Selenophosphoric Acids and their Interactions

Dissertation

Zur Erlangung des Doktorgrades der Naturwissenschaften

(Dr. rer. nat.)

an der Fakultät für Chemie und Pharmazie

der Universität Regensburg

vorgelegt von

Johannes Eder

aus Obergessenbach

im Jahr **2025**

Die vorliegende Dissertation beruht auf Arbeiten, die zwischen Januar 2022 und Februar 2025 im Arbeitskreis von Professorin Dr. Ruth M. Gschwind am Institut für Organische Chemie der Universität Regensburg durchgeführt wurden.

Promotionsgesuch eingereicht am:	07.02.2025
Die Arbeit wurde angeleitet von:	Prof. Dr. Ruth M. Gschwind
Promotionsausschuss:	
Vorsitzender:	Apl. Prof. Dr. Rainer Müller
1. Gutachterin:	Prof. Dr. Ruth M. Gschwind
2. Gutachterin:	Prof. Dr. Julia Rehbein
3. Prüfer:	Apl. Prof. Werner Kremer

„Wer hohe Türme bauen will, muss lange am Fundament verweilen“

~ Anton Bruckner, oft zitiert von Marianne Karrer

Table of Contents

1 Introduction and Outline

1.1 Brønsted acid catalysis

"Chemistry without catalysis would be a sword without a handle, a light without brilliance, a bell without sound." ~ Alwin Mittasch[1]

At the beginning of the 20th century, Mittasch played a pivotal role in the development of the iron catalysts that made the Haber-Bosch process for ammonia production viable on an industrial scale.[2] This advancement underscores the essential role of catalysis in both chemistry and life itself. In fact, estimates from the early 2000s suggest that nearly half of the global population is fed thanks to nitrogen fertilizers made possible by the Haber-Bosch process.[3]

Another significant advancement in catalysis emerged in the 1960s with the development of asymmetric catalysis using organometallic complexes. Research in this area has become essential for the production of pharmaceuticals, agrochemicals, fungicides, and more, often surpassing the efficiency of natural biological processes. This approach marked a significant shift in synthetic methodologies, enabling chemists to achieve higher selectivity and yields in complex chemical reactions.[4]

In the 1970s, pioneering research introduced metal-free organocatalysis as a third major approach alongside bio- and metal catalysis in asymmetric catalysis, motivated by the environmental impact and sustainability issues associated with metal catalysts - particularly regarding toxicity and resource depletion.[5,6] Nevertheless, the field was primarily established in the 21st century, beginning with the contributions of Benjamin List and David MacMillan, who were awarded the Nobel Prize in Chemistry in 2021 for their work in this emerging area of research.[7,8]

It is noteworthy, that advancements in catalysis are inherently linked to the need for detailed structural investigations to understand how complex reactions operate at a fundamental level.

1.1.1 Chiral Phosphoric Acids (CPAs)

One of the most important advancements in the field of asymmetric organocatalysis occurred in 2004 when the research groups of Akiyama and Terada introduced BINOL-based chiral phosphoric acids (Figure 1-1).[9,10] These catalysts combine chirality from their C_2 symmetric BINOL backbone with a bifunctional active center featuring a Brønsted acidic P–OH group and a Lewis basic P=O moiety, enabling both nucleophilic and electrophilic activation of substrates.

The size and reactivity of the active center can be fine-tuned via steric and electronic effects through substitutions at the 3,3'-positions. These catalysts are highly efficient, showing broad applicability across various reaction types, often delivering high stereoselectivities and yields.[11]

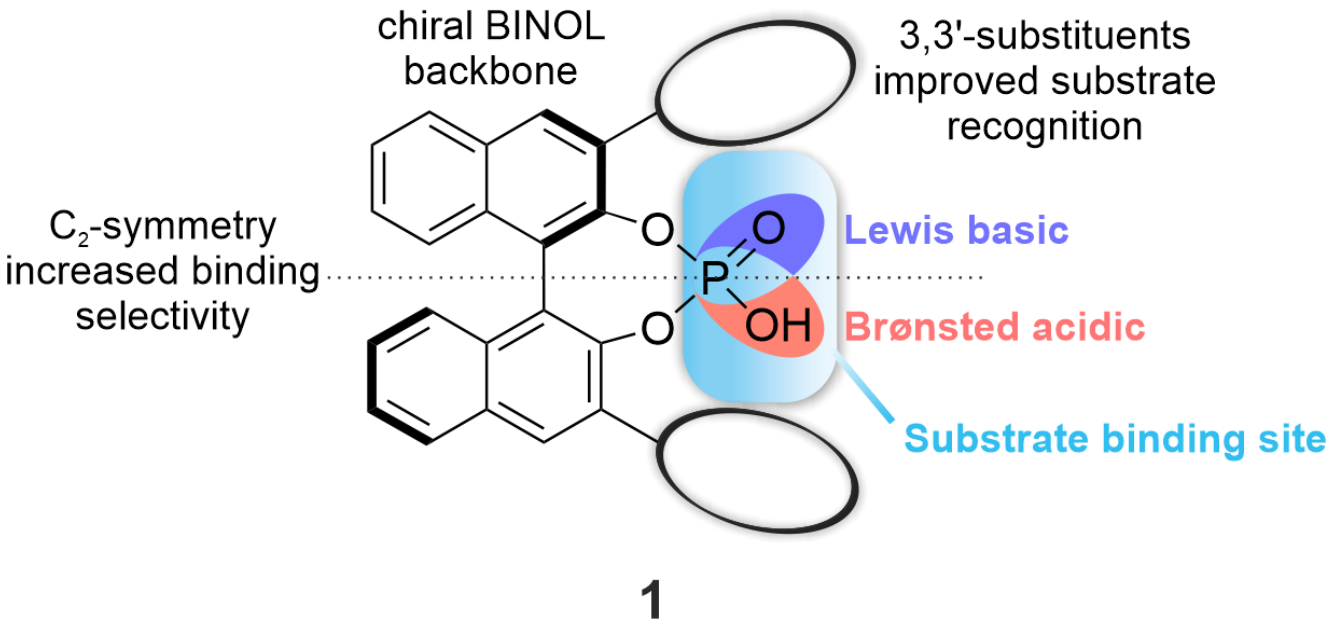

1

Figure 1-1: Structural design of chiral phosphoric acid catalysts. The chirality is integrated in the C_2-symmetric BINOL backbone and transferred onto the substrate by the 3,3'-substituents. The dual functionality consisting of Lewis basic P=O and Brønsted acidic P-OH moieties allows for effective dual activation of substrates.

Despite the broad range of reactions catalyzed by chiral phosphoric acids (CPAs), their relatively moderate acidity confines their application primarily to basic substrates, such as imines, quinolines, aziridines or alkenes.[12–17] Recognizing that enhanced catalyst acidity is often linked to increased reactivity,[18,19] various efforts over the past two decades have focused on modifying BINOL-based catalysts to broaden the spectrum of viable substrates in asymmetric organocatalysis.

Several pathways to more acidic catalysts were developed starting from the BINOL-based CPA **1**. These routes generally involve either the substitution of the phosphoryl P=O oxygen, of the P-OH hydroxy group, a combination of both, or the substitution of the entire phosphate POOH group (see Figure 1-2). This review is focused on the approach to access “superacidic” chiral BINOL-based Brønsted catalysts.

The following review centers on the pathways outlined above. It begins with the substitution of the P–OH hydroxyl group, followed by the substitution of the P=O oxygen. Next, the simultaneous substitution of both the P–OH and P=O groups is addressed. Finally, non-phosphoric acids are examined, while developments and changes to the backbone (e.g. [H_8]-BINOL or SPINOL) are outside the scope of this review. The BINOL backbone is always be displayed in its (*S*)-form for the catalysts’ syntheses. BINOL-based catalysts that are not used as Brønsted, but as Lewis acids (such as BALT[20]), are not incorporated in this review.

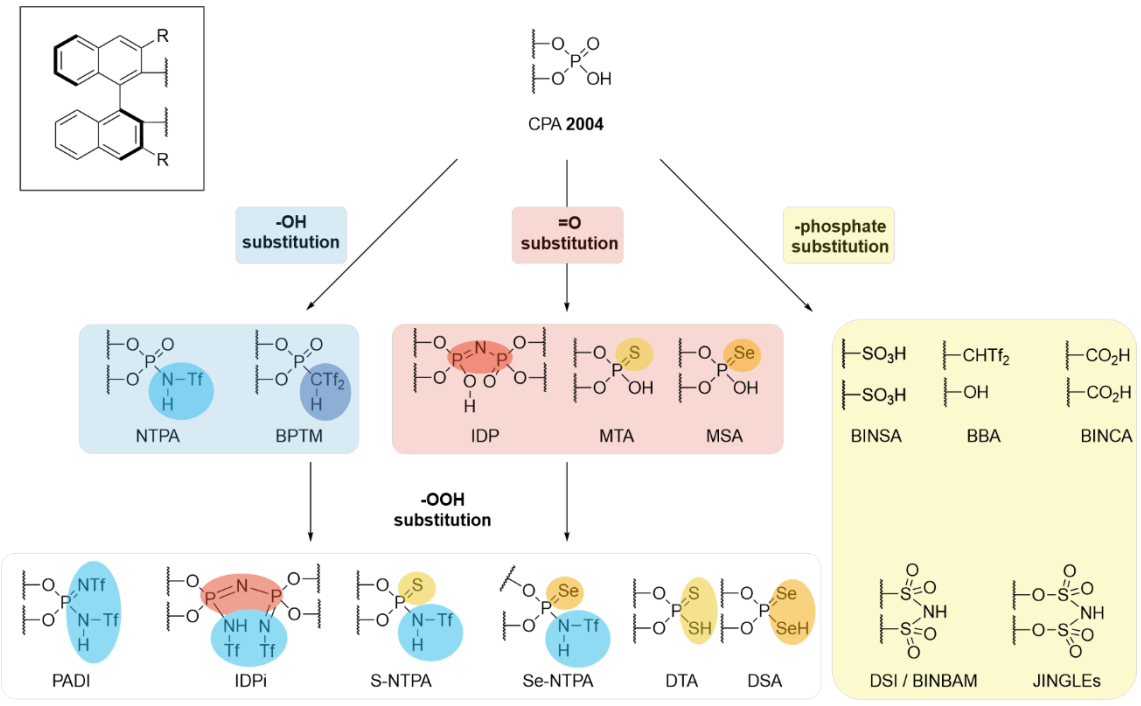

Figure 1-2: Variations and developments of BINOL-based Brønsted acidic organocatalysts.

1.1.2 Substitution of the P-OH hydroxy group

1.1.2.1 *N*-Triflyl Phosphoramides 2 (NTPAs)

In 2006, the Yamamoto group introduced a more acidic alternative to traditional CPAs by incorporating an *N*-triflyl group (-NHTf) into the phosphoric acid framework (see Figure 1-3).[21]

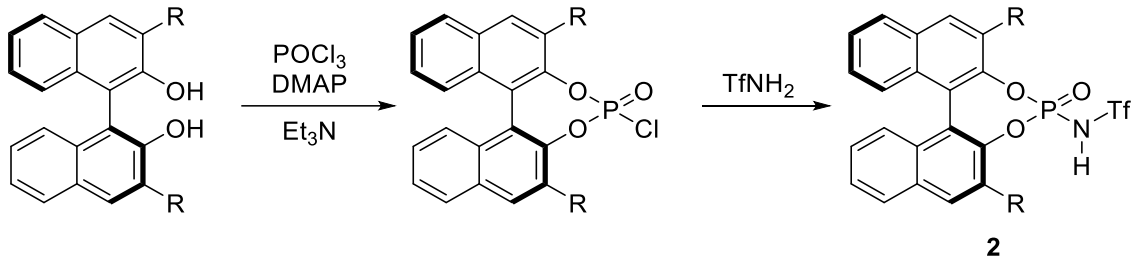

2a: R = Ph
2b: R = 2,4,6-(^{i}Pr)$_3$C$_6$H$_2$
2c: R = 4-(CF$_3$)C$_6$H$_4$
2d: R = SiPh$_3$
2e: R = 9-anthracenyl
2f: R = 3,5-(CF$_3$)$_2$C$_6$H$_3$

Figure 1-3: Synthetic pathway to NTPAs **2**. BINOLs are converted to phosphoryl chlorides and subsequently reacted with trifluoromethanesulfonamide.[21]

This increased acidity allowed the *N*-Triflyl Phosphoramide (NTPA) catalysts to effectively activate a broad range of substrates and enantioselectively catalyze numerous reactions, including Diels-Alder reactions,[21] Friedel-Crafts alkylations,[22,23] 1,4-additions,[24] cycloadditions[25] and many more.[26] Rueping provided a comprehensive review of NTPA-catalyzed reactions, which was later expanded upon by Goodman in reviews published in 2010 and 2021.[27,28] With this in mind, this review will focus on developments that have emerged since 2021, highlighting advances in understanding the binding interactions and novel applications of NTPAs in asymmetric organocatalysis.

Despite the extensive use of NTPAs in asymmetric catalysis since 2006, the catalyst-substrate binding mode remained poorly understood until 2021. That year, the Yoon group made a breakthrough by isolating a substrate-acid complex and resolving its structure via X-ray crystallography (see Figure 1-4).[29] Their findings revealed that the protonated imidazolium substrate interacts with the oxygen atom of the phosphoramide rather than the nitrogen atom, challenging prior assumptions. This insight was underlined in 2024, when the Gschwind group performed a detailed hydrogen bond analysis and low-temperature NMR spectroscopic investigations in solution, providing further clarity on the interaction mechanism.[30]

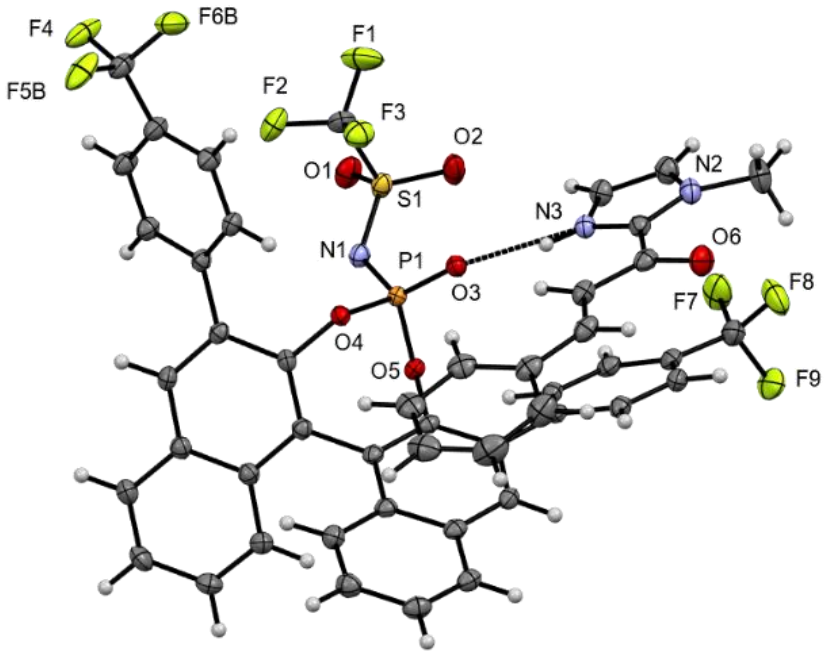

Figure 1-4: Crystal structure of a substrate-acid complex with NTPA by the Yoon group.[29] The protonated imidazolium substrate interacts with the NTPA-oxygen instead of the nitrogen.

Recent studies published after 2021 have focused on expanding the application scope of NTPAs and exploring their potential in new reaction types and substrates (see Figure 1-5).

In 2021, the Yoon group demonstrated that chiral Brønsted acids can activate enones by modifying their absorption properties, enabling them to serve as effective catalysts for enantio- and diastereoselective [2+2] photocycloadditions, leading to the formation of various substituted cyclobutanes (see Figure 1-5, A).[29] In the same year, NTPA **2b** was employed as a catalyst for an intramolecular cyclization reaction to synthesize 1-aminoindene derivatives, which can serve as valuable precursors for pharmaceutical agents such as rasagiline (see Figure 1-5, B).[31] Another example of an intramolecular reaction catalyzed by **2b** was reported in 2023, when Zhu *et al.* successfully carried out the carbocyclization of vinylidene ortho-quinone methides (VQMs). Furthermore, they demonstrated nucleophilic addition to the alkyne moiety using a range of diverse substrates (see Figure 1-5, C).[32]

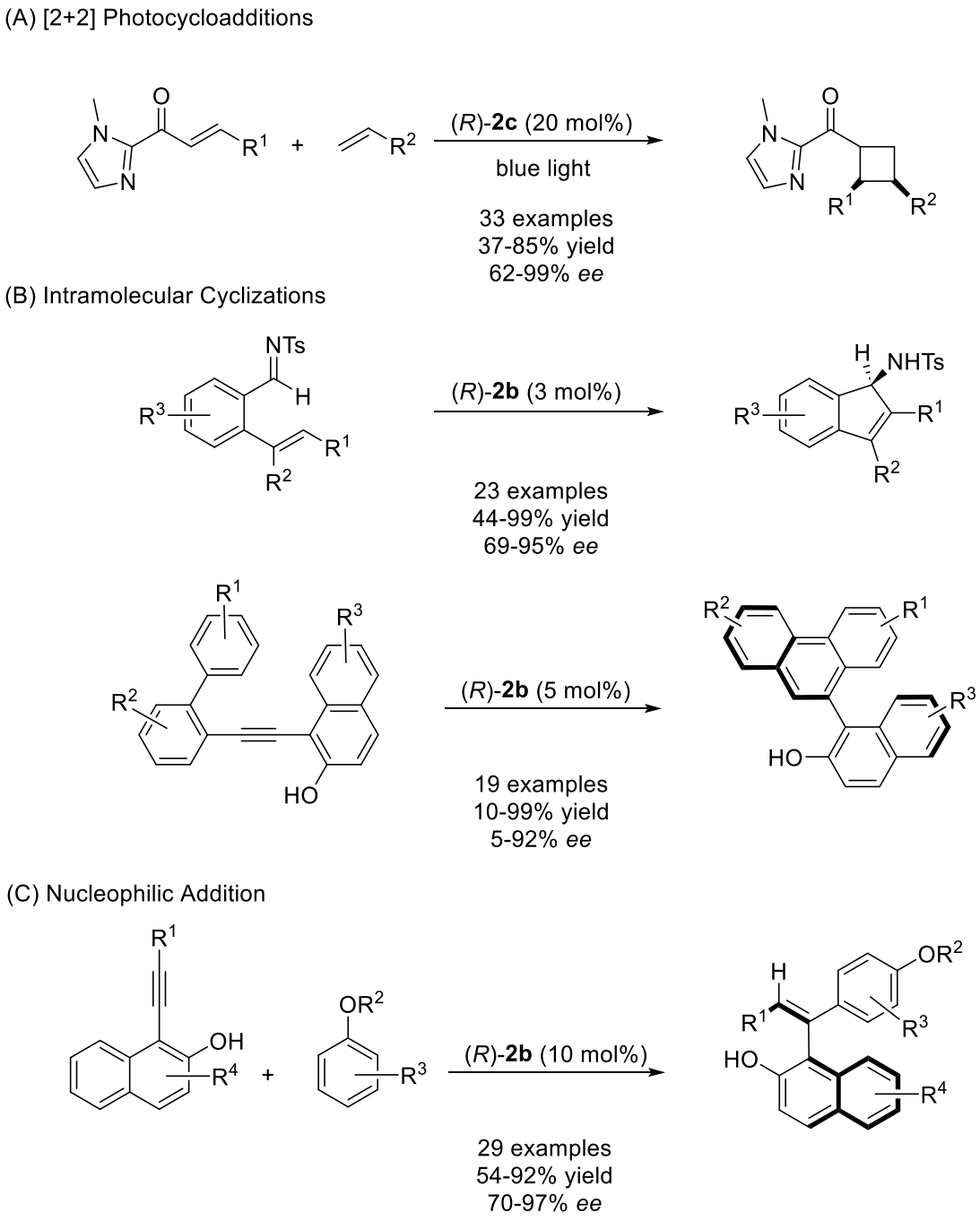

Figure 1-5: Summary of NTPA-catalyzed reactions since 2021. (A) displays a [2+2]-photocycloaddition,[29] (B) shows intramolecular cyclizations[31] and (C) a nucleophilic addition.[32]

1.1.2.2 BINOL-derived phosphoryl bis(trifluoromethyl)sulfonyl) methanes 3 (BPTMs)

In 2022, Peng *et al.* designed a new type of catalyst by substitution of the P-OH hydroxy group with a bis(trifluoromethyl)sulfonyl methane group, using a bis((trifluoromethyl)sulfonyl)methyl dianion as reagent (see Figure 1-6).[33]

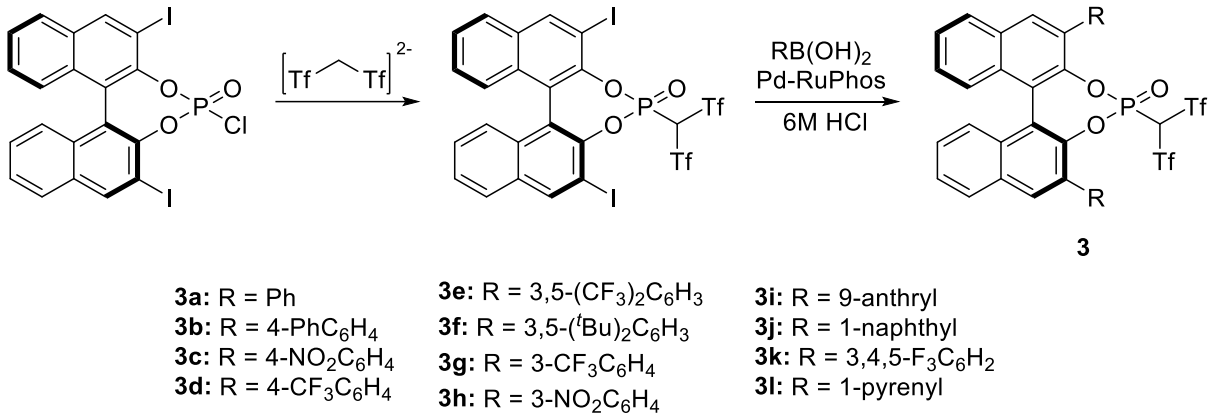

3a: R = Ph
3b: R = 4-PhC_6H_4
3c: R = 4-$NO_2C_6H_4$
3d: R = 4-$CF_3C_6H_4$
3e: R = 3,5-$(CF_3)_2C_6H_3$
3f: R = 3,5-$(^tBu)_2C_6H_3$
3g: R = 3-$CF_3C_6H_4$
3h: R = 3-$NO_2C_6H_4$
3i: R = 9-anthryl
3j: R = 1-naphthyl
3k: R = 3,4,5-$F_3C_6H_2$
3l: R = 1-pyrenyl

Figure 1-6: Synthesis of BPTMs **3** by addition of a bis((trifluoromethyl)sulfonyl)methyl dianion to a phosphoryl chloride and subsequent 3,3'-substitution.[33]

This led to C-H acidic catalysts with much higher Brønsted acidity (pK_a MeCN 1.3) compared to CPAs (pK_a MeCN 12-14) or NTPAs (pK_a MeCN 6-7). These catalysts allowed them to effectively active substrates in various transformations such as asymmetric Mukaiyama-Mannich reaction, allylic amination, three-component coupling of allyltrimethylsilane with 9-fluorenylmethyl carbamate and aldehydes, and protonation of silyl enol ethers with excellent enantioselectivites. (see Figure 1-7).[33]

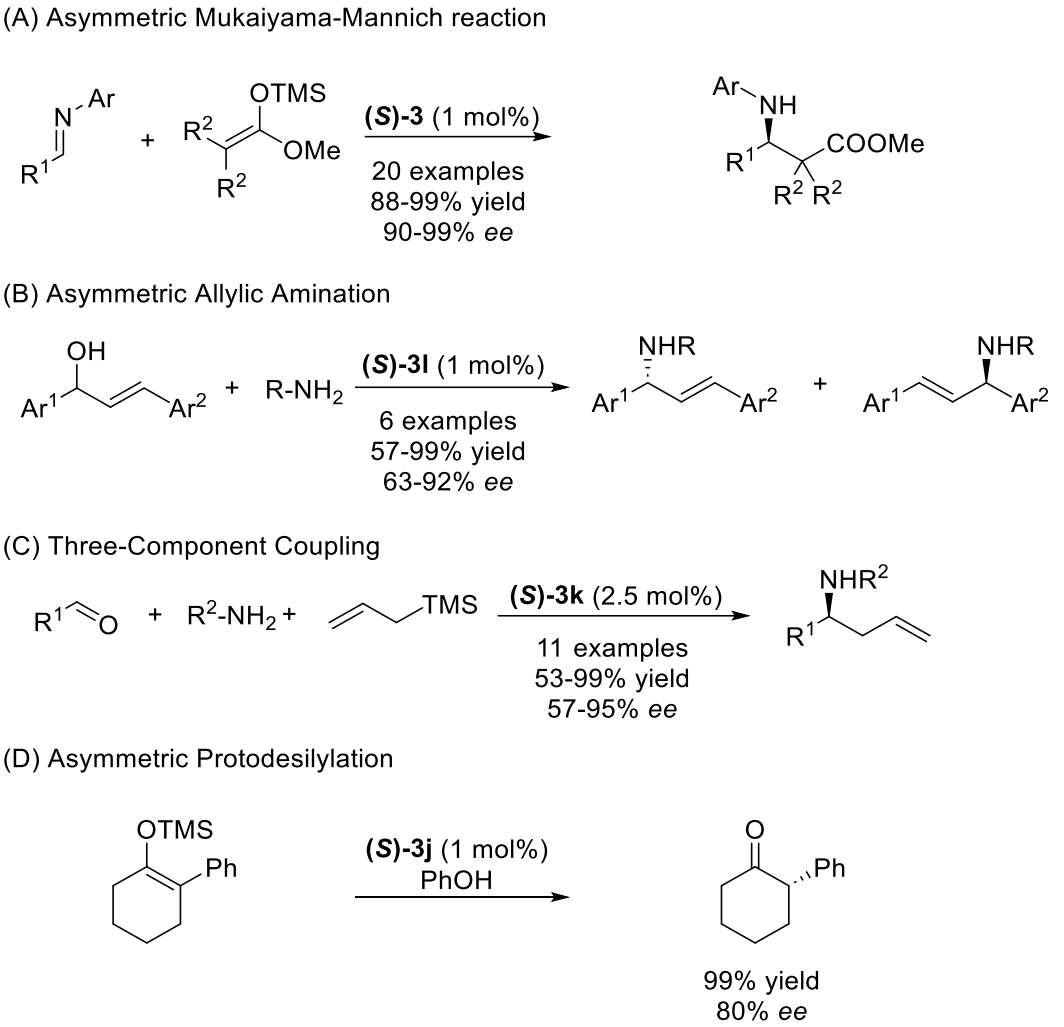

Figure 1-7: Summary of BPTM-catalyzed reactions. BPTMs **3** were successfully used in reactions like Mukaiyama-Mannich (A), allylic amination (B), three-component coupling (C) and protodesilylation (D).[33]

1.1.3 Substitution of the P=O phosphoryl group

1.1.3.1 Monothiophosphoric Acids 4 (MTAs)

The exchange of oxygen with sulfur in urea and thiourea catalysts has been shown to significantly enhance their acidity.[34,35] Consequently, it was anticipated that substituting the phosphoryl oxygen (P=O) in phosphoric acids with other chalcogen atoms would similarly lead to a significant increase in acidity. Building on this concept, considerable efforts have been devoted to incorporating various chalcogens into CPAs.

The structural aspects of these catalysts, particularly the modifications introduced by substituting different chalcogen atoms, have also been thoroughly investigated. Previous studies have demonstrated that thiophosphoric acids exist in a tautomeric equilibrium between their thiolic and thionic forms, with the equilibrium heavily favoring the thionic form (see Figure 1-8).[36,37] Thus, in this context, monothiophosphoric acids **4** and monoselenophosphoric acids **5** will consistently be represented with a double-bonded sulfur or selenium, respectively.

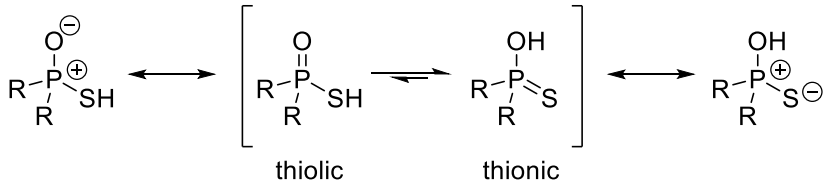

Figure 1-8: Tautomeric equilibrium between the thiolic and thionic form of monothiophosphoric acids.[36,37]

Monothiophosphoric acids (MTAs) **4** can be efficiently prepared through a simple two-step reaction using $Cl_3P{=}S$ and water starting from BINOLs (see Figure 1-9).[38]

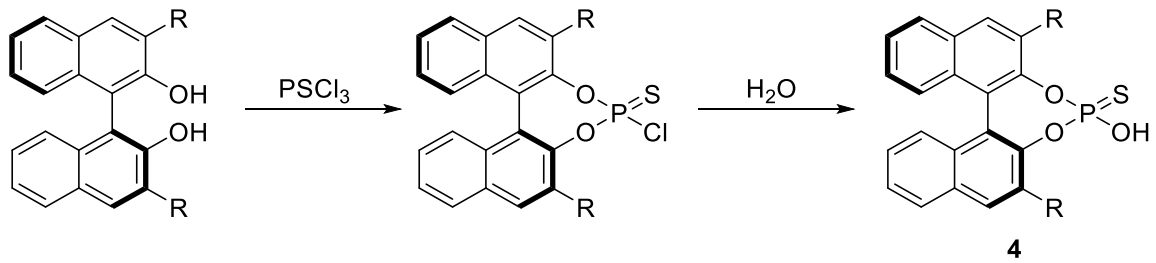

4a: R = Ph
4b: R = 2,4,6-$(CH_3)_3C_6H_2$
4c: R = 2,4,6-$^{i}Pr_3C_6H_2$
4d: R = 4-(1-adamantyl)-2,6-$^{i}Pr_2C_6H_2$
4e: R = 4-^{t}Bu-2,6-$^{i}Pr_2C_6H_2$
4f: R = H
4g: R = 2,4,6-$(CH_3)_3$-3,5-$(NO_2)_2C_6$
4h: R = 9-anthracenyl

Figure 1-9: MTAs **4** are synthesized by addition of thiophosphoryl chloride and water to BINOLs.[38]

Although MTAs **4** are more acidic than **1**, to the best of our knowledge, there are only a few reported instances of their application in organocatalysis. It is worth mentioning that, in two cases, **4** has demonstrated lower catalytic efficiency compared to other catalysts, such as CPAs **1** (see Figure 1-10).[39,40]

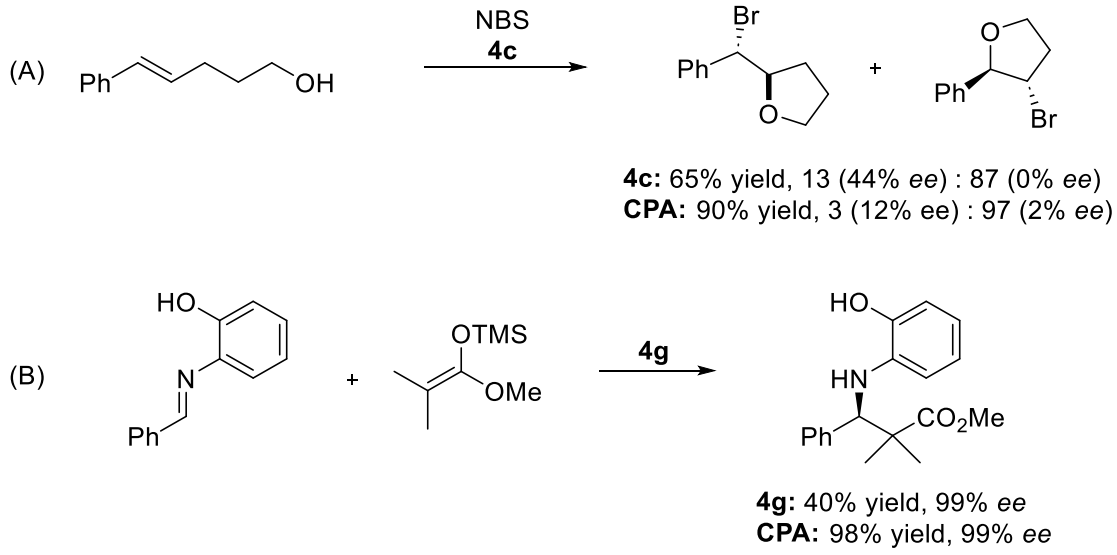

Figure 1-10: MTA-catalyzed reactions. (A) displays a heterocyclization, (B) a Mukaiyama-Mannich reaction.[39,40] Both transformations can be more efficiently catalyzed by CPAs.

Xie *et al.* efficiently catalyzed an N-H functionalization of indoles with α,β-unsaturated γ-lactams with MTA **4b** (see Figure 1-11, A).[41] While the reactivity was enhanced with the corresponding CPA **1** in some cases, the enantioselectivity provided by **4b** was slightly better. It has been shown, that MTA can also be used for asymmetric cyclization and coupling reactions of indoles (see Figure 1-11, B-C).[42,43]

To the best of our knowledge, the potential of MTAs in organocatalysis was not investigated further. However, in the field of photocatalysis, Xu *et al.* identified **4f** (R = H) as an effective catalyst for the Umpolung Trifluoromethylthiolation of tertiary ethers.[44]

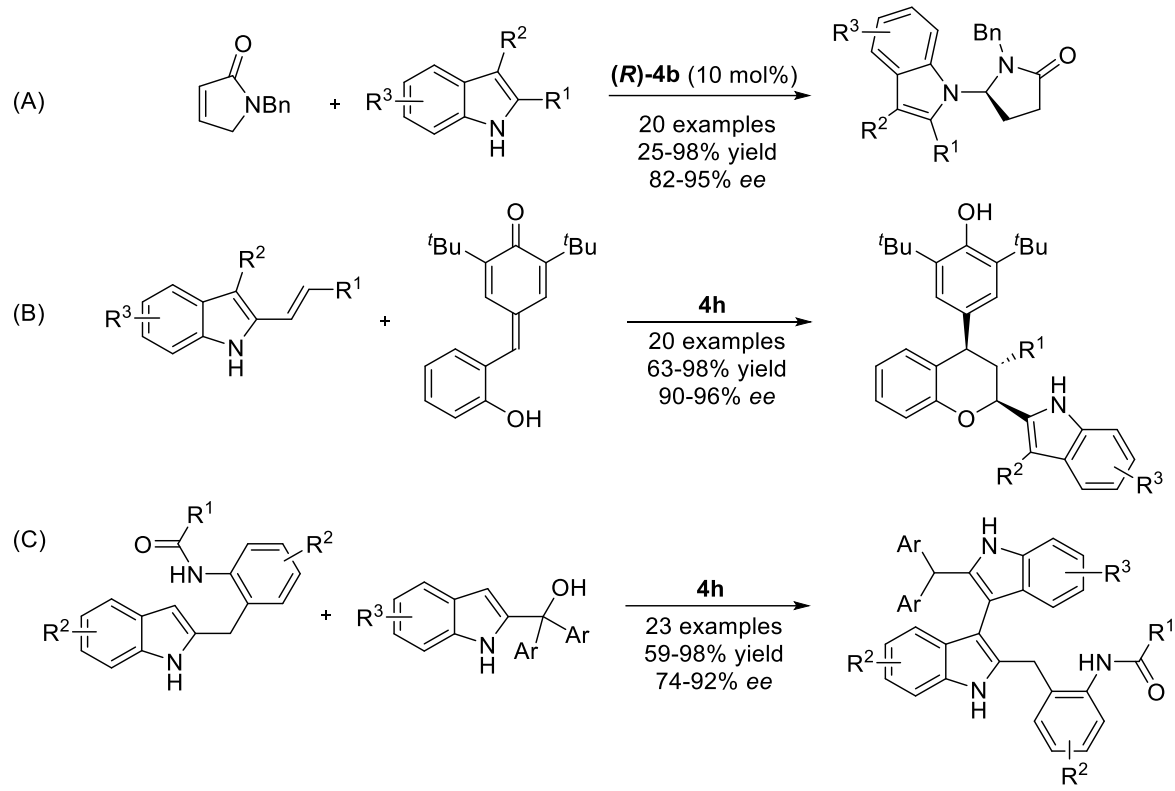

Figure 1-11: Summary of MTA-catalyzed reactions of indole N-H functionalization (A),[41] cyclization (B)[42,43] and coupling (C).[44]

1.1.3.2 Monoselenophosphoric Acids 5 (MSAs)

MSAs **5** can be prepared in a similar fashion to MTAs **4** by treatment of BINOLs with phosphorus(III) chloride and elemental selenium (see Figure 1-12).[45]

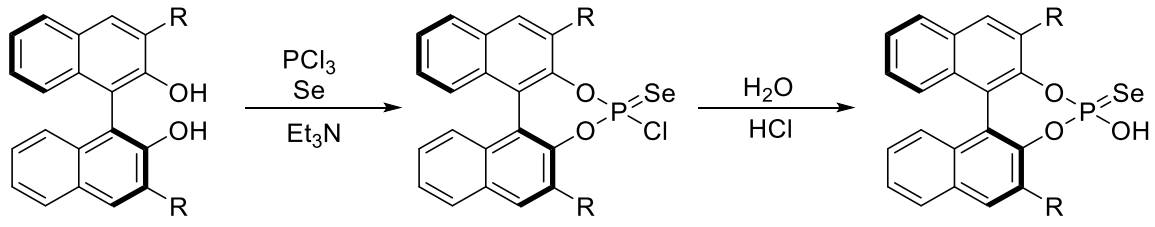

5a: R = H
5b: R = Br
5c: R = $SiPh_3$
5d: R = 2,4,6-$^{i}Pr_3C_6H_2$
5e: R = 2,4,6-$(CH_3)_3$-3,5-$(NO_2)_2C_6$

Figure 1-12: Synthetic pathway to MSAs **5**, prepared by treatment of BINOL with phosphorus(III) chloride, elemental selenium and water.[45]

In DMSO, these catalysts are approximately two magnitudes of order more acidic than their MTA counterparts **4**.[46] Despite their increased acidity, the catalysts **5** are not widespread used

in organocatalysis yet. It was previously shown, that it can catalyze an asymmetric transfer hydrogenation (ATH) reaction[47] and a Mukaiyama-Mannich reaction[39] with inferior results in comparison to traditional CPAs **1** or NTPAs **2** (see Figure 1-13).[48]

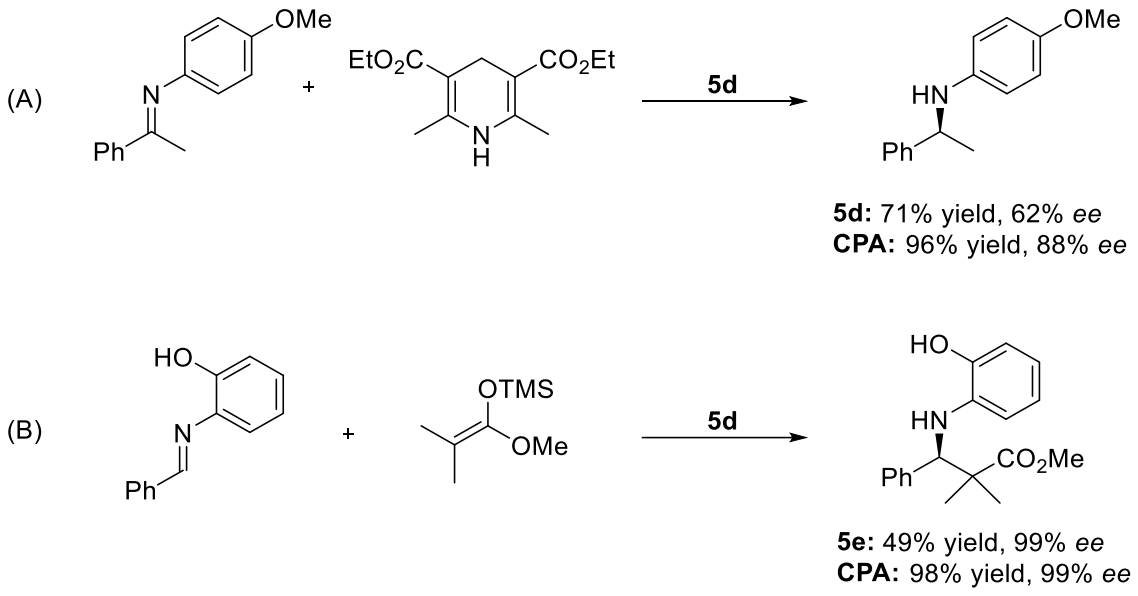

Figure 1-13: MSA-catalyzed reactions. (A) displays an asymmetric transfer hydrogenation (ATH),[47] (B) a Mukaiyama-Mannich reaction.[48] Both transformations can be more efficiently catalyzed by CPAs.

1.1.3.3 Imidodiphosphates 6 (IDPs)

In 2012, the List group introduced a novel imidodiphosphate (IDP) catalyst **6** by treating a BINOL-based phosphoryl chloride with a BINOL-based phosphoramide (see Figure 1-14).[49]

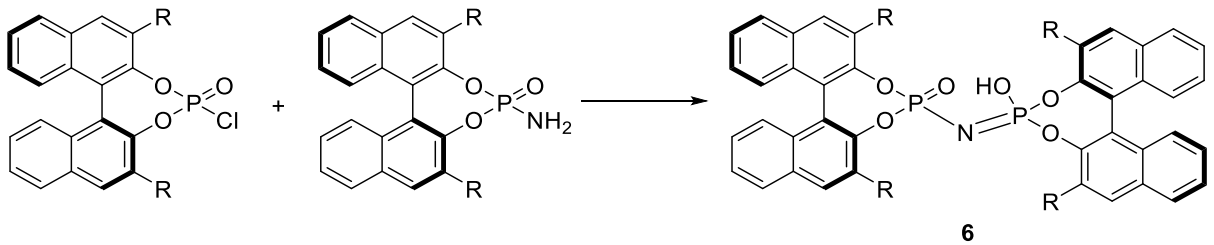

6a: R = 2,4,6-$(C_2H_5)_3C_6H_2$
6b: R = 2,6-$(C_2H_5)_2C_6H_3$
6c: R = 9-anthracenyl
6d: R = H
6e: R = Ph
6f: R = 1-naphthyl
6g: R = 2-^{i}Pr-5-$CH_3C_6H_3$

Figure 1-14: IDPs **6** can be obtained by coupling of a BINOL-based phosphoryl chloride with a BINOL-based phosphoramide.[49]

Those catalysts were effectively utilized for the asymmetric spiroacetalization reaction, exemplified by the first reported direct enantioselective synthesis of the natural product olean in organocatalysis alongside various other 5- and 6-membered ring formations (see Figure 1-15, A).[49] In the same year, Chen *et al.* also reported the synthesis of this catalyst type and performed highly efficient and selective three-component Mannich reactions (see Figure 1-15, B).[50]

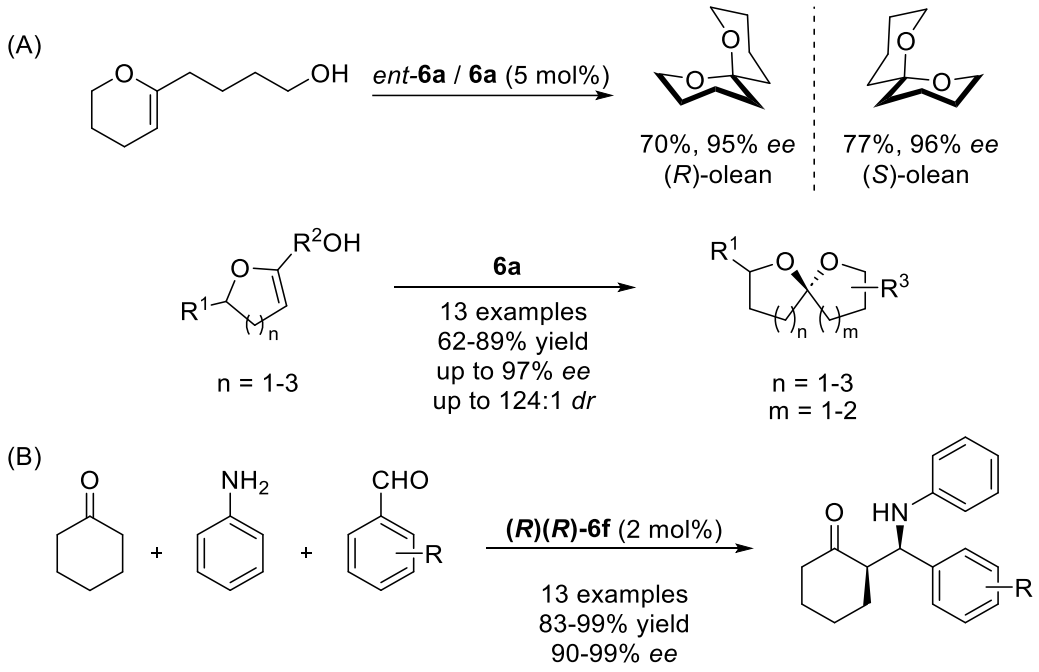

Figure 1-15: First IDP-catalyzed reactions – spiroacetalization (A)[49] and three-component Mannich reaction (B).[50]

These IDP catalysts are of particular interest due to their sterically constrained active site, made possible by the presence of two BINOL backbones with 3,3'-substituents. In contrast, regular BINOL-based catalysts face challenges in modifying their steric environment, as the 3,3'-substituents extend outward, away from the active site (see Figure 1-16).[49]

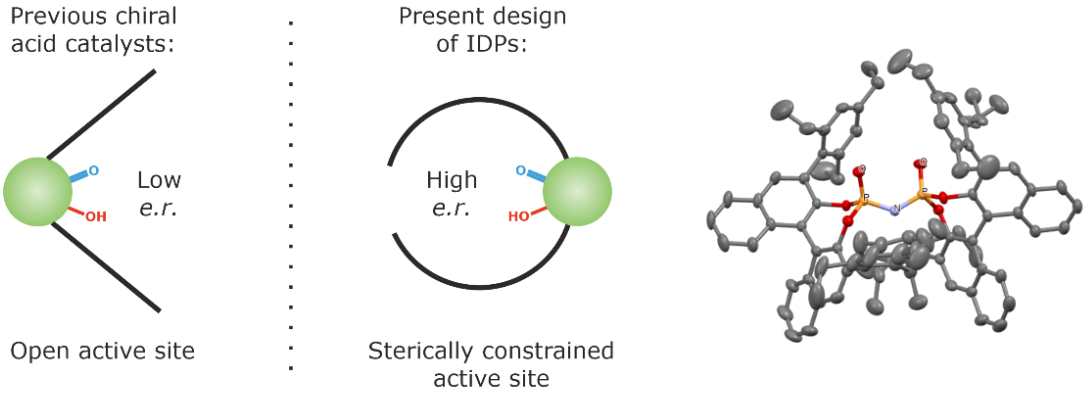

Figure 1-16: Schematic representation of the binding sites of CPA **1** and IDP **6**, along with the crystal structure of **6**. H-atoms are omitted for clarity.[49]

Some of the reactions of IDPs **6** were already covered in a review of Rueping and thus will not be inside the scope of this review.[51] Wu *et al.* [52] and Zhuo *et al.*[53] demonstrated that IDPs **6** are effective catalysts for the Friedel-Crafts reaction of indoles and 3-indolylphenylmethanol, respectively (see Figure 1-17, A). In 2013, the List group employed **6g** in asymmetric acetalization reactions of both aliphatic and aromatic aldehydes (see Figure 1-17, B).[54] In 2014, the Sunoj group reported a novel application of **6** in the asymmetric sulfoxidation of an achiral sulfide to a chiral sulfoxide (see Figure 1-17, C).[55] That same year, the Zhu group utilized **6** for the desymmetrization of bicyclic bislactones (see Figure 1-17, D), enabling the total syntheses of the alkaloids (-)-Rhazinilam and (-)-Leucomidine B.[56]

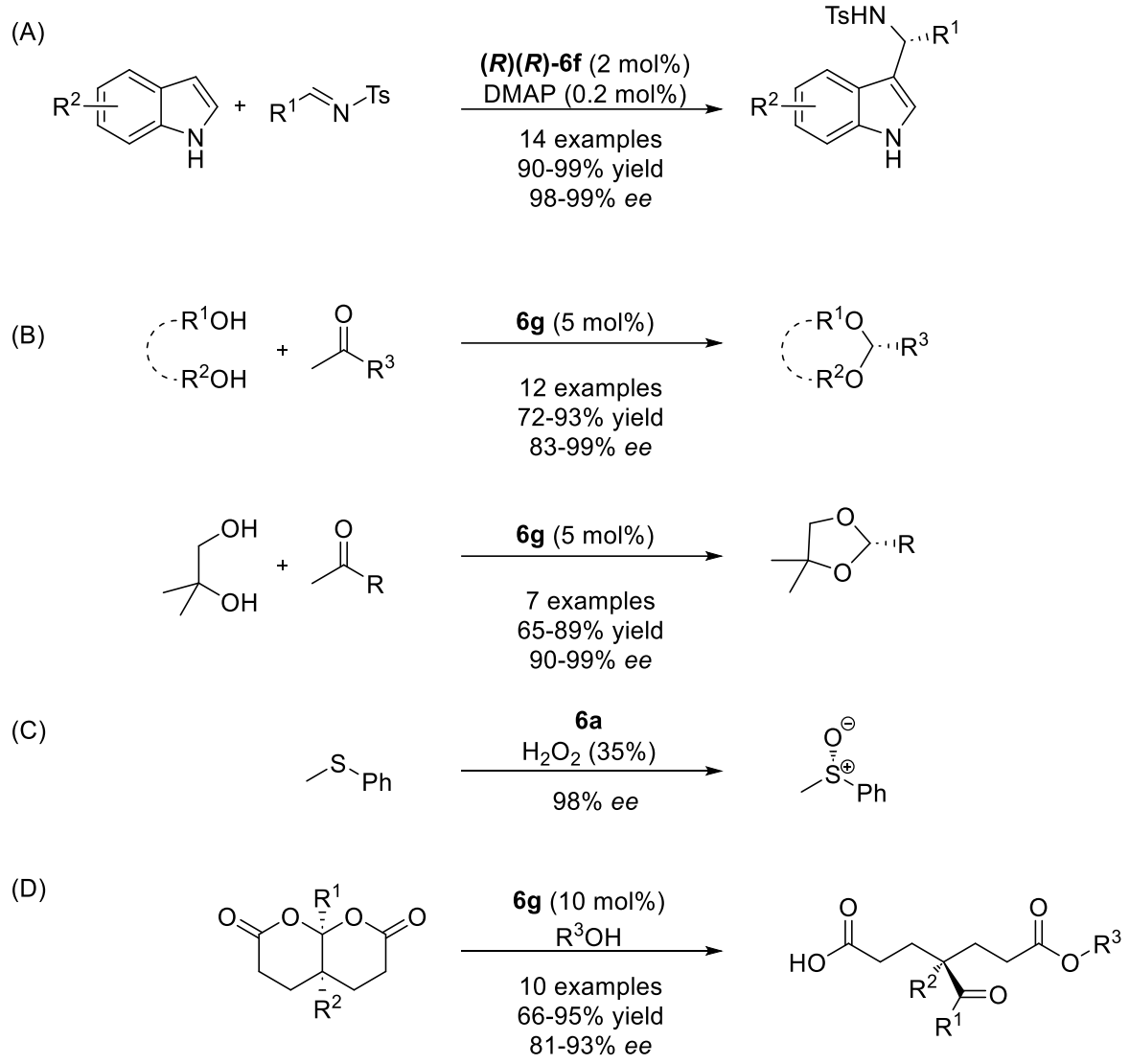

Figure 1-17: Summary of IDP-catalyzed transformations including Friedel-Crafts (A),[52,53] acetalizations (B),[54] sulfoxidation (C)[55] and desymmetrization (D)[56] reactions.

1.1.4 Simultaneous substitution of P-OH hydroxy and P=O phosphoryl groups

1.1.4.1 Dithiophosphoric Acids 7 (DTAs)

Dithiophosphoric Acid catalysts **7** (DTAs) can be easily synthesized by reacting BINOLs with phosphorus(V) sulfide (see Figure 1-18).[57,58]

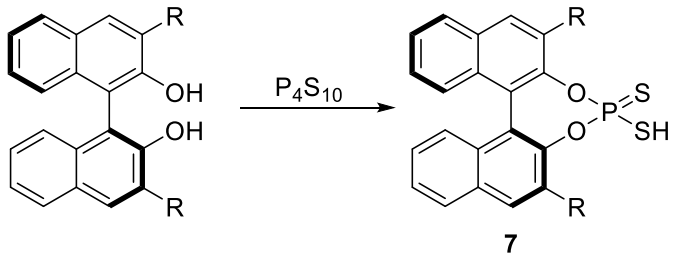

Figure 1-18: Synthesis of DTAs by treatment of BINOLs with phosphorus(V) sulfide.[57,58]

While theoretical studies have shown that DTAs surpass CPAs by approximately six orders of magnitudes in terms of pK_a values in DMSO,[46] they have not gained significant prominence in asymmetric Brønsted acid organocatalysis.

Although Shapiro *et al.* demonstrated that DTAs, unlike CPAs and NTPAs, can catalyze asymmetric hydroaminations to produce *N*-heterocycles, the *ee* values are rather low (see Figure 1-19).[57]

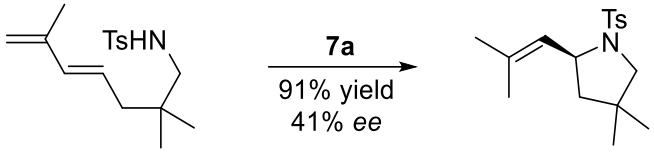

Figure 1-19: DTA-catalyzed hydroamination reaction.[57]

1.1.4.2 Diselenophosphoric Acids 8 (DSAs)

The very first chiral diselenophosphoric acid (DSA) **8a** was reported by the Gschwind group in 2024. DSA **8a** was prepared by the subsequent treatment of potassium BINOLate with phosphorus selenide and ethereal hydrogen chloride solution (for details see Chapter 2).[59] DSAs **8a-e** can be prepared by treatment of phosphoroselenoyl chloride with potassium selenide (for synthesis see Figure 1-20, for further details see Chapter 3).

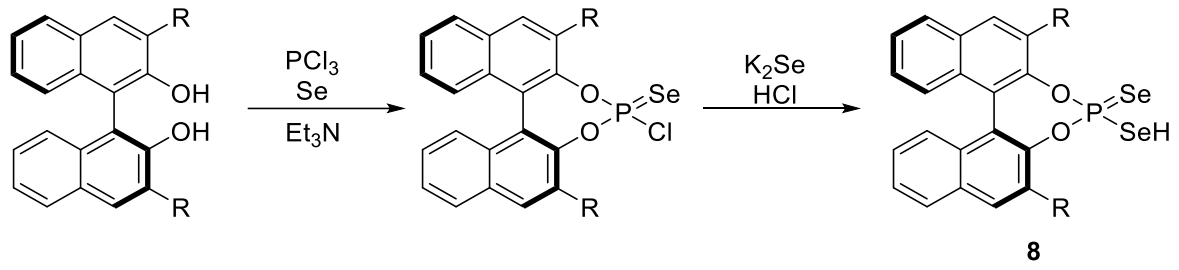

8a: R = H
8b: R = 2,4,6-$^{i}Pr_3C_6H_2$
8c: R = 9-anthracenyl
8d: R = 2,4,6-$(CH_3)_3C_6H_2$
8e: R = 3,5-$(CF_3)_2C_6H_3$

Figure 1-20: Synthesis of DSAs **8** by addition of potassium selenide to phosphoroselenoyl chlorides.

Initial reactivity tests demonstrated that DSA **8a** can efficiently activate Mukaiyama Mannich reaction and function as catalyst Asymmetric Counteranion-Directed Catalysis (ACDC, for details see Chapter 2, 3).[59]

Due to the novelty of DSAs **8**, their full potential is unexplored to date.

1.1.4.3 *N*-Triflyl Thiophosphoramide 9 (S-NTPAs) / *N*-Triflyl Selenophosphoramide 10 (Se-NTPAs)

In 2008, the Yamamoto group developed Thio- and Selenophosphoramide catalysts **9** and **10** which are expected to provide higher Brønsted acidity than NTPA **2** (see Figure 1-21).[17] The synthesis of these compounds is similar to the previously shown MTA **4** and MSA **5** catalysts and based on the reaction of phosphorothionyl chlorides / phosphoroselenoyl chlorides with trifluoromethanesulfonamide.

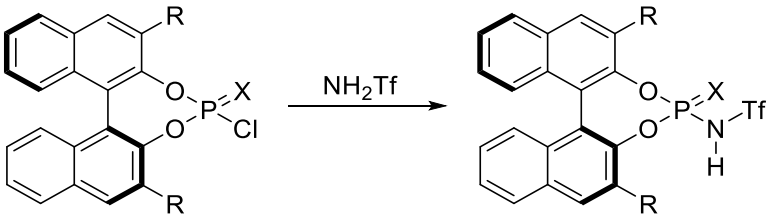

9: X = S
10: X = Se

9a: R = Ph
9b: R = 2,4,6-$(CH_3)_3C_6H_2$
9c: R = 2,4,6-$^{i}Pr_3C_6H_2$
9d: R = 4-(1-adamantyl)-2,6-$^{i}Pr_2C_6H_2$

9e: R = 2,6-$^{i}Pr_2$-4-$^{t}BuC_6H_2$
9f: R = 2,6-$^{i}Pr_2C_6H_3$
9g: R = 2,6-$^{i}Pr_2$-4-(2,4,6-i$Pr_3C_6H_2$)C_6H_2
9h: R = 2,6-$^{i}Pr_2$-4-(9-anthryl)C_6H_2

10a: R = 2,4,6-$^{i}Pr_3C_6H_2$

Figure 1-21: Thio- and selenophosphoramides are obtained by reacting the respective phosphoryl chloride with trifluoromethanesulfonamide.[17]

The Yamamoto group used **9c,e** and **10a** to protodesilylate silyl enol ethers – a transformation which is not effectively catalyzed by CPA **1** and MTA **4** – achieving higher enantiomeric excesses than with NTPAs **2** (see Figure 1-22, A.).[17] Furthermore, S-NTPA **9h** can be used as catalyst in a Mukaiyama aldol reaction of aldehydes with silyl enol ethers as nucleophiles.[60] The potential of Se-NTPA **10** remains largely unexplored.

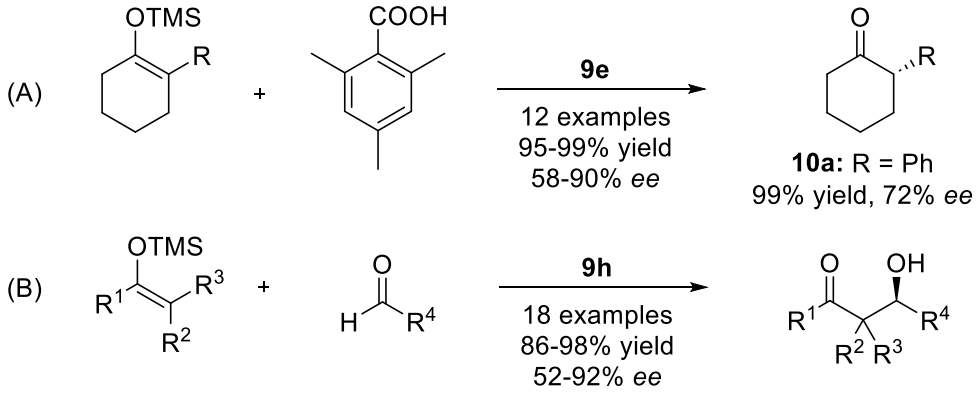

Figure 1-22: S- and Se-NTPA-catalyzed protodesilylation (A)[17] and S-NTPA catalyzed Mukaiyama aldol (B)[60] reaction.

1.1.4.4 Phosphoramide Imidates 11 (PADIs)

In 2016, the List group reported the synthesis of a novel phosphoramidimidate **11** (PADI) catalyst by reacting BINOLs with phosphorus pentachloride and subsequently with sulfonamides (see Figure 1-23).[61]

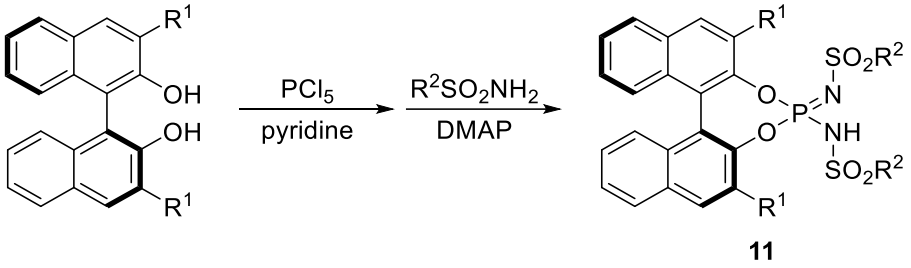

11a: R^1 = 2,4,6-^{i}Pr$_3$C$_6$H$_2$ R^2 = CF_3
11b: R^1 = 3,5-$(CF_3)_2C_6H_3$ R^2 = CF_3
11c: R^1 = 1-naphthyl R^2 = CF_3
11d: R^1 = 9-phenanthryl R^2 = CF_3
11e: R^1 = 2,6-(3,5-$(CF_3)_2C_6H_3)_2C_6H_3$ R^2 = CF_3
11f: R^1 = 2,4,6-^{i}Pr$_3$C$_6$H$_2$ R^2 = 3,5-$(CF_3)_2C_6H_3$
11g: R^1 = 3,5-$(CF_3)_2C_6H_3$ R^2 = 3,5-$(CF_3)_2C_6H_3$

Figure 1-23: Synthetic pathway for the synthesis of PADIs **11**, where BINOL is treated with phosphorus(V) chloride and sulfonamides.[61]

In 2017, the List group improved their synthesis of PADIs by employing *N*-triflylphosphorimidoyl trichloride as a reagent, achieving **11** in high yields of 72-98% under mild reaction conditions (r.t., 10 min). Additionally, both NTPA **2** and S-NTPA **9** can be synthesized by the same procedure (see Figure 1-24).[62]

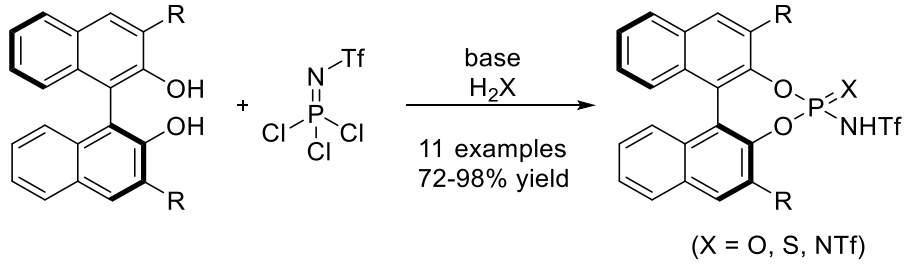

Figure 1-24: Improved synthesis of PADIs **11** with N-triflylphosphorimidoyl trichloride as reagent.[62]

Catalyst **11a** was only tested in the synthesis of α-tocopherol from (7*R*,11*R*)-isophytol – a transformation which could not be catalyzed using CPA **1** or NTPA **2**.[61] Despite the successful activation, both yield and *d.r.* values are very low (see Figure 1-25).

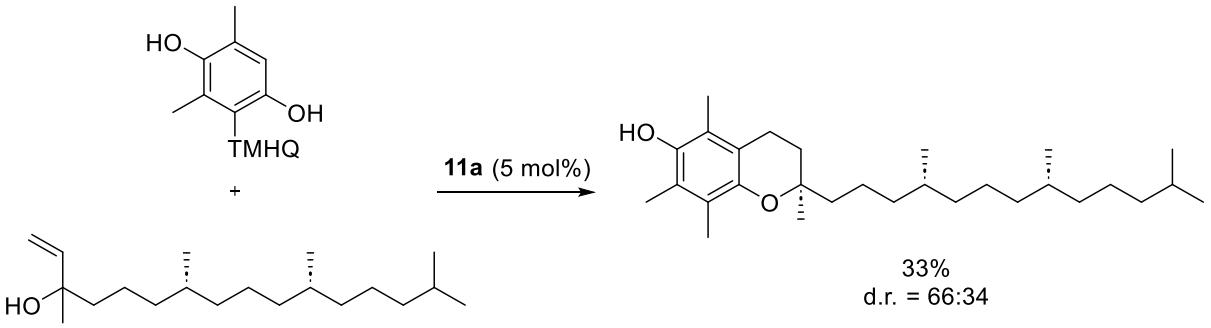

Figure 1-25: PADI-catalyzed synthesis of α-tocopherol.[61]

To date, the potential of PADI catalysts in asymmetric organocatalysis remains largely unexplored, however, they have been successfully utilized by the Liao group for polymerization reactions.[63,64]

1.1.4.5 Imidodiphosphateimidate 12 (IDPis)

In 2016, the List group introduced a novel imidodiphosphateimidate organocatalyst by treatment of BINOLs with sulfonylphosphorimidoyl trichlorides followed by triethylamine and ammonia (see Figure 1-26).[65]

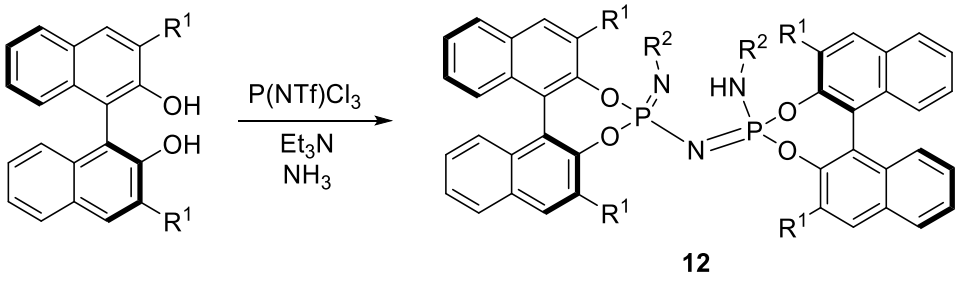

12a: R^1 = Ph, R^2 = Tf
12b: R^1 = 1-naphthyl, R^2 = Tf
12c: R^1 = 3-FC_6H_4, R^2 = Tf
12d: R^1 = 3,5-$(CF_3)_2C_6H_3$, R^2 = Tf
12e: R^1 = 7,9-$(CH_3)_2$-pyrenyl, R^2 = Tf
12f: R^1 = 9*H*-fluorene, R^2 = Tf
12g: R^1 = 4-^{t}BuC_6H_4, R^2 = F_7-1-naphthyl

Figure 1-26: IDPi synthesis with BINOL and sulfonylphosphorimidoyl trichlorides, triethylamine and ammonia as reactants.[65]

These IDPi catalysts **12** combine the high activity of PADIs **11** with the exceptional selectivity of IDPs **6** (see Figure 1-27).[65]

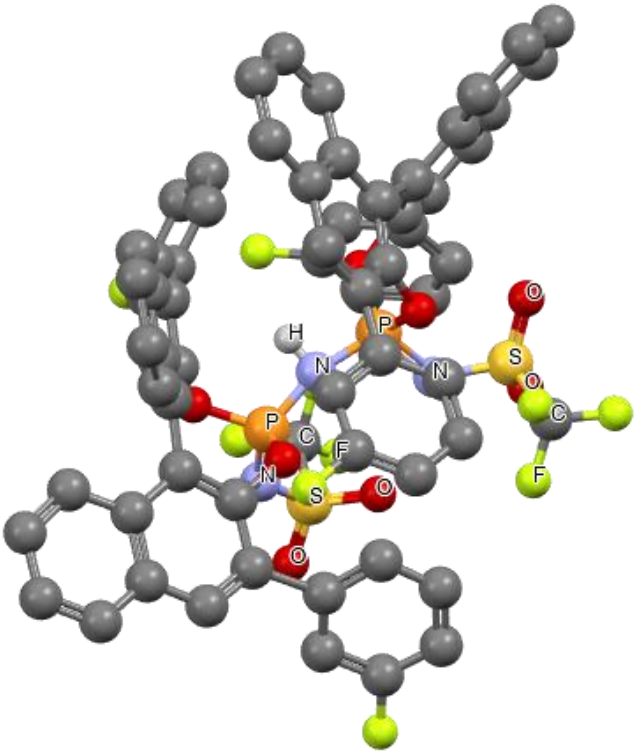

Figure 1-27: Structure of **12c**. Solvent molecules and H-atoms (except the acidic proton) are omitted for clarity. Molecular disorder is omitted for clarity.[65]

Since the List group reviewed the performance of these catalysts in Lewis and Brønsted acid catalysis in 2019, this review will focus solely on research published thereafter.[66]

Recently, Maji *et al*. demonstrated that IDPi can function as Brønsted acid catalysts in lactonization reactions to yield 5- and 6-membered heterocycles (see Figure 1-28).[67]

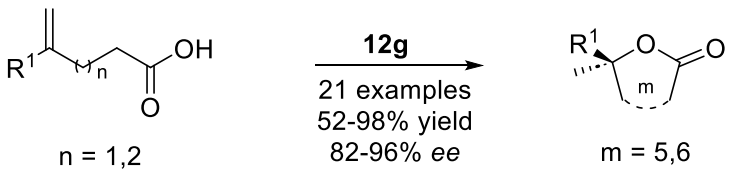

Figure 1-28: IDPi-catalyzed lactonization reaction to 5- and 6-membered heterocycles.[67]

In general, research on IDPi catalysts has primarily centered on stereoselective polymerization reactions[68–70] and Lewis-catalyzed asymmetric (de)silylation processes[71–74]. Nevertheless, it is worth mentioning that IDPIs can serve as Brønsted acid pre-catalysts to generate an active Lewis acid catalyst form (see Figure 1-29).[75,76]

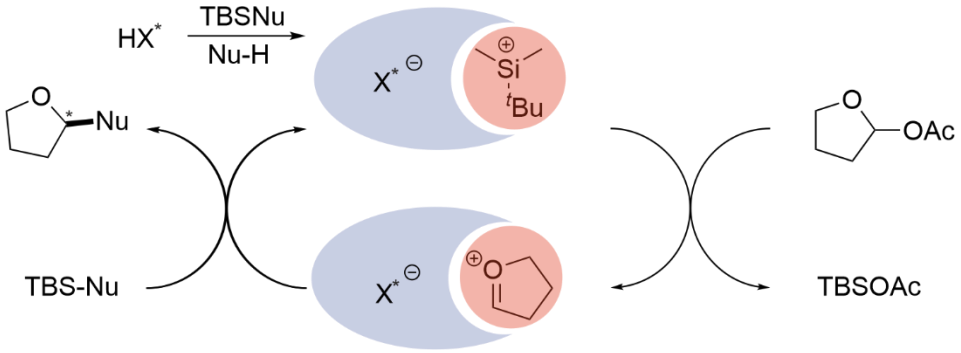

Figure 1-29: IDPi serves as a Brønsted acidic pre-catalyst, activating the silyl Lewis acid catalyst and providing stereocontrol for the reaction.[75,76]

1.1.5 Substitution of the POOH phosphate group

1.1.5.1 Binaphthyl-2,2'-disulfonates 13 (BINSAs)

Binaphthyl-2,2'-disulfonates **13** (BINSA) can be synthesized by oxidizing dithio-BINOL[77,78] and were introduced to the realm of asymmetric organocatalysis by the Ishihara group in 2008 (see Figure 1-30).[79]

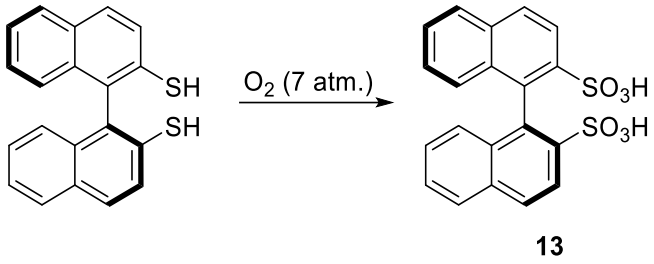

Figure 1-30: BINSA **13** can be obtained by oxidation of dithio-BINOL.[77,78]

In 2014, computational studies by Yang *et al.* revealed the surprisingly high acidity of **13** in DMSO (pK_a = -9.06), significantly exceeding that of NTPA **2** (pK_a = -3.40) and Disulfonimides **15** (pK_a = 0.15).[80]

Hatano and Ishihara published a comprehensive review on BINSA and its derivatives for asymmetric catalysis in 2014.[81] Since then - despite this remarkable acidity - BINSA was predominantly employed as a chiral ligand in Lewis acid catalysis or as the chiral component of catalyst clusters (see Figure 1-31).[82–84]

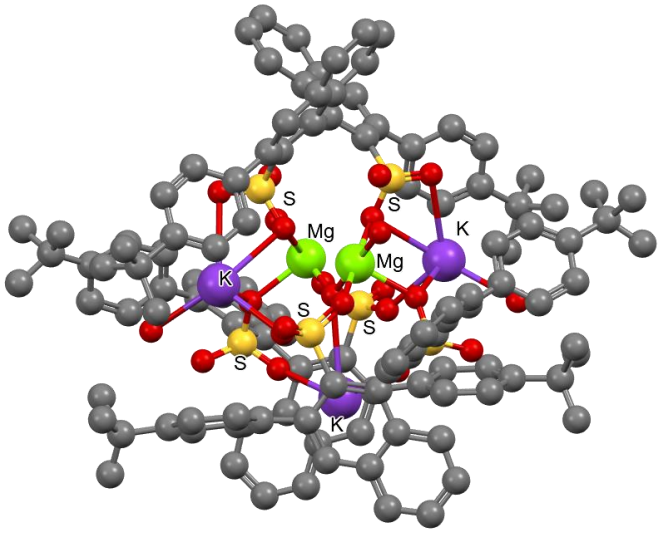

Figure 1-31: BINSA as part of a catalytic 3:1:4 complex of (R)-BINSA / Mg / K.[82]

1.1.5.2 (S)-2'-(bis((trifluoromethyl)sulfonyl)methyl)-[1,1'-binaphthalen]-2-ol 14 (BBA)

In 2006, a new chiral Brønsted acid-assisted chiral Brønsted acid (BBA) catalyst was developed by replacing a hydroxy group of BINOL with a bis(trifluoromethanesulfonyl)methyl group (see Figure 1-32).[85]

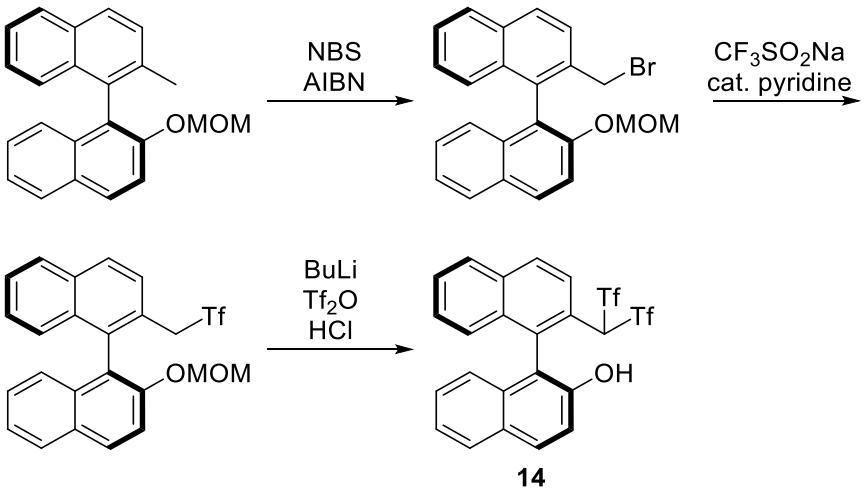

Figure 1-32: Synthetic access of **14** by replacing a hydroxy group of BINOL with a bis(trifluoromethanesulfonyl)methyl group.[85]

A cooperative H-bonding interaction can be anticipated, ensuring strong fixation of the reagent within the chiral pocket and eliminating the necessity for 3,3'-substituents (see Figure 1-33).[85]

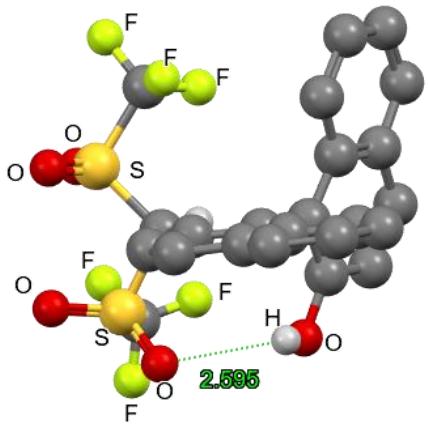

Figure 1-33: X-Ray structure of BBA **14**. An intramolecular hydrogen bond between the hydroxy group and the sulfonyl group can be expected.[85]

This modification resulted in a significantly stronger catalyst for organocatalysis. Remarkably, even in the absence of 3,3'-substituents, catalyst **14** was successfully employed in an enantioselective Mukaiyama-Mannich reaction (see Figure 1-34).[85]

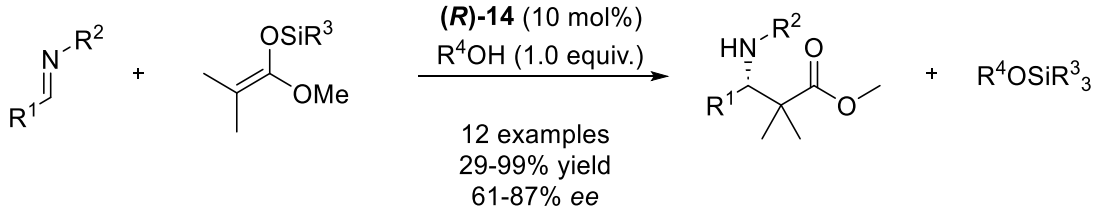

Figure 1-34: Successful application of BBA **14** in a Mukaiyama-Mannich reaction.[85]

It should be mentioned, that the reaction required the addition of a stoichiometric amount of an achiral proton source (R^4OH) to trap the silicon species formed during the process. Without this additive, the enantioselectivity dropped significantly, yielding only 14%.

To the best of our knowledge, BBAs were not further investigated.

1.1.5.3 Disulfonimides (DSIs) / Binaphthyl-2,2‘-bis(sulfon)amides (BINBAMs) 15

In 2009, the groups of List and Giernoth reported the syntheses of BINOL-based disulfonimide catalysts **15** (DSIs).[86,87] These catalysts are derived from BINSAs **13** through addition of thionylchloride with a catalytic amount of DMF and subsequent treatment with ammonia (see Figure 1-35).

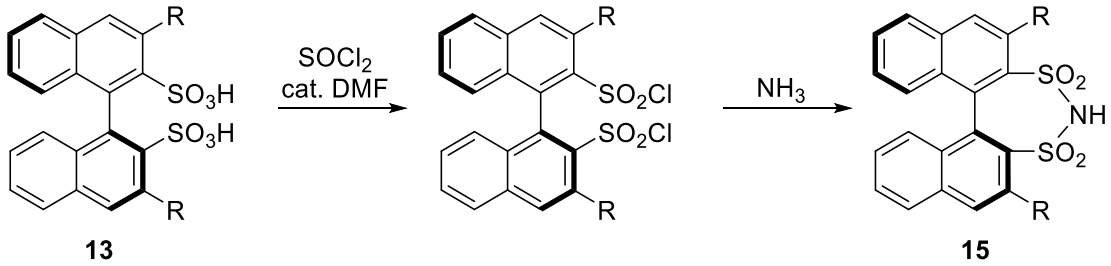

15a: R = H
15b: R = 3,5-$(CF_3)_2C_6H_3$
15c: R = phenyl
15d: R = 2-naphthyl
15e: R = 4-$CF_3C_6H_4$
15f: R = 4-CNC_6H_4
15g: R = 3,5-$F_2C_6H_3$
15h: R = 4-(1-naphthyl)C_6H_4
15i: R = 3-PhC_6H_4
15j: R = 1-naphthyl
15k: R = 3,5-$[CF(CF_3)_2]_2C_6H_3$
15l: R = 3,5-$[3,5\text{-}CF_3)_2C_6H_3]_2C_6H_3$
15m: R = 3,5-$(NO_2)_2$-4-$(CH_3)C_6H_2$
15n: R = 4-NO_2-C_6H_4
15o: R = 3,5-$[1\text{-}(3,7\text{-}(CF_3)_2)\text{-naphthyl})]_2C_6H_3$
15p: R = 3,5-$(C_6H_5)_2C_6H_3$
15q: R = 3,5-F_2-4-$CF_3C_6H_2$
15r: R = 1,3-$(CH_3)_2$-9-phenanthryl
15s: R = C-C-2-$CF_3C_6H_4$

Figure 1-35: DSIs/BINBAMs can be obtained by the treatment of BINSAs **13** with thionylchloride, a catalytic amount of DMF and subsequent addition of ammonia.[86,87]

Structurally, DSI catalysts exhibit perfect C_2-symmetry, unlike the “pseudo C_2-symmetry” of CPAs **1**. Furthermore, the proton-carrying functional group is positioned deeper within the chiral pocket compared to its placement in the corresponding CPA (see Figure 1-36).[87]

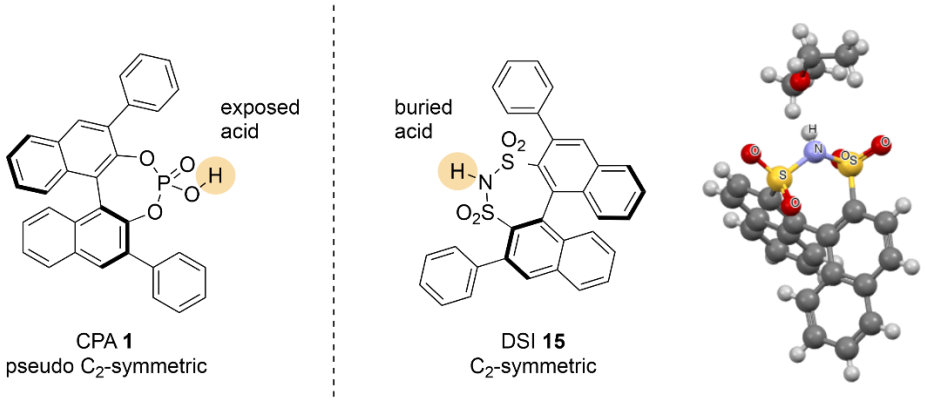

Figure 1-36: Structures and position of the acidic proton within the chiral pockets of CPA **1** and DSI **15**. The X-Ray structure of **15** shows the buried acidic proton.[87]

The modification of the active center introduces a multi-acceptor environment for hydrogen bonding. In-depth NMR studies and theoretical calculations conducted by the Gschwind group on DSI/imine complexes revealed that, in addition to the strong hydrogen bond acceptor (nitrogen), the four oxygen atoms also participate in hydrogen bonding. Notably, high structural flexibility does not conflict with the efficient performance of a catalytic system (see Figure 1-37).[88]

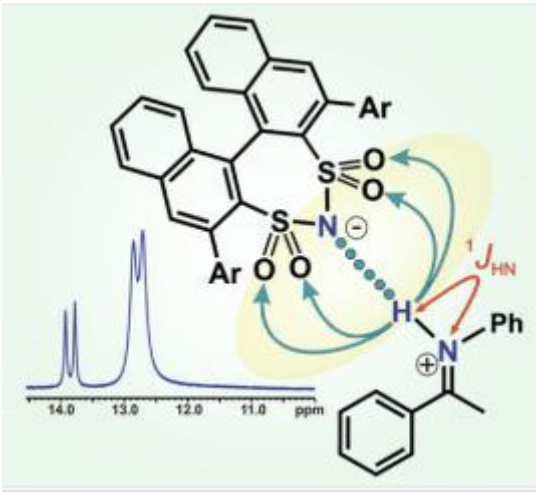

Figure 1-37: Multiple H-bond acceptors in DSI catalysts. The increased structural flexibility is not accompanied by a drop of the catalysts' performance.[88]

It was demonstrated, that DSI catalysts can efficiently catalyze Mukaiyama aldol reactions of aldehydes with simple (see Figure 1-38, A),[87] vinylogous (B),[89] bisvinylogous (C),[89] and alkynylogous (D)[90] silyl enol ethers.

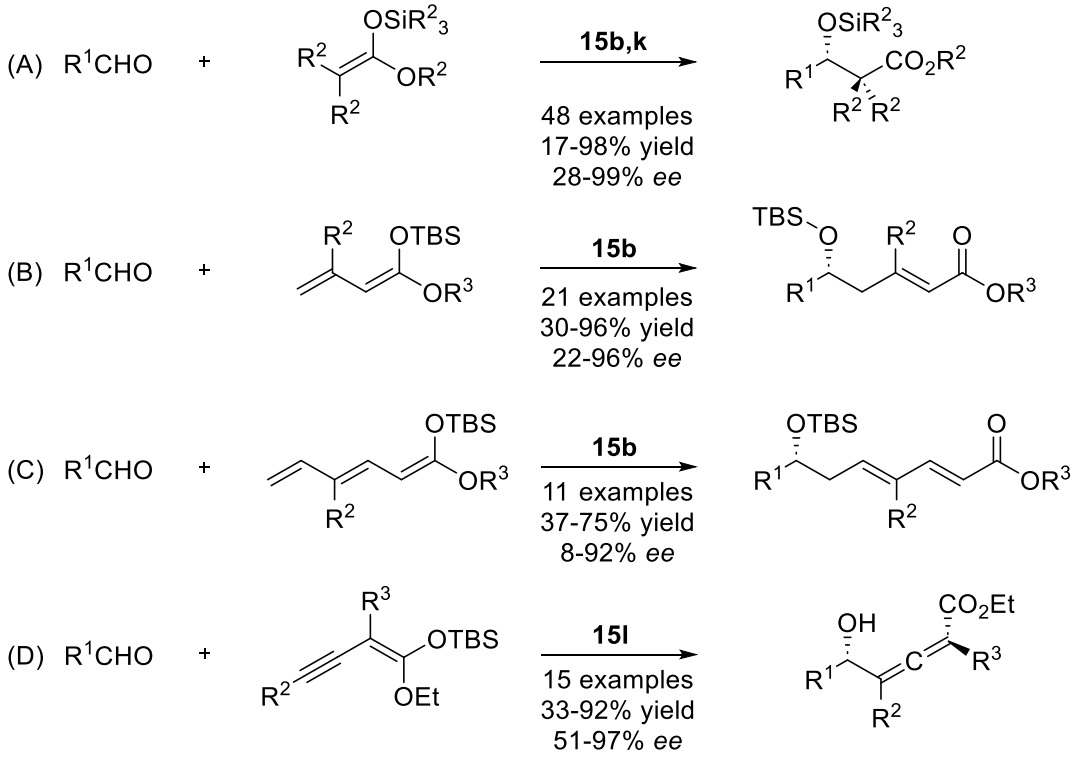

Figure 1-38: DSI-catalyzed Mukaiyama aldol reactions of simple (A),[87] vinylogous (B),[89] bisvinylogous (C)[89] and alkynylogous (D)[90] silyl enol ethers.

The List group also identified a suitable DSI catalyst, **15m**, for a Hosomi-Sakurai reaction, achieving high yields and enantioselectivities (see Figure 1-39, A).[91] A similar application was reported in 2013 involving a three-component-synthesis of an aldehyde, a carbamate and an allylsilane (see Figure 1-39, B).[92] In this case, it is assumed that the aldehyde and the carbamate form an iminium ion, which subsequently undergoes a Hosomi-Sakurai reaction.

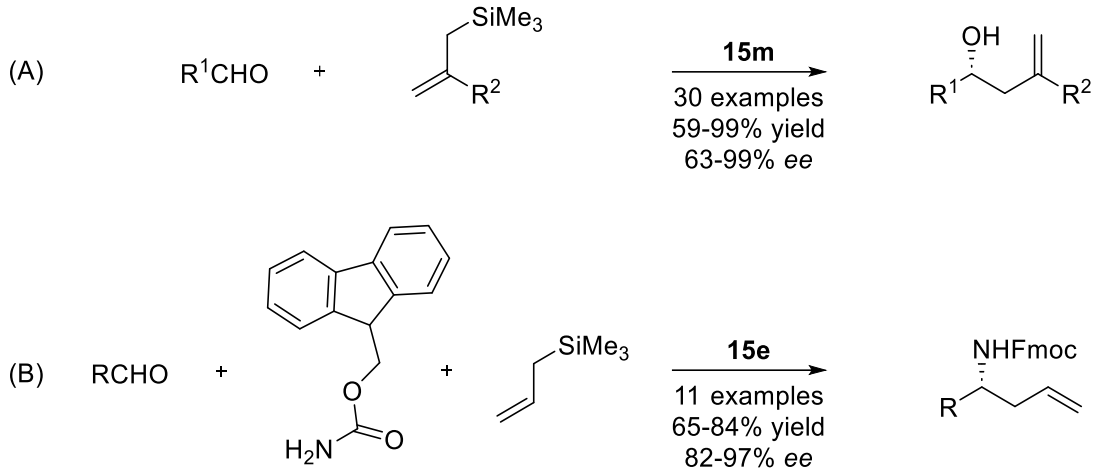

Figure 1-39: DSI-catalyzed Hosomi-Sakurai reactions (A)[91] and (B)[92].

In addition, DSIs were also successfully applied in Mannich[93,94] and Mukaiyama-Mannich[95] reactions (see Figure 1-40).

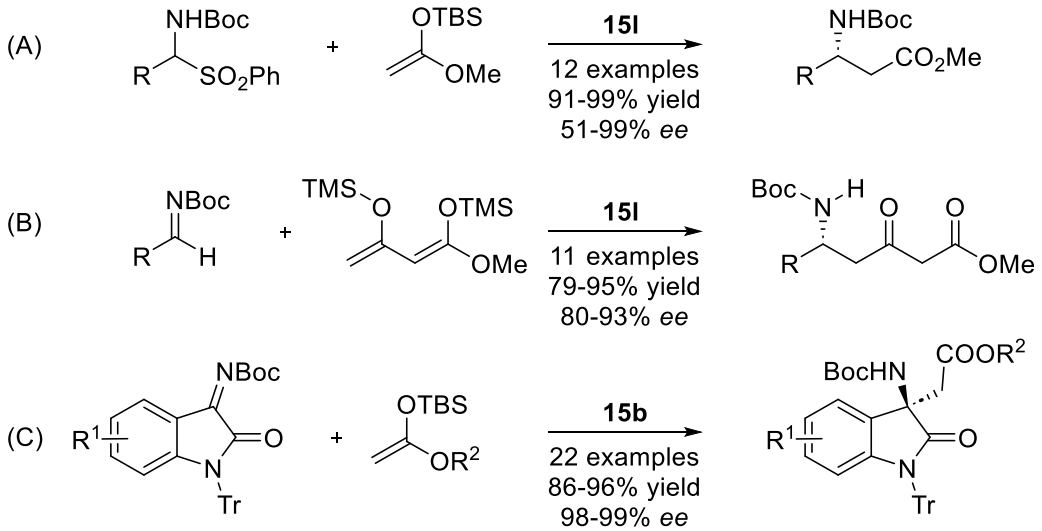

Figure 1-40: DSI-catalyzed Mannich (A,B)[93,94] and Mukaiyama-Mannich (C)[95] reactions.

Another application of DSIs in asymmetric organocatalysis was demonstrated when the groups of Lee[96] and Chen[97] employed DSI **15b** as a catalyst for Friedel-crafts reactions, enabling the substitution of indoles at the 2- and 3-positions (see Figure 1-41, A). It has been shown by Jia *et al.* that 1,3,5-trialkoxy benzenes can also undergo Friedel-crafts alkylation with *N*-sulfonyl aldimines (see Figure 1-41, B).[98]

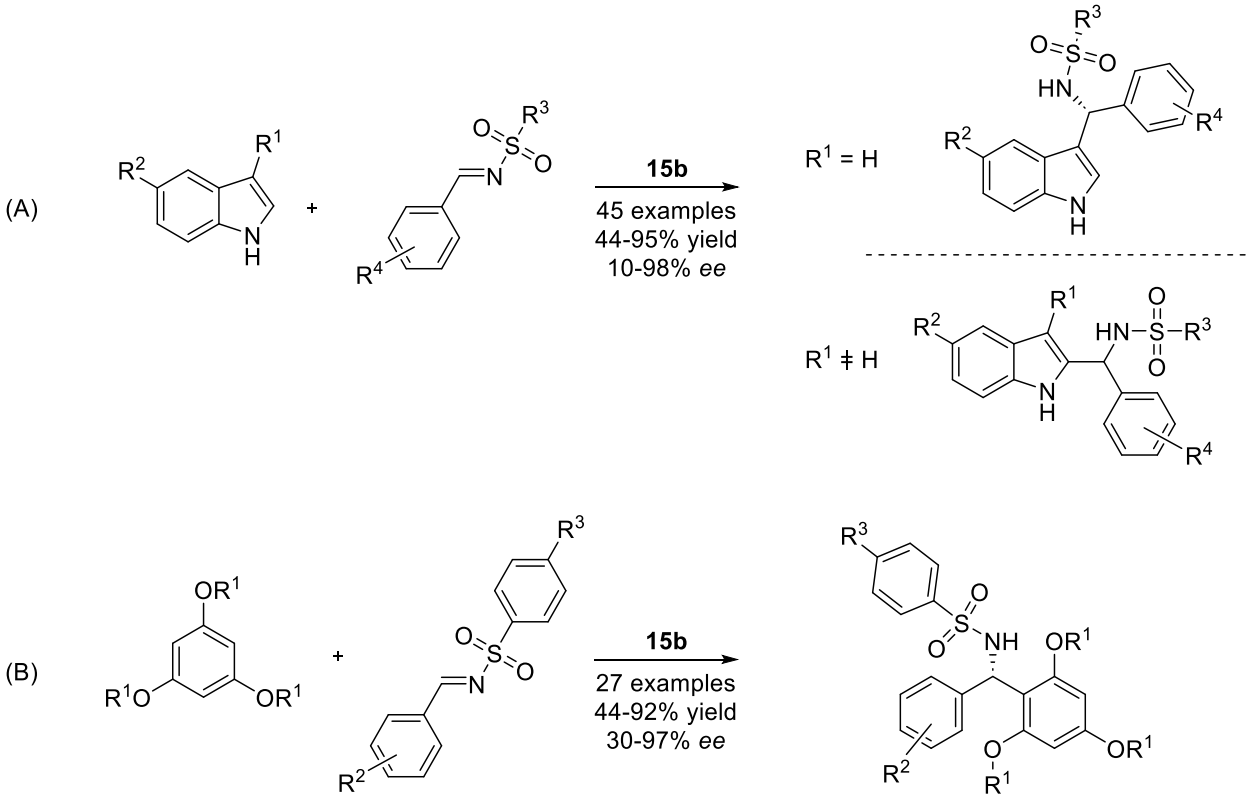

Figure 1-41: DSI-catalyzed Friedel-Crafts reactions of indoles (A)[96] and 1,3,5-trialkoxy benzenes (B)[98].

An additional implementation for DSI catalysts was found by the Sparr group in 2022, when they made Friedel-Crafts electrocyclization reactions of *ortho*-quinone methides to obtain the respective cyclic iminium ions (see Figure 1-42).[99]

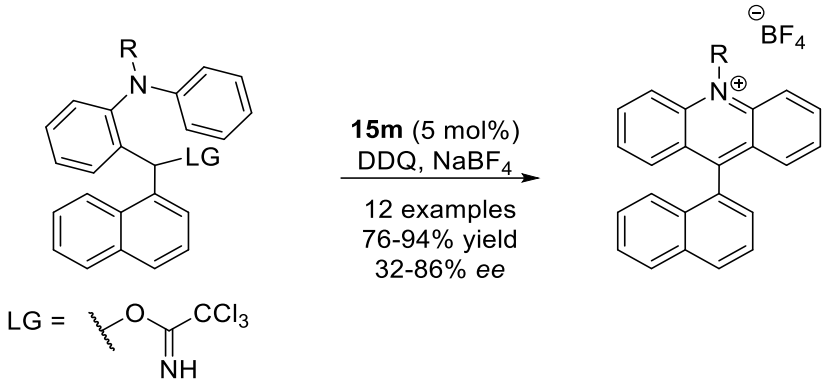

Figure 1-42: DSI-catalyzed Friedel-Crafts electrocyclization reaction.[99]

Chiral disulfonimides can also be employed for imine reductions such as asymmetric transfer hydrogenation reactions (see Figure 1-43, A).[100–102] Using this method, the List group synthesized a pharmacophore precursor for (*S*)-rivastigmine, a drug used to treat Alzheimer's disease, which they achieved with excellent enantioselectivity (99% *ee*).[100] Notably it has been shown, that also imine hydrochlorides can be reduced with this method (see Figure 1-43, B).[102] In addition it has been shown, that DSIs are capable of reductive ammonia condensation reactions, where two imines are coupled in a highly enantioselective way (C).[103]

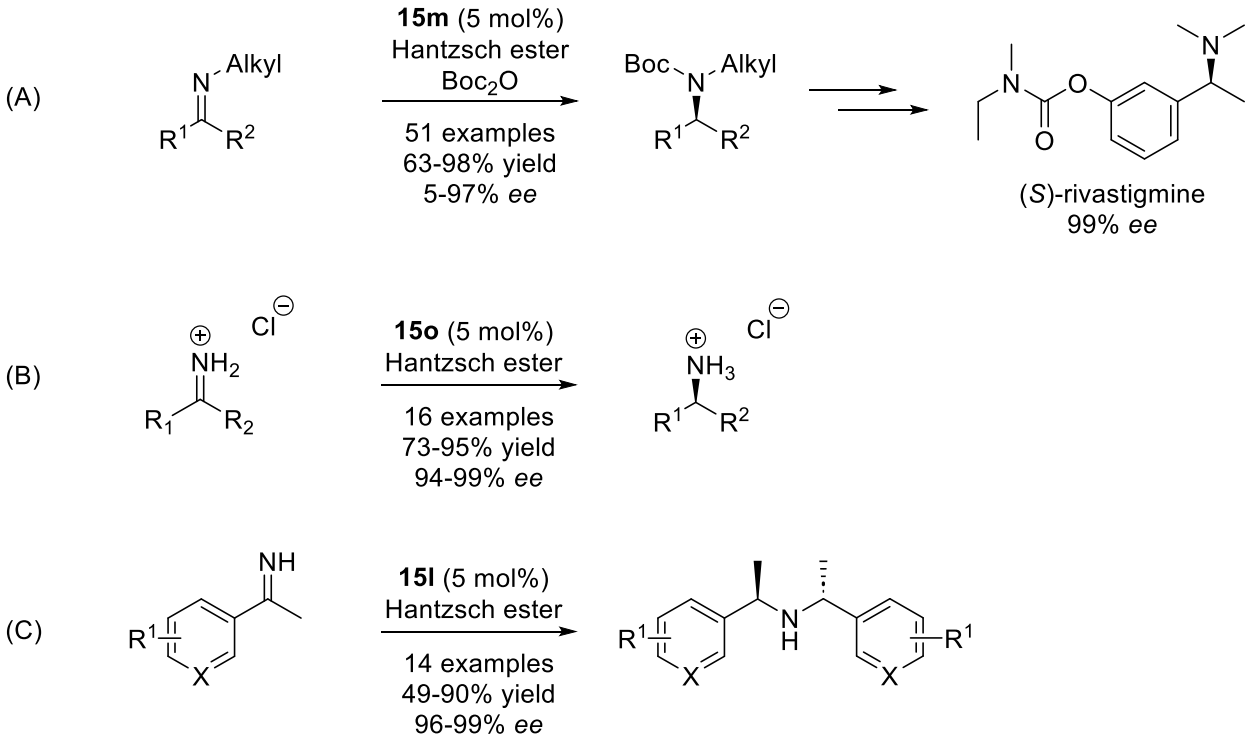

Figure 1-43: DSI-catalyzed ATH (A),[100–102] imine hydrochloride reduction (B)[102] and condensation reaction (C).[103]

In 2015, the List group reported a DSI-catalyzed asymmetric Abramov reaction where they coupled phosphites with aldehydes (see Figure 1-44).[104]

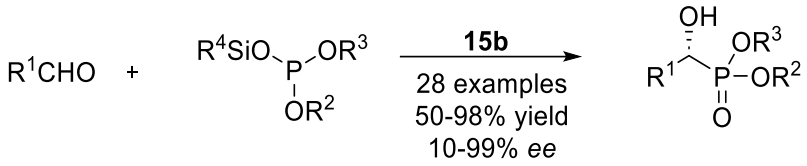

Figure 1-44: DSI-catalyzed asymmetric Abramov reaction.[104]

To date, there are a few publications about DSI-catalyzed cyclization reactions. In 2016, Galvan *et al.* synthesized pyrrolo-[1,2-*α*] indoles in a three-component reaction (see Figure 1-45, A).[105] In 2017, Li *et al.* synthesized isoquinolinonaphthyridines from tetrahydroisoquinolines and 2-methyl-3-aldehydeazaarenes (see Figure 1-45, B).[106] In 2020, Tan *et al.* synthesized enantioselective azirdines from anilines (C).[107] As shown by He *et al.* in 2021, DSI catalysts can also effectively catalyze Pictet-Spengler reactions (D).[108] In the same year, Takagi *et al.* performed reductive intramolecular hydroaminations with DSI catalysts (E).[109]

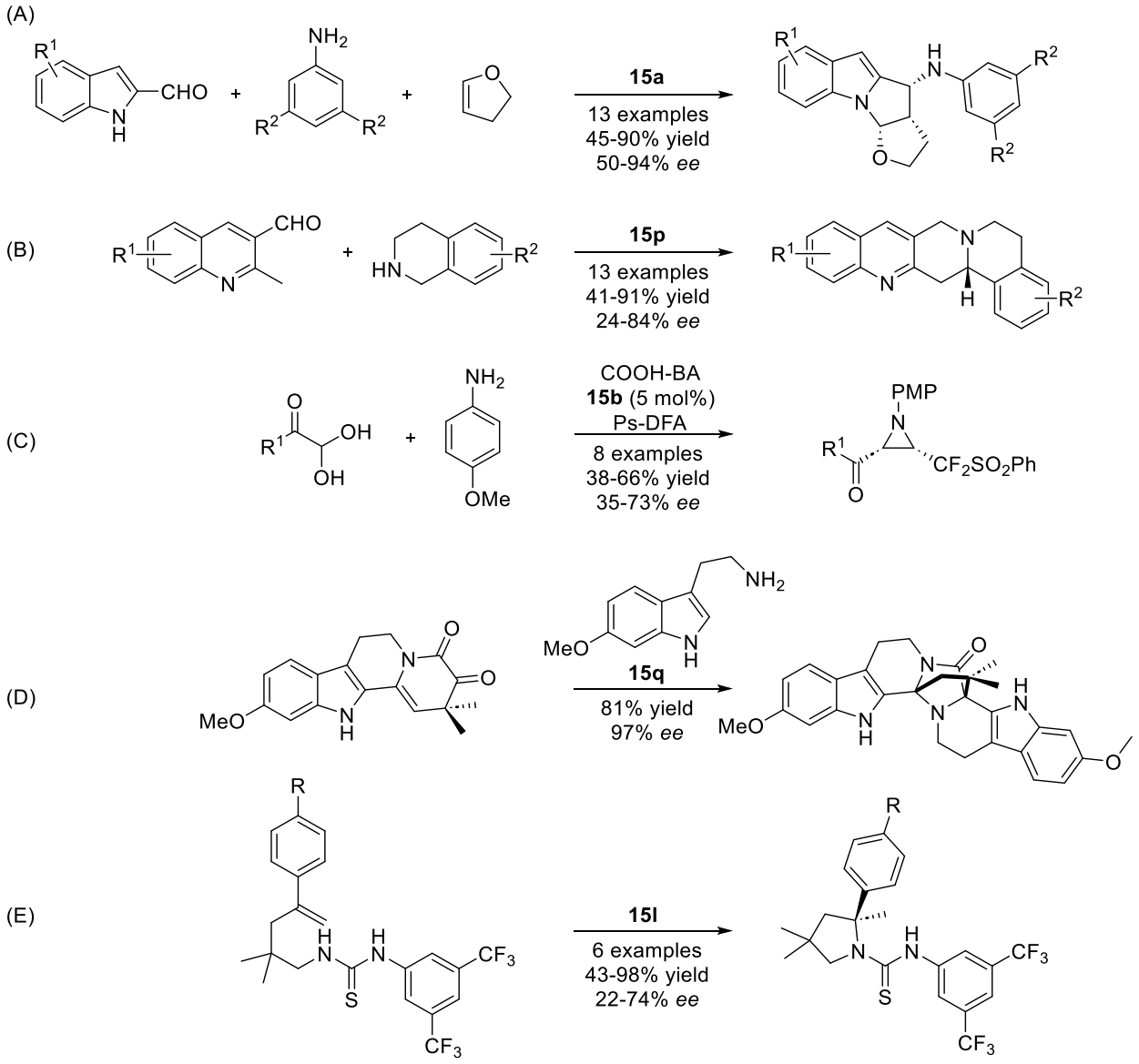

Figure 1-45: DSI-catalyzed cyclization reactions: Three-component coupling (A),[105] isoquinolinonaphthyridines synthesis (B),[106] aziridine synthesis (C),[107] Pictet-Spengler reaction (D),[108] intramolecular hydroaminations (E).[109]

Another significant finding of the List group was the DSI-catalyzed protodesilylation reaction, enabling the synthesis of drugs such as (*S*)-Ibuprofen with high enantioselectivity (see Figure 1-46).[110]

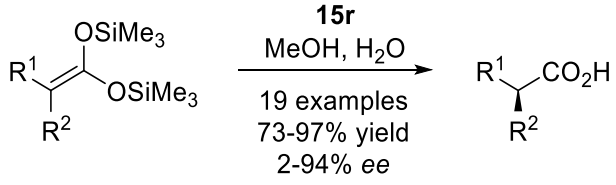

Figure 1-46: DSI-catalyzed protodesilylation reaction.[110]

Furthermore, Rose *et al.* discovered DSI-catalyzed iodination reactions of 2-amino-6-arylpyridines (see Figure 1-47).[111]

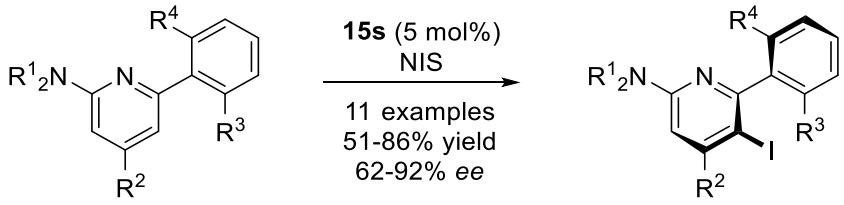

Figure 1-47: DSI-catalyzed iodination reaction.[111]

1.1.5.4 Binaphthyl-2,2‘-bis(sulfuryl)imides 16 (JINGLEs)

JINGLEs were first synthesized in 2010 when Berkessel *et al.* utilized imidobis(sulfuryl chloride) to convert BINOL sodium salts into **16** (see Figure 1-48).[112]

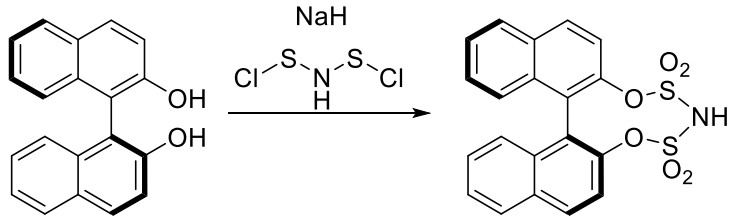

16

16a: R = H
16b: R = CH_3
16c: R = 2,4,6-$^{i}Pr_3C_6H_2$
16d: R = 1-naphthyl

Figure 1-48: Synthesis of JINGLEs **16** out of BINOL sodium salts and imidobis(sulfuryl chloride).[112]

It has been shown, that the acidity of **16** is comparable to DSI **15** and more acidic than NTPA **2**.[18,19]

The potential of JINGLEs in organocatalysis is mainly unexplored, however, in 2020, the Hodgson group utilized **16a** for the enantioselective desymmetrization of an achiral epoxide derived from an epoxytropinone (see Figure 1-49).[113]

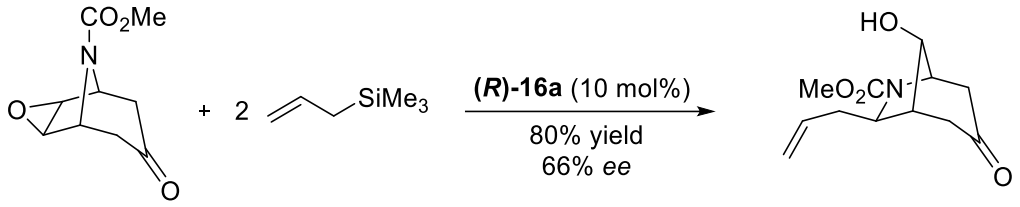

Figure 1-49: JINGLE-catalyzed desymmetrization of an achiral epoxide.[113]

Apart from this, JINGLEs were used for enantio-differentiation of chiral *O*-heterocycles or in Asymmetric Counteranion-Directed Catalysis (ACDC) in combination with a Lewis-acidic cation.[114,115]

1.1.5.5 Binaphthyl-2,2'-dicarboxylates 17 (BINCAs)

Binaphthyl-2,2'-dicarboxylates **17a-e** (BINCAs) can be synthesized through the 3,3'-substitution of commercially available unsubstituted **17** (see Figure 1-50).[116]

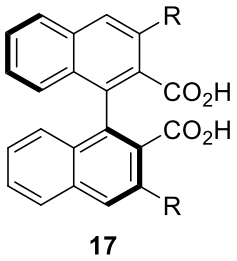

17

17a: R = 4-^{t}Bu-2,6-$(CH_3)_2C_6H_2$
17b: R = Ph
17c: R = 3,5-$(CF_3)_2C_6H_3$
17d: R = 4-^{t}BuC_6H_4
17e: R = 2,4,6-$(CH_3)_3C_6H_2$

Figure 1-50: Different 3,3'-substituents of BINCA **17**.[116]

Despite their relatively low pK_a of 3.97 in DMSO compared to DSI **15**, NTPA **2** or BINSA **13**,[80] BINCAs have been successfully applied to the asymmetric Mannich reaction of an arylaldehyde *N*-Boc imine with *tert*-butyl diazoacetate (see Figure 1-51, A.) or dimethyl diazomethylphosphonate (see Figure 1-51, B). Both reactions exhibited exceptionally high enantio-selectivity.[116]

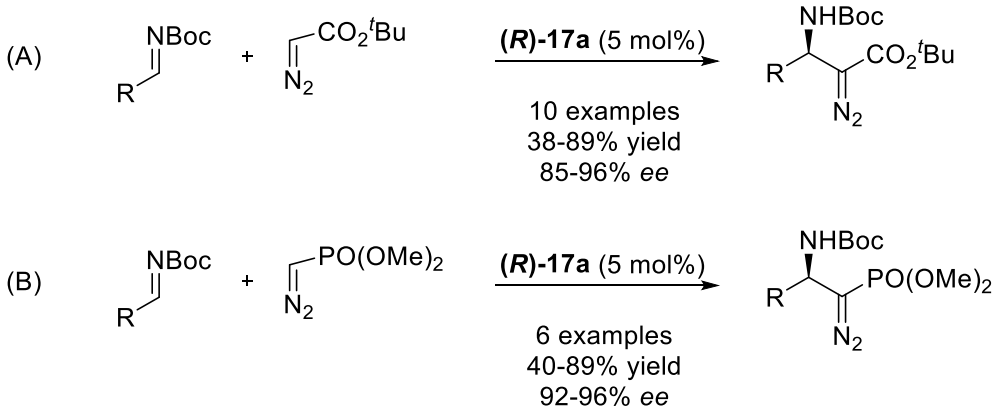

Figure 1-51: BINCA-catalyzed Mannich reactions of an arylaldehyde *N*-Boc imine with a diazoacetate (A) and a diazophosphonate (B).[116]

1.1.6 Development of Asymmetric Organocatalysis

Over the past two decades, numerous attempts have been made to enhance the acidity of Brønsted acid catalysts, particularly those derived from CPAs. To achieve this, a variety of substituents, such as NTf, sulfur, and selenium, have been incorporated. These modifications have enabled the activation of substrates that are more inert than imines. The most effective catalysts to date - NTPAs, DSIs, and IDPis - stand out due to their broad applicability, high yields, and high to excellent enantioselectivities.[27,28,66]

Yet, these catalysts either disrupt the favorable C_2-symmetry of the backbone or introduce multiple hydrogen bond acceptors, complicating substrate binding. This structural complexity increases the number of possible intermediates and transition states, necessitating detailed structural studies to elucidate their reaction mechanisms.[30,88]

An alternative approach is the substitution of oxygen in CPAs with heavier chalcogens, which would enhance the acidity while preserving the structural features of the BINOL backbone. Despite this, their potential in the context of asymmetric organocatalysis is largely unexplored to date.

1.2 Magnesium Cobaltate Complexes in Metal Catalysis

The investigation of low-valent transition metalate anions has attracted considerable interest due to their unique reactivity in synthesis, small molecule activation, and catalysis.[117] These anionic complexes, stabilized by ligands such as carbonyls, phosphines, and redox-active nitrogen donors, exhibit remarkable chemical properties that are strongly influenced by their surrounding environment. While extensive research has focused on their electronic structures and reactivity, the role of countercations in solution has emerged as an area of growing interest, as they have been shown to exert a significant influence.[118] Previous studies on a cobalt-magnesium complex demonstrated that its ion-pairing behavior is highly solvent-dependent: in toluene, it forms contact ion pairs, whereas in THF, it exists as solvent-separated ion pairs (see Figure 1-52, A.).[119] This pronounced difference in ion-pairing leads to substantial variations in reactivity, underscoring the critical role of counterions and solvation effects in determining catalytic performance. Despite these findings, the behavior and influence of countercations on the reactivity and stability of low-valent transition metalate anions are not yet fully understood, highlighting the need for further investigation in this field.

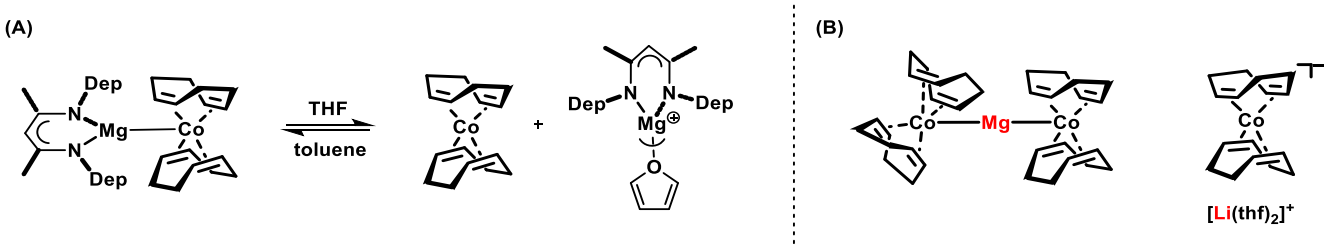

Figure 1-52: (A) Contact ion-pair of the magnesium cobaltate in toluene and solvent-separated ion-pair in THF.[119] (B) Investigated magnesium and lithium cobaltate complexes in this work (in toluene).

1.3 Outline

This thesis explores the design and structural analysis of catalysts for both asymmetric organocatalysis and metal catalysis.

On the one hand, a bifurcated approach combining synthesis and structural analysis is employed to iteratively refine the understanding, efficiency and selectivity of DSA catalyst synthesis. By systematically optimizing the reaction conditions, conversions, yields, and product purity are improved. This process is complemented by reactivity studies to evaluate catalytic performance. Another key focus is the investigation of substrate binding and catalyst aggregation, which is studied through a combination of X-ray crystallography, computational chemistry, and 1D NMR techniques. The latter includes satellite analysis to gain deeper insights into molecular interactions and structural dynamics. Together, these methods provide a comprehensive understanding of the structural and functional properties of DSA catalysts, aiding their rational design and future applications. Furthermore, a successful enantioselective application of a DSA catalyst in asymmetric ion pair catalysis is part of the scope of this work.

On the other hand, cobaltate-based catalysts for alkene hydrogenation were examined with a focus on their ionic environment, as their reactivity and selectivity are strongly influenced by their ion-pairing behavior.[117–119] To gain deeper insights into this aspect, Diffusion Ordered Spectroscopy (DOSY) for ^{1}H and ^{7}Li was employed to analyze the interactions between the metalate anion and its countercation in solution. These measurements revealed that these complexes predominantly form contact ion pairs, indicating that the counterion remains closely associated rather than fully dissociating into the solvent. This finding suggests that counterions play a more direct role in modulating the catalytic performance of these systems than previously assumed. A thorough understanding of this effect not only enhances our knowledge of the underlying reaction mechanisms but also provides a foundation for optimizing catalytic activity through strategic counterion selection.

Chapter 2 outlines the initial development of DSA synthesis. As a model system, unsubstituted and commercially available (*R*)-BINOL was selected and subjected to a reaction with phosphorus selenide. Previous reports had indicated that the reaction of simple alcohols with P_2Se_5 led to the formation of non-isolable and unstable achiral acids.[120] Phosphorus selenide ("P_2Se_5") itself is a polymeric reagent that was found to be non-storable and nearly insoluble in common organic solvents, posing challenges for its use in synthesis. To address this, different

preparation methods for both P_2Se_5 and P_4Se_3 - a molecular reagent with improved handling properties - were explored. Reaction progress and conversions were monitored via ^{1}H NMR, employing DMSO quenching to oxidize the products for better analytical resolution. Once conversion optimization was achieved, selectivity was assessed using ^{31}P and $\{^1H\}^{31}$P NMR spectroscopy. This analysis focused on chemical shifts, $^1J_{PSe}$, $^2J_{PP}$, and $^1J_{PH}$ spin-spin couplings, as well as the integral ratios of the ^{31}P-^{xx}Se ($xx \neq 77$) parent line to the ^{31}P-^{77}Se satellite signals. These investigations revealed that the catalyst synthesis required an *in situ* oxidative selenation step, which was found to proceed incompletely under standard conditions. A test reaction with externally introduced hydrogen selenide gas confirmed the necessity of this step.

To overcome this limitation, the synthesis was modified to enhance the reactivity of BINOL by first converting it into potassium BINOLate, followed by treatment with phosphorus selenide. This adaptation led to complete conversion of the starting material and significantly improved selectivity. The resulting potassium DSA salt (DSA-K) was found to be storable and could be easily transformed into DSA upon hydrogen chloride addition. However, due to its high reactivity, the free acid exhibited a strong tendency toward oxidation and hydrolysis.

Despite these stability concerns, the synthesized catalyst effectively activated substrates that CPA catalysts were unable to. Furthermore, it was demonstrated that the P=Se moiety exhibited enhanced Lewis basicity, enabling the formation of ion pairs with protonated THF. Even $^2J_{PH}$ coupling constants could be determined, highlighting the stability of these ion pairs. These experimental results were further validated by quantum chemical calculations. This research confirmed that replacing oxygen in CPAs with selenium not only increased Brønsted acidity but also significantly enhanced Lewis basicity.

Chapter 3 explores the incorporation of 3,3’-substituents into DSAs, as these are expected to significantly influence the structure of the catalysts' active center, thereby enabling enantioselective transformations. However, initial attempts revealed that 3,3’-substituted potassium BINOLates exhibited insufficient reactivity toward phosphorus selenide, necessitating the development of an alternative synthetic strategy. It was found that 3,3’-substituted BINOLs could be efficiently converted into phosphoroselenoyl chlorides, which, upon subsequent treatment with two equivalents of potassium selenide, yielded the corresponding DSA-K salts. Notably, when only one equivalent of potassium selenide was used,

a dimeric byproduct formed due to a reaction between the in situ generated DSA-K and the phosphoroselenoyl chloride precurso

Following optimization of the reaction conditions, four different 3,3'-substituted DSA-K derivatives - excluding hydrogen - were successfully synthesized. Moreover, it was demonstrated that this methodology extends beyond BINOL-based systems, as other diols, such as VANOL, could also be functionalized in the same manner. To assess the catalytic potential of these newly synthesized compounds, DSA-TRIP was tested in an asymmetric transfer hydrogenation reaction. The results revealed that the presence of potassium ions in the reaction mixture (introduced as potassium chloride) significantly reduced enantioselectivity. This effect was attributed to salt metathesis, which led to the disruption of the DSA-valine ester catalyst. Consequently, potassium had to be thoroughly removed from the reaction mixture, either by filtration or through complexation. Despite these challenges, a 3,3'-substituted DSA catalyst was successfully applied in asymmetric organocatalysis, demonstrating the feasibility of structural modifications for enhanced performance.

Chapter 4 provides an in-depth exploration of the Wolf group's study on the trinuclear magnesium cobaltate salt, $Mg[Co(\eta^4\text{-cod})_2]_2$ (where cod refers to 1,5-cyclooctadiene), which features a linear Co-Mg-Co arrangement. This compound's potential as a catalyst in alkene hydrogenation reactions is thoroughly examined. Previous studies have demonstrated the significant influence of counterions on the reactivity of metal cobaltate catalysts, with magnesium (Mg) showing superior performance compared to alkali metals.[118] This has positioned magnesium-based cobaltates as particularly promising candidates for catalytic applications. In this investigation, the reactivity and ionic structure of the complex were studied using Diffusion Ordered Spectroscopy (DOSY) NMR, specifically ^1H and ^7Li NMR, to measure the diffusion coefficients and hydrodynamic volumes of both $Mg[Co(\eta^4\text{-cod})_2]_2$ and $[Li(THF)_{1.92}][Co(\eta^4\text{-cod})_2]$. The results indicated that the magnesium cobaltate catalyst exists as a contact ion-pair in solution. This characteristic was shown to be particularly advantageous, as the catalyst's behavior in hydrogenation reactions confirmed its effectiveness. The Wolf group's findings highlight the critical role that ion-pairing behavior plays in optimizing catalytic performance, demonstrating that Mg-based cobaltate catalysts can be highly effective in hydrogenation processes.

1.4 References

[1] R. E. Oesper, *J Chem Educ* **1948**, *25*, 531–532.

[2] A. Mittasch, *Eur J Inorg Chem* **1926**, *59*, 13–36.

[3] M. A. Sutton, D. Simpson, P. E. Levy, R. I. Smith, S. Reis, M. van Oijen, W. de Vries, *Glob Chang Biol* **2008**, *14*, 2057–2063.

[4] R. Noyori, *Angewandte Chemie - International Edition* **2002**, *41*, 2008–2022.

[5] G. Guillena, C. Nájera, D. J. Ramón, *Tetrahedron Asymmetry* **2007**, *18*, 2249–2293.

[6] D. S. Su, J. Zhang, B. Frank, A. Thomas, X. Wang, J. Paraknowitsch, R. Schlögl, *ChemSusChem* **2010**, *3*, 169–180.

[7] B. List, R. A. Lerner, C. F. Barbas, *J Am Chem Soc* **2000**, *122*, 2395–2396.

[8] K. A. Ahrendt, C. J. Borths, D. W. C. MacMillan, *J Am Chem Soc* **2000**, *122*, 4243–4244.

[9] T. Akiyama, J. Itoh, K. Yokota, K. Fuchibe, *Angewandte Chemie - International Edition* **2004**, *43*, 1566–1568.

[10] D. Uraguchi, M. Terada, *J Am Chem Soc* **2004**, *126*, 5356–5357.

[11] D. Parmar, E. Sugiono, S. Raja, M. Rueping, *Chem Rev* **2014**, *114*, 9047–9153.

[12] X. F. Cai, R. N. Guo, G. S. Feng, B. Wu, Y. G. Zhou, *Org Lett* **2014**, *16*, 2680–2683.

[13] J. Liu, Y. Y. Du, Y. S. He, Y. Liang, S. Z. Liu, Y. Y. Li, Y. M. Cao, *Chem Sci* **2023**, *14*, 12152–12159.

[14] T. Akiyama, J. Itoh, K. Yokota, K. Fuchibe, *Angewandte Chemie - International Edition* **2004**, *43*, 1566–1568.

[15] D. Uraguchi, M. Terada, *J Am Chem Soc* **2004**, *126*, 5356–5357.

[16] L. Ackermann, A. Althammer, *Synlett* **2008**, 995–998.

[17] H. C. Cheol, H. Yamamoto, *J Am Chem Soc* **2008**, *130*, 9246–9247.

[18] P. Christ, A. G. Lindsay, S. S. Vormittag, J. M. Neudörfl, A. Berkessel, A. C. O'Donoghue, *Chemistry - A European Journal* **2011**, *17*, 8524–8528.

[19] K. Kaupmees, N. Tolstoluzhsky, S. Raja, M. Rueping, I. Leito, *Angewandte Chemie - International Edition* **2013**, *52*, 11569–11572.

[20] Z. Zhang, H. Y. Bae, J. Guin, C. Rabalakos, M. Van Gemmeren, M. Leutzsch, M. Klussmann, B. List, *Nat Commun* **2016**, *7*, DOI 10.1038/ncomms12478.

[21] D. Nakashima, H. Yamamoto, *J Am Chem Soc* **2006**, *128*, 9626–9627.

[22] M. Zeng, W. Zhang, S. You, *Chin J Chem* **2012**, *30*, 2615–2623.

[23] S. G. Wang, L. Han, M. Zeng, F. L. Sun, W. Zhang, S. L. You, *Org Biomol Chem* **2012**, *10*, 3202–3209.

[24] M. Rueping, B. J. Nachtsheim, S. A. Moreth, M. Bolte, *Angewandte Chemie - International Edition* **2008**, *47*, 593–596.

[25] A. Borovika, P. Nagorny, *Tetrahedron* **2013**, *69*, 5719–5725.

[26] L. Simón, J. M. Goodman, *J Am Chem Soc* **2008**, *130*, 8741–8747.

[27] M. Rueping, B. J. Nachtsheim, W. Ieawsuwan, I. Atodiresei, *Angewandte Chemie - International Edition* **2011**, *50*, 6706–6720.

[28] G. Caballero-García, J. M. Goodman, *Org Biomol Chem* **2021**, *19*, 9565–9618.

[29] E. M. Sherbrook, M. J. Genzink, B. Park, I. A. Guzei, M. H. Baik, T. P. Yoon, *Nat Commun* **2021**, *12*, DOI 10.1038/s41467-021-25878-9.

[30] M. Hecht, P. Dullinger, W. Silva, D. Horinek, R. M. Gschwind, *Chem Sci* **2024**, *15*, 9104–9111.

[31] X. Wu, D. Ding, Y. Zhang, H. J. Jiang, T. Wang, L. P. Zhao, *Chemical Communications* **2021**, *57*, 9680–9683.

[32] X. Q. Zhu, H. Y. Yang, L. W. Ye, *Chemistry - A European Journal* **2024**, *30*, e202402247.

[33] B. Peng, J. Ma, J. Guo, Y. Gong, R. Wang, Y. Zhang, J. Zeng, W. W. Chen, K. Ding, B. Zhao, *J Am Chem Soc* **2022**, *144*, 2853–2860.

[34] M. T. Robak, M. Trincado, J. A. Ellman, *J Am Chem Soc* **2007**, *129*, 15110–15111.

[35] A. G. Doyle, E. N. Jacobsen, *Chem Rev* **2007**, *107*, 5713–5743.

[36] M. I. Kabachnik, T. A. Mastrukova, A. E. Ship~v, T. A. Melen~yeva, *10 to 28. Pergamon Reu Ltd*, **1960**.

[37] K. R. Winters, J. L. Montchamp, *Beilstein Journal of Organic Chemistry* **2022**, *18*, 1471–1478.

[38] S. Kato, Y. Saga, M. Kojima, H. Fuse, S. Matsunaga, A. Fukatsu, M. Kondo, S. Masaoka, M. Kanai, *J Am Chem Soc* **2017**, *139*, 2204–2207.

[39] F. Zhou, H. Yamamoto, *Angewandte Chemie - International Edition* **2016**, *55*, 8970–8974.

[40] S. E. Denmark, M. T. Burk, *Org Lett* **2012**, *14*, 256–259.

[41] Y. Xie, Y. Zhao, B. Qian, L. Yang, C. Xia, H. Huang, *Angewandte Chemie - International Edition* **2011**, *50*, 5682–5686.

[42] X. L. Jiang, S. F. Wu, J. R. Wang, G. J. Mei, F. Shi, *Adv Synth Catal* **2018**, *360*, 4225–4235.

[43] F. T. Sheng, S. Yang, S. F. Wu, Y. C. Zhang, F. Shi, *Chin J Chem* **2022**, *40*, 2151–2160.

[44] W. Xu, J. Ma, X. Yuan, J. Dai, J. Xie, C. Zhu, *Angewandte Chemie* **2018**, *130*, 10514–10518.

[45] T. Murai, in *Phosphorus Sulfur Silicon Relat Elem*, **2008**, pp. 889–896.

[46] C. Yang, X. S. Xue, J. L. Jin, X. Li, J. P. Cheng, *Journal of Organic Chemistry* **2013**, *78*, 7076–7085.

[47] T. Murai, M. Monzaki, T. Katoh, T. Suzuki, T. Akiyama, *Phosphorus Sulfur Silicon Relat Elem* **2010**, *185*, 964–973.

[48] S. Hoffmann, A. M. Seayad, B. List, *Angewandte Chemie - International Edition* **2005**, *44*, 7424–7427.

[49] I. Čorić, B. List, *Nature* **2012**, *483*, 315–319.

[50] Y. Y. Chen, Y. J. Jiang, Y. Sen Fan, D. Sha, Q. Wang, G. Zhang, L. Zheng, S. Zhang, *Tetrahedron Asymmetry* **2012**, *23*, 904–909.

[51] D. Parmar, E. Sugiono, S. Raja, M. Rueping, *Chem Rev* **2014**, *114*, 9047–9153.

[52] K. Wu, Y. J. Jiang, Y. Sen Fan, D. Sha, S. Zhang, *Chemistry - A European Journal* **2013**, *19*, 474–478.

[53] M. H. Zhuo, Y. J. Jiang, Y. Sen Fan, Y. Gao, S. Liu, S. Zhang, *Org Lett* **2014**, *16*, 1096–1099.

[54] J. H. Kim, I. Čorič, S. Vellalath, B. List, *Angewandte Chemie - International Edition* **2013**, *52*, 4474–4477.

[55] G. Jindal, R. B. Sunoj, *Angewandte Chemie - International Edition* **2014**, *53*, 4432–4436.

[56] J. B. Gualtierotti, D. Pasche, Q. Wang, J. Zhu, *Angewandte Chemie - International Edition* **2014**, *53*, 9926–9930.

[57] N. D. Shapiro, V. Rauniyar, G. L. Hamilton, J. Wu, F. D. Toste, *Nature* **2011**, *470*, 245–250.

[58] D. Fabbri, G. Delogu, O. De Lucchi, *Thiopbosphonates of l,l'-Binaphthol as Cbiral Equivalents of I&S. Preparation of 2-Mercaptonorbornanes and 2-Mercaptonorbornenes*, **1993**.

[59] J. Eder, A. S. Antonov, E. Y. Tupikina, R. M. Gschwind, *Chemistry - A European Journal* **2024**, *30*, e202401793.

[60] C. H. Cheon, H. Yamamoto, *Org Lett* **2010**, *12*, 2476–2479.

[61] P. S. J. Kaib, B. List, *Synlett* **2016**, *27*, 156–158.

[62] S. Lee, P. S. J. Kaib, B. List, *Synlett* **2017**, *28*, 1478–1480.

[63] X. Zhang, P. Sun, Y. Jiang, S. Liao, *Chem Asian J* **2023**, *18*, e202201127.

[64] X. Zhang, Z. Yang, Y. Jiang, S. Liao, *J Am Chem Soc* **2022**, *144*, 679–684.

[65] P. S. J. Kaib, L. Schreyer, S. Lee, R. Properzi, B. List, *Angewandte Chemie* **2016**, *128*, 13394–13397.

[66] L. Schreyer, R. Properzi, B. List, *Angewandte Chemie* **2019**, *131*, 12891–12908.

[67] R. Maji, S. Ghosh, O. Grossmann, P. Zhang, M. Leutzsch, N. Tsuji, B. List, *J Am Chem Soc* **2023**, *145*, 8788–8793.

[68] H. Zhu, Y. Jiang, Z. Yang, X. Zhang, S. Liao, *Giant* **2023**, *14*, DOI 10.1016/j.giant.2023.100151.

[69] Y. Liao, X. Yan, H. Zhu, S. Zhou, S. Liao, *Chemistry - A European Journal* **2024**, DOI 10.1002/chem.202403170.

[70] Y. Zhou, Y. Sun, Y. Zhang, M. Hong, *Macromolecules* **2024**, *57*, 7227–7236.

[71] H. Zhou, R. Properzi, M. Leutzsch, P. Belanzoni, G. Bistoni, N. Tsuji, J. T. Han, C. Zhu, B. List, *J Am Chem Soc* **2023**, *145*, 4994–5000.

[72] H. Zhou, H. Y. Bae, M. Leutzsch, J. L. Kennemur, D. Bécart, B. List, *J Am Chem Soc* **2020**, *142*, 13695–13700.

[73] M. Zhu, H. J. Jiang, I. Sharanov, E. Irran, M. Oestreich, *Angewandte Chemie - International Edition* **2023**, *62*, e202304475.

[74] J. T. Han, H. Zhou, B. List, *Synlett* **2023**, *34*, 2393–2395.

[75] H. Y. Bae, D. Höfler, P. S. J. Kaib, P. Kasaplar, C. K. De, A. Döhring, S. Lee, K. Kaupmees, I. Leito, B. List, *Nat Chem* **2018**, *10*, 888–894.

[76] S. Lee, P. S. J. Kaib, B. List, *J Am Chem Soc* **2017**, *139*, 2156–2159.

[77] B. W. L F Armarego, E. E. Turner, *Diaryl-2 : 2'-Disulfihmic Acids*, **n.d.**

[78] B. Harry James Barber, S. Smiles, *CYCLIC DISULPHIDES DERIVED FROM DIPHENYL. CXLV.-Cyclic Disulphides Derived from Diphenyl*, **n.d.**

[79] M. Hatano, T. Maki, K. Moriyama, M. Arinobe, K. Ishihara, *J Am Chem Soc* **2008**, *130*, 16858–16860.

[80] C. Yang, X. S. Xue, X. Li, J. P. Cheng, *Journal of Organic Chemistry* **2014**, *79*, 4340–4351.

[81] M. Hatano, K. Ishihara, *Asian J Org Chem* **2014**, *3*, 352–365.

[82] M. Hatano, K. Nishikawa, K. Ishihara, *J Am Chem Soc* **2017**, *139*, 8424–8427.

[83] W. Bin Xie, Z. Li, *ACS Catal* **2021**, *11*, 6270–6275.

[84] M. Hatano, X. Zhao, T. Mochizuki, K. Maeda, K. Motokura, K. Ishihara, *Asian J Org Chem* **2021**, *10*, 360–365.

[85] A. Hasegawa, Y. Naganawa, M. Fushimi, K. Ishihara, H. Yamamoto, *Org Lett* **2006**, *8*, 3175–3178.

[86] M. Treskow, J. Neudörfl, R. Giernoth, *European J Org Chem* **2009**, 3693–3697.

[87] P. García-García, F. Lay, P. García-García, C. Rabalakos, B. List, *Angewandte Chemie* **2009**, *121*, 4427–4430.

[88] K. Rothermel, M. Žabka, J. Hioe, R. M. Gschwind, *Journal of Organic Chemistry* **2019**, *84*, 13221–13231.

[89] L. Ratjen, P. García-García, F. Lay, M. E. Beck, B. List, *Angewandte Chemie - International Edition* **2011**, *50*, 754–758.

[90] A. Tap, A. Blond, V. N. Wakchaure, B. List, *Angewandte Chemie* **2016**, *128*, 9108–9111.

[91] M. Mahlau, P. García-García, B. List, *Chemistry - A European Journal* **2012**, *18*, 16283–16287.

[92] S. Gandhi, B. List, *Angewandte Chemie - International Edition* **2013**, *52*, 2573–2576.

[93] Q. Wang, M. Leutzsch, M. Van Gemmeren, B. List, *J Am Chem Soc* **2013**, *135*, 15334–15337.

[94] Q. Wang, B. List, *Synlett* **2015**, *26*, 807–809.

[95] S. Hajra, S. Laskar, B. Jana, *Chemistry - A European Journal* **2019**, *25*, 14688–14693.

[96] L. Y. Chen, H. He, W. H. Chan, A. W. M. Lee, *Journal of Organic Chemistry* **2011**, *76*, 7141–7147.

[97] P. Sun, Z. H. Jia, L. Tang, H. Zheng, Z. R. Li, L. Y. Chen, Y. Li, *Org Biomol Chem* **2022**, *20*, 1916–1925.

[98] Z. H. Jia, L. Y. Chen, H. Zheng, Z. R. Li, Q. C. Song, Y. Li, *Journal of Organic Chemistry* **2023**, *88*, 9720–9729.

[99] X. Wu, C. Sparr, *Angewandte Chemie - International Edition* **2022**, *61*, e202201424.

[100] V. N. Wakchaure, P. S. J. Kaib, M. Leutzsch, B. List, *Angewandte Chemie* **2015**, *127*, 12019–12023.

[101] J. Mazuela, T. Antonsson, M. J. Johansson, L. Knerr, S. P. Marsden, *Org Lett* **2017**, *19*, 5541–5544.

[102] V. N. Wakchaure, C. Obradors, B. List, *Synlett* **2020**, *31*, 1707–1712.

[103] V. N. Wakchaure, B. List, *Angewandte Chemie* **2016**, *128*, 16007–16010.

[104] J. Guin, Q. Wang, M. Van Gemmeren, B. List, *Angewandte Chemie - International Edition* **2015**, *54*, 355–358.

[105] A. Galván, A. B. González-Pérez, R. Álvarez, A. R. de Lera, F. J. Fañanás, F. Rodríguez, *Angewandte Chemie* **2016**, *128*, 3489–3493.

[106] J. Li, Y. Fu, C. Qin, Y. Yu, H. Li, W. Wang, *Org Biomol Chem* **2017**, *15*, 6474–6477.

[107] X. F. Tan, F. G. Zhang, J. A. Ma, *Beilstein Journal of Organic Chemistry* **2020**, *16*, 638–644.

[108] G. He, B. List, M. Christmann, **2021**, DOI 10.26434/chemrxiv.14054558.v1.

[109] R. Takagi, D. T. Duong, T. Ichiki, *Tetrahedron* **2021**, *94*, DOI 10.1016/j.tet.2021.132332.

[110] F. Mandrelli, A. Blond, T. James, H. Kim, B. List, *Angewandte Chemie* **2019**, *131*, 11603–11606.

[111] B. T. Rose, J. C. Timmerman, S. A. Bawel, S. Chin, H. Zhang, S. E. Denmark, *J Am Chem Soc* **2022**, *144*, 22950–22964.

[112] A. Berkessel, P. Christ, N. Leconte, J. M. Neudörfl, M. Schäfer, *European J Org Chem* **2010**, 5165–5170.

[113] R. E. Shelton, S. Sezer, D. M. Hodgson, *Tetrahedron* **2020**, *76*, DOI 10.1016/j.tet.2020.131701.

[114] S. Ni, V. Ramesh Naidu, J. Franzén, *European J Org Chem* **2016**, *2016*, 1708–1713.

[115] A. Couffin, O. Thillaye du Boullay, M. Vedrenne, C. Navarro, B. Martin-Vaca, D. Bourissou, *Chemical Communications* **2014**, *50*, 5997–6000.

[116] T. Hashimoto, K. Maruoka, *J Am Chem Soc* **2007**, *129*, 10054–10055.

[117] V. R. Landaeta, T. M. Horsley Downie, R. Wolf, *Chem Rev* **2024**, *124*, 1323–1463.

[118] M. Gawron, F. Gilch, D. Schmidhuber, J. A. Kelly, T. M. Horsley Downie, A. Jacobi von Wangelin, J. Rehbein, R. Wolf, *Angewandte Chemie - International Edition* **2024**, *63*, e202315381.

[119] J. A. Kelly, J. Gramüller, R. M. Gschwind, R. Wolf, *Dalton Transactions* **2021**, *50*, 13985–13992.

[120] M. V Kudchadker, R. A. Zingaro, K. J. Irgolic, *Chemistry of Phosphorus Pentaselenide. I. Its Reaction with Alcohols*, **1968**.

2 Chiral Diselenophosphoric Acids for Ion Pair Catalysis: A Novel Approach to Enhance Both Proton Donating and Proton Accepting Properties

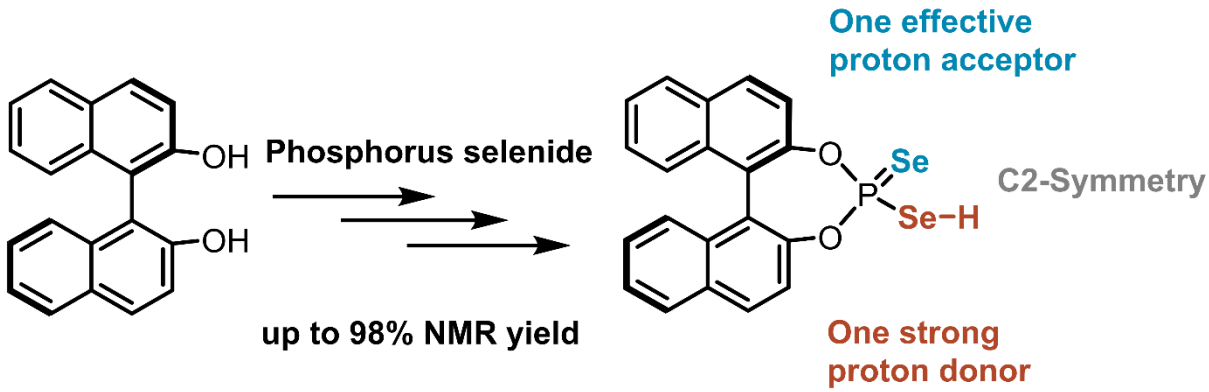

J. Eder, A. S. Antonov, E. Y. Tupikina, and R. M. Gschwind

Chem. Eur. J. **2024**, *30*, e202401793. **DOI:** 10.1002/chem.202401793

A) Johannes Eder planned, performed and analyzed most of the experiments, especially the synthesis of DSA-K out of potassium BINOLate and the protonation reactions towards acid and overprotonated acid. He also contributed to the writing of the manuscript. B) Alexander S. Antonov planned and analyzed experiments and performed initial studies on the synthesis of DSA out of BINOL. He wrote the majority of the manuscript. C) Elena Yu. Tupikina planned, performed and analyzed the computational studies and contributed to the manuscript by writing parts about the computational studies. D) Ruth M. Gschwind contributed to the design of experiments and the interpretation of data. She also contributed in writing and proof-reading of the manuscript part and provided funding.

Text and Figures may differ slightly from the original publication.

2.1 Abstract

The activation of poorly reactive substrates via strong chiral acids is a central topic in asymmetric ion pair catalysis these days. Despite highly successful scaffolds such as N-triflylphosphoramides, these catalysts either lack C_2-symmetry or provide multiple H-bond acceptor sites, leading to lower ee values for certain reactions. We present BINOL-based diselenophosphoric acids (DSA) as an extremely promising alternative. Using an intertwined approach of synthesis and NMR studies, we developed a synthetic approach to DSA with up to 98% NMR yield. The obtained acids provide both very high proton donor and proton acceptor properties, a bifunctionality, which is key to catalytic applications. Indeed, first reactivity test proved the much higher acidity of DSA and its ability to initiate Mukaiyama–Mannich reaction and protodesilylation of silyl ethers. Together with their C_2-symmetry, the single donor and single acceptor situation, the decreased tendency of self-association, and the straightforward synthesis with potential 3,3'-substitution, the DSA provide all features ideal for the further development of ion pair catalysis.

2.2 Introduction

The remarkable level of sophistication achieved in modern organic synthesis is attributed to the discovery of effective catalytic processes. Organocatalysis has also significantly contributed to the modern synthetic chemistry of complex chiral molecules in this case.[1–6] In the different fields of organocatalysis, e.g., enamine, iminium and ion pair catalysis various non-covalent interactions such as hydrogen, halogen, and chalcogen bonds or electrostatic and steric interactions, are successfully applied and combined.

One major breakthrough in metal-free ion pair catalysis[7–9] was the development of chiral phosphoric acid (CPA) catalysts with a 1,1'-bi-2-naphthyl backbone (Scheme 2-1).[10,11] The success of chiral Bronsted acids is based on their vast applicability, high substrate tolerance, excellent stereoselectivity and high yields.[12] These catalysts have proven effective in numerous stereoselective reactions, including inter- and intramolecular heterocyclizations,[13–15] alkylation,[16–18] reductive amination,[19,20] and hydrogenation[21,22].

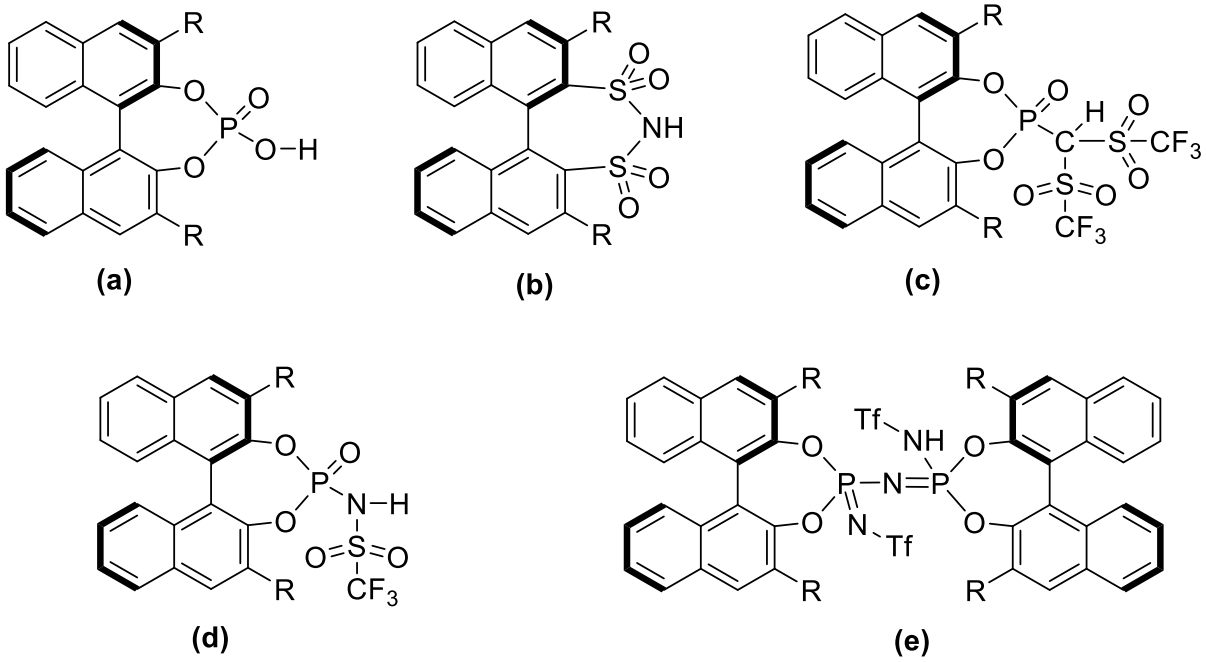

Scheme 2-1. 1,1'-bi-2-naphthyl based chiral phosphoric acid and some other highly acidic ion pair catalysts.

To adapt the 1,1'-bi-2-naphthyl based phosphoric acids to certain substrates and substrate classes, the substituents in 3 and 3' positions of the binaphthyl core are generally varied. Despite their extensive use, most reactions catalyzed by chiral phosphoric acids typically require extended reaction times, ranging from several hours to even days, particularly when using low

catalyst loadings. Raising the catalyst load is generally undesirable since, first, it increases the cost, and second, potentially leads to the realization of a dimeric catalytic path and the loss (or even reversal) of enantioselectivity.[23] Furthermore, in some cases, phosphoric acids are not acidic enough to activate certain substrate classes.[24] Therefore, numerous new chiral acids have been developed, which mostly focus on introducing a higher acidity via strong electron-accepting substituents, such as disulfonimides (Scheme 2-1b), (trifluoromethyl)sulfonyl methanes (pK_a ≈ 1, Scheme 2-1c) and *N*-triflylphosphoramides (pK_a ≈ 6, Scheme 2-1d and e).[24–27] This approach has indeed significantly enhanced the catalysts' acidities and enabled the activation of otherwise inert substrates. However, the presence of multiple H-bond acceptors in these highly acidic chiral acids multiplies the potential structures of intermediates and transition states as especially shown for disulfonimides (Scheme 2-1b).[26] Furthermore, in many catalysts (see c, d, e in Scheme 2-1) either asymmetry disrupts the favorable C_2-symmetry or huge catalyst structures raise questions about the compatibility with large and diverse substrates. In addition, these catalysts tend to provide lower enantiomeric excess values compared to classic chiral phosphoric acids. Classic chiral phosphoric acid structures with a higher acidity would offer a solution to these problems and potentially combine high acidity with a C_2-symmetry and a single H-bond acceptor. Considering that the acidity of H_2Se is ten orders of magnitudes higher than that of H_2O, one would anticipate that substitution of the OH moiety with SeH could provide acidity levels comparable to those of the known leaders illustrated in Scheme 1, while conserving the highly successful structural features of CPAs. Simultaneously, due to the larger size of selenium and the reduced electronegativity in comparison to oxygen, the alignment for H-bonding is more constrained.[28] Consequently, complexation of the substrate with SeH is expected to provide less conformational freedom and to alter the impact of the dimeric pathway on enantioselectivity.[23] Additionally, replacing oxygen with selenium introduces NMR-visible, non-quadrupolar nuclei, specifically ^{77}Se, with a reasonable natural abundance (7.58%). This provides an exceptional tool for investigating the mechanisms of organocatalyzed reactions: selenium is a direct participant in H-bonding, and thus its chemical shift and spin-spin coupling constants are highly sensitive to any structural changes. Finally, given the current active development of the applications of Se-containing molecules for organocatalysis,[29] the development of chiral systems bearing selenium possesses a high potential for both synthetic and mechanistic developments. Despite the potential advantages of the selenophosphoric acids mentioned above, there have been relatively few efforts to modify the chalcogen atoms in BINOL-based CPAs so far (Scheme 2-2). Only a couple of papers

concerning the preparation of chiral dithiophosphoric **2**[30] and monoselenophosphoric **3**[31–33] acids have been published. Only one attempt was reported to construct dialkyldiselenophosphoric acids, which stopped at the level of potassium salts.[34,35] However, on one hand, the catalytic activity of these systems has not been systematically investigated, except for the observation that **3** provides lower *ee* values than **1** in the hydrogenation of imines with Hantzsch ester.[32] On the other hand, the obtained monoselenophosphoric acids exist in a Se=P-OH tautomeric form, thus they don't provide the advantages of a Se-H moiety. In principle, this issue could be solved with the preparation of diselenophosphoric acids with a binaphthyl backbone such as **4**, however, this step has not been attempted so far.

An approach to novel binaphthyl-based chiral phosphoric acids should involve readily available, enantiomerically pure 1,1'-bi-2-naphthols (BINOLs). Typically, these BINOLs are subjected to treatment with $POCl_3$ to yield the corresponding phosphoric acids **1**, or with PCl_3 in the presence of selenium to prepare monoselenophosphoric acids **3** (see Scheme 2-2).[32,36] In both cases, further hydrolysis of the intermediates introduces an oxygen atom. In contrast, the treatment of BINOL with P_4S_{10} directly yields the dithiophosphoric acid **2**, without the need for any additional S-nucleophile.[30]

The high yields achieved with phosphorus sulfide may suggest that using phosphorus selenide would offer a straightforward route to obtain diselenophosphoric acid **4**. However, this task is very challenging due to the structural peculiarities of phosphorus selenide. Unlike diphosphorus pentoxide and diphosphorus pentasulfide, which exist in the molecular form of P_4O_{10} and P_4S_{10}, respectively, diphosphorus pentaselenide forms a polymeric glass.[37–39] Only extended extraction with CS_2 facilitates the disruption of the polymeric structure, resulting in molecular P_2Se_5 with a very modest yield of approximately 6% (Figure 2-1).[37,40] In addition, the phosphorus in P_2Se_5 exists in a +3 oxidation state, in contrast to $POCl_3$, P_4O_{10}, or P_4S_{10}, containing phosphorus +5. Therefore, the synthesis of diselenophosphoric acids necessitates a subsequent oxidative selenation.

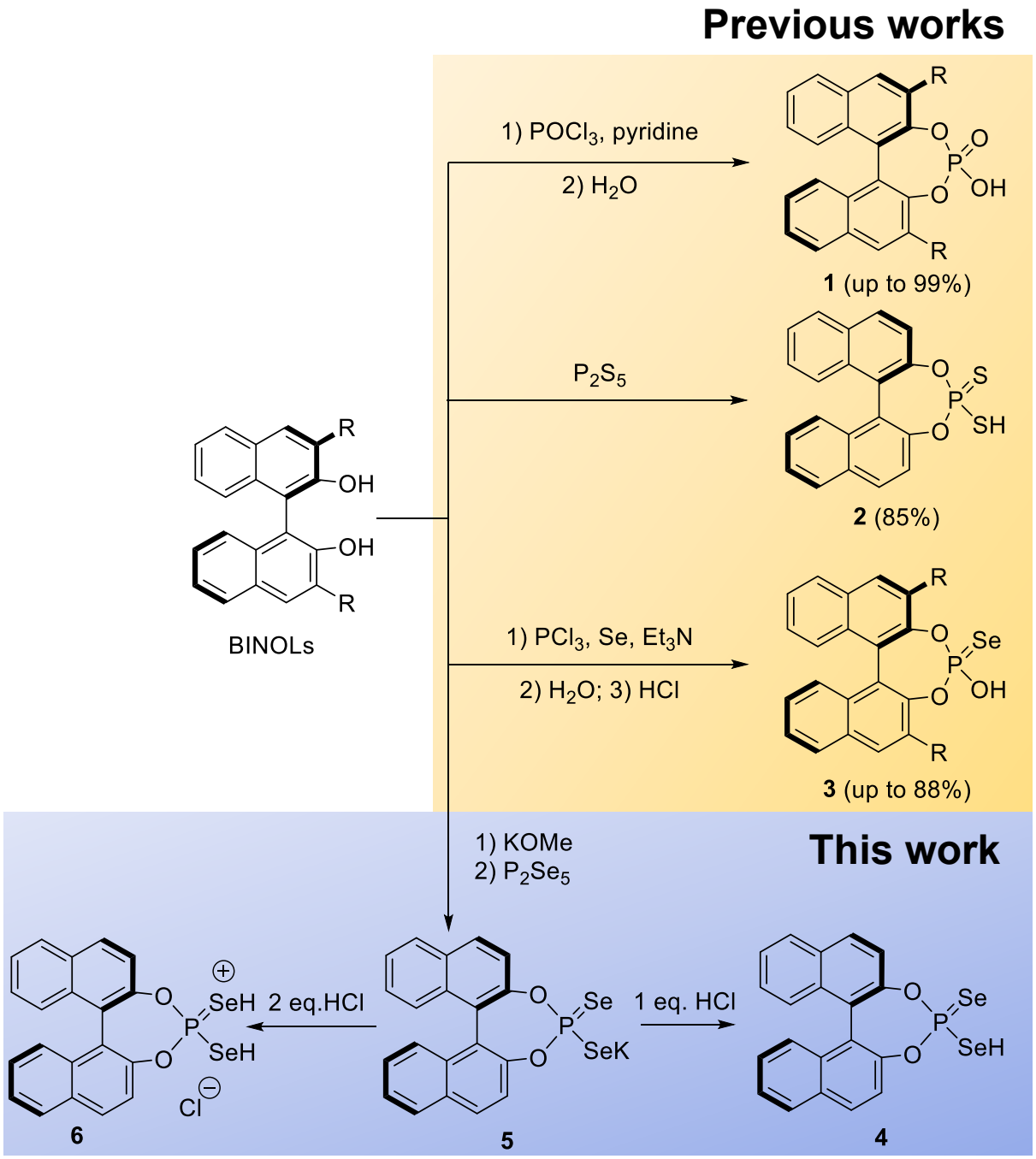

Scheme 2-2. Synthesis of chiral 1,1'-bi-2-naphthyl based chalcophosphoric acids.

In addition, the detailed mechanism of how phosphorus selenide interacts with alcohols and phenols is elusive so far. Thus, a rational access is not possible, which might be one of the reasons why free diselenophosphoric acids have not yet been successfully prepared. The sole exception lies in the preparation of their potassium salts through subsequent treatment of phosphorus selenide with alcohols and potassium hydroxide.[34,35] Unfortunately, this complicated reaction suffers from poor reproducibility, with no significant advancements since the 1970s.

Therefore, in this study, we present an in-depths *in situ* NMR identification of products and intermediates formed upon the reaction of phosphorus selenide and unsubstituted (*R*)-BINOL as well as an intertwined approach between mechanistic studies and synthetic experiments allowing us to boost the NMR yields up to 95%. The oxidation of P^{+3} with *in situ* formed H_2Se and elemental selenium allows for a simple, safe, and high yielding synthesis of the first diselenophosphoric acid **4** without implementation of any additional selenating agents, showcasing the possibility of synthesizing chiral (*R*)-BINOL-based diselenophosphoric acids. One-pot deprotonation of (*R*)-BINOL with potassium methoxides followed by treatment with phosphorus selenide provides an effective synthesis of the potassium diselenophosphate **5**, which is stable in air and can be further in situ converted in the corresponding acid to avoid any possible decomposition. Additionally, we demonstrate the unexpectedly enhanced basicity of the P=Se moiety, allowing the protonation of **4** with either HCl or H_2Se, leading to the formation of the stable protonated diselenophosphoric acid **6**. Overall, a new and effective synthetic pathway to diselenophosphoric acids including its mechanistic details is presented, which should pave the way to applications of diselenophosphoric acids in ion pair catalysis.

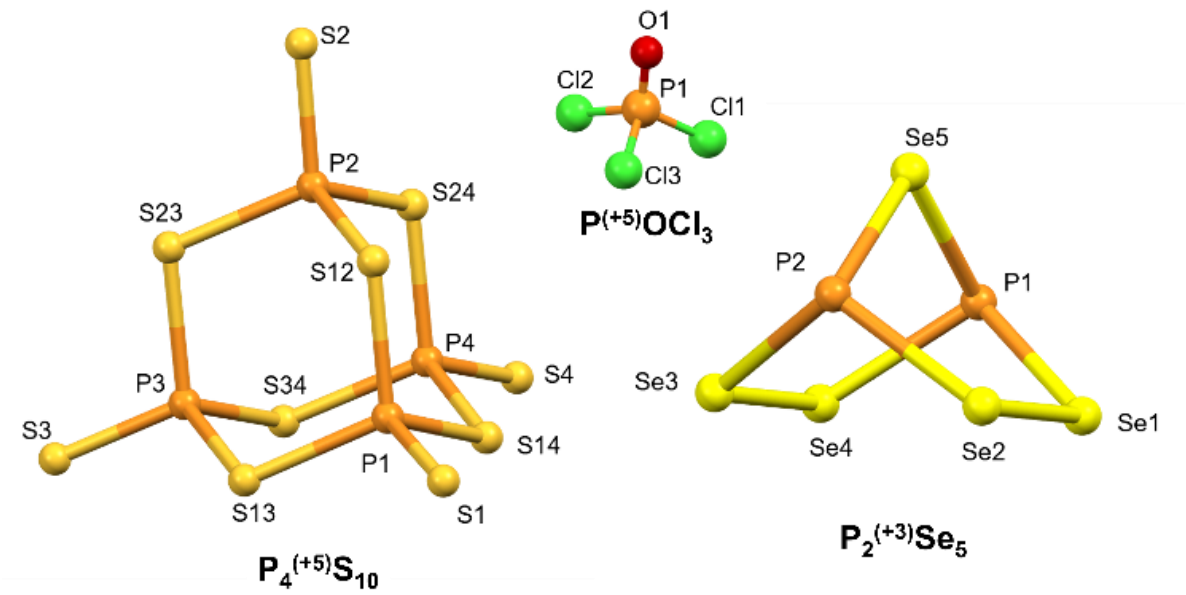

Figure 2-1. $POCl_3$ and P_4S_{10} as typical reagents for dichalcophosphoric acids synthesis provide P^{+5} and readily available in molecular form. In contrast, molecular P_2Se_5 contains P^{+3} and requires prolonged but low-yielding CS_2-extraction from polymeric glass.[37–39] The X-Ray structures are shown.

In both cases, further hydrolysis of the intermediates introduces an oxygen atom. In contrast, the treatment of BINOL with P_4S_{10} directly yields the dithiophosphoric acid 2, without the need for any additional S-nucleophile.[30]

2.3 Results and Discussion

2.3.1 Model System

The basis of the outstanding enantioselectivity of CPAs is the BINOL moiety, and the refinement for certain substrate classes is most often conducted via the adaption of the substituents in 3,3'-positions. In this study, unsubstituted (*R*)-BINOL was selected as model system since it is readily available, cheap, and thus very suitable for test reaction. Considering the polymeric nature, the insolubility of phosphorus selenide and the resulting low reactivity showcased in the beginning of the study, unsubstituted BINOL offers clear advantages for a proof of principle study. Additionally, the simple, commercially available, and cost-effective unsubstituted (*R*)-BINOL as a model system allows for extensive and rigorous tests of various synthetic approaches. In contrast, sterically hindered 3,3' substituents are expected to reduce the reactivity. Therefore, high conversions and reactivity for the unsubstituted BINOL model system are the goals to lay the basis for future implementation of our synthesis into more complex 3,3'-disubstituted derivatives.

2.3.2 Reaction of (*R*)-BINOL with Phosphorus Selenide

We started our experiments with tests of reactivity of (*R*)-BINOL towards freshly prepared phosphorus selenide. The previously mentioned extraction of molecular P_2Se_5 with CS_2 proves highly inefficient for synthetic purposes due to its prolonged time and low yield. To address this challenge, our approach commenced with the synthesis of polymeric phosphorus selenide, accompanied by efforts to enhance its reactivity. Several publications have reported the synthesis of this compound from its elemental components, proposing various reaction conditions. For instance fusing at temperatures of 400–450 °C in a sealed or open tube using an electric or flame burner from 25 minutes – 12 hours up to as long as 12 days is reported.[34,35,37,43–45] According to our experiments (for details see Table S2-1 in SI) the most convenient method involves heating a 2:5 mixture of dried red phosphorus and gray selenium under an argon atmosphere at 650 °C for 10-15 minutes using a heat gun. The obtained solid product was immediately ground within an inert atmosphere (glovebox) and mixed with (*R*)-BINOL in toluene or mesitylene under an argon atmosphere. The final heterogeneous mixture was stirred at 100–160 °C for up to 144 hours to achieve noticeable conversion.

2.3.3 Identification of Intermediates and Products

In a typical experiment, the formation of a complex mixture and an incomplete conversion were observed. Therefore, we focused on the NMR identification of the products in the raw mixture to learn something about the mechanism of this reaction and to improve the synthesis via mechanistic insights. To determine the composition, a sample of the reaction mixture was filtered, and the solution was directly used for NMR measurements. The resulting ^{31}P NMR spectra display three main signals, along with several minor signals corresponding to different phosphorus-containing species. This observation suggests a more intricate reaction mixture than originally anticipated (Figure 2-2).

First, we analyzed the satellite signals regarding integral intensities and ^{31}P-^{77}Se spin-spin coupling constants to identify the number of selenium atoms bound to the respective phosphorus atom and their bonding order. It's worth noting that the natural abundance of ^{77}Se is 7.58%.[46] As a result, when one phosphorus atom is bound to one ^{77}Se atom, the ratio between the parent line and both of the satellite signals is approximately 92.4:7.6.

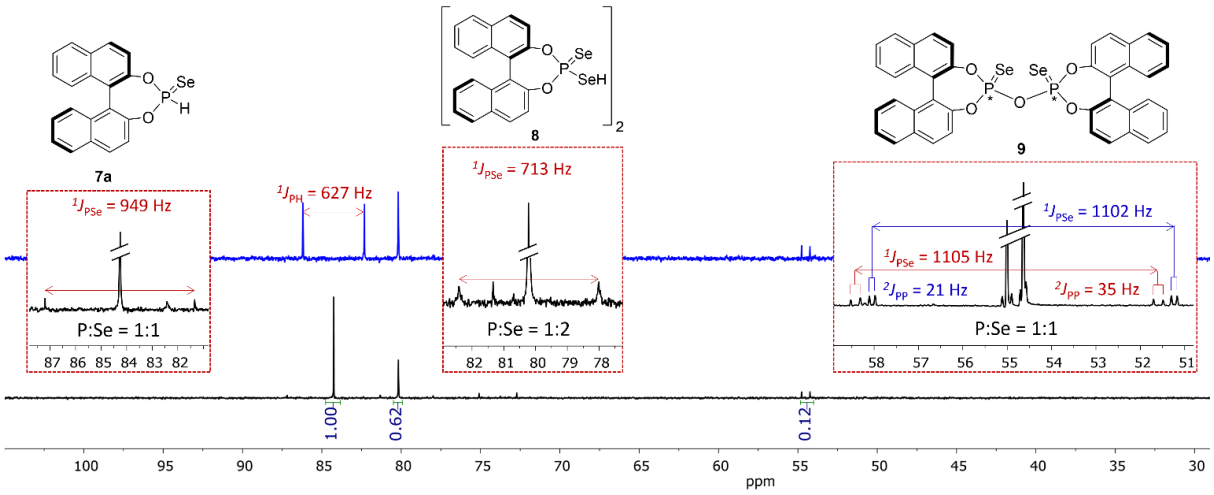

Figure 2-2. Intermediate/product identification from the crude reaction mixture of (*R*)-BINOL and phosphorus selenide (for reaction conditions see Table 1, entry 5). A P^{+3} containing compound **7a**, the dimer of diselenophosphoric acid **8** and a covalent dimer with a bridging oxygen atom **9** were observed as main products in the ^{31}P (top) and the $\{^1H\}^{31}$P (bottom) NMR spectra (toluene, 298 K). For details see text.

If a phosphorus atom is bound to two ^{77}Se, this ratio shifts to approximately 84:16. The size of the $^{1}J_{PSe}$ scalar coupling is associated with the bond order. For a P-Se single bond typical $^{1}J_{PSe}$ values range from 200 – 620 Hz, for a P=Se double bond from 800 – 1200 Hz.

Thus, the phosphorus atom associated with the signal at 84.3 ppm (integral ratio 92.4:7.6) is bonded to only one selenium atom. The observed $^{1}J_{PSe}$ value of 949 Hz corresponds to a phosphorus atom with a double bond to selenium.[46,47] Furthermore, in proton coupled ^{31}P NMR spectra, this signal appears as a doublet with a spin-spin coupling constant of 627 Hz (Figure 2-2, top), indicating the presence of a P-H bond, as typical $^{1}J_{PH}$ values fall within the range of 600 - 700 Hz.[48-50] Combining a P-H bond with a Se-P double bond, we assign the signal at 84.3 ppm to the P^{+3} compound **7a**, which is the tautomer of **7** and results from the initial nucleophilic attack of (*R*)-BINOL on phosphorus selenide (Scheme 2-3). Similar P-OH to (P=O)H tautomerizations are well-documented for compounds such as phosphonates, secondary phosphine oxides, and phosphinates.[51] While the structure of **7a** formally contains hypervalent phosphorus and could be represented in resonance form as **7b**, the $^{1}J_{PSe}$ value strongly indicates the presence of a P=Se double bond. Consequently, this compound will be further discussed in the form of **7a**. The signal exhibiting a chemical shift of 80.2 ppm corresponds to a phosphorus atom bonded to two selenium atoms, as evident from the integral intensities of the satellite signals (84:16). In agreement with the structure of a diselenophosphoric acid, the value of $^{1}J_{PSe}$ = 713 Hz suggests an intermediate bond order. However, the chemical shift is puzzling at first glance. It is well-established that substituting an oxygen atom with selenium causes a substantial low-field shift. For example, in $CDCl_3$, δ^{31}P for **1** is approximately 5 ppm, while for **3** it is approximately 70 ppm.[30]

Thus, replacing two oxygen atoms with selenium should result in an even more pronounced low-field shift. Hence, the question arises whether the relatively low chemical shift of 80.2 ppm could be caused by dimerization (or oligomerization) of the diselenophosphoric acid into a complex, such as dimer **8** (Scheme 2-3), which is typical for phosphoric acids.[47,52,53]

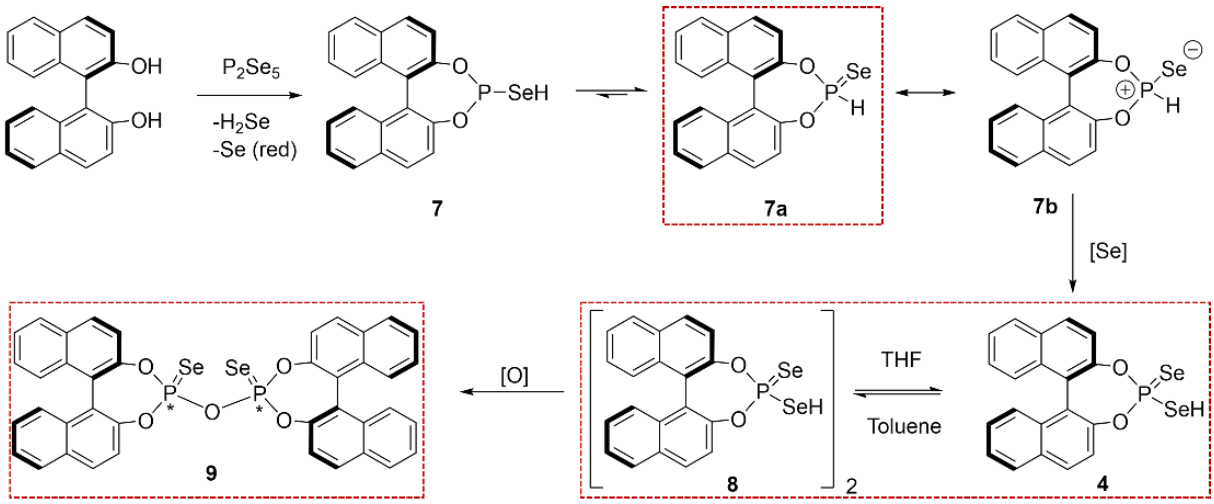

Scheme 2-3. Sequence of transformation of (*R*)-BINOL with phosphorus selenide: nucleophilic substitution followed by oxidative selenation and side oxidation/hydrolysis of the formed diselenophosphoric acid. NMR identified species are highlighted in dashed boxes.

In fact, the breakdown of the aggregation via the addition of THF to the reaction mixture caused a low-field shift to 108.5 ppm. This confirms that an unusually high-field chemical shift in toluene originates from an aggregation and that the formation of the monomeric compound **4** occurs in the presence of THF (see Figure S2-1a and b in SI).[54]

Next, quantum-chemical calculations were conducted to further validate this disaggregation hypothesis. Indeed, in a vacuum, two molecules of **4** form the hydrogen-bonded dimer depicted in Figure 2-3a. In contrast to most phosphoric acids preferring cyclic self-associates,[52,53] for **8**, a non-cyclic dimer corresponds to the energy minimum on the potential energy surface. This phenomenon can be attributed to the geometric constraints of H-bonding with selenium. Due to the larger atomic radius and polarization as well as the reduced dipole moment, the electron density of selenium forms a toroid-like structure around the nucleus, which reduces the flexibility of H-bonding compared to oxygen. A similar restriction of H-bond geometries occurs upon transition from oxygen- to sulfur-containing proton acceptors.[28] As a result, **4** tends to form H-bonded chains rather than cyclic dimers. Confirming this trend, three molecules of **4** led to the formation of a distorted dimer, with the third molecule attached via π-stacking (see Figure S12 in SI). Consequently, dimerization of **4** appears to be the most favorable complex structure in the absence of additional H-bond acceptors.

In agreement with the experimental observation, repeating the calculations with the addition of THF molecules to the dimer **8** results in its disruption and the formation of monomeric **4**, H-

bonded with the oxygen atom of THF (Figure 2-3b). It should be noted that the calculated absolute ^{31}P chemical shift values for **4** and **6** show offsets of around 100 ppm compared to the experimental ones. However, as often observed for systematic offsets, the relative chemical shift change between dimer to monomer fits much better ($\Delta\delta^{31}P_{exp.}$ = 28.3 ppm and $\Delta\delta^{31}P_{calc.}$ = 18.3 ppm), strongly corroborating the monomerization of **4** upon the addition of THF. The third set of signals, which is located at approximately 54 ppm in the ^{31}P NMR spectrum in Figure 2-2 is particularly intriguing. Both observable signals correspond to a similar species, each containing one selenium atom per one phosphorus atom. The $^{1}J_{PSe}$ = 1102 and 1105 Hz indicate the presence of typical P=Se double bonds. In contrast to the other components **7a** and **8**, this compound displays a doublet splitting of the satellite signals with typical $^{2}J_{PP}$ values of 21 and 35 Hz, respectively.[55]

All these characteristics point toward the existence of a covalent dimer bridged by oxygen, denoted as **9** (Scheme 2-3). Exposure of the reaction mixture to air results in the predominant formation of **9**. Given the stability of selenophosphites like **7**, [56,57] we hypothesize that **9** forms during the oxidation of **8**. The results of an HRMS study support the suggested structure of **9** (calc. for $C_{40}H_{25}O_5P_2Se_2^+$ $[M+H]^+$ 806.9503, found 806.9513). In different synthetic approaches, significant variations in the relative integral intensities of the two signal sets are observed. This indicates that the two signals do not belong to one species but to two closely related diastereomeric complexes, and that the process is not stereoselective in a reproducible way.

2.3.4 Mechanism Driven Synthetic Optimization

Next, the insights into the principal mechanistic steps gained via NMR spectroscopy (see Scheme 2-3) were used to optimize the phosphoselenation of BINOL. Vice versa synthetic approaches were used to refine the mechanism. Given that the phosphorus in P_2Se_5 exists in the +3 oxidation state, **7a** is the obvious first product of the nucleophilic attack of (*R*)-BINOL to phosphorus selenide. Further transformation to diselenophosphoric acid **4** necessitates oxidative selenation. Conducting the reaction in the presence of additional gray selenium or Woollins' reagent did not improve the **4**:**7a** ratio. This observation rules out conventional selenation of **7a**. Considering the propensity of thiophosphites to react with nucleophiles in the presence of an oxidant,[58] we propose that the transformation from **7a→4** might occur in a similar manner. Specifically, during the initial nucleophilic attack of (*R*)-BINOL to phosphorus selenide, hydrogen selenide and elemental selenium are released. In this context, hydrogen selenide could serve as a nucleophile and elemental selenium as an oxidant. Indeed, treatment

of the reaction mixture with hydrogen selenide leads to complete selenation of **7a** (see Figure S2-1c). Thus, the so far undefined selenation reagent in Scheme 2-3 can be identified as hydrogen selenide and elemental selenium (see Scheme 2-4), both *in situ* formed in the reaction of BINOL with P_2Se_5.

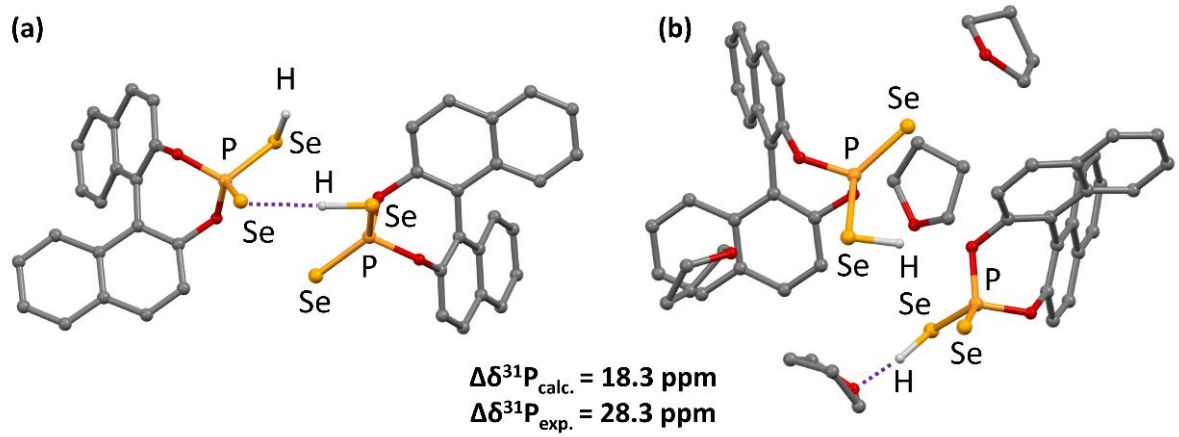

Figure 2-3. Disruption of the non-cyclic dimer **8** in vacuum (a) in the presence of THF molecules (b). The free dimer is stabilized by a single hydrogen bond. The THF molecules break the Se···H···Se bonding, resulting in a monomer that is H-bonded to a THF molecule. Calculated and experimental $\Delta\delta^{31}P$ are provided. B3LYP-D3BJ/6-311++G(d,p), hydrogen atoms (except for SeH) are omitted for clarity.

With these mechanistic steps at hand, the synthetic conditions for the phosphoselenation of BINOL were optimized next. For this, a straightforward method had to be developed to determine the conversion and NMR *in situ* yield. The proton spectra of the mixtures are by far too crowded in toluene to differentiate BINOL from the phosphoselenated species. However, we found that in DMSO-d_6, all components of the reaction mixture shown in Figure 2-2 undergo complete oxidation.

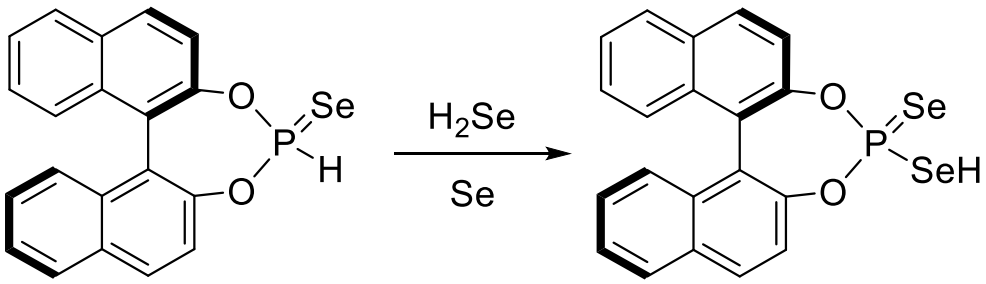

7a **4**

Scheme 2-4. Selenation of **7a** with *in situ* formed hydrogen selenide and elemental selenium.

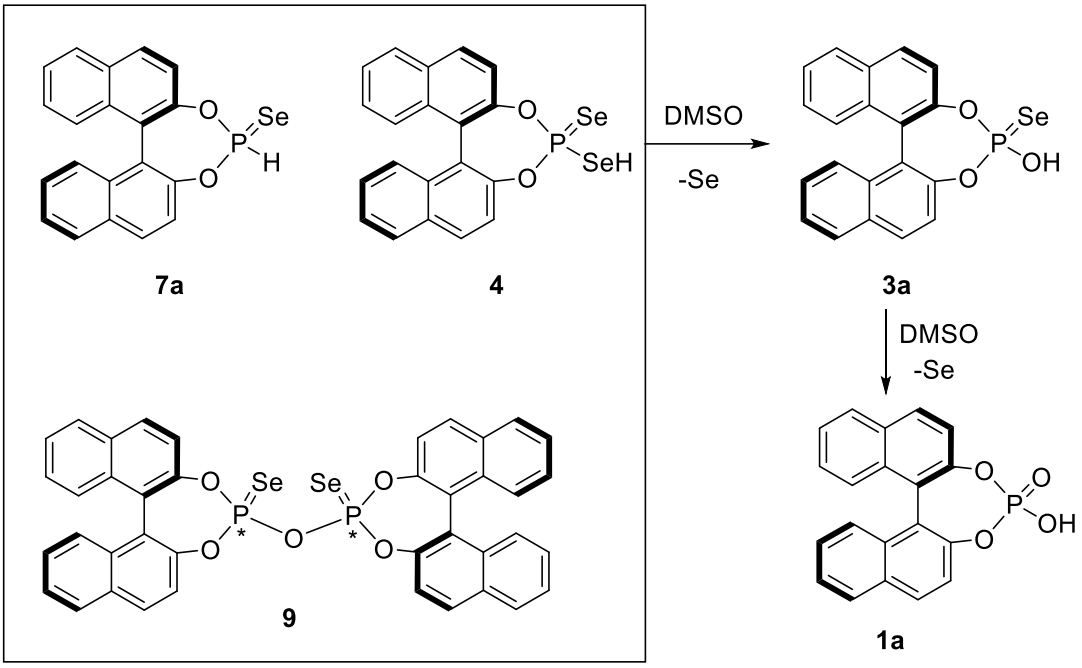

Scheme 2-5. Oxidation of the components of the reaction mixture in Figure 2-2 with DMSO.

This leads to the precipitation of red selenium and the formation of phosphoric acid **1a** (R=H) as the sole phosphorus-containing compound (Scheme 2-5).

Consequently, the respective ^{1}H NMR spectra become significantly simplified, allowing us to determine the conversion by comparing the integral intensities of (*R*)–BINOL and **1a** (R=H), which are the only components present in the mixture (Figure 2-4).

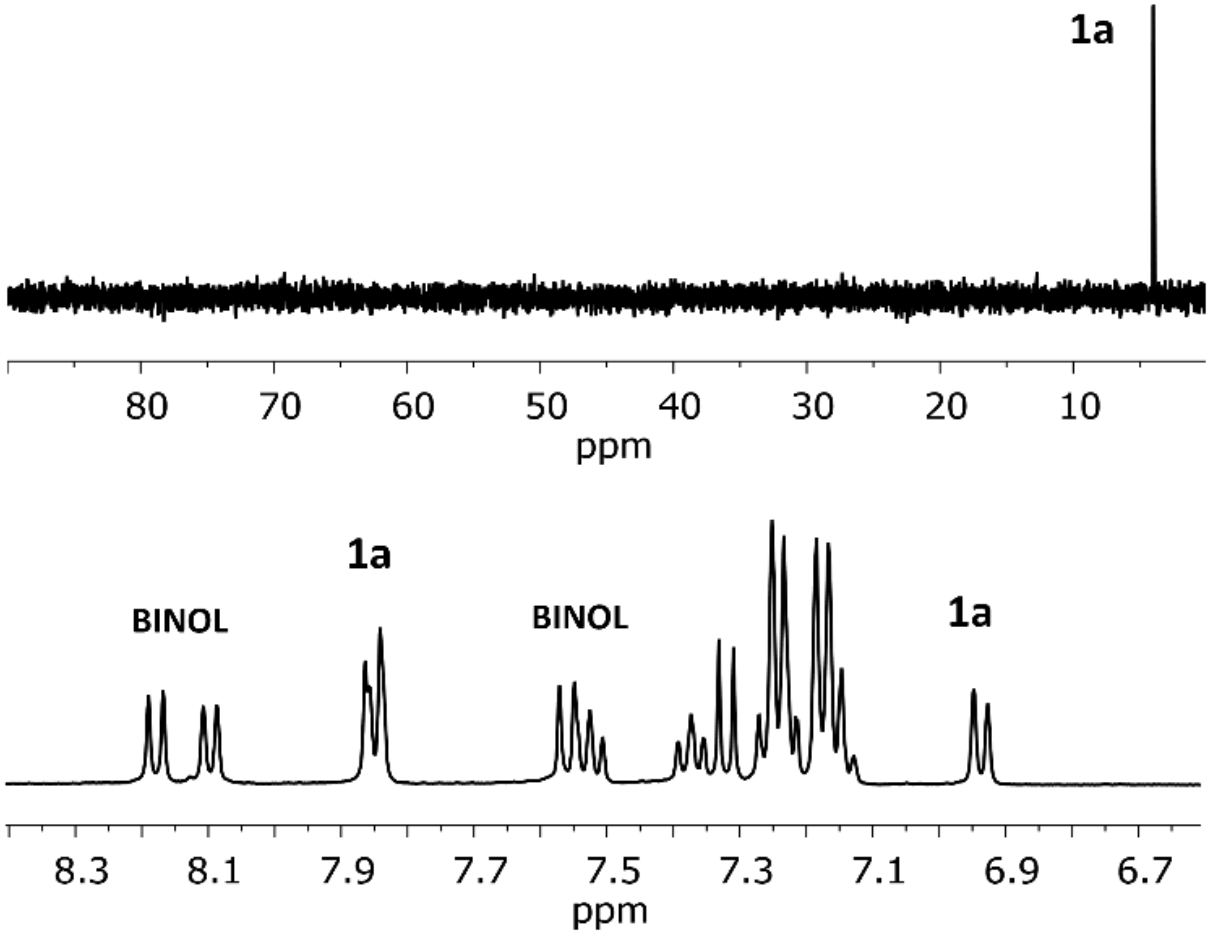

Figure 2-4. Conversion determination via oxidation of the reaction mixture shown in Figure 2 with DMSO. The ^{31}P spectrum shows CPA **1a** only (top) while the ^{1}H spectrum (bottom) allows for integration of (*R*)-BINOL versus **1a**.

We employed this approach to assess the reactivity of phosphorus selenide towards (*R*)-BINOL under various conditions, with the goal of achieving a higher conversion of the starting material (Table 2-1). According to the mechanism in Scheme 2-3 upon first transformation of BINOL with phosphorous selenide 1 equivalent of H_2Se is released, which is exactly the amount necessary for the later transformation to **4**. In addition, H_2Se is a highly toxic gas. Therefore, we tried to achieve high phosphoselenation yields relying only on *in situ* formed H_2Se released from phosphorous selenide.

In all experiments, we used 5 equivalents of phosphorus selenide. Heating freshly prepared phosphorus selenide with (*R*)-BINOL in toluene at 100 °C for 24 hours yielded only 5% conversion (entry 1). Extending the reaction time to 72 hours increased the conversion to 29%, but further prolongation did not lead to further improvements (entry 4).

Table 2-1. Reaction of phosphorus selenide with (*R*)-BINOL and (*R*)-BINOLates

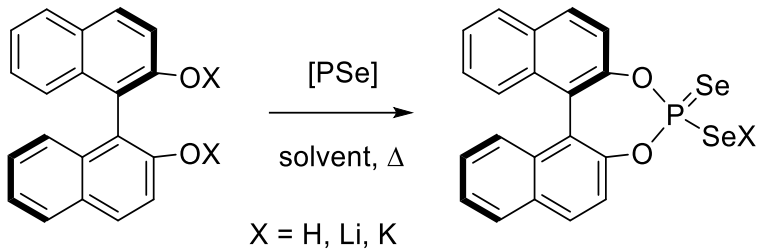

Entry	X	Solvent	T, °C	Time, h	NMR yield, %
1 [a]	H	toluene	100	24	5[d]
2 [a]	H	toluene	100	48	10[d]
3 [a]	H	toluene	100	72	29[d]
4 [a]	H	toluene	100	144	30[d]
5 [a]	H	toluene	120	72	70[d]
6 [a]	H	mesitylene	160	72	72[d]
7 [b]	H	toluene	120	72	82[d]
8 [c]	H	toluene	120	72	0[d]
9 [b]	K	toluene	120	72	95
10 [b]	Li	toluene	120	72	83

[a] with phosphorus selenide prepared by fusion of elements at 450-500 °C for 10-15 minutes; [b] with phosphorus selenide sublimated in vacuum at 650 °C after fusion; [c] with molecular P_4Se_3; [d] detected in the form of **1a** due to the oxidation in DMSO shown in Scheme 5.

During this reaction, the fine powder of phosphorus selenide tended to fuse back into a single solid mass, resulting in a significant reduction in the reaction rate. To address this issue and maintain a more manageable reaction time, the reaction temperature was increased to 120 °C, achieving a 70% conversion (entry 5). Heating at 160 °C in mesitylene did not yield a noticeable improvement (entry 6). Sublimation of the crude phosphorus selenide under a vacuum or in an argon stream proved effective in breaking the polymeric structure and enhancing reactivity, resulting in a conversion of up to 82% (entry 7). Attempts to utilize the well-soluble molecular P_4Se_3[59] in toluene led to no observable reaction (entry 8).

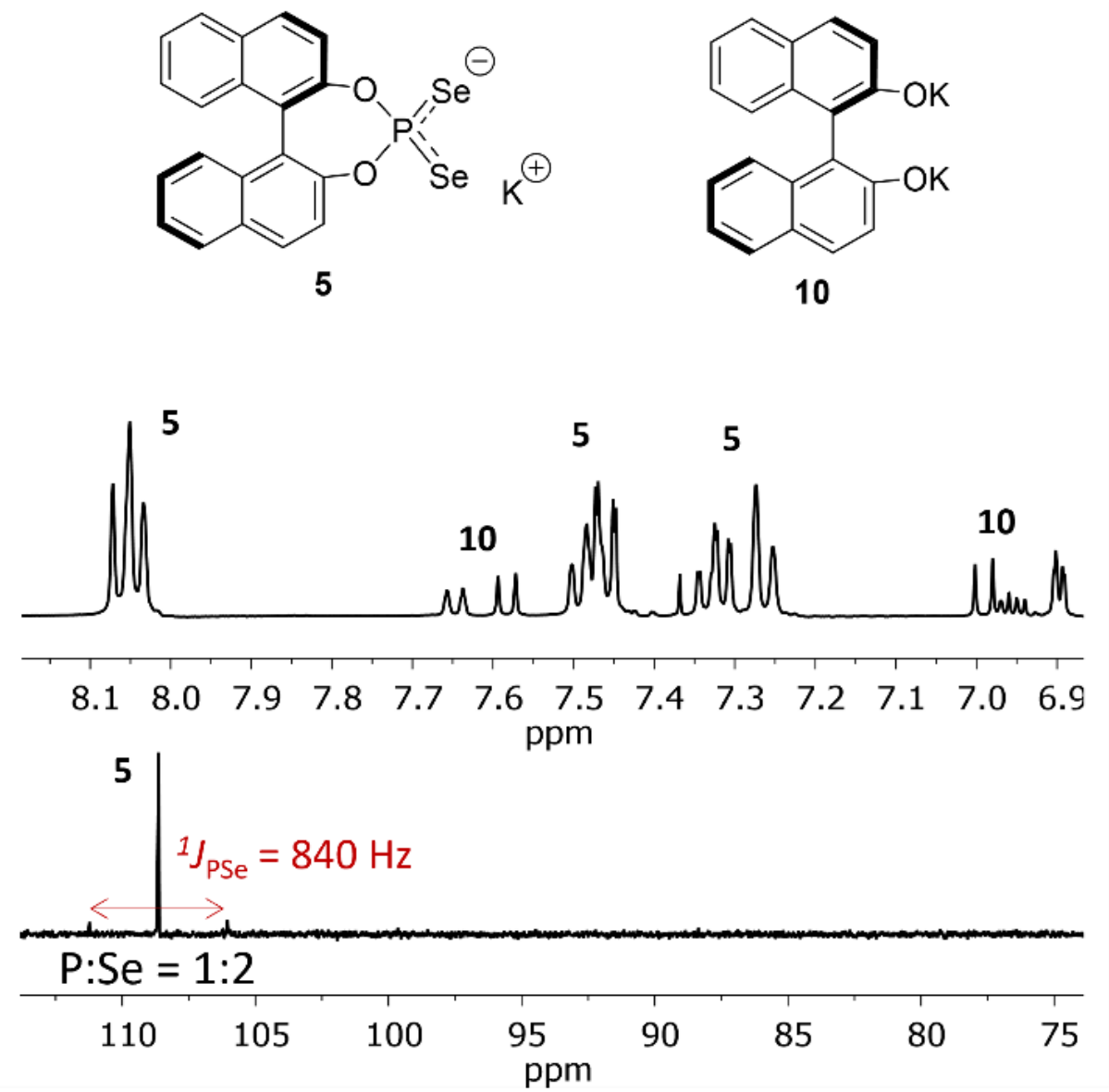

Figure 2.5. Full conversion of phosphorus containing species towards **5** upon addition of KOMe to the reaction mixture shown in Figure 2. ^{1}H (top) and ^{31}P (bottom) NMR spectra (DMSO-d_6, 298 K).

Since **4** is prone to oxidation and hydrolysis, its isolation from the reaction mixture using conventional separation techniques (*i.e.* chromatography) is unfeasible. A similar issue was previously reported by Kudchadker *et al.*, as they also failed in isolating pure selenophosphoric acids after treatment of simple alcohols with P_2Se_5.[35] However, they successfully prepared the corresponding potassium salts by treating their reaction mixtures with KOH or KOEt. In line with these findings, we added KOMe to our reaction mixture (depicted in Figure 2-2). This resulted in the precipitation of potassium salt **5**, along with a minor quantity of deprotonated (*R*)-BINOLate **10** (Figure 2-5). The remaining solution contained **5** with traces of **7a** indicating a highly effective overall selenation upon addition of KOMe. This observation corroborates our selenation hypothesis *via* the combination of H_2Se/Se discussed above (see Scheme 2-4). KOMe in presence of H_2Se should lead to the formation of KSeH, a much stronger nucleophile, which facilitates the transformation of **7a** into **5**. In accordance with **5** as the exclusive product, the ^{31}P NMR spectrum reveals only one signal with a P:Se ratio of 1:2 and a coupling constant of $^1J_{PSe}$ = 840 Hz. This indicates that both Se atoms share the same binding order towards the phosphorus atom and the relatively small coupling (in comparison with **9**) suggests a binding order between 1 and 2. With the higher reactivitiy of KHSe in mind, we wanted to generate it *in situ* without any additives and further improve the overall yield of the phosphoselenation. Starting the reaction with potassium (*R*)-BINOLate **10** has the additional advantage that it facilitates not only the second selenation step but also the initial nucleophilic attack to phosphorous selenide. Indeed, this approach resulted in extremely pure NMR spectra providing the signals of over 95% **5** and below 5% BINOL (Scheme 2-6, Table 2-1 entry 9, for spectra see Figure S2-11 in SI). Purification from NMR-invisible inorganic side products resulted in a 54% isolated yield of solid **5**. Additionally, lithium salt **11** was tested. However, it neither improved the yield nor facilitated the purification process (Table 2-1 entry 10).The obtained potassium salt **5** is stable in air and easy to handle. However, for some of the later catalytic applications, the free acid is required. Therefore, we treated potassium salt **5** with one equivalent of an ethereal solution of hydrogen chloride in dry THF to obtain diselenophosphoric acid **4** (Scheme 2-7, top). Conducting this reaction at room temperature resulted in the partial decomposition of **4** despite inert conditions (glovebox, argon atmosphere). However, performing this reaction at -80 °C allowed the stabilization of **4** and provided much cleaner spectra. Conveniently, the potassium chloride formed in this reaction precipitates from the reaction mixture due to its low solubility in THF. Fortunately, in most of the catalytic reactions involving chiral CPAs the acidic proton is transferred to the substrate forming an anionic CPA and a protonated substrate. Thus, the poor

stability of the acid **4** at elevated temperatures can be well-compensated by an excellent stability of its anion substrate complex. Indeed, we could stabilize diselenophosphoric acid/amine complexes for many days.[60] From these experiences we expect that diselenophosphoric acids can be successfully applied in ion-pair catalysis in the future.

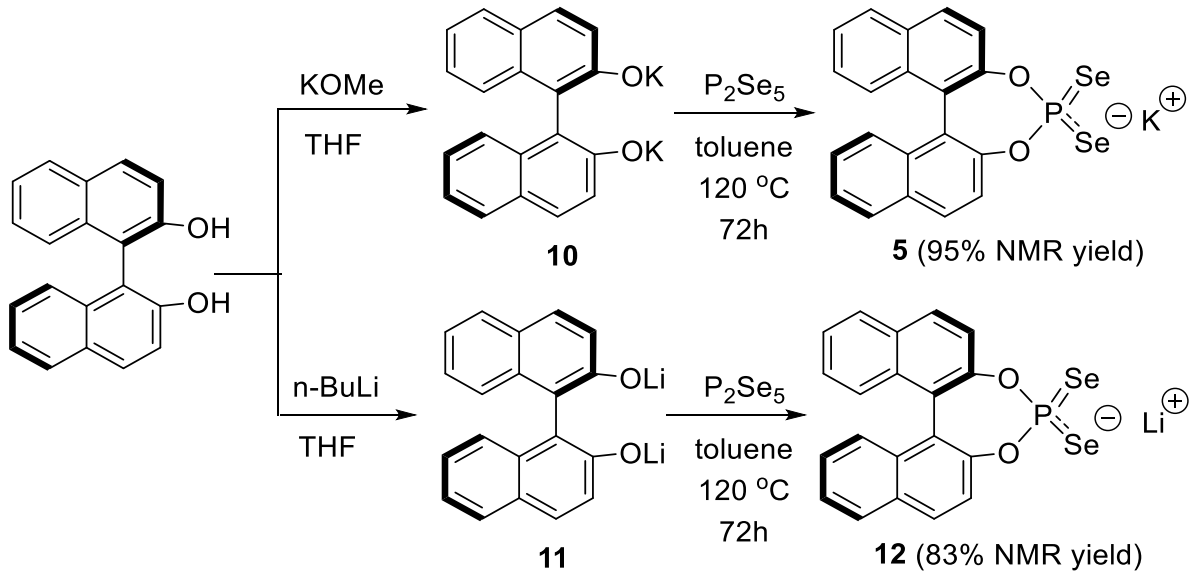

Scheme 2-6. Preparation of (*R*)-BINOLates **10** and **11** enhances the reactivity towards phosphorus selenide.

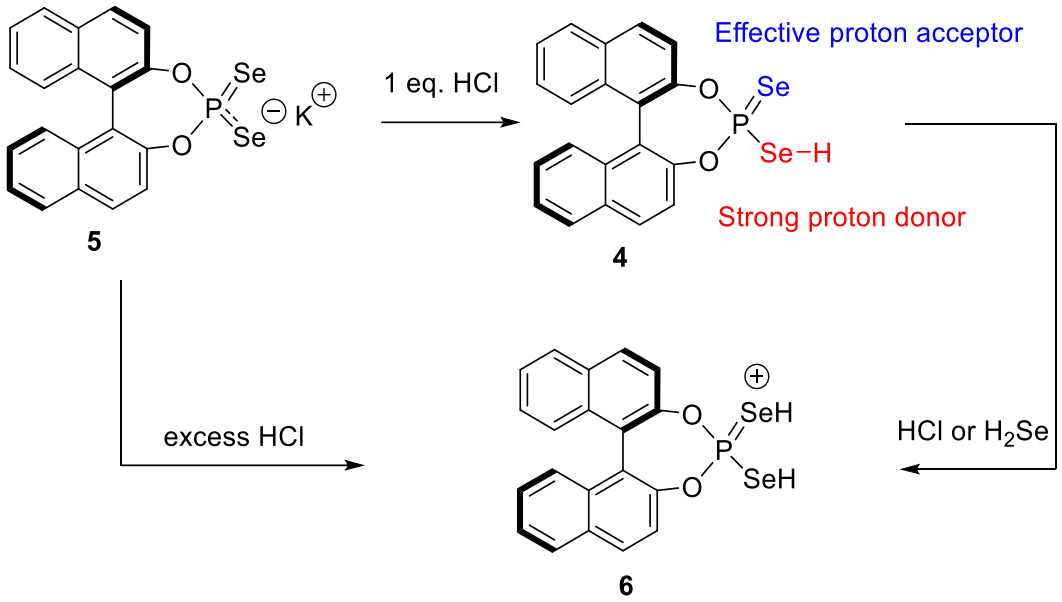

Scheme 2-7. Preparation of the free acid **4** and its high proton-acceptor property shown via protonation with HCl and H_2Se.

Next, the structural properties of the diselenophosphoric acid derivatives were investigated. Upon transition from **5→4**, the ^{1}H and the ^{31}P chemical shifts exhibit negligibly small differences while the ^{77}Se signal undergoes a high-field shift of approximately 10 ppm, which indicates an interaction with Se (see Figure 2-6a and Figures S2-2 and S2-4 in SI). However, the proton exhibits a fast exchange between the two Se atoms on the NMR time scale even at 180 K. As a result, only one type of Se is observed in the ^{77}Se and the ^{31}P spectrum as well as a mixed binding order in the $^{1}J_{PSe}$ and no scalar couplings to the proton is detected (see Figure S2-8 in SI).

To our surprise, **4** demonstrates unprecedented high basicity of the selenium double bond moiety. When the potassium salt **5** is treated with an excess of hydrogen chloride in Et_2O, the initially formed **4** undergoes further protonation, yielding the cation **6** (Scheme 2-7, bottom). The identical cationic species was even observed upon protonation with the by far less acidic H_2Se (see Figure S2-1c). The protonation stops the proton exchange between the two Se atoms and allows the first time observation of a single-bonded and a double bonded Se atom in the same molecule. As a result, two sets of satellite signals are observed in the ^{31}P NMR spectra: a $^{1}J_{PSe}$ coupling constants of 514 Hz, signifying a single bond, and 966 Hz, indicating a double bond (see Figure 2-6b). In accordance with two differently bound protons, the proton-coupled ^{31}P spectrum displays the signal splitting into a doublet of doublets with $^{2}J_{PH}$ coupling constants of 17 and 22 Hz (Figure 2-6c).

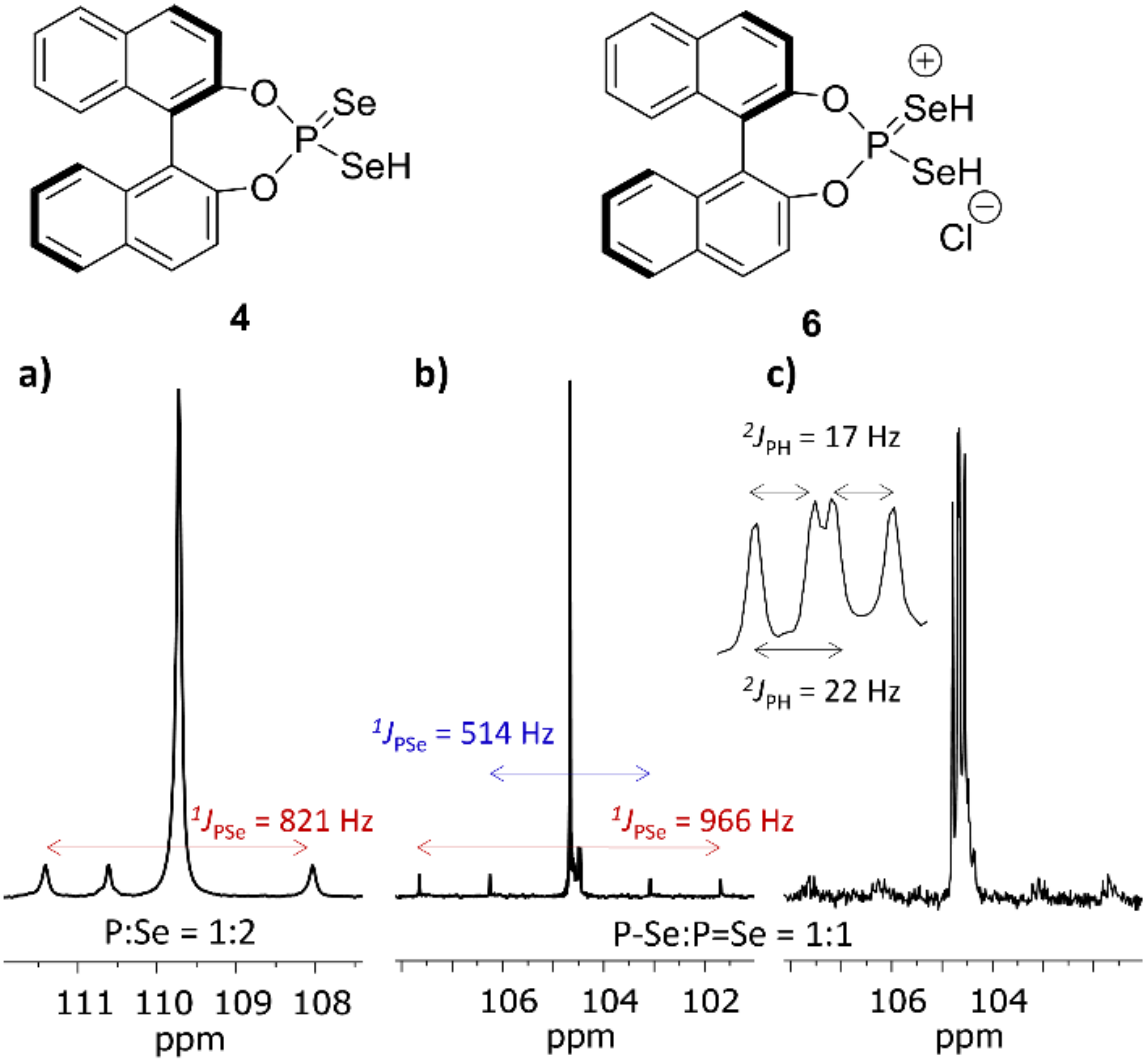

Figure 2-6. First experimental differentiation of the H-bonding situation to chalcogens in phosphoric acid derivatives. The ^{77}Se satellites in the ^{31}P NMR spectra of **4** (a) show a rapid exchange of the acidic proton in **4** resulting in a decoupled singlet phosphorus signal and an intermediate P-Se binding evidenced by the $^{1}J_{PSe}$ coupling constant. In contrast, both ^{31}P NMR and $\{^{1}H\}^{31}$P NMR spectrum of **6** (b, c) show two distinct ^{77}Se satellite pairs. This reveals the presence of a P-Se single and a P=Se double bond and is corroborated by the two $^{2}J_{PH}$.coupling constants detected (c). THF-d_8, 180 K.

Given that phosphine selenides typically exhibit lower basicity in comparison to their phosphine oxide counterparts,[61] the behavior of **4** underscores the unprecedentedly high basicity of the P=Se moiety. Thus, diselenophosphoric acids provide both a highly acidic SeH moiety and a highly basic P=Se moiety. This might be an additional key factor for application of diselenophosphoric acid in ion pair catalysis compared to other highly acidic catalysts shown in Scheme 2-1. The bifunctional properties of ion pair catalysts are essential for the formation of the ternary complexes in many reactions catalyzed by chiral Brønsted acids. Especially, we

found that in reductive aminations, the binding constants for Hantzsch ester to form the ternary complex was very low[62,63] reducing significantly the overall effectiveness of the catalysis. Indeed, quantum chemical calculations of **6** in the presence of two THF molecules have revealed a cooperative nature of hydrogen bonding: transitioning from the complex **4**·THF to **6**·THF_2 leads to a reduction in the Se…O distance, thereby strengthening the hydrogen bond (Figure 2-7). Furthermore, protonation of the **4**·THF complex facilitates the transfer of a hydrogen atom from selenium to oxygen within the Se···H···O hydrogen bond. Consequently, the formation of a hydrogen bond with the P=Se moiety enhances the acidity of the Se-H bond, which is particularly advantageous for reactions requiring highly potent chiral Brønsted acids.

Regarding reactivity, our findings suggest that diselenophosphoric acids are likely to facilitate both significant substrate activation and effective reagent binding. From a selectivity perspective, the C_2-symmetry of these compounds, coupled with their diminished propensity for dimerization, holds substantial promise for future enantioselective catalysis applications.

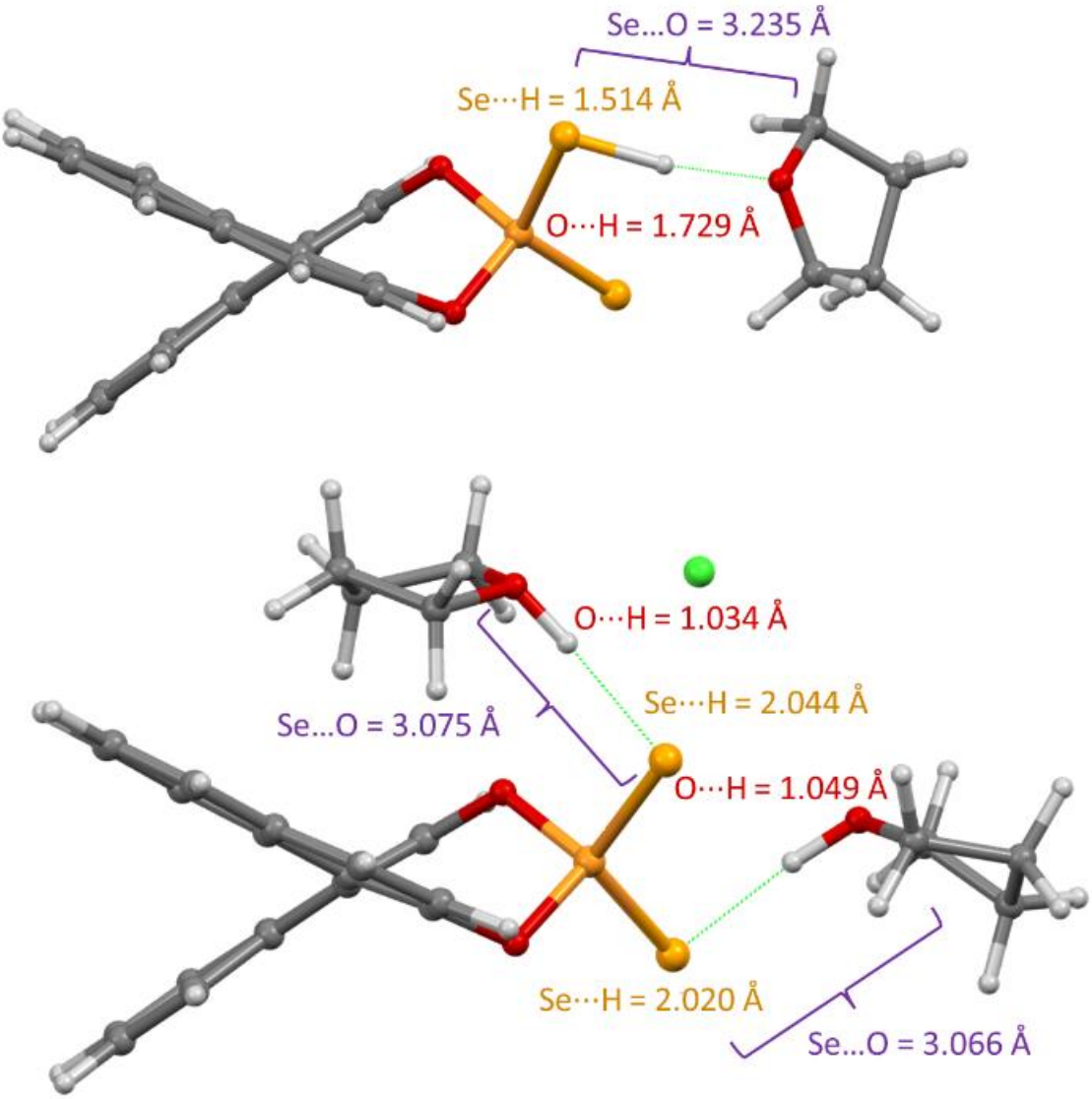

Figure 2-7. Protonation of **4**·THF (top) with the formation of **6**·THF_2 (bottom) results in the strengthening of hydrogen bonds (cooperative bonding) and proton transfer from selenium to oxygen atom: the formation of H-bond with P=Se moiety increases the acidity of Se-H bond. B3LYP-D3BJ/6-311++G(d,p).

For NMR practitioners, diselenophosphoric acids offer an unprecedented opportunity to directly observe the bonding dynamics between the two donor and acceptor sites in chiral phosphoric acids. Taken together, the enhanced acidity and potent proton-accepting capabilities position diselenophosphoric acids as an exceptionally promising new category of ion pair catalysts.

2.3.5 First Reactivity Tests

The reactivity of **4** was evaluated in the context of the Mukaiyama-Mannich reaction (Scheme 2-8).[64] It was previously shown that substrates lacking an OH group in the N-Ph moiety cannot be effectively activated by BINOL-based chiral phosphoric acids **1**. In contrast, more acidic catalysts, such as *N*-triflylphosphoramides (Scheme 2-1d) and (trifluoromethyl)-sulfonyl methanes (Scheme 2-1c), provide fast reactivity, good yields and excellent *ee* values.[24,65]

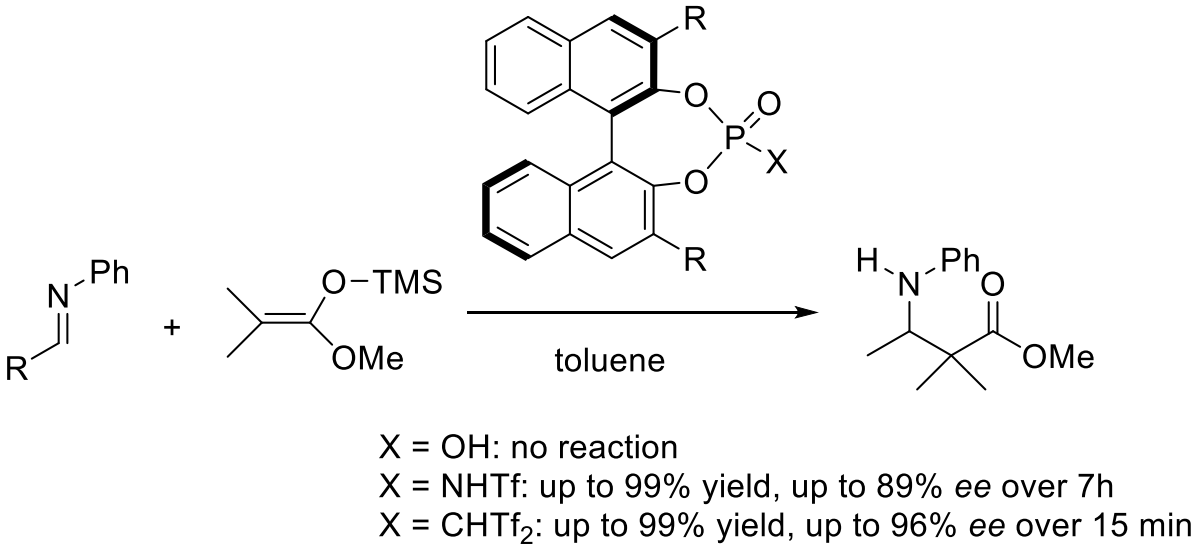

Scheme 2-8. Activation of imines lacking an OH group in the NPh moiety for Mukaiyama–Mannich reaction requires stronger chiral Brønsted acids, such as *N*-triflylphosphoramides and (trifluoromethyl)sulfonyl methanes.

Given that the free acid **4** is prone to oxidation and hydrolysis, the reactive complex **14** was prepared in situ in a way avoiding the presence of free acid. First imine **13** is mixed with an ethereal solution of HCl (10 mol%) forming the iminium hydrochloride. Then the reaction mixture is evacuated to dryness to ensure that no free HCl is left. Next potassium salt **5** (10 mol%) in THF is added yielding a mixture of **13** and complex **14** while KCl precipitates. The fact that the resulting mixture is stable on air indicates that there is no free acid **4** in THF. The evaporated reaction mixture composed of **14** and **13** (for details see experimental procedure) was then treated with silyl ether **15** (2 equiv.) in dry toluene at room temperature (Scheme 2-9). After 24 hours, the NMR spectrum of the crude reaction mixture demonstrated the presence of the anticipated product **16**, along with an unexpected ester **17**, in a **16**:**17** ratio of 1:2.6. Employing

a stoichiometric amount of **14** facilitates the formation of **17** elevating the **16**:**17** ratio to 1 :16.9. These results demonstrated excellent reproducibility.

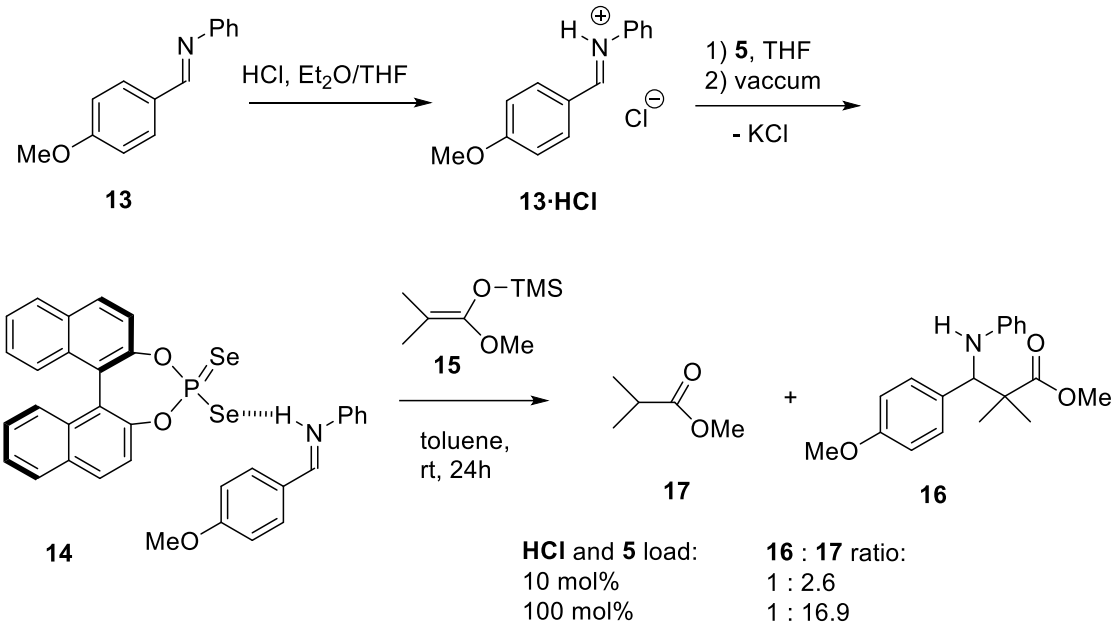

Scheme 2-9. Diselenophosphoric acid activates Mukaiyama–Mannich reaction together with protodesilylation transformation.

Product **17** originates from protodesilylation of silyl ether **15**, a transformation that typically requires strong acids such as *N*-triflylphosphoramides and (trifluoromethyl)sulfonyl methanes for the activation.[24] Interestingly, this side reaction has not been previously reported as significant in Mukaiyama-Mannich reactions. The observation of this transformation in the case of complex **14** is particularly unexpected, in case that the proton is attached to the imine nitrogen. Given the poor solubility of ionic species such as **14** in toluene we assume an equilibrium of the ion pair **14** with neutral **4** and **13**. Under these conditions, while the Mukaiyama-Mannich reaction proceeds slowly due to its heterogenous nature, the presence of free **4** in the solution facilitates a rapid, homogenous protodesilylation.

2.4 Conclusion

BINOL-based diselenophosphoric acids offer in principle an ideal scaffold for enantioselective ion pair catalysis providing very high acidities, C_2-symmetry and only one acceptor site but haven't been used in this field so far. Therefore, their principle synthetic access, formation pathway, stability and structural properties were investigated on the example of (*R*)-BINOL-based diselenophosphoric acids using an intertwined approach of synthesis, NMR spectroscopy and quantum chemical calculations. The key step in the reaction of BINOL with phosphorus selenide is the oxidative selenation of the initially formed selenophosphide **7** with H_2Se in the presence of elemental selenium. Fortunately, *in situ* formation of the exactly required amount of H_2Se from P_2Se_5 prevents handling of this exceptionally toxic gas. Starting from potassium (*R*)-BINOLate and phosphorus selenide produces *in situ* the even more effective and non-volatile selenation agent KHSe, resulting in up to 98% diselenophosphate **5** formation. The latter was isolated with a good yield and can be stored for months at ambient temperature. The diselenophosphate **5** can be converted into the more instable free diselenophosphoric acid **4** via treatment with hydrogen chloride. However, in most catalytic applications, diselenophosphoric acids should be instantly deprotonated by the substrate forming stable ion pairs again. Indeed, complexes with ammonium substrates were found to be stable for days.[60] An unexpected discovery with a high potential for catalytic applications is the exceptionally high basicity of the P=Se moiety. Treatment of the free diselenophosphoric acid **4** with an excess of hydrogen chloride or hydrogen selenide led to the formation of stable **4**·H^+ species with such a slow proton exchange that for the first time P=SeH and P-SeH moieties can be differentiated. This protonation might be also supported by the reduced trend of diselenophosphoric acids to self-aggregate compared to phosphoric acids, as shown by the computational studies. The bifunctionality of chiral acids is a key feature for their catalytic applications. Here, we show that diselenophosphoric acids provide both very high proton donor and proton acceptor properties. The initial tests on reactivity have underscored the markedly higher acidity of diselenophosphoric acids relative to the commonly employed phosphoric acids. This increased acidity enables the initiation of both the Mukaiyama-Mannich reaction and the protodesilylation of silyl ethers. Coupled with the C_2-symmetry of the catalysts, the unique single donor and single acceptor scenario, a reduced propensity for self-association, straightforward synthesis, and the feasibility of 3,3'-substitution, these diselenophosphoric acids embody an optimal blend of desirable characteristics. Consequently, they stand out as highly promising candidates for advancing the field of ion pair catalysis.

Experimental Details

General

Toluene, acetonitrile and THF were dried by the mbraun solvent purification system SPS 5.

Liquid-state NMR experiments were either performed using a Bruker Avance III HD NMR spectrometer (600 MHz for ^{1}H) equipped with a 5 mm triple resonance broadband inverse probe with ^{19}F-selective channel (TBI-F) with z gradient or a Bruker Avance III HD 400 MHz spectrometer with 5 mm BBO BB-^{1}H/D probe head. Chemical shifts are referenced to TMS or solvent for ^{1}H and ^{13}C, to H_3PO_4 (85% in H_2O) for ^{31}P and to Me_2Se for ^{77}Se. Spectrometer control was performed by Bruker Software TopSpin 3.2 PL 7.

Mass-spectra were obtained either on a Jeol AccuTOF GCX or an Agilent Q-TOF 6540 UHD. Methanol, DCM or chloroform were used as the solvent.

Synthesis

Phosphorus Selenide

Dry red phosphorus (109 mg, 3.50 mmol) and gray selenium (692 mg, 8.75 mmol) were weighed into a test tube inside the glove box and mixed thoroughly. The tube was sealed with a septum and ejected. The mixture was heated under 10 mbar of argon atmosphere at 650 °C for 15 min. The formed liquid was allowed to cool down to room temperature. The glassy product was mortared inside the glove box to create a fine blend. The product was obtained as a glassy amorphous solid (657 mg, 1.42 mmol, 82%).

General Reaction of (R)-BINOL with Phosphorus Selenide

Inside the glove box, (*R*)-1,1'-Binaphthol (100.2 mg, 0.35 mmol, 1 equiv.) was dissolved in toluene (SPS dry, 2 mL). Phosphorus selenide (801 mg, 1.75 mmol, 5 equiv.) was added to the solution. The heterogenous mixture was sealed, ejected from the glove box, and refluxed for 72 h. Afterwards, the reaction mixture was allowed to cool down and was filtered inside the

glove box. The solution was subjected to NMR measurements, or the solvent was removed under reduced pressure and the residue was dissolved in DMSO-d_6 to determine the conversion.

Potassium Diselenophosphate ***5***

Inside the glove box, (*R*)-1,1'-Binaphthol (0.35 mmol, 1 equiv.) and potassium methoxide (49.1 mg, 0.70 mmol, 2 equiv.) were dissolved in THF (SPS dry, 2 mL). The solution was stirred at room temperature for 1 h. Afterwards, the solvent and the formed methanol were removed under reduced pressure to yield **9** as yellow crystals. To a 10 mL pressure tube a solution of **9** in toluene (SPS dry, 2 mL) and phosphorus selenide (808 mg, 1.75 mmol, 5 equiv.) were added inside the glove box. The suspension was stirred at 120 °C for 72 h under argon atmosphere. The reaction mixture was diluted with THF (SPS dry, 20 mL) and the solution was separated via centrifugation. The solvent was removed under reduced pressure. The formed yellow solid was washed with boiling toluene (3×5 mL) to yield **5** as colorless crystals (96 mg, 0.19 mmol, 54%) decomp. over 240 °C.

^{1}H NMR (THF-d_8, 400 MHz): δ = 7.94 (d, 4H, *J*=8.5 Hz), 7.59 – 7.52 (m, 2H), 7.45 – 7.35 (m, 4H), 7.22 (t, 2H, *J*=7.8 Hz) ppm.

^{13}C NMR (THF-d_8, 101 MHz): δ = 150.23 (d, *J*=14.2 Hz), 132.80, 131.40, 128.57, 128.11, 126.91, 125.18, 124.20, 123.79 (d, *J*=2.1 Hz), 123.59 (d, *J*=3.2 Hz) ppm. ^{31}P NMR (THF-d_8, 162 MHz): δ = 107.65 ppm.

^{77}Se NMR (THF-d_8, 76 MHz): δ = 111.45 (d, *J*=817.1 Hz) ppm.

HRMS (ESI): m/z $[M - K]^-$ calcd. for $C_{20}H_{12}O_2PSe_2^-$: 474.8911; found: 474.8919.

*Diselenophosphoric acid **4***

At −80 °C, potassium diselenophosphate **5** (15.23 mg, 0.03 mmol, 1 equiv.) was dissolved in dry THF-d_8 (0.6 mL) and treated with ethereal hydrogen chloride (2.0 M, 15 µL, 0.03 mmol, 1 equiv.). The formed non-isolable diselenophosphoric acid **4** was directly measured at 180 K.

^{1}H NMR (400 MHz, THF-d_8) δ = 7.87 (d, J = 8.7 Hz, 4H), 7.48 (dd, J = 8.8, 1.3 Hz, 2H), 7.38 – 7.30 (m, 4H), 7.18 – 7.11 (m, 2H).

^{31}P NMR (243 MHz, THF-d_8) δ = 109.72 (d, J = 821.4 Hz).

^{77}Se NMR (114 MHz, THF-d_8) δ = 101.16 (d, J = 823.0 Hz).

*Diselenophosphoric acid hydrochloride **6***

At −80 °C, potassium diselenophosphate **5** (15.23 mg, 0.03 mmol, 1 equiv.) was dissolved in dry THF (2 mL) and treated with ethereal hydrogen chloride (2.0 M, 45 µL, 0.09 mmol, 3 equiv.). The reaction mixture was filtered inside the glovebox and the solvent was removed under reduced pressure. The resulting non-isolable diselenophosphoric acid cation **6** was dissolved in dry THF-d8 (0.6 mL) and measured at 180 K.

^{1}H NMR (600 MHz, THF-d_8) δ = 10.68 (br. s, 3H), 8.52 – 8.20 (m, 4H), 7.96 – 7.33 (m, 8H).

^{31}P NMR (243 MHz, THF-d_8) δ = 109.34 (d, J = 817.0 Hz).

Reactivity Test

Mukaiyama-Mannich reaction and protodesilylation reaction

At room temperature, potassium diselenophosphate **5** (8.85 mg, 0.017 mmol, 0.1 eq.) and imine **13** (36.49 mg, 0.170 mmol, 1.0 eq.) were dissolved in dry toluene (0.6 mL) and treated with ethereal hydrogen chloride (2.0 M, 8.6 µL, 0.017 mmol, 0.1 eq.). The solvents were removed under reduced pressure and toluene-d_8 was added. Silyl acetal **15** (60.22 mg, 0.340 mmol, 2.0 eq.) was added. A closer NMR analysis of the reaction mixture at room temperature revealed

the presence of both Mukaiyama-Mannich reaction product **16** and the protodesilylation product **17**.

Computational Details

Geometry optimization and harmonic vibrational frequency calculations were performed at the B3LYP-D3BJ/6-311++G(d,p) level using the Gaussian 16 revision A03 software.[124] All structures were checked for the absence of imaginary frequencies and for satisfying standard convergence criteria. Solvation effects for **4** were considered implicitly (CPCM model with THF dielectric constant) and explicitly (four THF molecules placed in the proximity of **4**). NMR parameters were calculated using the GIAO approach at the same level of theory. Shielding constants were converted to chemical shift using ^{31}P nuclei shielding for H_3PO_4.

2.5 Acknowledgements

This project was financed by the German Science Foundation (DFG; RTG 2620) project number 426795949. The authors thank Mr. Dominik Kreutzer for his help with experiments with H2Se, Mr. Martin Schmid for the help with phosphorus selenide analysis and Mr. Daniel Raith for proofreading the paper with regard to the English language. Open Access funding enabled and organized by Projekt DEAL.

2.6 References

[1] M. P. van der Helm, B. Klemm, R. Eelkema, *Nat. Rev. Chem.* **2019**, *3*, 491–508.

[2] S. H. Xiang, B. Tan, *Nat. Commun.* **2020**, *11*, 3786.

[3] H. Guo, Y. C. Fan, Z. Sun, Y. Wu, O. Kwon, *Chem. Rev.* **2018**, *118*, 10049–10293.

[4] B. Han, X. H. He, Y. Q. Liu, G. He, C. Peng, J. L. Li, *Chem. Soc. Rev.* **2021**, *50*, 1522–1586.

[5] O. García Mancheño, M. Waser, *European J. Org. Chem.* **2023**, *26*, e202200950.

[6] K. L. Jensen, G. Dickmeiss, H. Jiang, L. Albrecht, K. A. Jørgensen, *Acc. Chem. Res.* **2012**, *45*, 248–264.

[7] K. Brak, E. N. Jacobsen, *Angew. Chemie - Int. Ed.* **2013**, *52*, 534–561.

[8] A. G. Doyle, E. N. Jacobsen, *Chem. Rev.* **2007**, *107*, 5713–5743.

[9] T. Akiyama, *Chem. Rev.* **2007**, *107*, 5744–5758.

[10] T. Akiyama, J. Itoh, K. Yokota, K. Fuchibe, *Angew. Chemie Int. Ed.* **2004**, *43*, 1566–1568.

[11] D. Uraguchi, M. Terada, *J. Am. Chem. Soc.* **2004**, *126*, 5356–5357.

[12] D. Parmar, E. Sugiono, S. Raja, M. Rueping, *Chem. Rev.* **2014**, *114*, 9047–9153.

[13] S. Rajkumar, M. Tang, X. Yang, *Angew. Chemie Int. Ed.* **2020**, *59*, 2333–2337.

[14] Z.-L. Xia, C. Zheng, R.-Q. Xu, S.-L. You, *Nat. Commun.* **2019**, *10*, 3150.

[15] Y. Bin Wang, S. C. Zheng, Y. M. Hu, B. Tan, *Nat. Commun.* **2017**, *8*, 1–9.

[16] T. Schnitzer, A. Budinská, H. Wennemers, *Nat. Catal.* **2020**, *3*, 143–147.

[17] E. Mensah, N. Camasso, W. Kaplan, P. Nagorny, *Angew. Chemie Int. Ed.* **2013**, *52*, 12932–12936.

[18] T. Inukai, T. Kano, K. Maruoka, *Angew. Chemie - Int. Ed.* **2019**, *59*, 2211–2214.

[19] R. I. Storer, D. E. Carrera, Y. Ni, D. W. C. MacMillan, *J. Am. Chem. Soc.* **2006**, *128*, 84–86.

[20] K. Saito, T. Akiyama, *Chem. Commun.* **2012**, *48*, 4573.

[21] M. Rueping, T. Theissmann, M. Stoeckel, A. P. Antonchick, *Org. Biomol. Chem.* **2011**, *9*, 6844.

[22] Q. Yin, S. G. Wang, S. L. You, *Org. Lett.* **2013**, *15*, 2688–2691.

[23] M. Franta, J. Gramüller, P. Dullinger, S. Kaltenberger, D. Horinek, R. M. Gschwind, *Angew. Chemie Int. Ed.* **2023**, e202301183.

[24] B. Peng, J. Ma, J. Guo, Y. Gong, R. Wang, Y. Zhang, J. Zeng, W. W. Chen, K. Ding, B. Zhao, *J. Am. Chem. Soc.* **2022**, *144*, 2853–2860.

[25] G. Caballero-García, J. M. Goodman, *Org. Biomol. Chem.* **2021**, *19*, 9565–9618.

[26] K. Rothermel, M. Žabka, J. Hioe, R. M. Gschwind, *J. Org. Chem.* **2019**, *84*, 13221–13231.

[27] P. S. J. Kaib, L. Schreyer, S. Lee, R. Properzi, B. List, *Angew. Chemie - Int. Ed.* **2016**, *55*, 13200–13203.

[28] T. Steiner, *Angew. Chemie - Int. Ed.* **2002**, *41*, 48–76.

[29] R. Sun, E. Viaud, R. Nomula, J. V. Naubron, N. Daugey, T. Buffeteau, F. Castet, P. Y. Toullec, S. Quideau, P. A. Peixoto, *Angew. Chemie - Int. Ed.* **2023**, e202310436.

[30] B. Q. Gong, W. Y. Chen, B. F. Hu, *Phosphorus. Sulfur. Silicon Relat. Elem.* **1991**, *57*, 87–94.

[31] T. Murai, M. Monzaki, F. Shibahara, *Chem. Lett.* **2007**, *36*, 852–853.

[32] T. Murai, M. Monzaki, T. Katoh, T. Suzuki, T. Akiyama, *Phosphorus, Sulfur Silicon Relat. Elem.* **2010**, *185*, 964–973.

[33] T. Murai, D. Matsuoka, K. Morishita, *J. Am. Chem. Soc.* **2006**, *128*, 4584–4585.

[34] N. I. Zemlyanskii, R. D. Gorak, *J. Gen. Chem. USSR* **1971**, *41*, 1691–1693.

[35] M. V. Kudchadker, R. A. Zingaro, K. J. Irgolic, *Can. J. Chem.* **1968**, *46*, 1415–1424.

[36] M. Klussmann, L. Ratjen, S. Hoffmann, V. Wakchaure, R. Goddard, B. List, *Synlett* **2010**, *2010*, 2189–2192.

[37] R. Blachnik, H.-P. Baldus, P. Lönnecke, B. W. Tattershall, *Angew. Chemie Int. Ed. English* **1991**, *30*, 605–607.

[38] H. Arnold, *Zeitschrift fur Krist. - New Cryst. Struct.* **1986**, *177*, 139–142.

[39] R. Blachnik, J. Matthiesen, A. Müller, H. Nowottnick, H. Reuter, *Zeitschrift fur Krist. - New Cryst. Struct.* **1998**, *213*, 247–248.

[40] R. Blachnik, P. Lönnecke, K. Boldt, B. Engelen, *Acta Crystallogr. Sect. C Cryst. Struct. Commun.* **1994**, *50*, 659–661.

[41] R. Blachnik, J. Matthiesen, A. Müller, H. Nowottnick, H. Reuter, *Zeitschrift fur Krist. - New Cryst. Struct.* **1998**, *213*, 247–248.

[42] K. Olie, *Acta Crystallogr. Sect. B Struct. Crystallogr. Cryst. Chem.* **1971**, *27*, 1459–1460.

[43] L. Roopesh Kumar, N. R. Sagar, K. Divya, C. Madhu, V. V Sureshbabu, *New J. Chem.* **2020**, *44*, 7261–7264.

[44] K. Geisler, A. Jacobs, A. Künzler, M. Mathes, I. Girrleit, B. Zimmermann, E. Bulka, W.-D. Pfeiffer, P. Langer, *Synlett* **2002**, 1983–1986.

[45] B. Y. Winer, S. M. Berry, R. D. Pike, D. C. Bebout, *Polyhedron* **2012**, *48*, 125–130.

[46] H. Duddeck, *Prog. Nucl. Magn. Reson. Spectrosc.* **1995**, *27*, 1–323.

[47] In the literature, ^{31}P-^{77}Se scalar couplings are often reported as negative values.[46] However, since our spectra do not permit the determination of the sign, all scalar coupling are presented as absolute values

[48] N. S. Golubev, R. E. Asfin, S. N. Smirnov, P. M. Tolstoi, *Russ. J. Gen. Chem.* **2006**, *76*, 915–924.

[49] V. V. Mulloyarova, I. S. Giba, M. A. Kostin, G. S. Denisov, I. G. Shenderovich, P. M. Tolstoy, *Phys. Chem. Chem. Phys.* **2018**, *20*, 4901–4910.

[50] T. Kupka, A. Wawer, J. O. Dzicegielewski, P. S. Zacharias, *Fresenius. J. Anal. Chem.* **1991**, *339*, 253–257.

[51] B. G. Janesko, H. C. Fisher, M. J. Bridle, J. L. Montchamp, *J. Org. Chem.* **2015**, *80*, 10025–10032.

[52] V. V. Mulloyarova, I. S. Giba, G. S. Denisov, A. S. Ostras', P. M. Tolstoy, *J. Phys. Chem. A* **2019**, *123*, 6761–6771.

[53] V. V. Mulloyarova, D. O. Ustimchuk, A. Filarowski, P. M. Tolstoy, *Molecules* **2020**, *25*, 1907.

[54] Since the ^{1}H NMR spectrum of the reaction mixture is too crowded to determine individual signals of the components no DOSY measurements could be performed.

[55] S. Berger, S. Braun, H.-O. Kalinowski, in *NMR-Spektroskopie von Nichtmetallen*, George Thieme, Stuttgart, **1996**, p. 205.

[56] J. Michalski, C. Krawiecki, *Rocz. Chem.* **1957**, *31*, 715–716.

[57] C. Krawiecki, J. Michalski, R. A. Y. Jones, A. R. Katritzky, *Rocz. Chem.* **1969**, *43*, 869–879.

[58] L. Riesel, R. Helbing, *ZAAC - J. Inorg. Gen. Chem.* **1992**, *617*, 148–154.

[59] M. K. Kurt Irgolic, Ralph A. Zingaro, *Inorg. Chem.* **2012**, *4*, 8–10.

[60] S. Knapp, Selenophosphoric Acids in Organocatalysis, **2023**.

[61] D. V. Krutin, Diagnostics of Intermolecular Hydrogen Bonds Using 31P and 77Se NMR Spectroscopy, Saint Petersburg State University, **2022**.

[62] M. Žabka, R. M. Gschwind, *Chem. Sci.* **2021**, *12*, 15263–15272.

[63] K. Rothermel, M. Melikian, J. Hioe, J. Greindl, J. Gramüller, M. Žabka, N. Sorgenfrei, T. Hausler, F. Morana, R. M. Gschwind, *Chem. Sci.* **2019**, *10*, 10025–10034.

[64] S. Kobayashi, Y. Mori, J. S. Fossey, M. M. Salter, *Chem. Rev.* **2011**, *111*, 2626–2704.

[65] F. Zhou, H. Yamamoto, *Angew. Chemie* **2016**, *128*, 9116–9120.

[66] 2H belong to the molecule of **6** and 1H – to the excess of HCl (3 equiv. of the latter were utilized to generate **6** from **5**).

[67] Gaussian 16, Revision C.01, M. J. Frisch, G. W. Trucks, H. B. Schlegel, G. E. Scuseria, M. A. Robb, J. R. Cheeseman, G. Scalmani, V. Barone, G. A. Petersson, H. Nakatsuji, X. Li, M. Caricato, A. V. Marenich, J. Bloino, B. G. Janesko, R. Gomperts, B. Mennucci, H. P. Hratchian, J. V. Ortiz, A. F. Izmaylov, J. L. Sonnenberg, D. Williams-Young, F. Ding, F. Lipparini, F. Egidi, J. Goings, B. Peng, A. Petrone, T. Henderson, D. Ranasinghe, V. G. Zakrzewski, J. Gao, N. Rega, G. Zheng, W. Liang, M. Hada, M. Ehara, K. Toyota, R. Fukuda, J. Hasegawa, M. Ishida, T. Nakajima, Y. Honda, O. Kitao, H. Nakai, T. Vreven, K. Throssell, J. A. Montgomery, Jr., J. E. Peralta, F. Ogliaro, M. J. Bearpark, J. J. Heyd, E. N. Brothers, K. N. Kudin, V. N. Staroverov, T. A. Keith, R. Kobayashi, J. Normand, K. Raghavachari, A. P. Rendell, J. C. Burant, S. S. Iyengar, J. Tomasi, M. Cossi, J. M. Millam, M. Klene, C. Adamo, R. Cammi, J. W. Ochterski, R. L. Martin, K. Morokuma, O. Farkas, J. B. Foresman, D. J. Fox, Gaussian, Inc., Wallingford CT, **2016**, https://gaussian.com/citation/..

2.7 Supporting Information

Table S2-1:

Conditions for the preparation of phosphorus selenide and their impact on the reactivity with (*R*)-BINOL

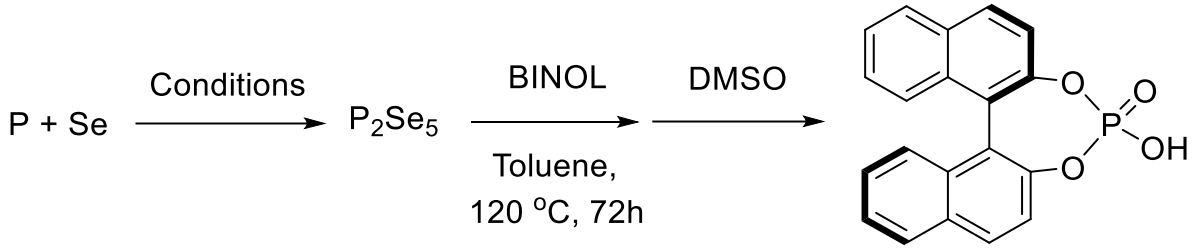

Run	P_2Se_5 synthesis conditions	BINOL conversion
1	fused for 15 min. in a test tube using heat gun (≈650 °C) under Ar atmosphere	70
2	fused for 72 hours in a sealed ampoule in an oven (≈ 500 °C) under Ar atmosphere	75
3	fused for 15 min. under Ar atmosphere using heat gun and afterwards sublimated in vacuum	82

Copies of NMR spectra

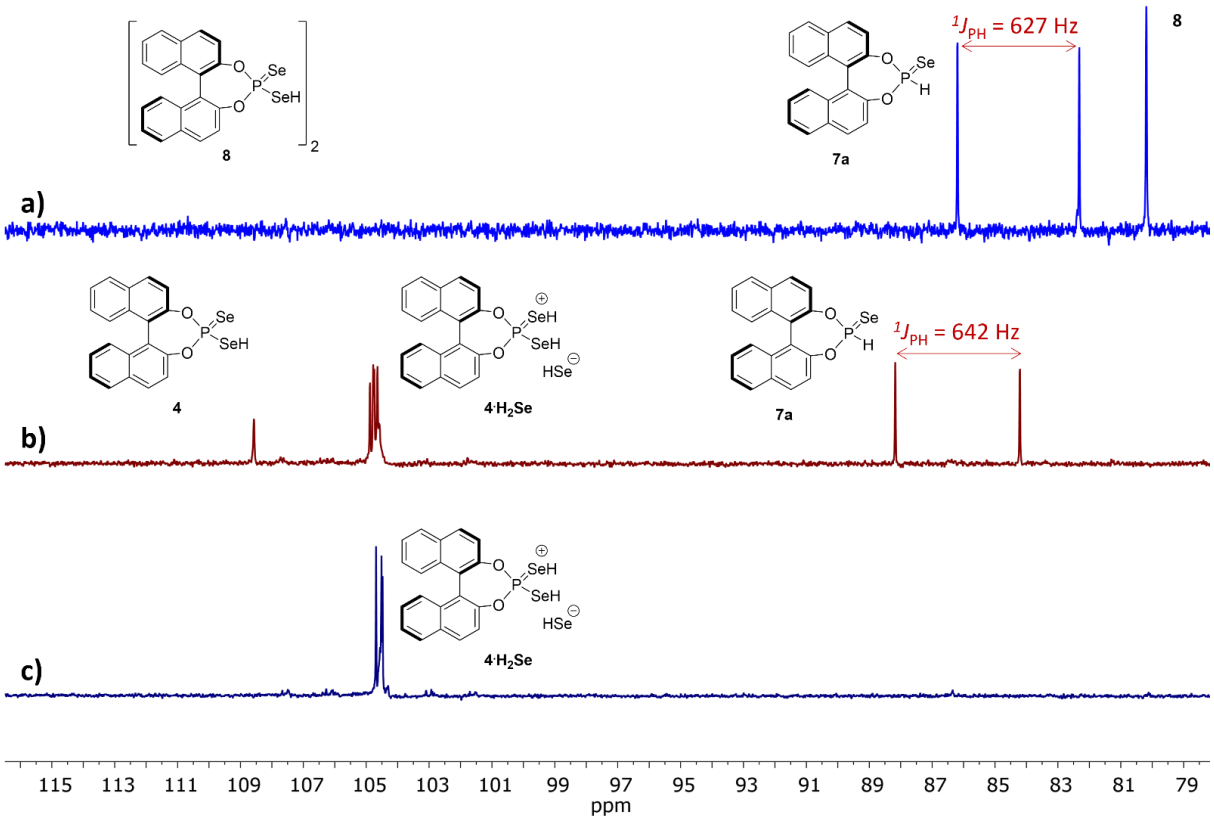

Figure S2-1. (a) ^{31}P NMR spectrum of the crude reaction mixture in toluene, obtained after treatment of BINOL with phosphorus selenide; (b) ^{31}P NMR spectrum of the same mixture after addition of THF: dimeric **8** transforms in monomeric **4**; (c) ^{31}P NMR spectrum of the same mixture after addition of hydrogen selenide in THF: **7a** undergoes oxidative selenation with the formation of **4**·H_2Se.

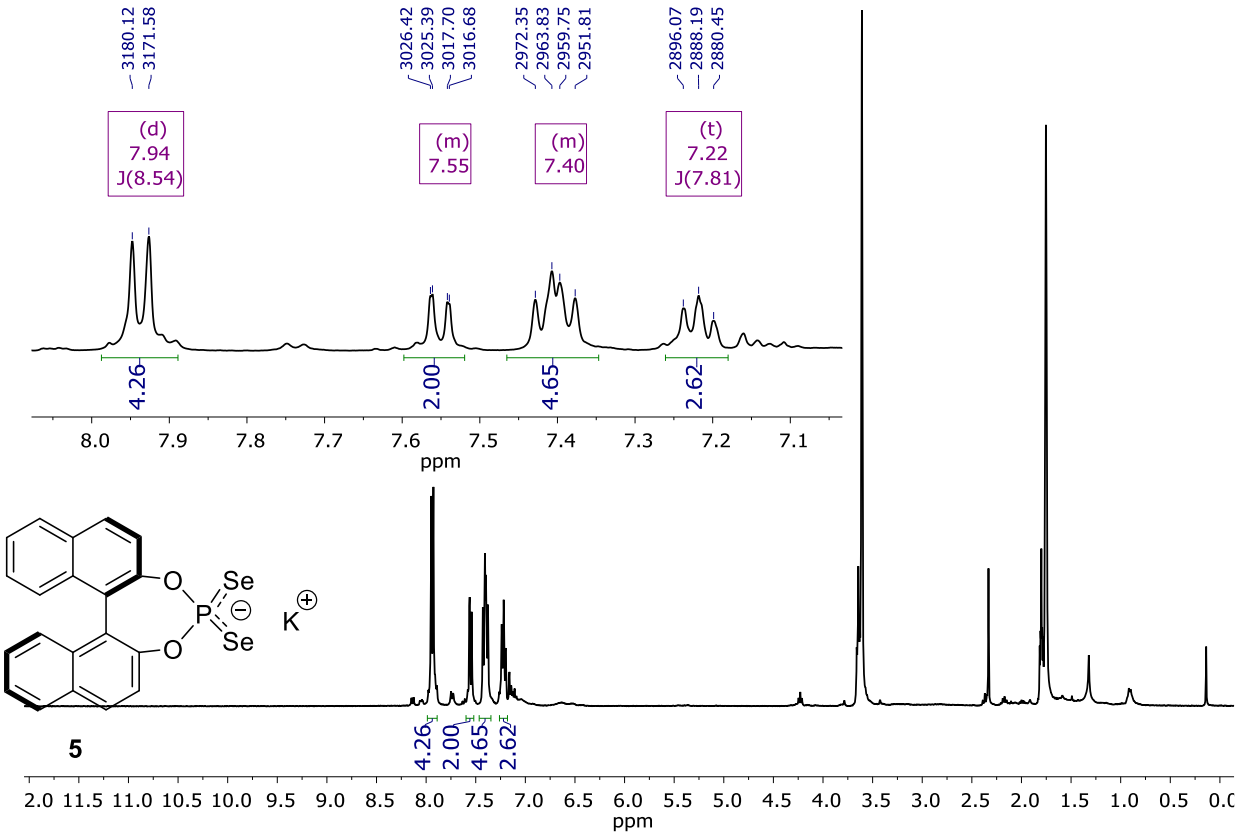

Figure S2-2. ^{1}H NMR spectrum of **5** (THF-d_8, 298 K, 400.1 MHz).

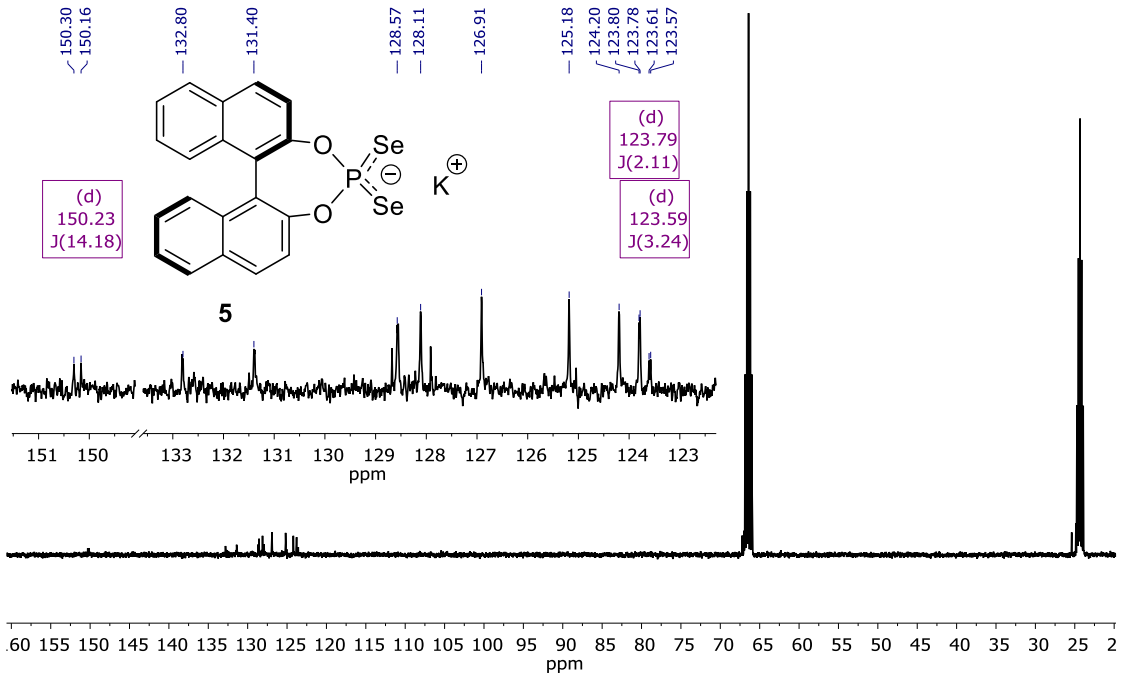

Figure S2-3. ^{13}C NMR spectrum of **5** (THF-d_8, 298 K, 100.6 MHz).

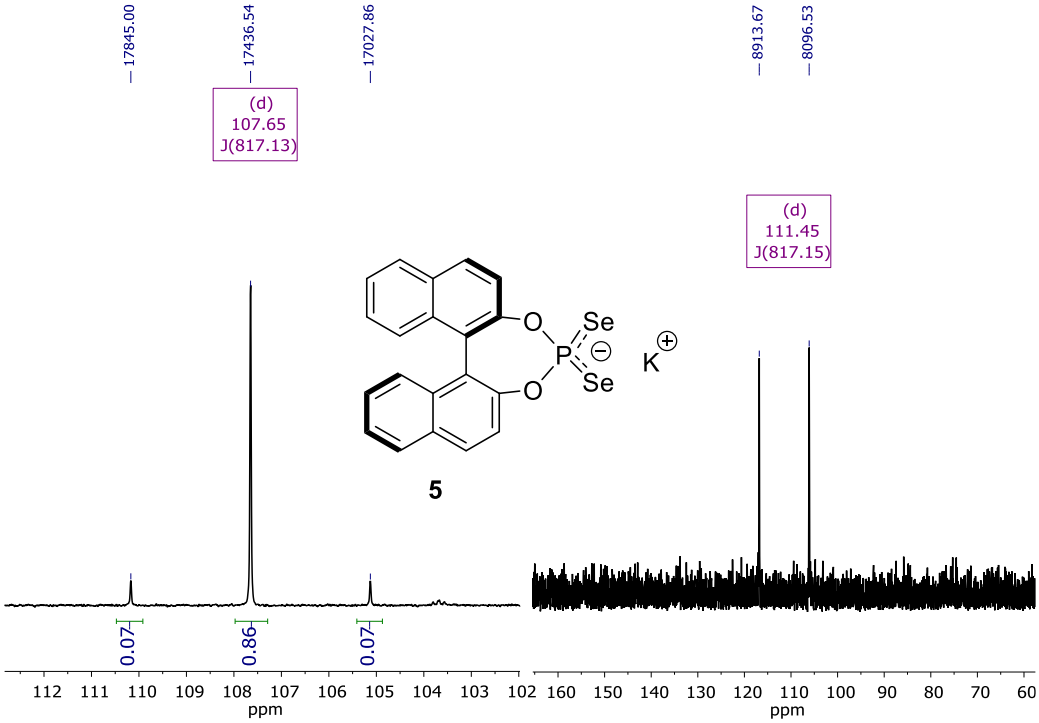

Figure S2-4. ^{31}P (left) and ^{77}Se (right) NMR spectra of **5** (THF-d_8, 298 K, 162.2 MHz for ^{31}P and 76.3 MHz for ^{77}Se).

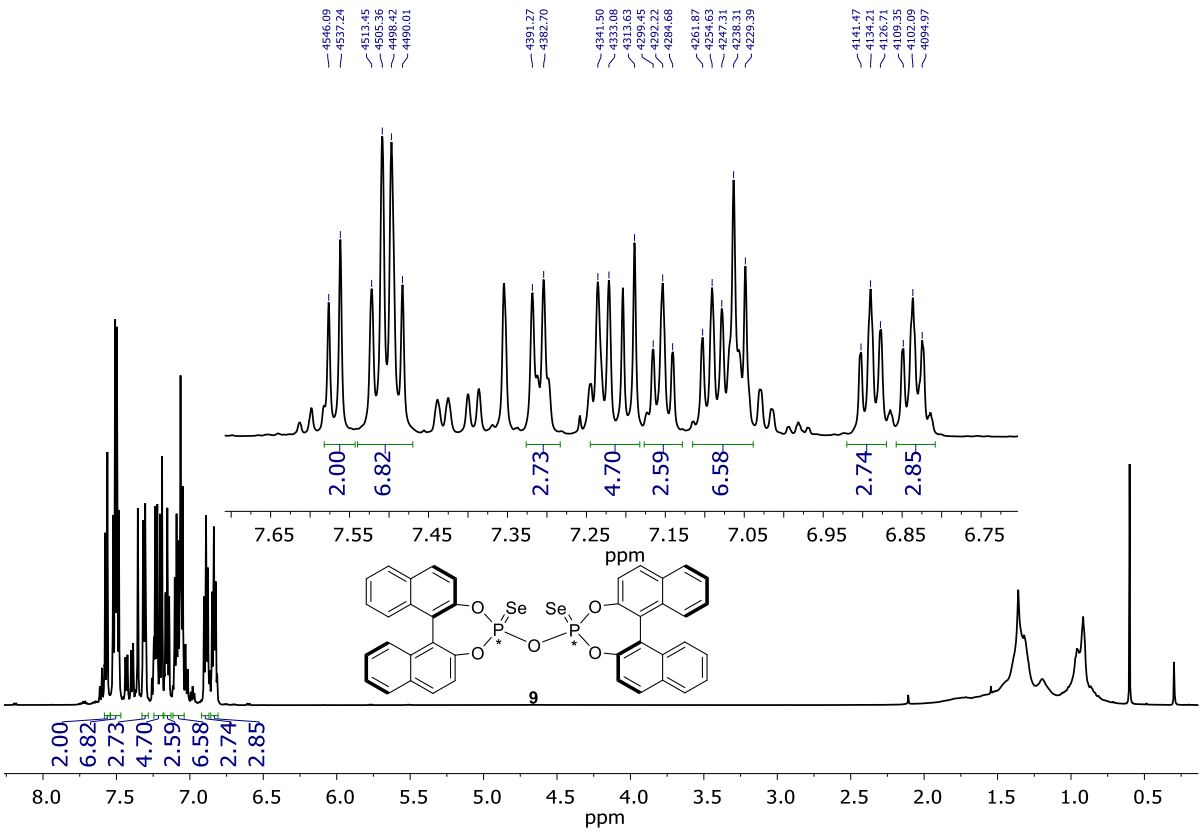

Figure S2-5. ^{1}H NMR spectrum of **9** (benzene-d_6, 298 K, 600.1 MHz).

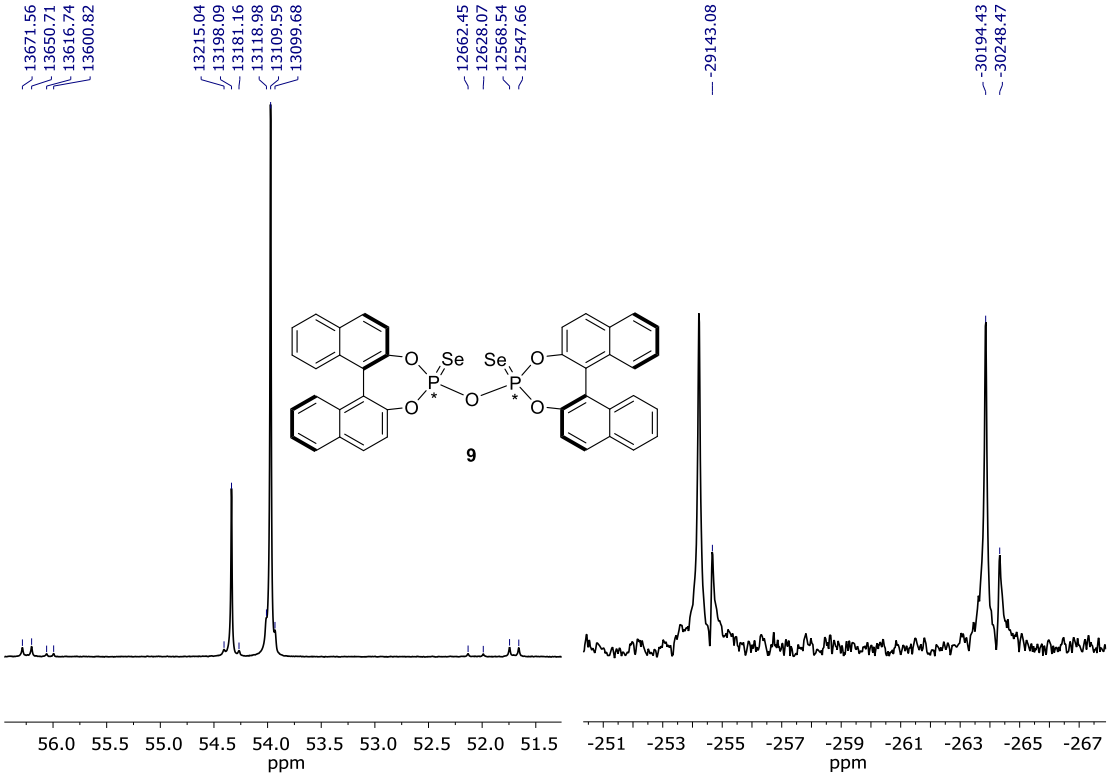

Figure S2-6. ^{31}P (left) and ^{77}Se (right) NMR spectra of **9** (benzene-d_6, 298 K, 242.9 MHz for ^{31}P and 114.5 MHz for ^{77}Se).

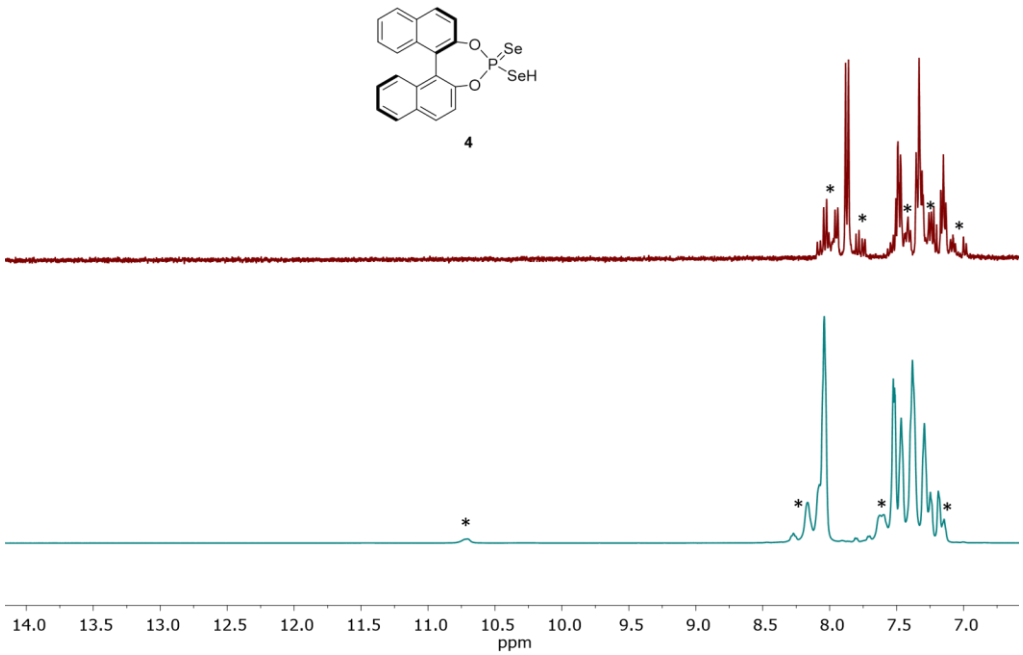

Figure S2-7. ^{1}H NMR spectra of **4** at 298 K(top) and 180 K (bottom) (THF-d_8, 600.1 MHz). The sample is obtained *in-situ* by mixing solution of **5** with 1 equiv. of ethereal solution of HCl. Signals of the decomposition products are marked with *.

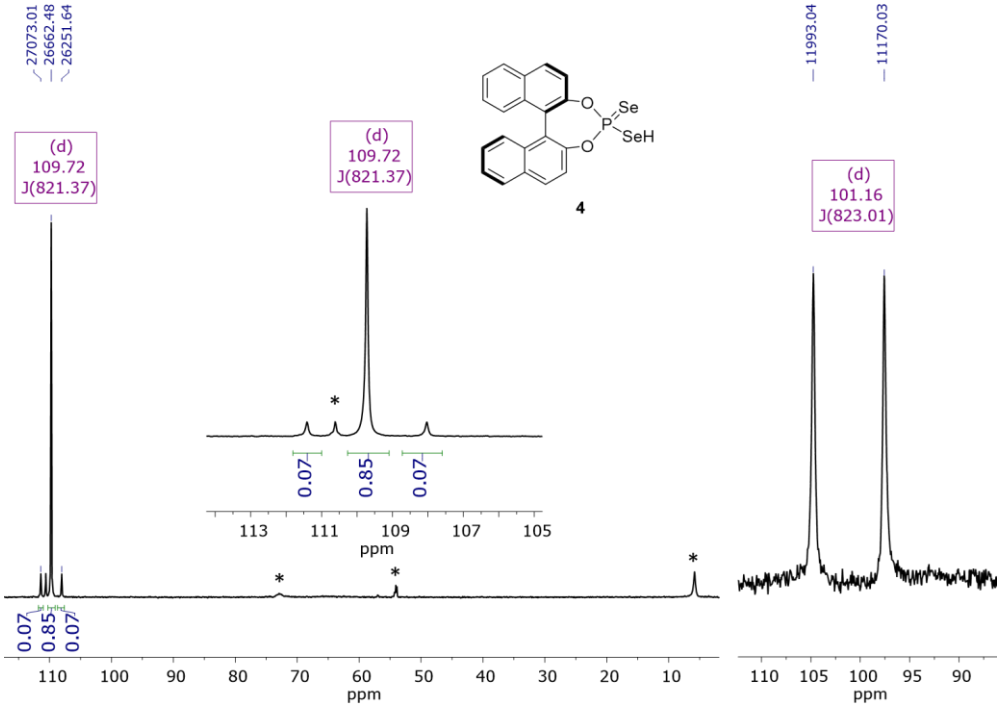

Figure S2-8. ^{31}P (left) and ^{77}Se (right) NMR spectra of **4** (THF-d_8,, 180 K, 242.9 MHz for ^{31}P and 114.5 MHz for ^{77}Se). The sample is obtained *in-situ* by mixing solution of **5** with 1 equiv. of ethereal solution of HCl. Signals of the decomposition products are marked with *.

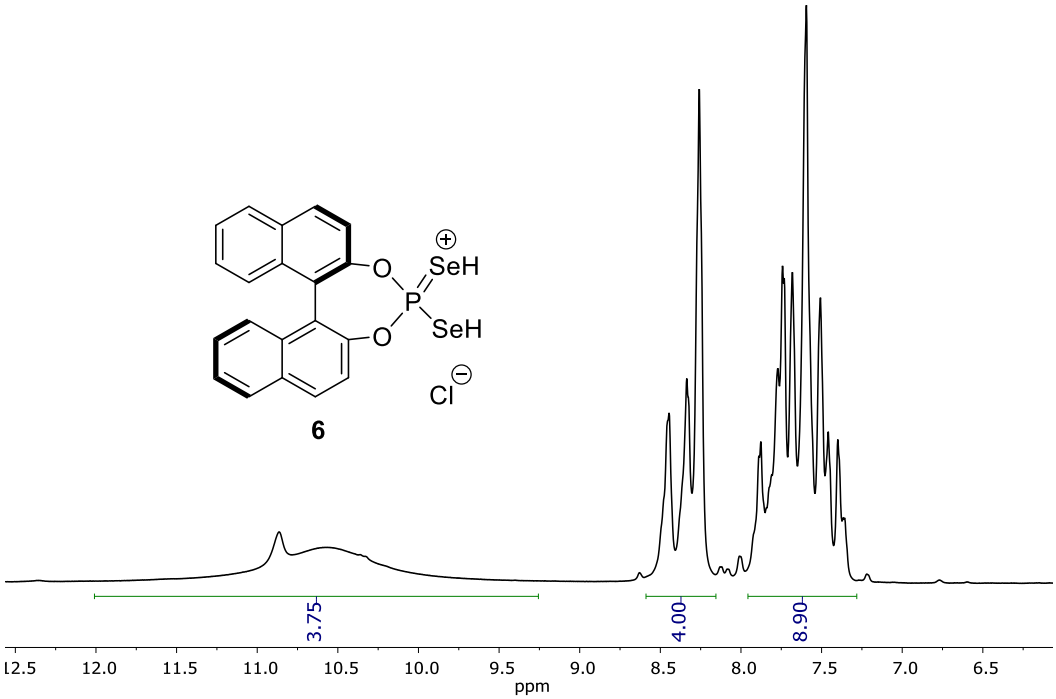

Figure S2-9. ^{1}H NMR spectrum of **6** (THF-d_8, 180 K, 600.1 MHz). The sample is obtained *in-situ* by mixing solution of **5** with 3 equiv. of ethereal solution of HCl.

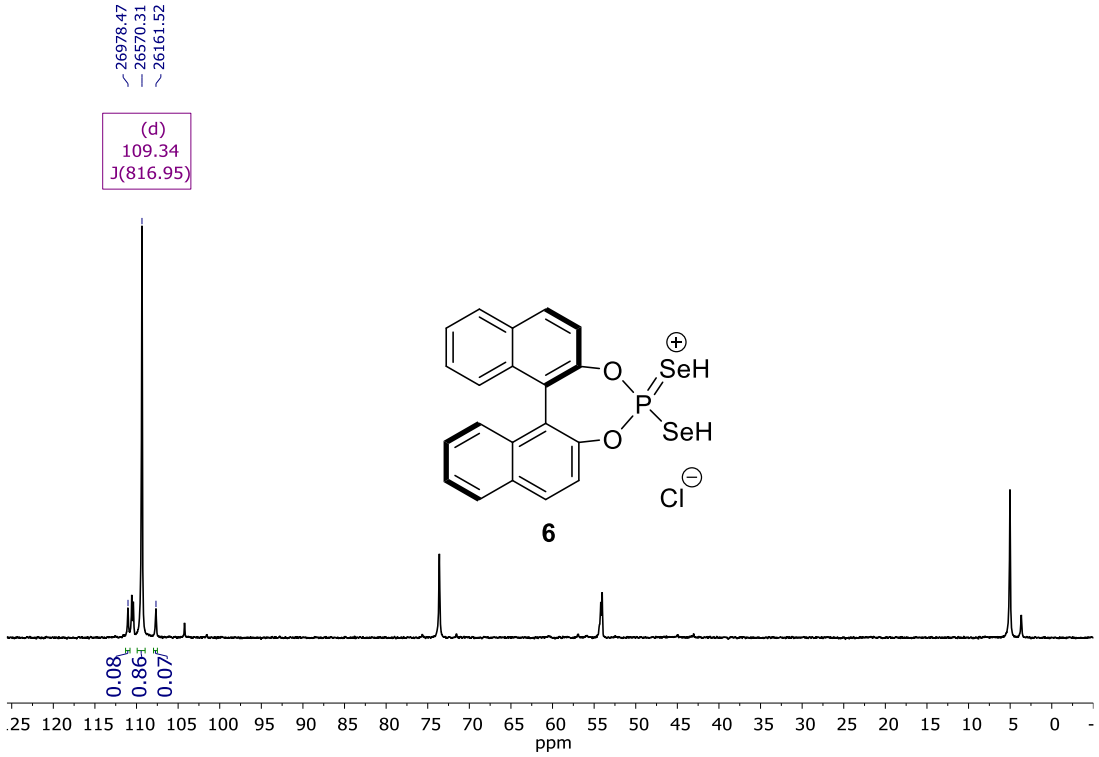

Figure S2-10. ^{1}H NMR spectrum of **6** (THF-d_8, 180 K, 600.1 MHz). The sample is obtained *in-situ* by mixing solution of **5** with 3 equiv. of ethereal solution of HCl.

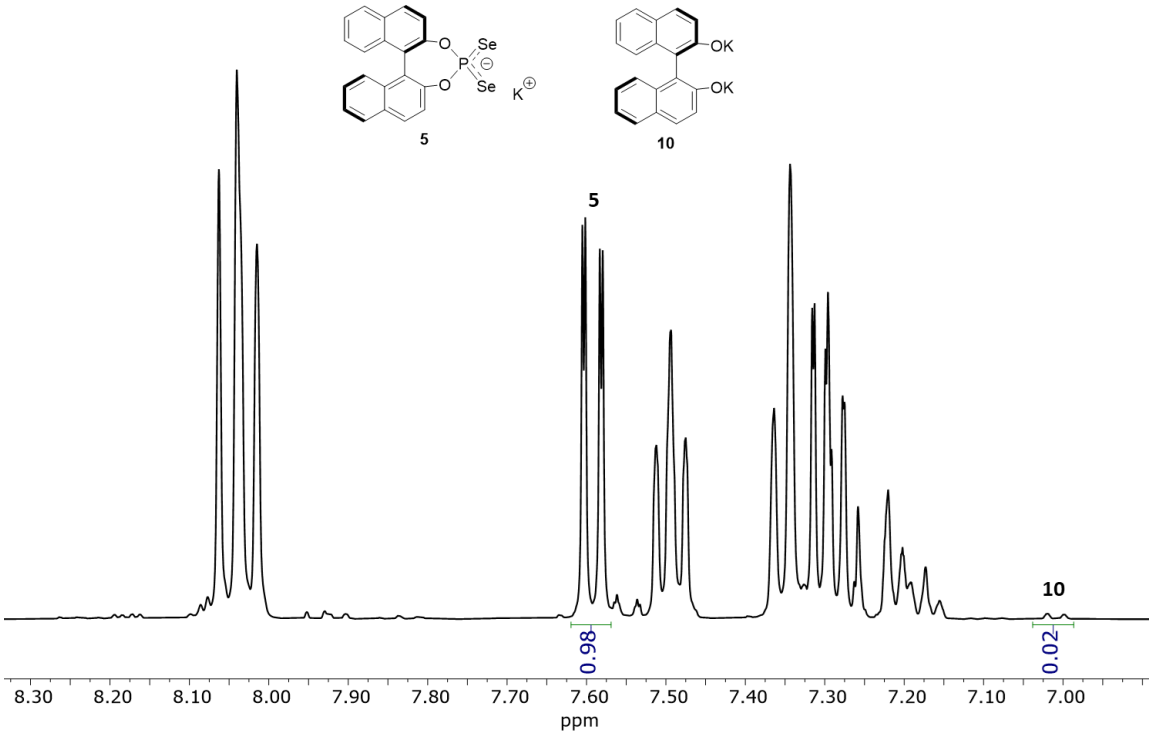

Figure S2-11. ^{1}H NMR spectrum of crude mixture after reaction of BINOLate **10** with phosphorus selenide (CD_3CN, 298 K, 400.1 MHz). Conversion of starting material reaches 98%.

Computational details

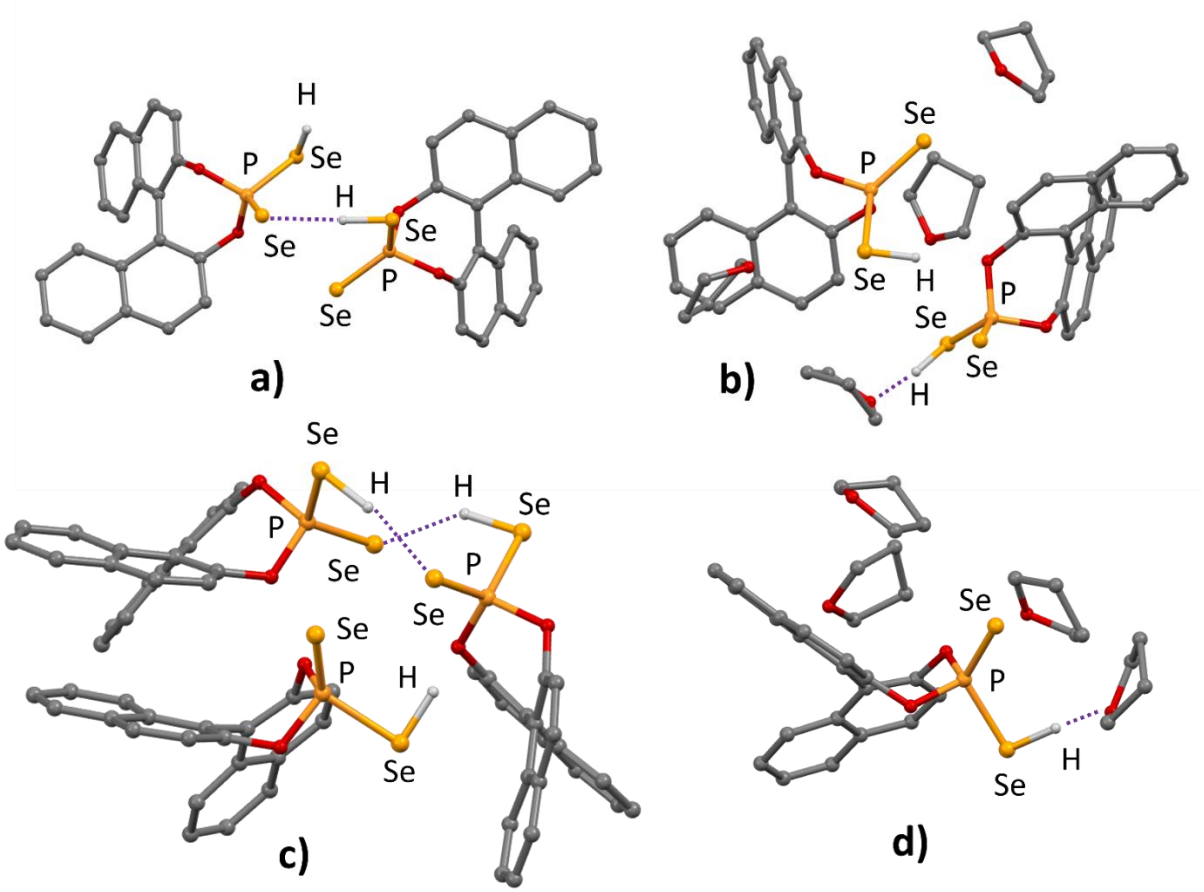

Figure S2-12. Optimized geometries of the dimer **6** in a vacuum (a) and the formation of monomeric **4** in the presence of THF molecules (b), mutual orientation of three molecules of **4** in vacuum (c), monomeric 4 in the presence of THF molecules (d) calculated using B3LYP-D3BJ/6-311++G(d,p) method. Hydrogen atoms (except for SeH) are omitted for clarity.

3 Improved Synthesis of Chiral Diselenophosphoric Acid Catalysts and Introduction of Substituents for Stereoselective Transformations

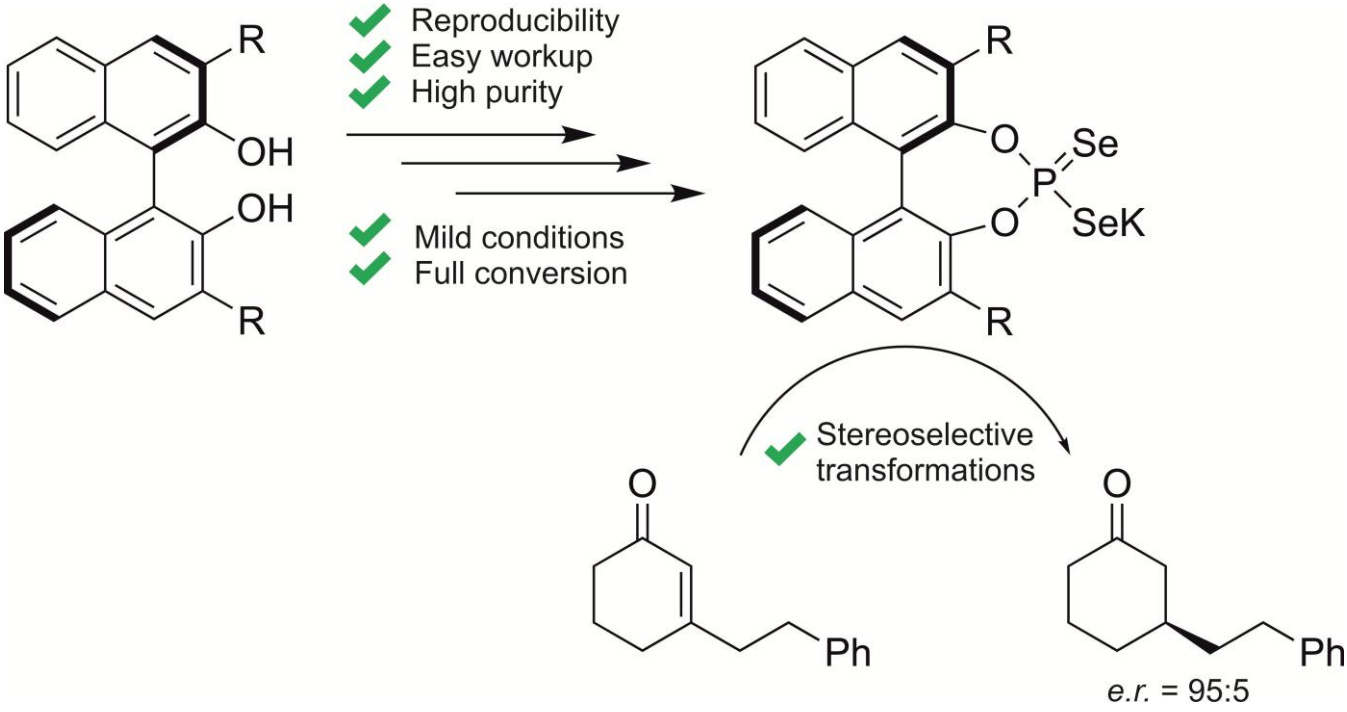

J. Eder, S. Knapp, N. Müller, F. Schmidt, N. Reisinger, J. E. A. Lavarda, A. S. Antonov, B. König, N. Korber, R. M. Gschwind

To be submitted

A) J. Eder planned all experiments, synthesized and analyzed the catalysts. B) S. Knapp synthesized starting materials and performed experiments, assisted by J. E. A. Lavarda. C) N. Müller and B. König planned, performed and analyzed HPLC measurements. D) F. Schmidt and N. Korber provided the potassium selenide reagent. E) N. Reisinger assisted in experiments, crystallization experiments and X-ray analysis. F) A. S. Antonov contributed to the design of experiments and interpretation of data and proofreading of the manuscript. G) R. M. Gschwind contributed to the project's conceptualization, experimental design, data interpretation, manuscript writing and proofreading, and secured funding.

Preliminary version – text and figures may differ from the final manuscript. In the Supporting Information, only the results of this work are displayed.

3.1 Abstract

In contemporary asymmetric organocatalysis, the development of acidic catalysts plays a key role by enabling the activation of diverse substrates. In this study, we present an enhanced and streamlined procedure for the synthesis of 3,3'-disubstituted chiral BINOL-based diselenophosphoric acids (DSA) – promising highly acidic Brønsted catalysts. Our approach is based on the reaction between easily available phosphoroselenoyl chlorides and potassium selenide. This optimized method offers mild reaction conditions, high yields, and great product purity. Additionally, it demonstrates excellent reproducibility, ensures complete conversion, and is highly atom-economic. The improved synthesis successfully yields BINOL-based DSAs as well as VANOL-based DSA, both of which exhibit increased acidity relative to conventional chiral phosphoric acids. The obtained DSAs demonstrate excellent performance in asymmetric transfer hydrogenation of enones, providing enantiomeric ratios (*e.r.*) of up to 95:5. The discovered negative influence of potassium ions on the *e.r.* value is successfully overcome by addition of a complexation reagent to the reaction mixture.

3.2 Introduction

The advanced capabilities of contemporary organic synthesis are largely due to the development of efficient catalytic methods. Metal-free organocatalysis, as an essential branch of asymmetric catalysis, has played a crucial role in advancing the modern synthesis of complex chiral molecules.[1–3] Within the diverse areas of organocatalysis, a range of non-covalent interactions, including hydrogen bonds, as well as electrostatic and steric effects, are effectively utilized and integrated.[4] A significant advancement in metal-free ion pair catalysis was the introduction of chiral phosphoric acid (CPA) catalysts featuring a 1,1'-bi-2-naphthyl (BINOL) backbone (Figure 1).[5,6]

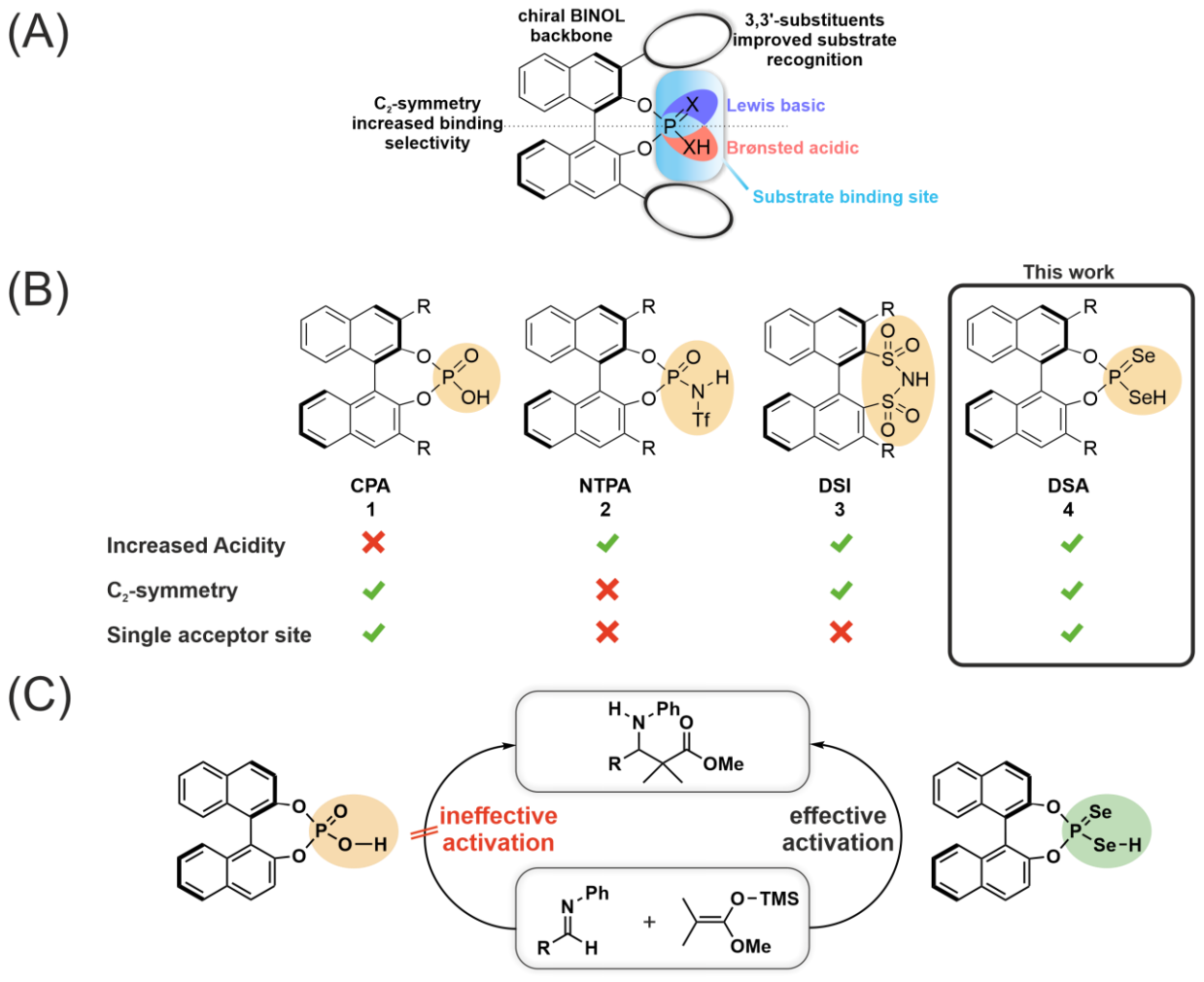

Figure 3-1: (A) Structure of a C_2-symmetric BINOL-based chiral phosphoric acid catalyst. The axial chirality of the BINOL-backbone alongside the bulky 3,3'-substituents create an active site guiding the reactants into a specific orientation. The phosphoric acid group functions as bifunctional scavenger, allowing activation of both electrophiles and nucleophiles. (B) Comparison of different organocatalysts. DSAs resembles the structural features of CPAs, such as C_2-symmetry and a single acceptor site, and show enhanced acidity. (C) Increased reactivity of DSAs was previously shown in the context of a Mukaiyama-Mannich reaction.

These chiral Brønsted acids are widely recognized for their broad substrate compatibility, excellent stereoselectivity, and ability to deliver high yields.[7] They have been successfully employed in a variety of stereoselective reactions, such as inter- and intramolecular heterocyclizations, Mannich-reactions, Strecker reactions, transfer hydrogenations, and many others. [8–13]

The exceptional performance of BINOL-based CPA catalysts can be attributed to their unique structural features (see Figure 3-1, A., X = O). These catalysts are characterized by an axially chiral BINOL backbone, C_2-symmetry, variable 3,3'-substituents, and a bifunctional phosphoric acid group. The axial chirality of the BINOL backbone is essential because it enables the CPA to distinguish between the enantiotopic faces of substrates. This occurs through the formation of specific hydrogen bonds, enabling stereochemical control of the reaction.[14,15] The bulky 3,3'-substituents introduce steric hindrance around the active site, effectively shielding one face of the substrate, influencing both the yield and the enantiomeric excess of the reactions.[16,17] The Brønsted acidic P-O-H group serves as a scavenger through hydrogen bonding. Simultaneously, the phosphoryl oxygen (P=O) in the catalyst exhibits Lewis basicity, providing the catalyst with dual functionality. This dual functionality is crucial, as it enables the activation of both the substrate and the reagent, thereby facilitating a broad range of reactions with high efficiency and selectivity.[15]

CPAs facilitate a wide range of reactions, but their relatively moderate acidity limits their application primarily to basic substrates such as ketimines or aziridenes.[18] Since increased catalyst acidity is often associated with enhanced reactivity,[19,20] numerous efforts over the past two decades have focused on modifying BINOL-based catalysts to expand the scope of asymmetric organocatalysis. Since then, researchers have developed a variety of new chiral "superacids"[27] with enhanced acidity, like *N*-triflylphosphoramides NTPAs **2**, disulfonimides DSIs **3**, and others (see Figure 3-1, B.).[21–24] These modifications have indeed improved the acidity of the catalysts and expanded their ability to activate otherwise unreactive substrates. However, these highly acidic catalysts introduce new complications, such as the possibility of formation of multiple intermediate structures and transition states due to the presence of multiple hydrogen bond acceptors.[25,26] Additionally, the substitution of the OH group with more complex functionalities disrupts the favorable C_2-symmetry. As a result, these acids provide imperfect enantiomeric excess values in some cases.[18]

To address this challenge, we developed a first chiral diselenophosphoric acid **DSA 4** (R=H) in our previous work (see Figure 3-2, previous work).[24] The replacement of the oxygen atoms with selenium not only enhances its acidity but also preserves the C_2-symmetry. In addition to these advantages, our DSA catalyst features only a single hydrogen bond acceptor site. The enhanced acidity and streamlined design of the DSA catalyst enable it to effectively activate substrates that are typically too inert for traditional CPAs. For instance, our DSA catalyst successfully activates certain aldimines which are usually challenging for classic CPAs (see Figure 3-1, C.).[21,27] Through this innovative approach, we have expanded the range of substrates that can be efficiently processed, offering new possibilities for catalytic applications.

Although we have already developed a synthetic route achieving up to 98% NMR yield of the unsubstituted potassium salts of a BINOL-based DSA (DSA-K), the introduction of 3,3'-substituents remained a challenge (see Figure 3-2, previous work). While the reaction showed high selectivity, the reactivity was dramatically decreased. This could be due to the bulkiness of the 3,3'-substituents which prevents efficient interaction with the polymeric phosphorus selenide.

Therefore, in this study, we present an improved and simplified synthesis for DSA-K **6** that delivers excellent NMR yields, high isolated yields, and allows for a range of different 3,3'-substituents (see Figure 3-2, this work, A.). This new approach not only improves efficiency but also broadens the scope of potential applications by accommodating diverse structural variations. Furthermore, the synthesis proceeds under very mild conditions and is completed quickly. The handling and workup are straightforward, ensuring high reproducibility and reduced chemical waste. Interestingly, the crystal structure of a DSA-K showed dimeric aggregation. Thereby, the dimerization occurs *via* potassium, which is coordinated to the selenium atoms of one DSA molecule and the aromatic ring of the 3,3'-substituent of the other one (see Figure 3-2, B.). Furthermore, in this work, the first enantioselective transformation catalyzed by chiral diselenophosphoric acids is reported, proofing its applicability in asymmetric ion-pair catalysis (see Figure 3-3, C.). Notably, it has been shown that DSA-K **6** can be easily transformed into its acid counterpart **4** by addition of ethereal hydrogen chloride solution.[24] Due to the high reactivity of **4**, the catalyst is stored as **6** and only prepared *in situ*, and is therefore displayed as the potassium salt **6** here.

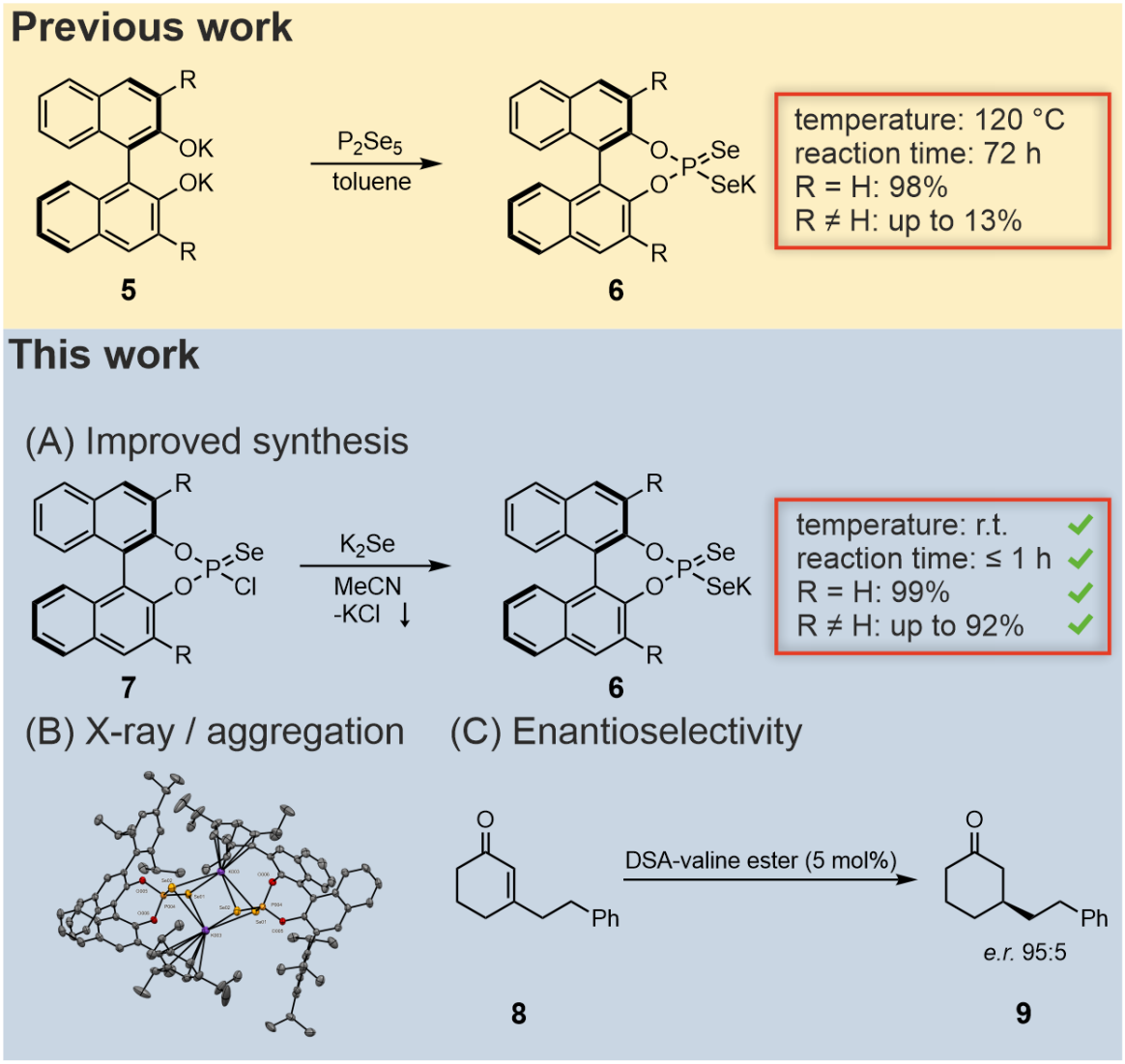

Figure 3-2: Previous work introduced a synthesis for DSA-K with R = H. This work not only improved the synthesis to mild conditions but also offers access to R ≠ H systems (A), provides X-ray data which shows dimeric aggregation (B) and incorporates successful selectivity studies of DSA-catalysts (C).

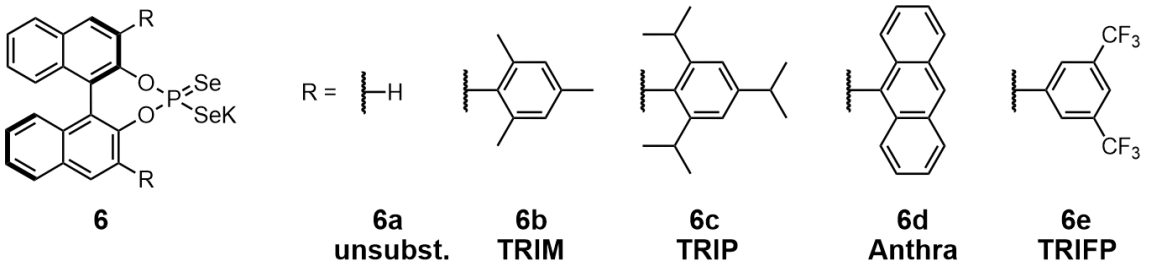

Figure 3-3: Various model systems of DSA-K, including unsubstituted **6a**, 2,4,6-trimethylphenyl **6b**, 2,4,6-triisopropylphenyl **6c**, 9-anthracenyl **6d**, and 3,5-trifluoromethylphenyl **6e** derivatives. These substituents vary in their electronical and steric properties, enabling fine-tuning of the active center.

Variation in 3,3'-substituents plays a crucial role in fine-tuning the size of the active center. This is particularly intriguing because selenium, being bulkier than oxygen, may lead to increased pocket angles. At the same time, the key advantage of selenium is its beneficial properties for NMR spectroscopy, in contrast to oxygen, which exhibits unfavorable characteristics in this regard. Incorporating selenium into DSA catalysts enables advanced spectroscopic analysis by utilizing the ^{77}Se isotope. Firstly, ^{77}Se has a natural abundance of 7.58%, which, while moderate, is sufficient for practical applications. Secondly, it possesses a positive gyromagnetic ratio, making it highly suitable for magnetic resonance studies. Most importantly, ^{77}Se is a non-quadrupolar nucleus, meaning it avoids quadrupolar broadening, a common issue that complicates NMR signals. These properties make ^{77}Se a powerful tool for investigating reaction mechanisms, particularly those involving DSA catalysts. Furthermore, selenium's direct participation in hydrogen bonding makes it highly sensitive to its local environment. This sensitivity is reflected in its coupling constants, allowing for the detection of subtle structural changes. By analyzing ^{77}Se satellites in ^{31}P spectra, researchers can gain detailed insights into reaction mechanisms, shedding light on molecular-level transformations in DSA-catalyzed processes.

3.3 Results and Discussion

In our previous work we have demonstrated full conversion of potassium (*R*)-BINOLate to DSA **4a** using phosphorus selenide with high reproducibility. In this study we attempted to expand this approach for the synthesis of 3,3'-substituted DSAs **4b-e**. Although the utilization of 3,3'-substituted BINOLates also showed high selectivity, the reactivity was notably worse (up to 13%, see SI Figure S3-1) not allowing preparative access to **4b-e**. We assume that the steric hindrance provided by the 3,3'-substituents limits the interaction of the BINOLate and the polymeric phosphorus selenide reagent.

In response to the limitations of the previous approach, we developed a novel synthetic pathway to access DSAs **4**. This new method involves the treatment of phosphoroselenoyl chlorides **7** with the monomeric potassium selenide reagent, offering a more efficient and streamlined process (see Table 3-1). Phosphoroselenoyl chlorides **7** can be synthesized by reacting BINOL **5** with phosphorus trichloride and elemental selenium, using triethylamine as a base to facilitate the reaction.[28] The use of phosphoroselenoyl chlorides **7** eliminates the need for complex reagents like polymeric phosphorus selenide, simplifying the overall reaction conditions. The subsequent treatment of the phosphoroselenoyl chloride with potassium selenide - a reagent that is stable and can be easily stored under an argon atmosphere - provides direct access to the potassium salt of diselenophosphoric acid **6** (DSA-K). During this transformation, potassium chloride is generated as the sole by-product.

Consequently, the reaction was subjected to screening and optimization of its parameters.

Table 3-1: Optimization of DSA-K **6a** synthesis.

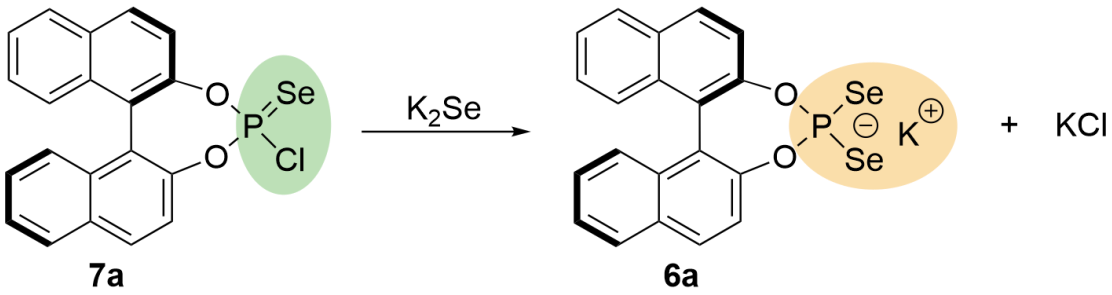

7a **6a**

Run	*Solvent*	*K_2Se, equiv.*	*T, °C*	*Time, h*	*NMR yield, %*
1	toluene	1	120	72	76
2	toluene	2	120	72	94
3	toluene	5	120	72	70
4	THF	1	70	72	78
5	MeCN	1	80	72	87
6	THF	2	70	72	97
7	***MeCN***	***2***	***80***	***72***	***99***
8	MeCN	2	80	18	98
9	MeCN	2	60	18	98
10	MeCN	2	25	18	98
11	***MeCN***	***2***	***25***	***10 min***	***97***

The initial experiment closely mirrored the conditions of previous studies,[24] employing high temperatures in toluene and extended reaction times (Run 1), which resulted in a 76% NMR yield. Increasing the amount of potassium selenide to 2 equivalents improved the yield to 94% (Run 2), while a further increase to 5 equivalents led to a notable decline (70%, Run 3). Next, a solvent screening was conducted, revealing MeCN as the most effective choice (Runs 4 and 5). For both THF and MeCN, the use of 2 equivalents of potassium selenide yielded the best results (Runs 6 and 7), with acetonitrile achieving an NMR yield of 99%. Since the solvent change coincided with a reduction in reaction temperature, this parameter - along with reaction time - was systematically optimized (Runs 8–11). The study demonstrated that the reaction could proceed efficiently even at room temperature, underscoring the robustness of the optimized conditions. This advancement enables lower-energy, faster reactions while maintaining excellent product yields. The new approach enhances control over the reaction process, reduces the dependence on high temperatures, and minimizes the reaction time to 10 min. Additionally, the improved method streamlines handling and workup, making the process more practical and reproducible for future catalytic applications. Using these optimized conditions, various substituted DSA-Ks **6** were successfully synthesized, achieving isolated yields of 86–92%. Keeping in mind the bulkiness of 3,3'-substituted **7** in a typical experiment, the reaction mixture was kept for 1 h to ensure full conversion (see experimental part for details).

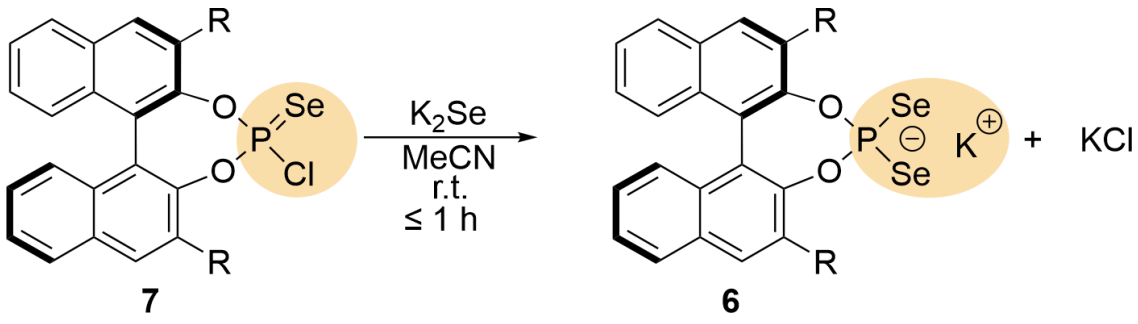

Product	H, **6a**	TRIM, **6b**	TRIP, **6c**	Anthra, **6d**	TRIFP, **6e**
isolated Yield	92%	86%	92%	90%	88%

Figure 3-4: Screening of different 3,3'-substituents with isolated yields of up to 92%.

Additionally, we have found that our novel procedure can also be effectively applied to other asymmetric diols such as VANOL – a known ligand in Lewis acid catalysis (for details, see SI Figure S3-2).[29,30]

3.4 First selectivity tests

Since the reactivity of the DSA catalyst was established in previous studies,[24] this work focuses on selectivity, enabled by the introduction of 3,3'-substituents. The applicability of DSAs in ion pair catalysis was assessed in an asymmetric transfer hydrogenation (ATH) with an α,β-unsatured ketone **8** as substrate and Hantzsch' ester **10** as hydride donor. Previous studies by the List group demonstrated that combining a chiral anion with a chiral cation, as employed in asymmetric counteranion-directed catalysis (ACDC), can generate highly active catalysts for this transformation.[31] Using a TRIP-CPA / valine ester catalyst **11**, they achieved excellent enantioselectivites with enantiomeric ratios (*e.r.*) of up to 98:2 (see Figure 3-5). This highly efficient reaction, which has been successfully established with CPA, was strategically selected for a proof-of-principle study. By testing our catalyst under these conditions, we aimed to demonstrate that the increased bulkiness of selenium compared to oxygen does not compromise key structural advantages, such as C_2 symmetry.

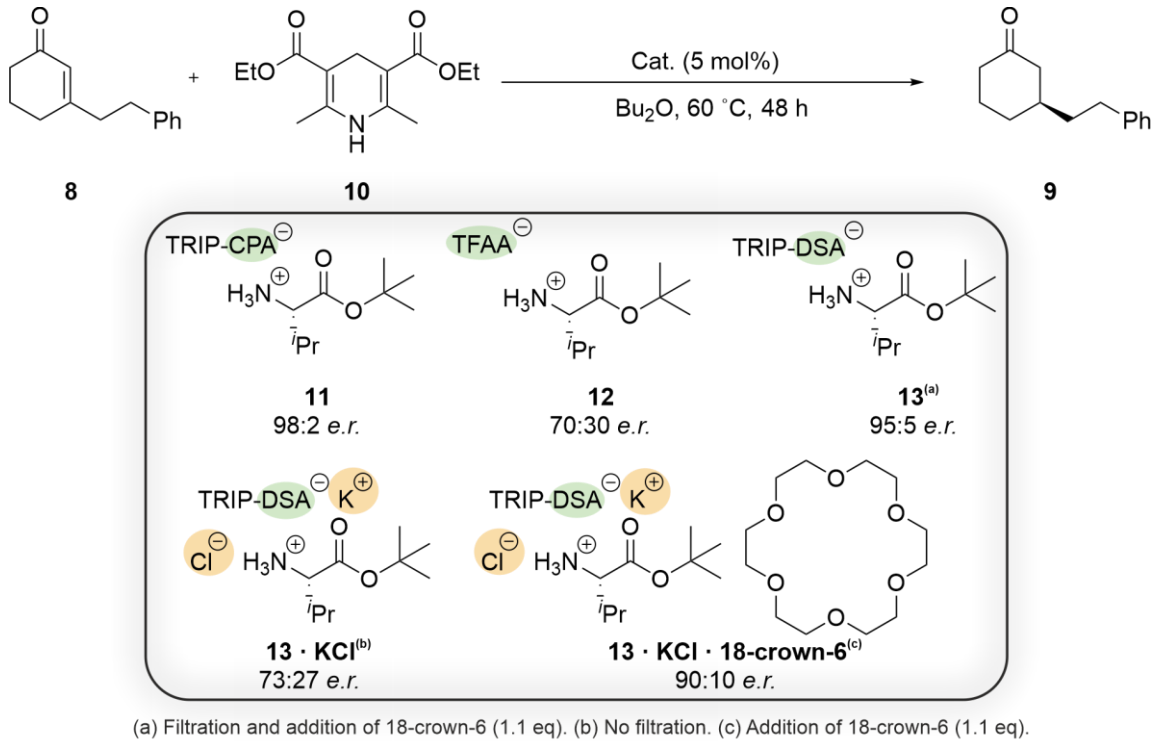

Figure 3-5: ATH of an α,β-unsatured ketone **8** with Hantzsch' ester **10** as hydride donor with different catalysts. Catalyst **13** shows comparable results to the established CPA-valine ester catalyst **11**.

To enable comparison, a TRIP-DSA valine ester catalyst **13** was prepared by combining valine ester hydrochloride with **6c**, followed by filtration and the addition of 18-crown-6 to remove most of the resulting KCl. This catalyst achieved an enantiomeric ratio of 95:5 for product **9**,

demonstrating a performance comparable to that of **11**. However, when KCl was not removed, the performance of **13·KCl** dropped significantly, yielding an *e.r.* of 73:27.

We propose that in the presence of KCl, the contact ion pair of **13** is disrupted due to the competitive coordination of the DSA anion with the potassium cation (see Figure 3-6). This interference likely forces the reaction to occur outside the chiral catalytic pocket, leading to a dramatic decrease in enantioselectivity. Supporting this hypothesis, the use of catalyst **12**, which consists of an achiral anion such as trifluoroacetic acid (TFAA) and valine ester, resulted in a similar decline in enantioselectivity, yielding an *e.r.* of 70:30.

Notably, adding 18-crown-6 to the reaction mixture containing KCl improved the *e.r.* to 90:10, suggesting that even stronger complexation agents, such as [2.2.2]-cryptand, accompanied by initial removal of KCl by filtration, could further enhance both reactivity and selectivity.

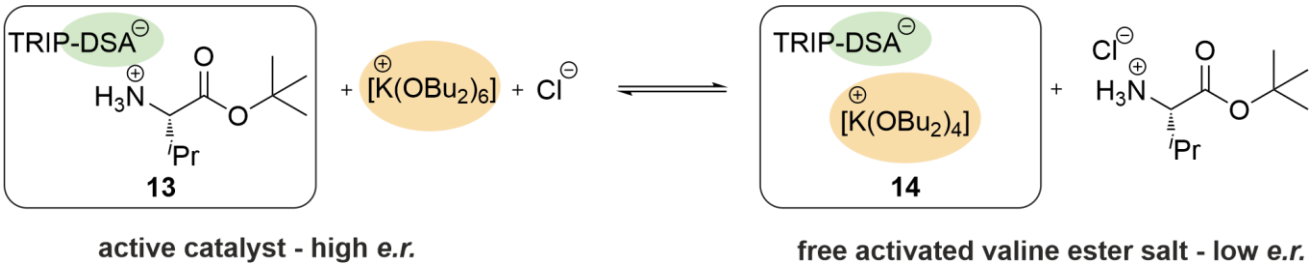

Figure 3-6: Catalyst de-activation by salt metathesis of **13** with solvated potassium chloride. The resulting free activated valine ester salt decreases *e.r.*

3.5 Conclusion

3,3'-Substituted BINOL-based diselenophosphoric acids represent a promising scaffold for enantioselective ion pair catalysis, offering exceptional acidity, C_2-symmetry, and a single acceptor site. This study explores their efficient synthesis and initial reactivity in catalytic applications. Building upon previous work, we identified limitations in our original synthetic route, which involved potassium BINOLate and phosphorus selenide, as it proved unsuitable for substituted derivatives. To overcome this challenge, we developed an improved and straightforward synthetic approach. By combining phosphoroselenoyl chlorides and potassium selenide under mild reaction conditions, we successfully synthesized various DSA-K derivatives **6a-e** with excellent yields, reproducibility, and purity.

While free DSAs are highly reactive and thus prone to oxidation and hydrolysis, their salts demonstrate excellent stability for catalytic applications. We have demonstrated that DSA-K **6c**, combined with valine ester chloride, forms an active catalyst **13**. This catalyst allows to achieve *e.r.* in asymmetric transfer hydrogenation reaction comparable to the previously published TRIP-CPA valine ester system **11**. Notably, the formation of KCl during the generation of catalyst **13** significantly diminished both *e.r.* and reactivity, highlighting the importance of rigorous KCl removal. This issue was successfully overcome by initial filtration of the solution of **13** and addition of 18-crown-6 to bind traces of potassium ions present in solution.

Overall, this work introduces a novel and efficient synthetic route to 3,3'-substituted BINOL-based diselenophosphoric acids (DSAs), which exhibit superior acidity compared to CPAs while retaining C_2 symmetry and a single acceptor site. We developed an enhanced pathway for their preparation and demonstrated their effectiveness in stereoselective transformations. These advancements position DSAs as highly promising tools for enantioselective ion pair catalysis, facilitating their broader application in both synthetic and mechanistic studies.

3.6 Experimental section

General

Toluene, acetonitrile and THF were dried by the mbraun solvent purification system SPS 5.

Liquid-state NMR experiments were either performed using a Bruker Avance III HD NMR spectrometer (600.1 MHz for ^{1}H) equipped with a 5 mm triple resonance broadband inverse probe with ^{19}F-selective channel (TBI-F) with z gradient or a Bruker Avance III HD 400.1 MHz spectrometer with a 5 mm BBO BB-^{1}H/D probe. Chemical shifts are referenced to TMS or solvent for ^{1}H and ^{13}C, to H_3PO_4 (85% in H_2O) for ^{31}P and to Me_2Se for ^{77}Se. Spectrometer control was performed by Bruker Software TopSpin 3.2 PL 7.

Mass-spectra were obtained either on a Jeol AccuTOF GCX or an Agilent Q-TOF 6540 UHD. Methanol, DCM or chloroform were used as the solvents.

Synthesis

Phosphoroselenoyl chlorides[28]

The 3,3´-substituted BINOL derivative (1 equiv.) as well as grey selenium (1 equiv.) were weighed in and transferred under argon atmosphere into a flame dried pressure tube containing a magnetic stir bar. Upon addition of PCl_3 (1 equiv.), everything was dissolved in SPS dry toluene (1.2 mL). Then, NEt_3 (2 equiv.) was added and the reaction mixture was stirred at 110 °C for 24 h. The products were obtained after column chromatography as colourless or yellowish powders with up to 81 % yield. (for details see SI).

Potassium Diselenophosphates

Inside the glovebox, phosphoroselenoyl chlorides (1 equiv.) and potassium selenide (2 equiv.) were weighed in and acetonitrile (2 mL, SPS dry) was added. The mixture was stirred at room temperature. After 1 h, the mixture was centrifuged (4000 rpm, 5 min) and the precipitate was filtered off. The solvent was evaporated under reduced pressure to yield potassium diselenophosphates (86-92%) as yellowish solid.

Valine ester chloride

Valine ester (1 equiv.) was dissolved in diethyl ether (1 mL). The solution was treated with an ethereal solution of hydrogen chloride (1 equiv.) and stirred for 10 minutes at room temperature. Then, the solvent was removed under reduced pressure yielding the product as white solid (99%).

TRIP-DSA · valine ester complex **13**

Inside the glovebox, **6c** (1 equiv.) and valine ester chloride (1 equiv.) were weighed in and dissolved in THF (1 mL, SPS dry). The mixture was stirred for 10 min at room temperature. The formed potassium chloride was filtered off and the solvent was evaporated under reduced pressure yielding the activated catalyst **13** as yellowish solid (up to 75%).

Reactivity Test

Asymmetric Transfer Hydrogenation of α,β-unsaturated Ketones

The α-substituted-α,β-unsaturated ketone (20 mg, 19.3 µL, 0.10 mmol) was dissolved in Bu_2O (0.3 mL) and added under argon atmosphere into a flame-dried pressure tube containing a magnetic stir bar. Upon addition of the corresponding catalyst (0.005 mmol) and Hantzsch ester (30.4 mg, 0.12 mmol), the reaction mixture was stirred at 60 °C under argon atmosphere for 48 h. The crude reaction mixture was treated with KOH aqueous solution. The organic phase was washed with KOH (3 x 0.3 mL), combined, dried over $MgSO_4$ and filtered. The resulting solution was analyzed by HPLC for *e.r.* determination.

3.7 Acknowledgements

This project was financed by the German Science Foundation (DFG; RTG 2620) project number 426795949.

3.8 References

[1] H. Guo, Y. C. Fan, Z. Sun, Y. Wu, O. Kwon, *Chem Rev* 2018, *118*, 10049–10293.

[2] B. Han, X. H. He, Y. Q. Liu, G. He, C. Peng, J. L. Li, *Chem Soc Rev* 2021, *50*, 1522–1586.

[3] M. P. van der Helm, B. Klemm, R. Eelkema, *Nat Rev Chem* 2019, *3*, 491–508.

[4] K. Brak, E. N. Jacobsen, *Angewandte Chemie - International Edition* 2013, *52*, 534–561.

[5] T. Akiyama, J. Itoh, K. Yokota, K. Fuchibe, *Angewandte Chemie - International Edition* 2004, *43*, 1566–1568.

[6] D. Uraguchi, M. Terada, *J Am Chem Soc* 2004, *126*, 5356–5357.

[7] D. Parmar, E. Sugiono, S. Raja, M. Rueping, *Chem Rev* 2014, *114*, 9047–9153.

[8] R. R. Gataullin, *Helv Chim Acta* 2020, *103*, DOI 10.1002/hlca.202000137.

[9] S. Rajkumar, M. Tang, X. Yang, *Angewandte Chemie* 2020, *132*, 2353–2357.

[10] M. Yamanaka, J. Itoh, K. Fuchibe, T. Akiyama, *J Am Chem Soc* 2007, *129*, 6756–6764.

[11] J. M. M. Verkade, L. J. C. Van Hemert, P. J. L. M. Quaedflieg, F. P. J. T. Rutjes, *Chem Soc Rev* 2008, *37*, 29–41.

[12] Y. Pan, D. Wang, Y. Chen, D. Zhang, W. Liu, X. Yang, *ACS Catal* 2021, *11*, 8443–8448.

[13] M. Rueping, E. Sugiono, C. Azap, T. Theissmann, M. Bolte, *Org Lett* 2005, *7*, 3781–3783.

[14] M. S. Sigman, E. N. Jacobsen, Schiff Base Catalysts for the Asymmetric Strecker Reaction Identified and Optimized from Parallel Synthetic Libraries, 1997.

[15] M. Terada, *Synthesis (Stuttg)* 2010, 1929–1982.

[16] K. Saito, T. Akiyama, *Chemical Communications* 2012, *48*, 4573–4575.

[17] S. Hoffmann, A. M. Seayad, B. List, *Angewandte Chemie - International Edition* 2005, *44*, 7424–7427.

[18] M. Rueping, B. J. Nachtsheim, W. Ieawsuwan, I. Atodiresei, *Angewandte Chemie - International Edition* 2011, *50*, 6706–6720.

[19] P. Christ, A. G. Lindsay, S. S. Vormittag, J. M. Neudörfl, A. Berkessel, A. C. O'Donoghue, *Chemistry - A European Journal* 2011, *17*, 8524–8528.

[20] K. Kaupmees, N. Tolstoluzhsky, S. Raja, M. Rueping, I. Leito, *Angewandte Chemie - International Edition* 2013, *52*, 11569–11572.

[21] B. Peng, J. Ma, J. Guo, Y. Gong, R. Wang, Y. Zhang, J. Zeng, W. W. Chen, K. Ding, B. Zhao, *J Am Chem Soc* 2022, *144*, 2853–2860.

[22] D. Nakashima, H. Yamamoto, *J Am Chem Soc* 2006, *128*, 9626–9627.

[23] P. Garcia-Garcia, F. Lay, P. Garcia-Garcia, C. Rabalakos, B. List, *Angewandte Chemie - International Edition* 2009, *48*, 4363–4366.

[24] J. Eder, A. S. Antonov, E. Y. Tupikina, R. M. Gschwind, *Chemistry - A European Journal* 2024, e202401793.

[25] K. Rothermel, M. Žabka, J. Hioe, R. M. Gschwind, *Journal of Organic Chemistry* 2019, *84*, 13221–13231.

[26] M. Hecht, P. Dullinger, W. Silva, D. Horinek, R. M. Gschwind, *Chem Sci* 2024, *15*, 9104–9111.

[27] F. Zhou, H. Yamamoto, *Angewandte Chemie - International Edition* 2016, *55*, 8970–8974.

[28] T. Murai, M. Monzaki, T. Katoh, T. Suzuki, T. Akiyama, *Phosphorus Sulfur Silicon Relat Elem* 2010, *185*, 964–973.

[29] J. C. Antilla, W. D. Wulff, *Angewandte Chemie - International Edition* 2000, *39*, 4518–4521.

[30] Z. Lu, Y. Zhang, W. D. Wulff, *J Am Chem Soc* 2007, *129*, 7185–7194.

[31] N. J. A. Martin, B. List, *J Am Chem Soc* 2006, *128*, 13368–13369.

3.9 Supporting Information

3.9.1 TRIP-DSA-K Synthesis with Previous Procedure

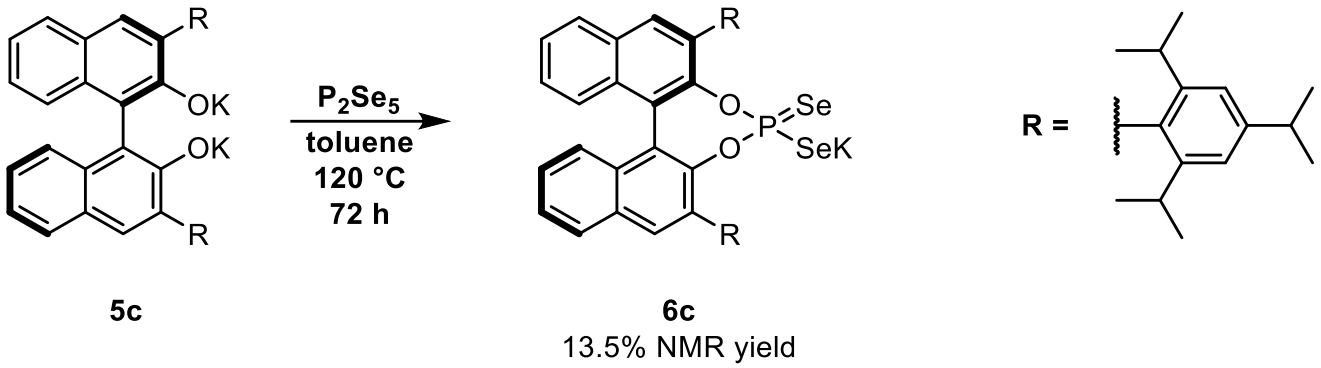

5c **6c**
13.5% NMR yield

Figure S3-1: Incomplete conversion of **5c** with phosphorus selenide to **6c**.

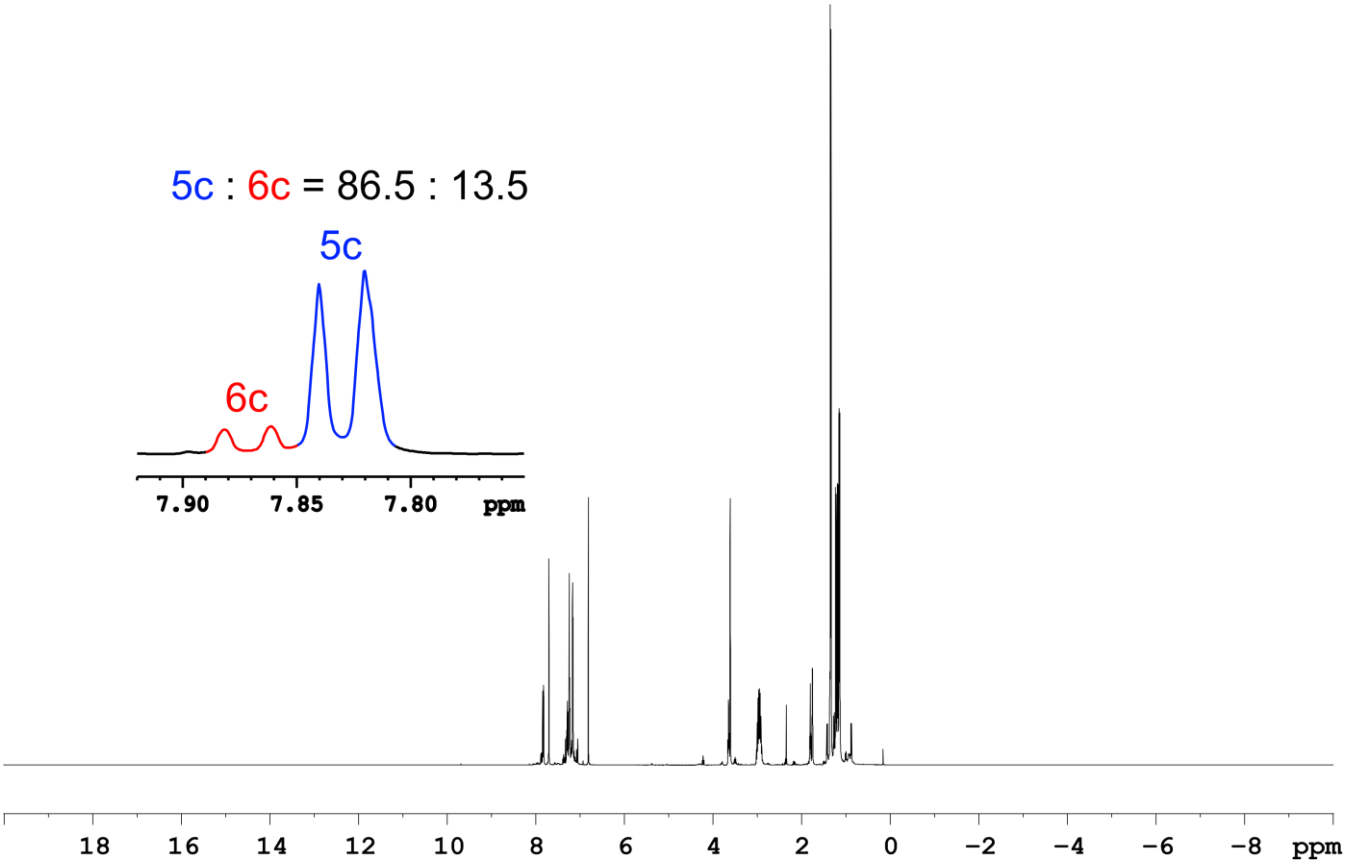

Figure S3-2: ^{1}H NMR spectrum (400.1 MHz, THF-d_8, 298 K) of the reaction mixture of **5c -> 6c**. Incomplete conversion of **5c** with phosphorus selenide to **6c** can be observed.

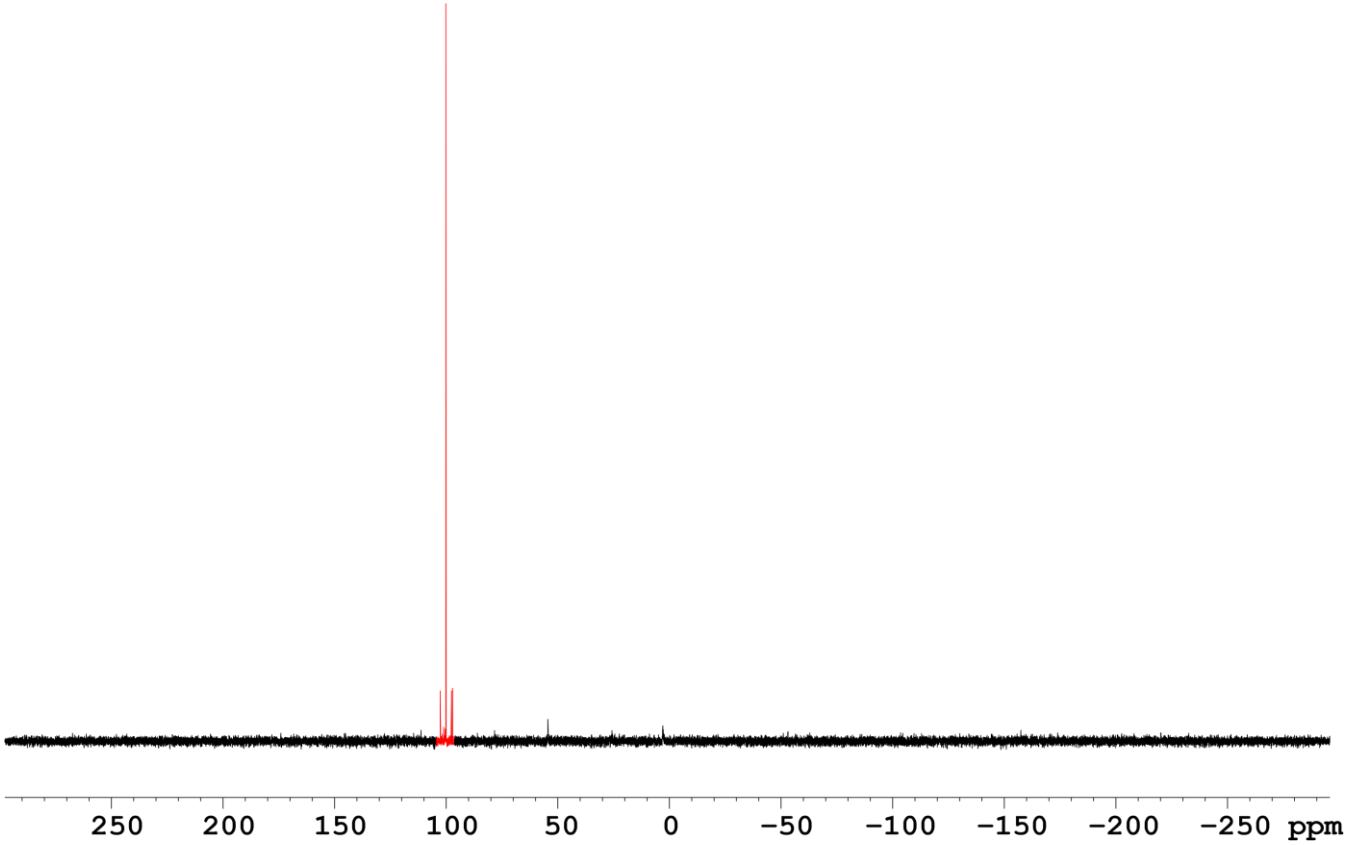

Figure S3-3: ^{31}P NMR spectrum (161.9 MHz, THF-d_8, 298 K) of the reaction mixture of **5c -> 6c**. The reaction proceeds with high selectivity. Starting material **5c** is invisible in ^{31}P spectra.

3.9.2 Synthesis and analysis of VANOL-DSA-K

The synthesis of VANOL-DSA-K follows the general procedure described in the experimental section (see Chapter 3.6). The product was obtained with 60% isolated yield (99% conversion).

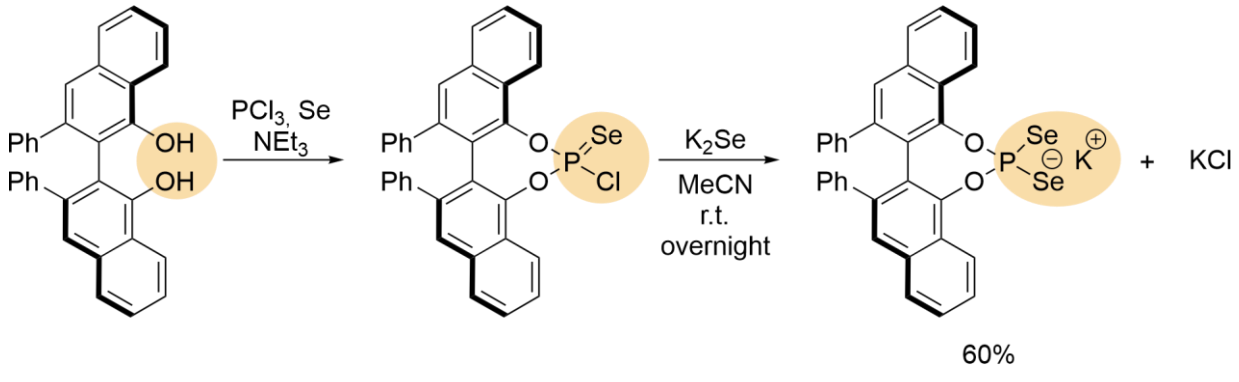

Figure S3-4: Synthesis of VANOL-DSA-K.

Mass Spectrometry

calc. for $C_{32}H_{20}O_2PSe_2^-$ $[M]^-$ 626.9537, found 626.9546.

NMR Spectroscopy

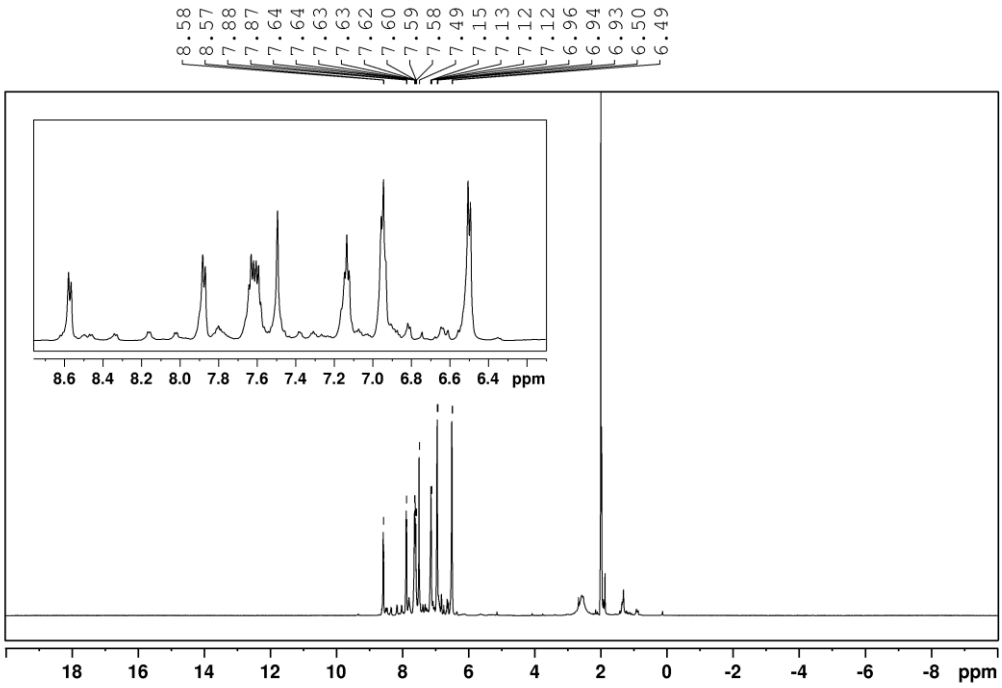

Figure S3-5: ^{1}H NMR spectrum of VANOL-DSA-K (600.1 MHz CD_3CN, 298 K,).

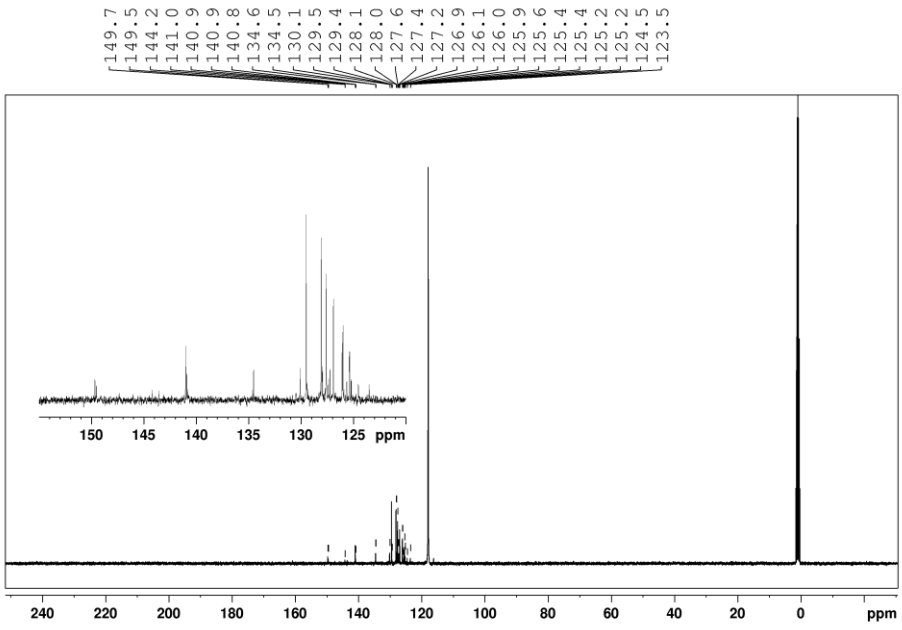

Figure S3-6: ^{13}C NMR spectrum of VANOL-DSA-K (150.9 MHz, CD_3CN, 298 K).

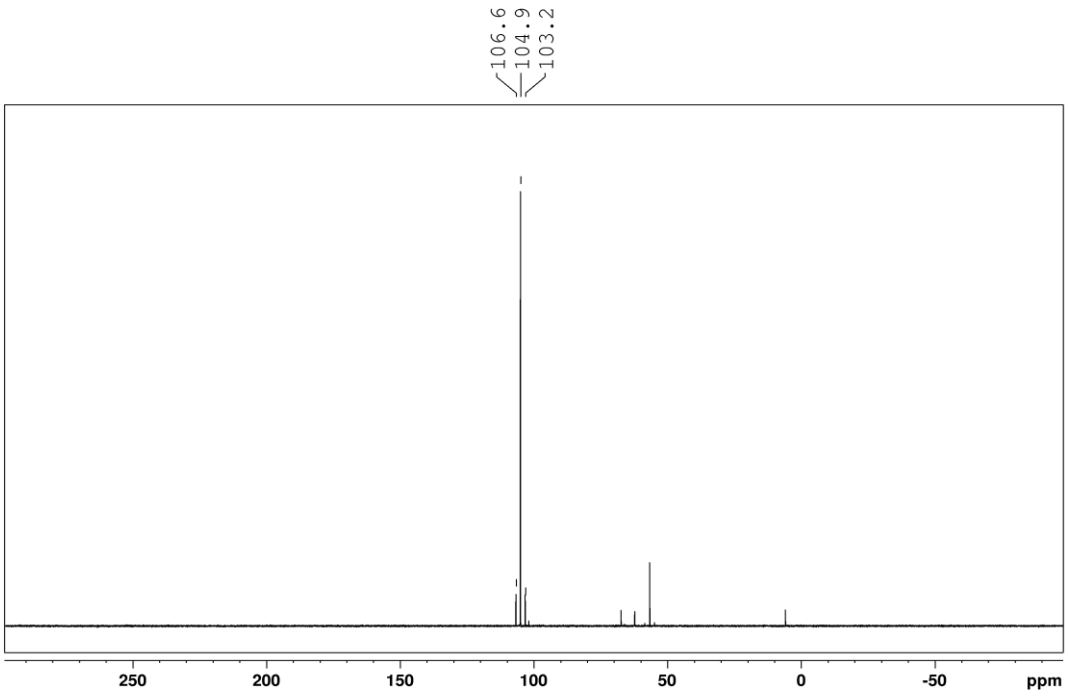

Figure S3-7: ^{31}P NMR spectrum of VANOL-DSA-K (242.9 MHz, CD_3CN, 298 K), $^1J_{PSe}$ = 841.0 Hz.

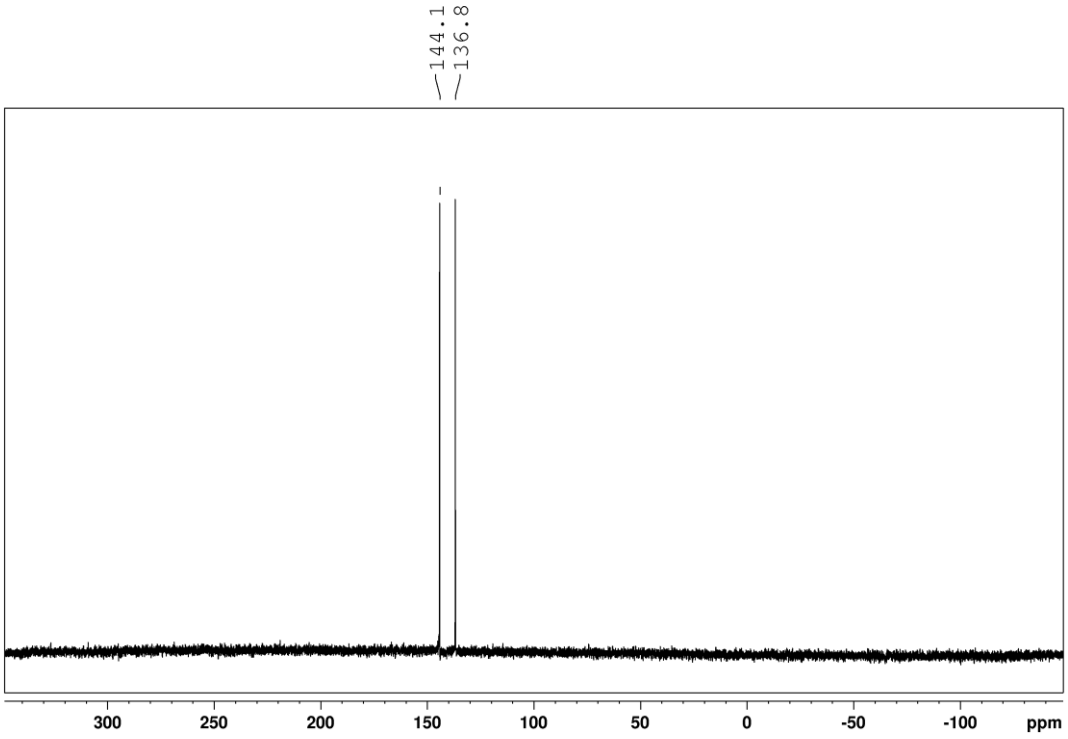

Figure S3-8: ^{77}Se NMR spectrum of VANOL-DSA-K (CD_3CN, 298 K, 114.5 MHz) $^1J_{PSe}$ = 841.0 Hz.

3.9.3 Synthesis and Analysis of DSA-K 6b-e

The synthesis of DSA-Ks **6b-e** follow the general procedure described in the experimental section (see Chapter 3.6). The products were obtained with 86-92% isolated yield (99% conversion).

Potassium bis[2,4,6-(CH_3)$_3$$C_6H_2$]-diselenophosphate salt (TRIM-DSA-K) 6b

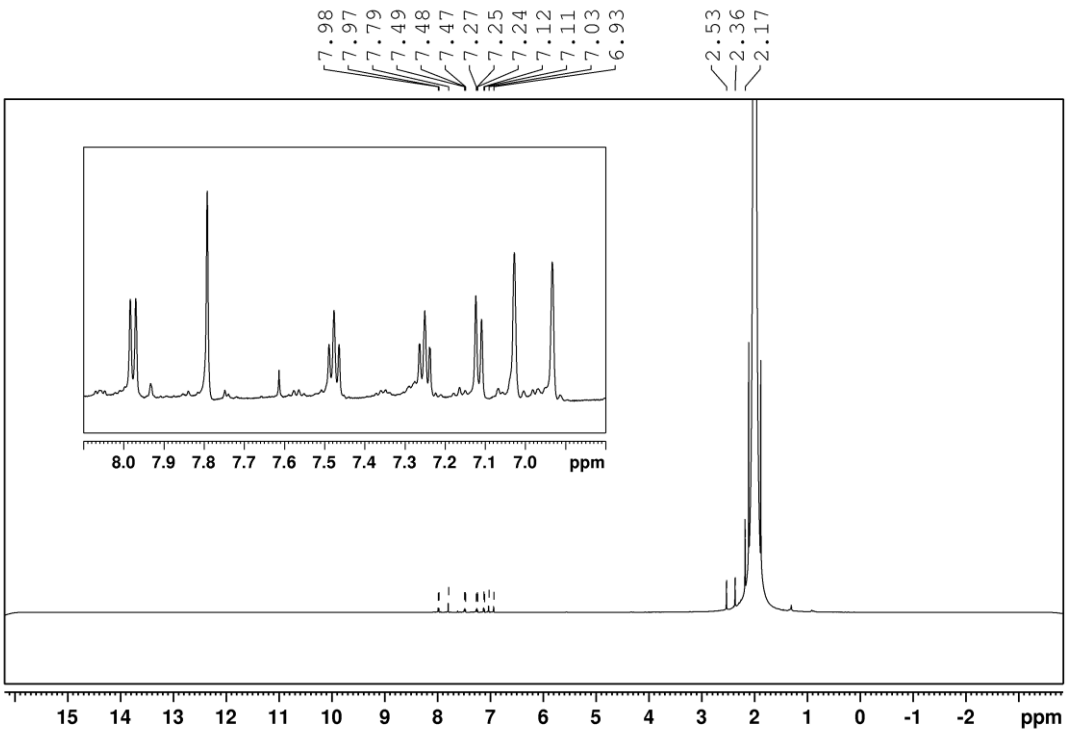

Figure S3-9: ^{1}H NMR spectrum of TRIM-DSA-K (600.1 MHz, CD_3CN, 298 K).

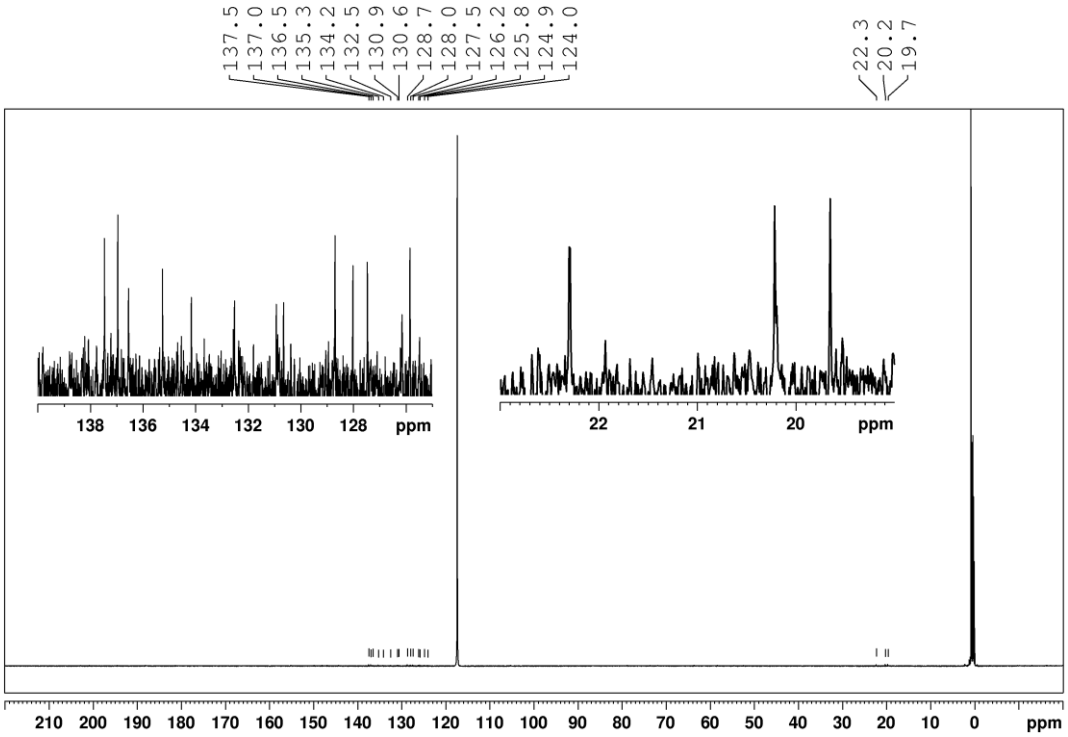

Figure S3-10: ^{13}C NMR spectrum of TRIM-DSA-K (150.9 MHz, CD_3CN, 298 K).

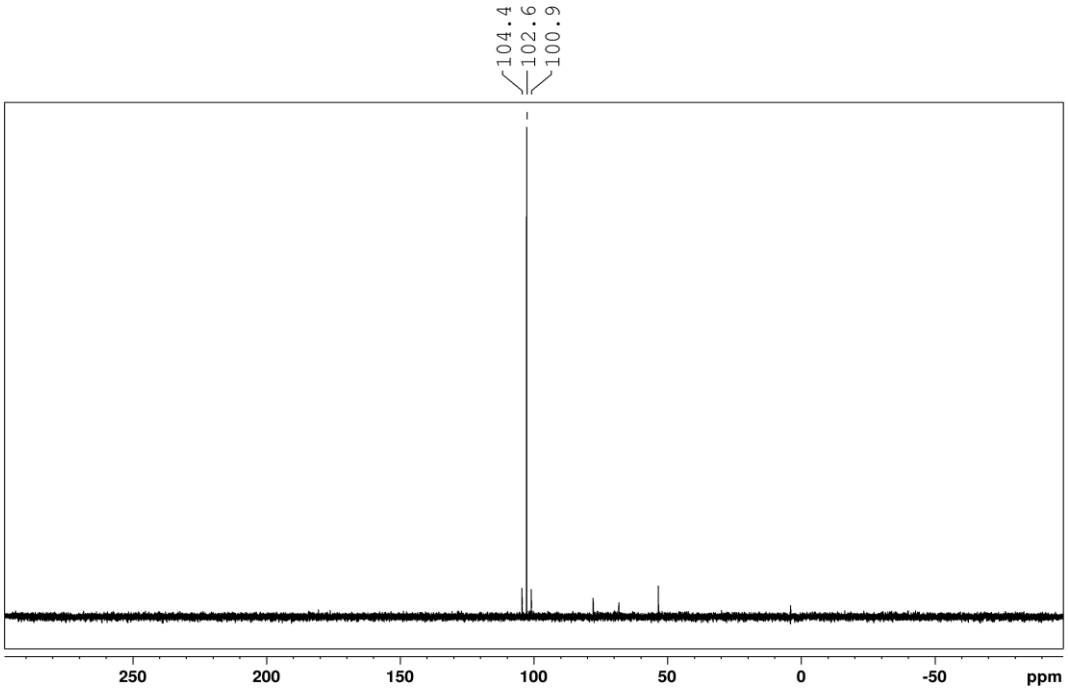

Figure S3-11: ^{31}P NMR spectrum of TRIM-DSA-K (CD_3CN, 298 K, 242.9 MHz), $^{1}J_{PSe}$ = 843.6 Hz.

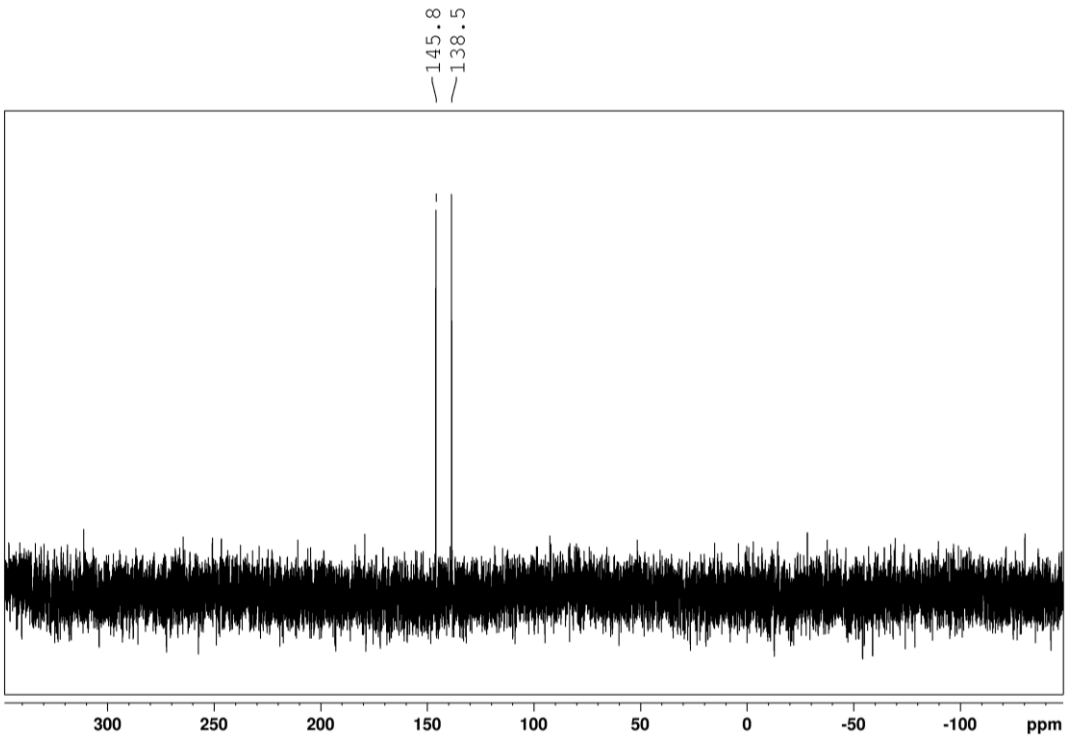

Figure S3-12: ^{77}Se NMR spectrum of TRIM-DSA-K (CD_3CN, 298 K, 114.5 MHz) $^{1}J_{PSe}$ = 843.6 Hz.

Potassium bis[2,4,6-(iPr)$_3$C$_6$H$_2$]-diselenophosphate salt (TRIP-DSA-K) 6c

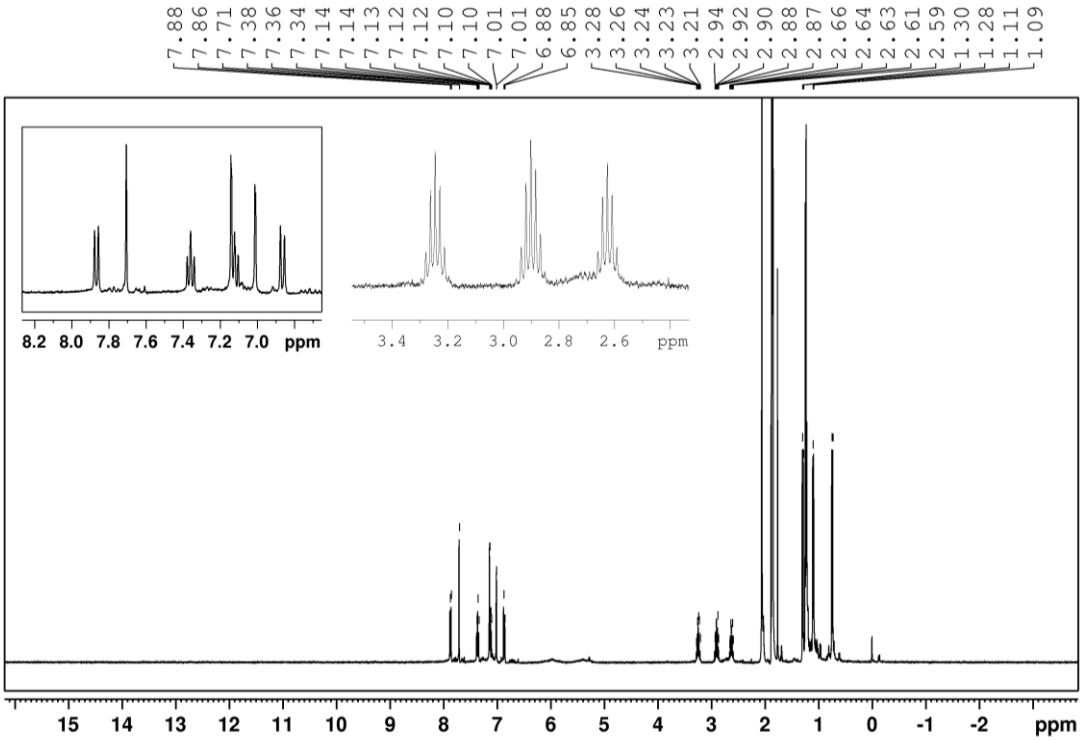

Figure S3-13: ^{1}H NMR spectrum of TRIP-DSA-K (400.1 MHz, CD_3CN, 298 K).

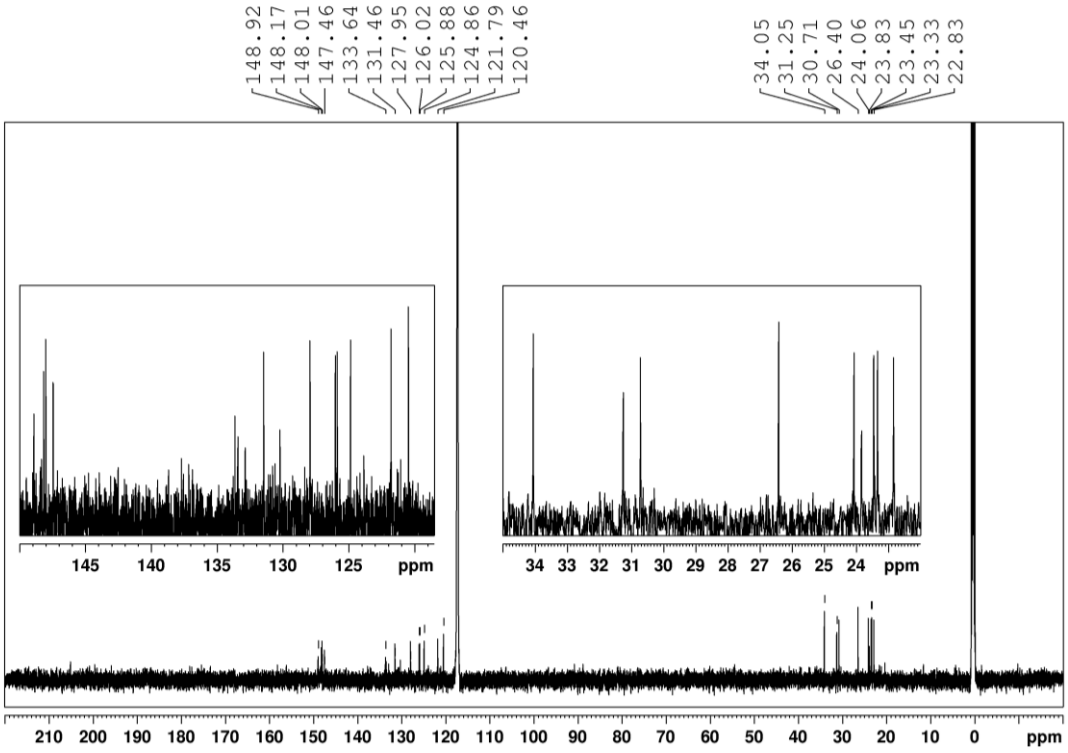

Figure S3-14: ^{13}C NMR spectrum of TRIP-DSA-K (100.6 MHz, CD_3CN, 298 K).

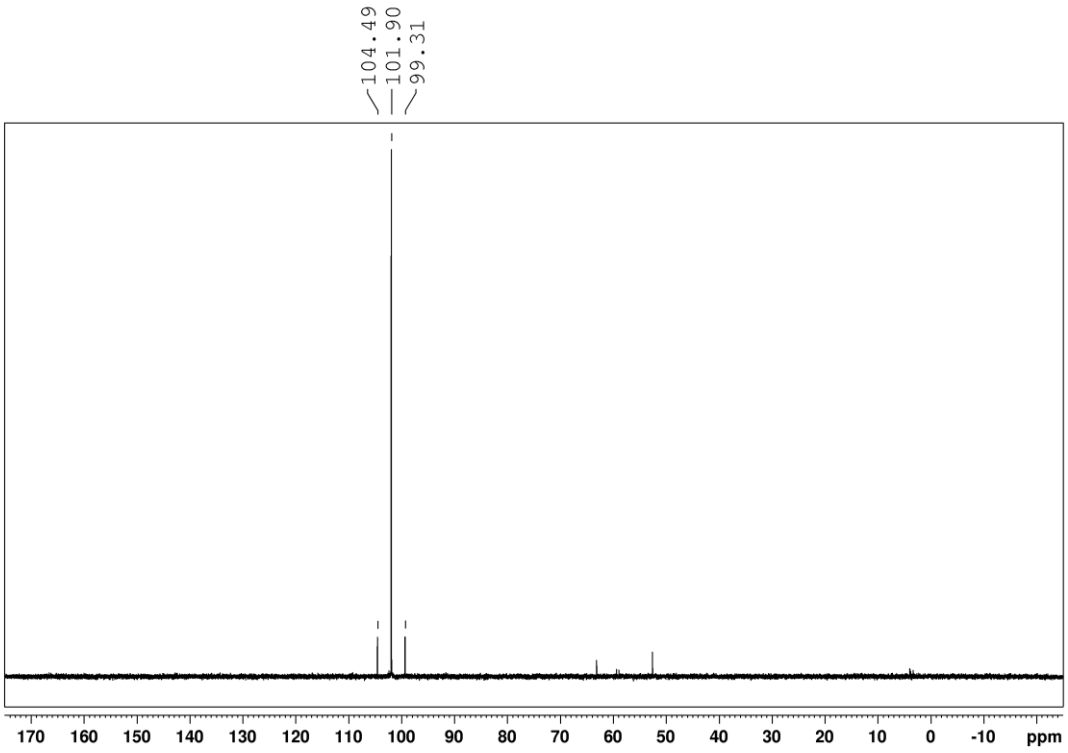

Figure S3-15: ^{31}P NMR spectrum of TRIP-DSA-K (162.2 MHz, CD_3CN, 298 K), $^{1}J_{PSe}$ = 840.1 Hz.

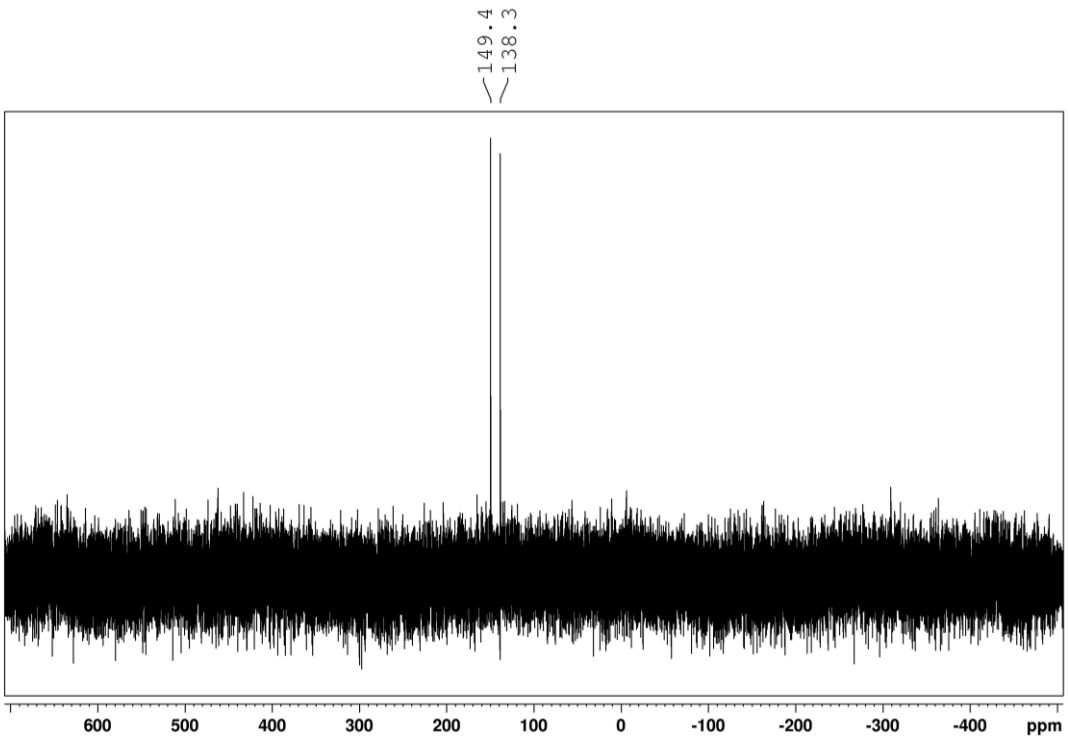

Figure S3-16: ^{77}Se NMR spectrum of TRIP-DSA-K (76.3 MHz, CD3CN, 298 K), $1J_{PSe}$ = 840.1 Hz.

Potassium bis(9-anthracenyl)-diselenophosphate salt (Anthra-DSA-K) 6d

Mass Spectrometry

calc. for $C_{48}H_{28}O_2PSe_2^-$ $[M]^-$ 827.0157, found 827.0172.

Melting Point

Decomposition > 240 °C.

NMR Spectroscopy

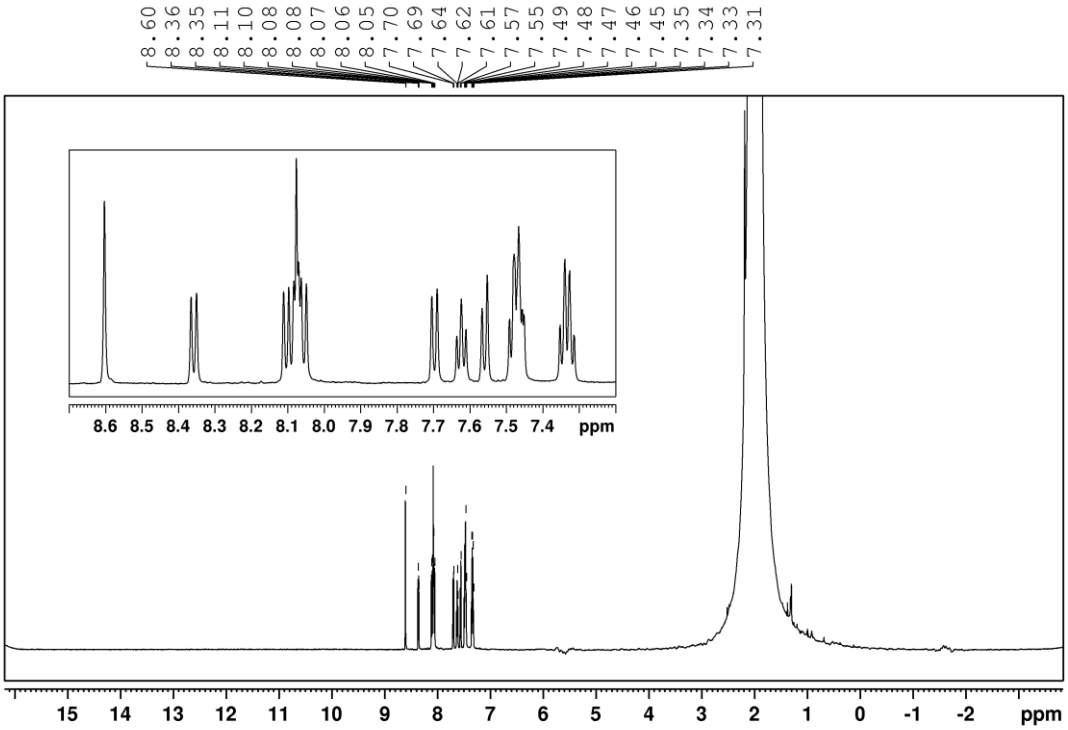

Figure S3-17: ^{1}H NMR spectrum of Anthra-DSA-K (600.1 MHz, CD_3CN, 298 K).

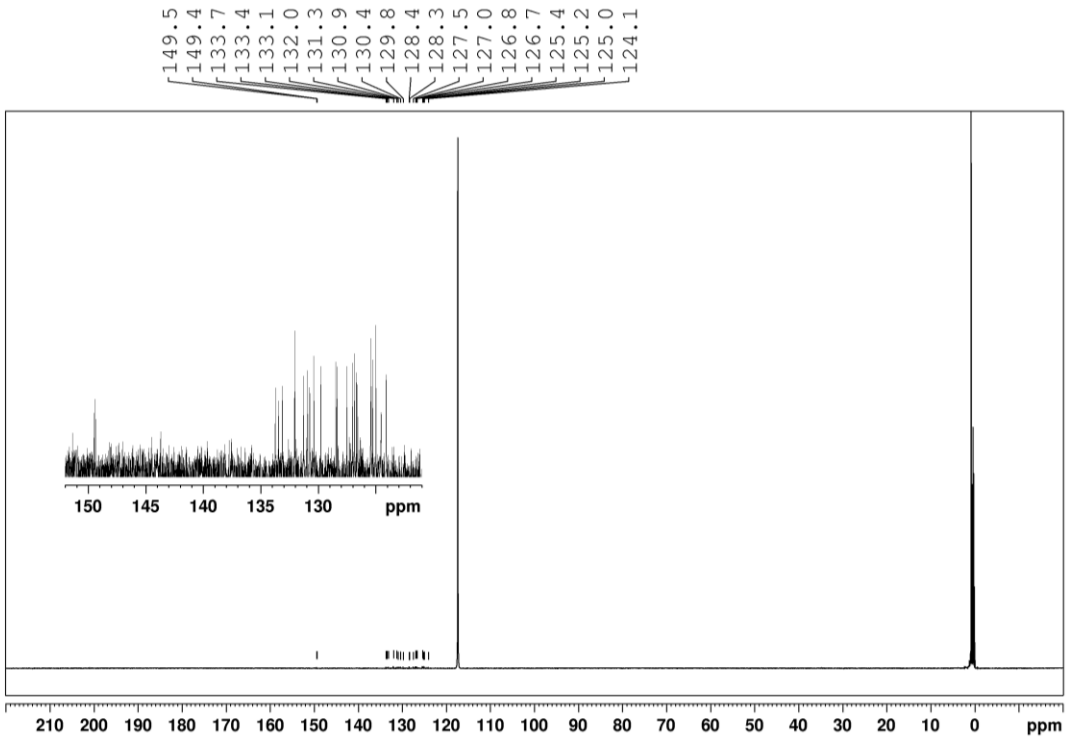

Figure S3-18: ^{13}C NMR spectrum of Anthra-DSA-K (150.9 MHz, CD_3CN, 298 K).

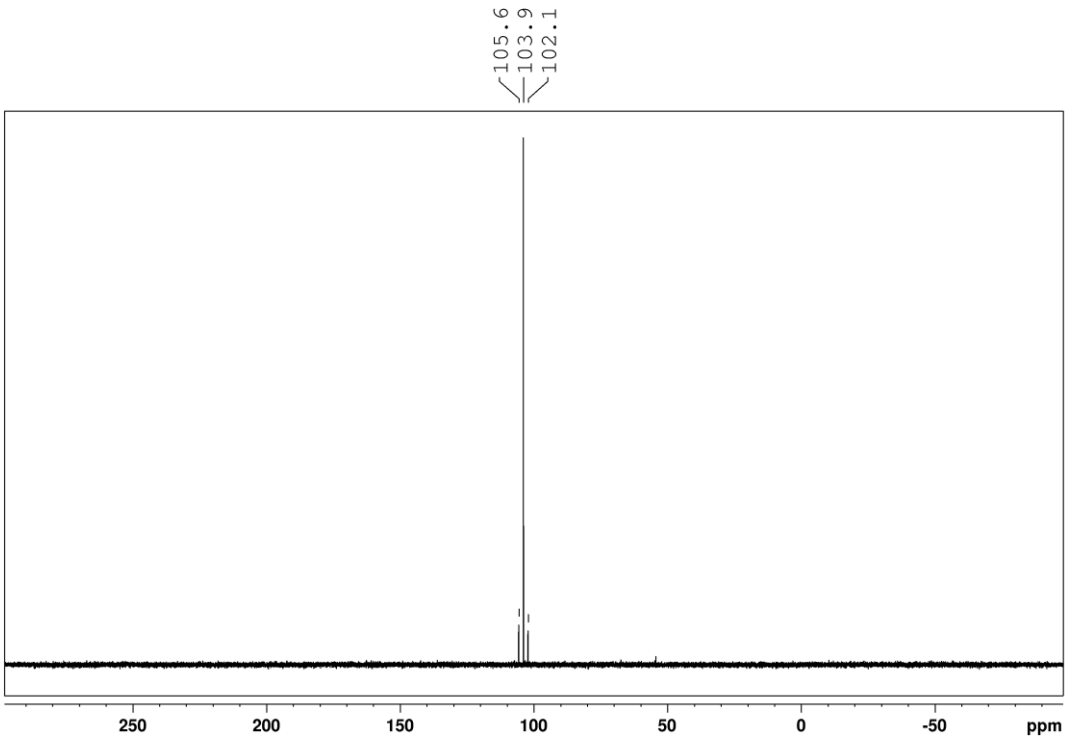

Figure S3-19: ^{31}P NMR spectrum of Anthra-DSA-K (242.9 MHz, CD_3CN, 298 K).

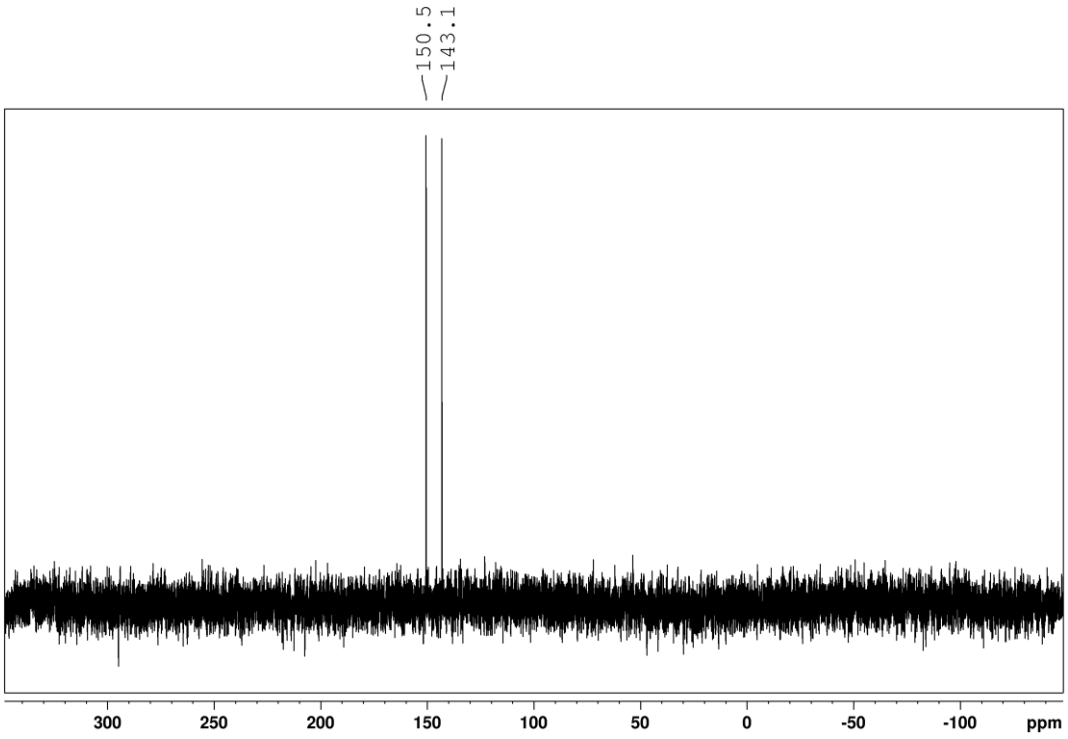

Figure S3-20: ^{77}Se NMR spectrum of Anthra-DSA-K (114.5 MHz, CD_3CN, 298 K).

Potassium bis[3,5-(CF$_3$)$_3$]-diselenophosphate salt (TRIFP-DSA-K) 6e

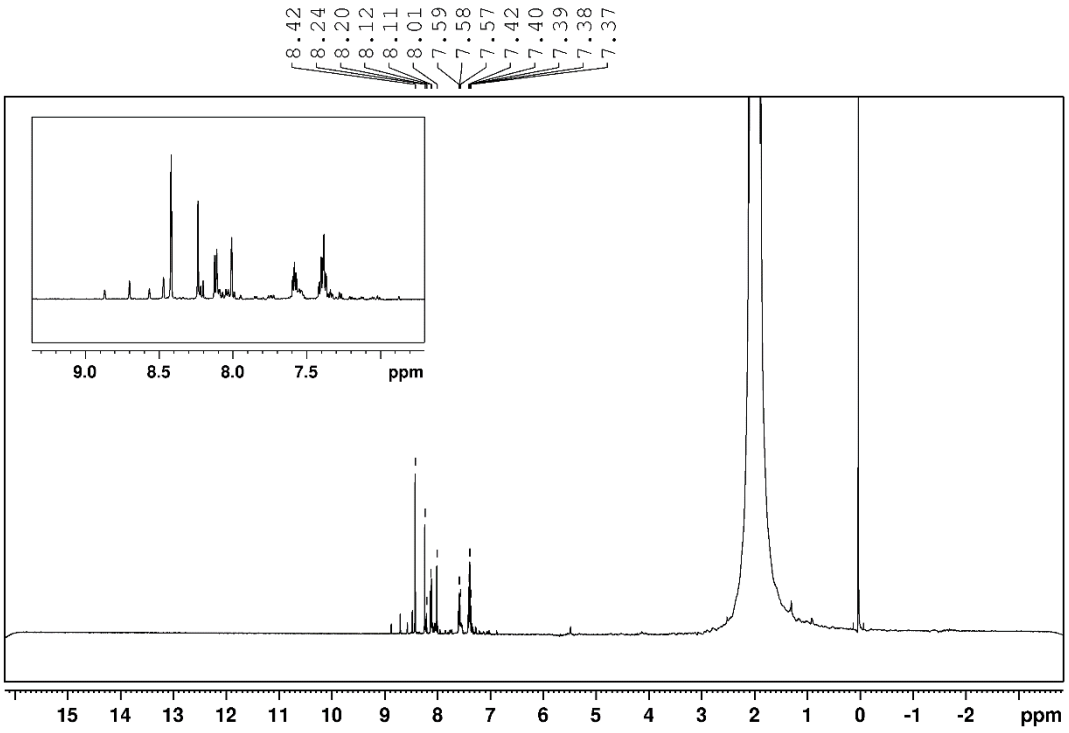

Figure S3-21: ^{1}H NMR spectrum of TRIFP-DSA-K (600.1 MHz, CD_3CN, 298 K).

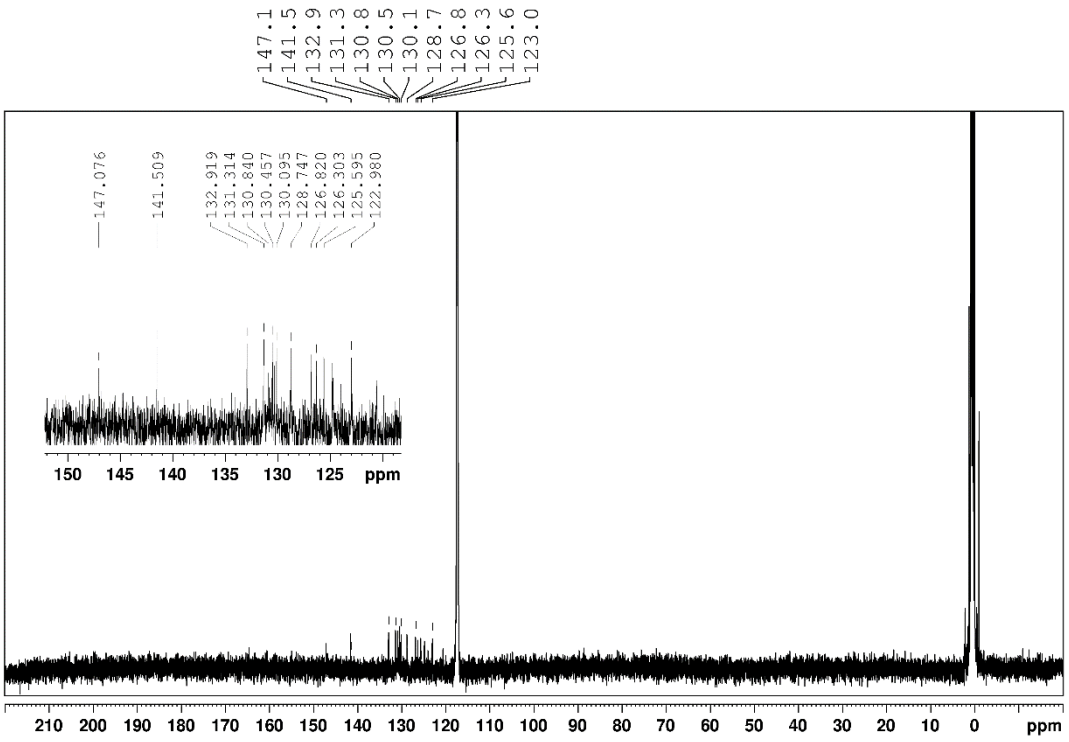

Figure S3-22: ^{13}C NMR spectrum of TRIFP-DSA-K (150.9 MHz, CD_3CN, 298 K).

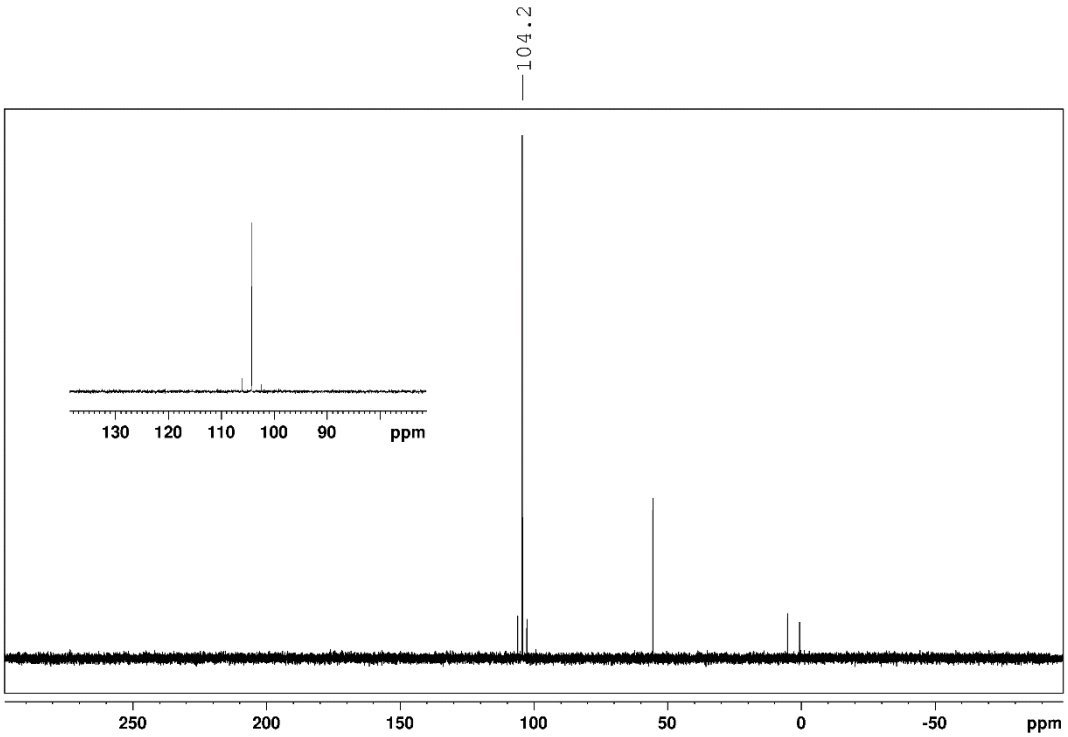

Figure S3-23: ^{31}P NMR spectrum of TRIFP-DSA-K (242.9 MHz, CD_3CN, 298 K).

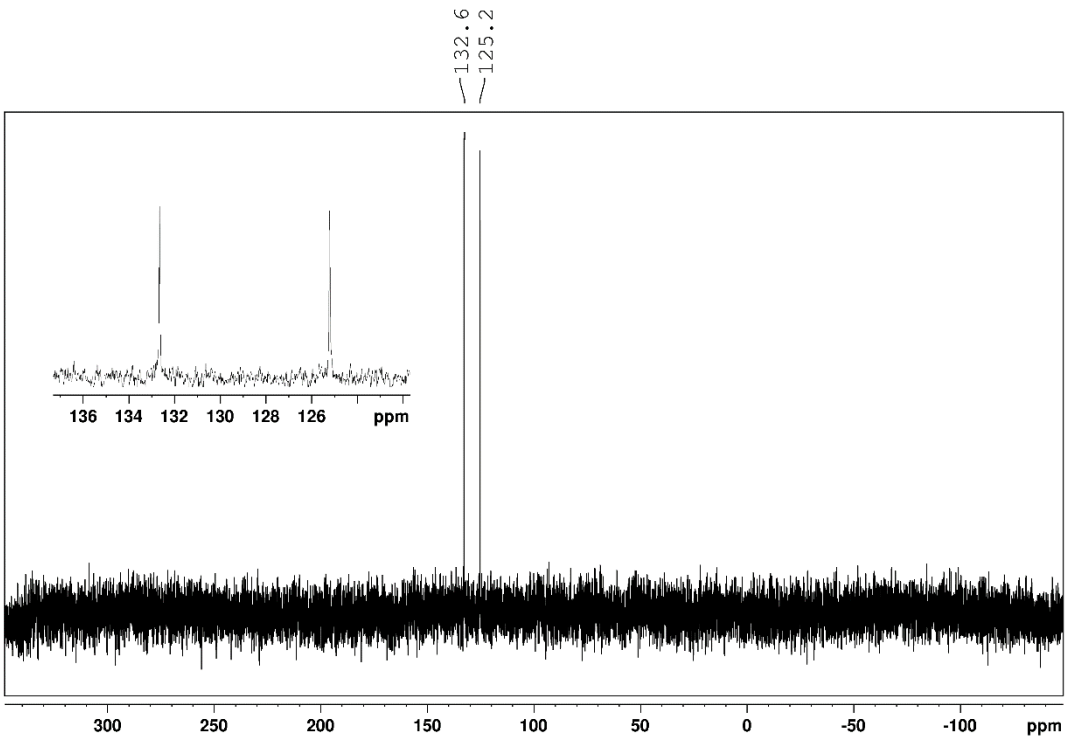

Figure S3-24: ^{77}Se NMR spectrum of TRIFP-DSA-K (114.5 MHz, CD_3CN, 298 K).

3.9.4 Crystallographic Data

A crystal structure of TRIP-DSA-K **6c** was obtained by slow vapor diffusion in toluene/*n*-hexane. Two DSA-K molecules form a dimer with bridging potassium atoms that interact with all selenium atoms and with the phenyl-moiety of a TRIP-substituent, respectively.

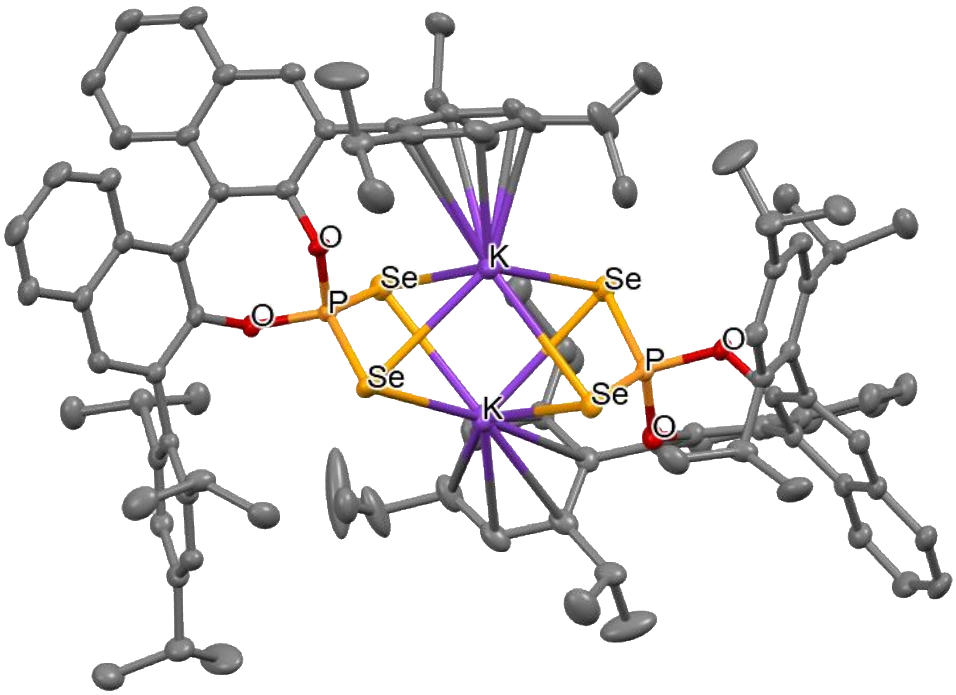

Figure S3-25: Crystal structure of TRIP-DSA-K **6c**. Two molecules of **6c** form a dimeric complex in solid state, with bridging potassium atoms.

Table S3-1: Crystal Data and structure refinement of TRIP-DSA-K **6c**

Empirical formula	$C_{100}H_{112}K_2O_4P_2Se_4$
Formula weight	1833.87
Temperature/K	123.15
Crystal system	monoclinic
Space group	I2
a/Å	16.0090(2)
b/Å	16.57970(10)
c/Å	19.2605(2)
α/°	90
β/°	114.3070(10)
γ/°	90
Volume/Å^3	4659.02(9)
Z	2
ρ_{calc}g/cm^3	1.307
μ/mm^{-1}	3.384
F(000)	1896.0
Crystal size/mm^3	0.126 × 0.095 × 0.024
Radiation	CuKα (λ = 1.54184)
2Θ range for data collection/°	6.078 to 150.478
Index ranges	$-20 \leq h \leq 19$, $-20 \leq k \leq 20$, $-23 \leq l \leq 23$
Reflections collected	58673
Independent reflections	9278 [R_{int} = 0.0334, R_{sigma} = 0.0224]
Data/restraints/parameters	9278/2/528
Goodness-of-fit on F^2	1.062
Final R indexes [I>=2σ (I)]	R_1 = 0.0263, wR_2 = 0.0687
Final R indexes [all data]	R_1 = 0.0278, wR_2 = 0.0695
Largest diff. peak/hole / e Å^{-3}	0.49/-0.35
Flack parameter	-0.013(6)

Table S3-2: Fractional Atomic Coordinates (×104) and Equivalent Isotropic Displacement Parameters (Å2×103). Ueq is defined as 1/3 of the trace of the orthogonalised UIJ tensor.

Atom	x	y	z	U(eq)
Se1	4957.1(2)	3952.8(2)	8824.5(2)	26.49(9)
Se2	5097.4(2)	6135.7(2)	8877.1(2)	28.77(9)
K1	3711.0(5)	5033.7(6)	9574.3(3)	31.84(14)
P1	4659.7(5)	5065.9(6)	8235.3(4)	21.16(14)
O1	5022.2(13)	5131.6(15)	7567.4(10)	22.0(4)
O2	3543.2(13)	5040.7(16)	7756.7(10)	23.2(4)
C007	2495(2)6	167(2)	7379.1(17)	24.6(6)
C008	4586(2)	4752.0(18)	6858.6(16)	21.1(6)
C009	3767(2)	4004(2)	5448.7(16)	25.5(6)
C00A	3275(2)	4602.8(19)	5655.4(17)	24.0(6)
C00B	7683(2)	4203(2)	7637.2(18)	26.8(7)
C00C	3732.9(19)	5014(2)	6370.4(15)	22.5(5)
C00D	6780(2)	4470(2)	7259.0(18)	24.6(6)
C00E	3117(2)	5650.5(19)	7231.6(17)	23.1(6)
C00F	2066(2)	6753(2)	6850.4(19)	28.0(7)
C00G	3318(2)	3571(2)	4755.8(18)	30.4(7)
C00H	6059.6(19)	3931(2)	7160.6(16)	22.0(6)
C00I	2268(2)	6032(2)	8050.1(18)	25.9(6)
C00J	2898(2)	6366(2)	6079.8(18)	26.0(6)
C00K	2278(2)	6894(2)	6217.6(18)	27.0(7)
C00L	7895(2)	3428(2)	7927.3(18)	26.8(7)
C00M	8882(2)	3131(2)	8312(2)	35.4(8)
C00N	4677(2)	3827.1(19)	5948.1(17)	24.4(6)
C00O	1471(2)	4700(2)	7442(2)	35.5(8)
C00P	6596(2)	5338(2)	6978(2)	29.0(7)
C00Q	7175(2)	2916(2)	7847.0(18)	26.3(7)
C00R	2488(2)	6608(2)	8633.5(19)	29.1(7)
C00S	5508(2)	2536(2)	7373(2)	31.3(7)
C00T	6256(2)	3146.8(19)	7462.3(18)	24.0(6)
C00U	1790(2)	5317(2)	8081(2)	30.8(7)

C00V	2420(3)	3702(2)	4306.4(18)	34.8(8)
C00W	9293(3)	2987(3)	7730(2)	42.8(9)
C00X	5095(2)	4164.6(18)	6660.6(17)	21.7(6)
C00Y	2944(2)	7408(2)	8609.6(19)	29.2(7)
C00Z	3135(2)	6540(2)	5464.4(19)	31.4(7)
C010	3261(2)	5690.4(19)	6577.9(17)	23.6(6)
C011	2773(3)	7197(2)	5005(2)	36.3(8)
C012	5664(3)	2094(2)	8115(2)	38.4(8)
C013	1925(3)	4278(2)	4517(2)	36.4(8)
C014	2339(2)	4726(2)	5167.4(19)	29.7(7)
C015	2127(3)	7693(2)	5119(2)	37.1(8)
C017	5421(3)	1910(2)	6759(2)	46.0(10)
C018	6992(3)	5525(2)	6395(2)	39.7(9)
C019	2250(3)	6456(2)	9244(2)	36.8(8)
C01A	3711(3)	7637(2)	9378(2)	38.8(8)
C01B	2221(3)	8080(2)	8351(2)	37.3(8)
C01C	1570(2)	5202(2)	8703(2)	37.2(9)
C01D	1799(3)	5758(2)	9292(2)	40.9(9)
C01E	1886(3)	7547(2)	5709(2)	34.5(8)
C01F	1613(4)	3832(3)	7735(3)	52.9(11)
C01G	465(3)	4852(3)	6913(3)	76.0(19)
C01H	1576(4)	5564(3)	9965(3)	65.7(16)
C01J	9494(3)	3700(4)	8929(3)	68.5(16)
C1	6970(3)	5926(2)	7644(2)	37.6(8)
C2	2215(3)	4909(3)	10462(2)	43.2(10)
C3	1413(4)	6257(4)	10345(3)	41.9(18)
C3A	832(8)	5727(9)	10048(7)	37(4)

Table S3-3: Anisotropic Displacement Parameters (Å2×103). The Anisotropic displacement factor exponent takes the form: -2π2[h2a*2U11+2hka*b*U12+…].

Atom	U11	U22	U33	U23	U13	U12
Se1	29.15(16)	25.25(18)	22.10(16)	5.10(14)	7.56(13)	5.82(14)
Se2	35.09(19)	27.00(19)	23.81(17)	-3.85(14)	11.70(14)	0.99(15)
K1	27.9(3)	42.2(4)	24.8(3)	1.3(4)	10.1(2)	3.8(3)
P1	22.0(3)	23.4(3)	16.3(3)	1.7(3)	6.1(3)	4.1(3)
O1	22.5(9)	26.6(12)	15.2(8)	-2.7(9)	6.2(7)	0.3(9)
O2	22.4(9)	25.1(9)	19.6(9)	5.0(11)	6.1(8)	5.5(10)
C007	21.0(13)	27.0(15)	24.3(14)	-0.3(13)	8.0(11)	2.8(13)
C008	24.6(14)	23.3(13)	14.3(12)	0.3(11)	7.0(11)	-1.0(11)
C009	30.2(15)	27.6(16)	18.0(13)	0.2(13)	9.1(12)	-3.4(14)
C00A	26.7(15)	25.8(16)	17.0(13)	3.0(12)	6.3(12)	0.1(12)
C00B	24.0(15)	31.0(16)	24.2(15)	-2.9(12)	8.6(13)	-6.1(12)
C00C	26.1(14)	23.5(13)	17.2(11)	2.9(14)	8.2(11)	2.6(13)
C00D	27.7(16)	26.4(16)	19.5(14)	-1.6(12)	9.5(12)	-1.3(12)
C00E	20.9(14)	22.3(15)	22.3(14)	1.4(12)	5.1(12)	3.0(11)
C00F	26.6(15)	27.3(16)	28.3(16)	1.8(13)	9.3(13)	6.5(13)
C00G	39.4(18)	30.1(17)	19.8(15)	-1.7(13)	10.3(14)	-3.6(14)
C00H	21.9(13)	23.8(14)	19.7(13)	-1.5(12)	8.0(11)	0.5(13)
C00I	21.1(14)	28.0(16)	29.1(15)	2.6(13)	10.9(12)	6.9(12)
C00J	25.5(15)	26.5(16)	20.7(14)	1.7(12)	4.3(12)	4.6(12)
C00K	26.1(15)	25.5(17)	23.0(15)	1.5(13)	3.7(12)	4.2(13)
C00L	21.4(15)	35.5(18)	20.5(15)	-3.2(13)	5.6(12)	0.7(13)
C00M	22.4(16)	43(2)	32.7(17)	-0.3(16)	3.5(14)	1.1(14)
C00N	27.7(14)	23.6(16)	22.7(14)	-0.4(12)	11.1(12)	1.8(12)
C00O	21.8(16)	36.5(18)	42(2)	2.9(16)	7.4(14)	0.0(14)
C00P	33.6(17)	24.8(16)	29.4(16)	1.5(13)	13.9(14)	-3.2(13)
C00Q	26.6(16)	24.7(16)	25.3(15)	0.4(12)	8.4(13)	3.5(12)
C00R	31.0(17)	28.7(17)	30.7(17)	5.0(13)	15.8(14)	9.1(13)
C00S	23.5(15)	25.0(17)	39.4(19)	4.2(14)	7.0(14)	-0.2(12)
C00T	23.1(15)	22.5(15)	24.1(14)	-1.7(12)	7.4(12)	1.5(12)
C00U	21.5(15)	29.0(16)	41.7(19)	6.5(14)	12.8(14)	5.5(12)

C00V	41.8(19)	35.2(19)	18.7(15)	-3.4(13)	3.7(14)	-6.6(15)
C00W	29.7(18)	52(2)	48(2)	4.1(19)	17.6(17)	3.9(17)
C00X	22.5(14)	22.0(15)	19.6(14)	2.1(11)	7.6(12)	1.0(11)
C00Y	35.4(17)	26.2(16)	28.8(16)	0.2(13)	15.9(14)	6.0(13)
C00Z	38.5(19)	29.6(17)	23.8(15)	3.9(13)	10.6(14)	8.8(14)
C010	23.1(14)	25.5(16)	19.2(14)	1.7(12)	5.6(12)	4.7(12)
C011	47(2)	33.7(19)	25.4(16)	6.7(14)	11.8(15)	5.9(16)
C012	39.4(19)	28.7(17)	51(2)	8.5(17)	22.2(17)	2.9(15)
C013	30.0(17)	43(2)	24.6(16)	4.8(15)	-0.7(14)	-2.0(15)
C014	28.5(17)	32.8(16)	23.9(15)	4.4(13)	6.8(13)	2.4(13)
C015	45(2)	29.6(18)	28.9(17)	8.1(15)	7.1(16)	9.6(16)
C017	47(2)	33(2)	41(2)	-2.7(16)	1.4(18)	-10.5(17)
C018	55(2)	33(2)	37(2)	1.9(16)	26.1(18)	-3.9(17)
C019	48(2)	31.4(18)	40.4(19)	3.5(16)	27.7(18)	12.5(16)
C01A	46(2)	35.1(19)	34.0(18)	-3.7(16)	15.5(17)	4.9(17)
C01B	46(2)	26.2(18)	43(2)	1.2(16)	21.3(17)	10.4(16)
C01C	32.9(17)	34(2)	53(2)	11.8(16)	25.5(16)	7.3(14)
C01D	48(2)	38(2)	52(2)	13.0(18)	36.0(19)	16.1(17)
C01E	37.1(19)	28.4(18)	30.9(17)	3.9(14)	6.9(15)	8.5(15)
C01F	69(3)	33(2)	70(3)	3(2)	42(2)	3(2)
C01G	34(2)	57(3)	97(4)	-24(3)	-14(2)	6(2)
C01H	100(4)	53(3)	84(4)	25(3)	79(4)	26(3)
C01J	31(2)	88(4)	57(3)	-28(3)	-11(2)	9(2)
C1	51(2)	29.0(19)	34.8(19)	-1.7(15)	19.4(17)	-4.3(15)
C2	59(2)	42(3)	37.3(18)	1.8(17)	28.5(18)	3.3(18)
C3	48(3)	51(4)	32(3)	5(2)	22(3)	13(3)
C3A	33(6)	53(8)	31(6)	-2(5)	19(5)	1(5)

4 A Highly Reduced Magnesium Dicobalt Complex for the Hydrogenation of Tri- and Tetra-Substituted Alkenes

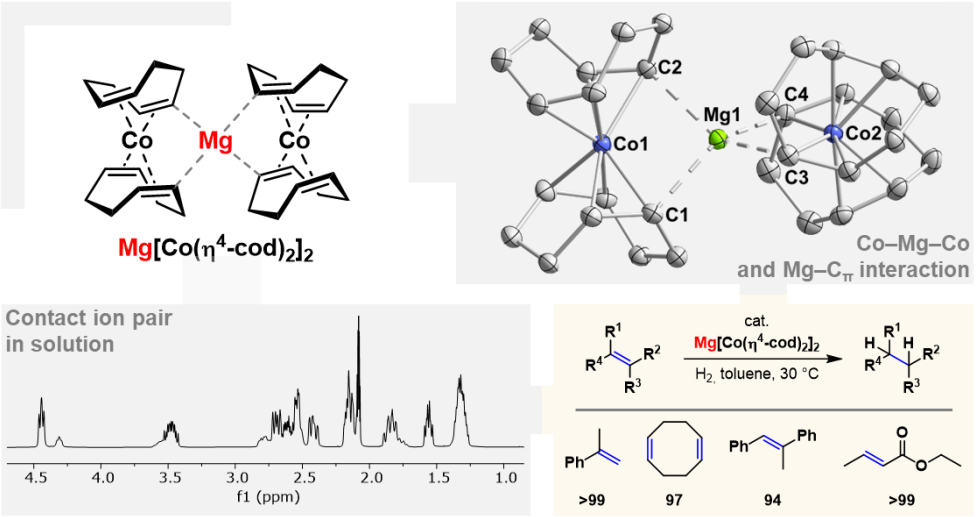

M. Gawron, **J. Eder**, X. Weichselgartner, G. Bálazs, R. M. Gschwind, R. Wolf

To be submitted

A). M. Gawron performed all reactions and characterisations and prepared the manuscript. B) J. Eder and R. M. Gschwind conducted and interpreted the DOSY NMR experiments. C) X. Weichselgartner assisted in the hydrogenation studies. D) G. Bálazs helped with the preparation of the manuscript. E) R. Wolf supervised and directed the project.

Preliminary version – text and figures may differ from the final manuscript. In the Supporting Information, only the results of this work are displayed.

4.1 Abstract

We describe the synthesis and structural characterization of the Mg^{2+} salt $Mg[Co(\eta^4\text{-cod})_2]_2$ (**1**; cod = 1,5-cyclooctadiene), forming a tight ion pair. Quantum chemical studies suggest that the interactions within the unsupported Co–Mg–Co motif are mainly electrostatic in nature. Importantly, the complex serves as a successful pre-catalyst for the hydrogenation of sterically tri- and tetra-substituted alkenes, surpassing the catalytic capabilities of related alkali metal and β-diketiminate magnesium complexes.

4.2 Introduction

Low-oxidation state alkali metal cobaltate salts, such as $[M(thf)_n][Co(\eta^2\text{-}C_2H_4)]$ (M = Li, **A**; M = K, **B**; C_2H_4 = ethylene), $[M(thf)_n][Co(\eta^4\text{-}cod)_2]$ (**C**: M = Li; **D**: M = Na; **E**: M = K; cod = 1,5-cyclooctadiene), and $[K([2.2.2]crypt.)][Co(\eta^4\text{-}C_{14}H_{10})_2]$ (**F**; $C_{14}H_{10}$ = anthracene, crypt. = cryptand), serve as versatile synthetic equivalents for the "Co^-" anion (Figure 4-, top).[1] These complexes have been utilized for the synthesis of various other cobalt species and have demonstrated promising reactivities in processes such as small molecule activation,[2] alkene hydrogenation,[1e,3] and other catalytic reactions.[4] The reactivity and catalytic properties of the cobaltate anions can be altered by coordinating heteroatomic ligands (e.g. phosphines or bipyridines)[1c,5] or redox-active ligands (e.g. α-diimines),[6] resulting in the formation of heteroleptic complexes. However, the effect of the counterions on their reactivity has not been thoroughly understood. As a result, only a few alkaline earth metal cobaltates are known, including the "inorganic Grignard reagent" $[MgBr(thf)_2][CpCo(\eta^3\text{-}C_3H_5)]$ (**G**) reported by Jonas, and the carbonyl complexes $[AE(thf)_n][Co(CO)_x(PCy_3)]_2$ reported by Mountford (where x = 1-3 and AE = Mg-Ba; see, for example, complex **H** in Figure 4-, bottom).[7] Additionally, only a very limited number of compounds containing counterions beyond group II are known.[1c],[8] Recently, we discovered that countercations have a significant impact on the catalytic properties of anionic cobaltates **C**-**E** and $[(^{Dep}nacnac)Mg][Co(\eta^4\text{-}cod)_2]$ (**J**; Dep = 2,6-diethylphenyl) during alkene hydrogenations.[1e]

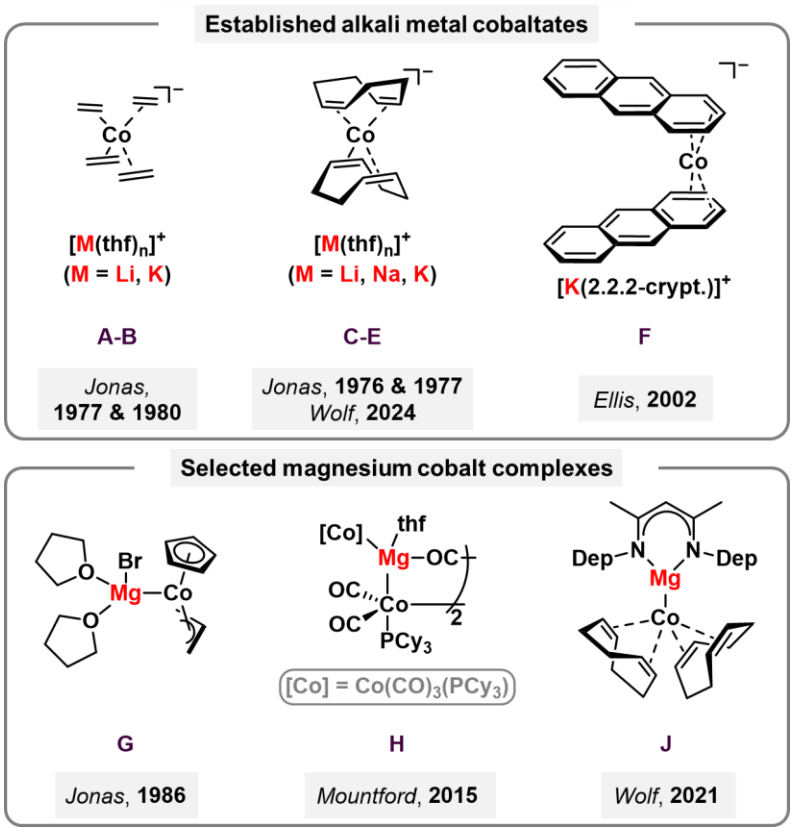

Figure 4-1: Established alkali metal cobaltates used as synthetic precursors, pre-catalysts or in the activation of small molecules (top) and selected examples of magnesium cobalt complexes (bottom). Dep = 2,6-diethylphenyl.

Our studies suggest that the counterion plays an active co-catalytic role in the hydrogenation reaction by coordinating with cobalt hydride intermediates. To investigate the enhanced reactivity of magnesium cobaltates compared to their alkali metal salts, we focused on the Mg^{2+} complex, $Mg[Co(\eta^4\text{-cod})_2]_2$ (**1**, Figure 4-2), which lacks any additional ligands on the magnesium cation. In this report, we outline the synthesis of **1**, whose molecular structure features a linear Co-Mg-Co arrangement. We analyze the bonding situation in **1** and demonstrate that this complex catalyzes the hydrogenation of tri- and tetra-substituted alkenes with greater efficiency than **J** or other s-block metal cobaltates.[1e]

4.3 Results and Discussion

Complex **1** was prepared by treating anhydrous $MgCl_2$ with $[K(thf)_{0.33}][Co(\eta^4\text{-cod})_2]$ (**E**) in THF/toluene. The compound was isolated as an orange-yellow powder in 63%. Crystals grown from a saturated toluene solution were analyzed by single crystal X-ray diffraction. In the solid state, **1** forms an ion triple with a Mg^{2+} cation sandwiched by two $Co(\eta^4\text{-cod})_2]^-$ units (Figure 4-2, bottom; Co1–Mg1–Co2 179.36(4)°).[9] The two $[Co(\eta^4\text{-cod})_2]^-$ anions are rotated towards each other at 61.20° along the Co–Mg–Co axis (plane$[Co(\eta^4\text{-cod})_2]$-to-plane$[Co(\eta^4\text{-cod})_2]$). The Co–Mg distances (2.631(6) and 2.615(6) Å) are similar to those in complex **J**.[2d] Close contacts of the Mg^{2+} cation with four carbon atoms of the cod ligands (C1, C2, C3 and C4; Mg–C 2.362(8)-2.415(8) Å) presumably arise from an interaction with the π-bonds of the cod ligand. A quantum chemical analysis using intrinsic bond orbitals (IBOs), second-order perturbation theory (SOPT) and quantum theory of atoms in molecules (QTAIM) indicates that these interactions are weakly covalent.

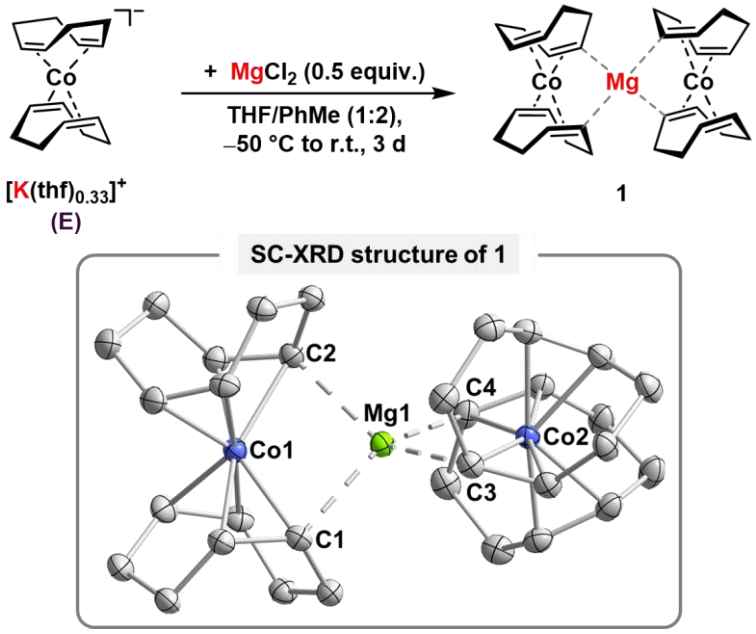

Figure 4-2: Top: Synthesis of $Mg[Co(\eta^4\text{-cod})_2]_2$ (1). Bottom: Solid state molecular structure of 1. Thermal ellipsoids are drawn at 40% probability level. H atoms are omitted for clarity. Selected bond lengths [Å] and angles [°]: Co1–Mg1 2.631(6), Co2–Mg1 2.615(6), Mg1–C1 2.411(2), Mg1–C2 2.362(2), Mg1–C3 2.363(2), Mg1–C4 2.415(2), Co1–Mg1–Co2 179.36(4).

The ^{1}H and ^{13}C NMR spectra of **1** show the presence of two species in a ratio of approximately 1:0.25, which is explained by the presence of rotamers with similar NMR spectra (Figure S4-3). ^{1}H NMR resonances at 1.2-4.5 ppm are assigned to the (chemically) inequivalent H atoms of the cod ligands (Figure S4-12). The cod ligands give rise to eight ^{13}C{^{1}H} NMR resonances at 27.0-83.0 ppm (Figure S4-13). This is in agreement with the contact-ion structure observed in the solid state, for which chemically inequivalent carbon atoms are expected.[2d] Broadening of the resonances is observed at elevated temperature (60 °C), which possibly indicates chemical exchange between the rotamers (Figure S4-17).

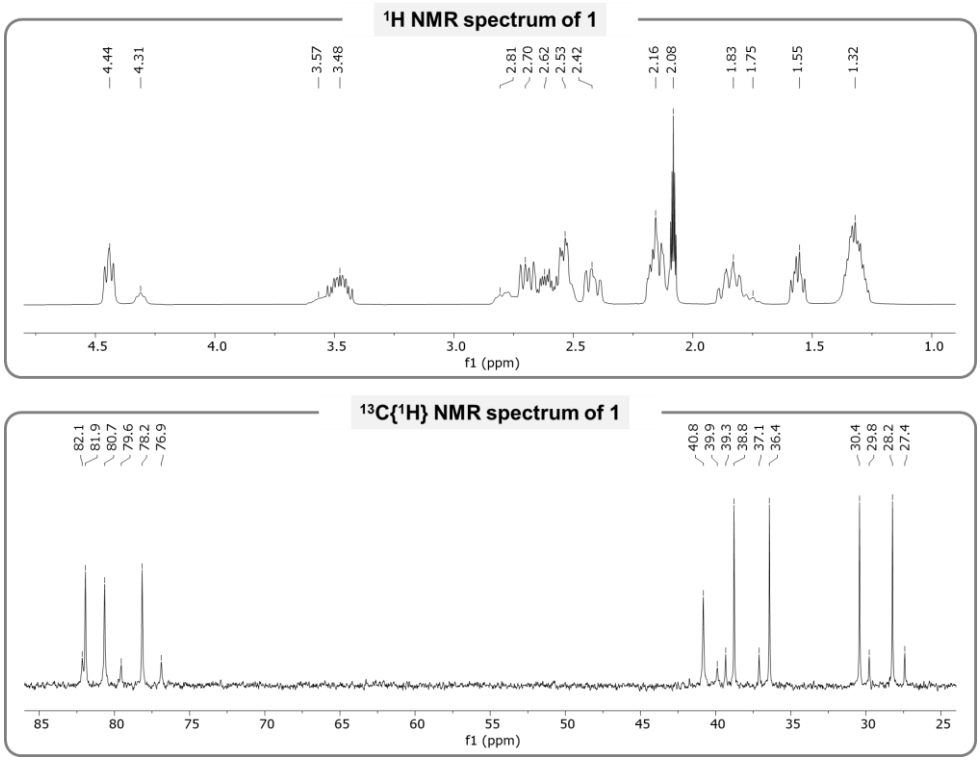

Figure 4-3: Cutouts of the ^{1}H and ^{13}C{^{1}H} NMR spectra (400.13/100.61 MHz, 298 K, toluene-d$_8$) of 1 in toluene-d$_8$.

Further confirmation of the intimate ion pair character in solution was provided by DOSY NMR studies of **1** and the lithium salt [Li(thf)$_{1.92}$][Co(η^4-cod)$_2$] (**C**) (section 0). For **1**, similar diffusion coefficients (D ≈ 9.1 x 10^{-10} m^2 s^{-1}) were obtained for all suitable cod ligand signals, which correspond to a hydrodynamic volume V_H ≈ 754 Å^3; for comparison, the diffusion coefficients for the 1,5-cod ligand signals (D ≈ 1.0 x 10^{-9} m^2 s^{-1}) and the Li$^+$ cation (D ≈ 9.9 x 10^{-10} m^2 s^{-1}; ^{7}Li NMR) of **C** give volumes V_H ≈ 566 Å^3 and V_H ≈ 448 Å^3, respectively. The larger hydrodynamic volume V_H of **1** strongly supports the presence of the magnesium salt as a contact ion pair in solution. NMR spectroscopic evidence of this C$_π$···Mg interaction can be found in the ^{13}C{^{1}H} NMR spectrum of **1**, which features one of four olefinic signals at an unusual chemical shift of

40.8 ppm, significantly high-field shifted compared to the other resonances at ≈ 80.0 ppm (see Figure S4-13 and Figure S4-14). The $^{13}C\{^{1}H\}$ NMR chemical shifts calculated at the PBE0/def2-TZVPP level of theory show that this resonance can be assigned to the four inward-facing C_{π} atoms (δ_{calc} = 44.9 ppm for C1/2/3/4; see Table S4-7). The ^{1}H NMR spectrum of **1** does not change significantly upon the addition of THF (see Figure S4-6). However, much simpler ^{1}H and ^{13}C NMR spectra are observed with 4-dimethylamino pyridine (DMAP), which indicate the formation of the ion-separated complex $[Mg(DMAP)_6][Co(\eta^4\text{-cod})_2]_2$ (**2**). In contrast to complex **J**, **1** does not react with styrene and dibenzo[*a,e*]cyclooctene even at elevated temperatures.[1e] This indicates that the tight ion-pairing in **1** significantly slows down ligand exchange.

Quantum chemical calculations confirm that the bonding in the Co–Mg–Co core of **1** is highly ionic, while weak donor-acceptor interactions between the Mg^{2+} center and four alkene C atoms provide partial covalent stabilization (*vide supra*). Natural bond order (NBO) and SOPT analyses show that any donor-acceptor interactions between the cobalt and magnesium atoms are negligible (<1 kcal mol^{-1}; see Table S8). The Wiberg bond index for the Co–Mg bond is 0.029 (0.030), and the QTAIM analysis displays no bond critical point (BCP) along the Co–Mg–Co motif (see Figure 4-4a,c). The charges from the natural population analysis (NPA) are positive for the Mg^{2+} cation (+1.74) and overall negative for the $[Co(\eta^4\text{-cod})_2]^-$ anions (–0.87), while the formal Co(–I) center itself has a positive charge (+0.25/+0.26). The C=C double bonds interacting with the Mg^{2+} are polarized (e.g. NPA charge (C4) of –0.54 vs. NPA charge (C8) of –0.20).

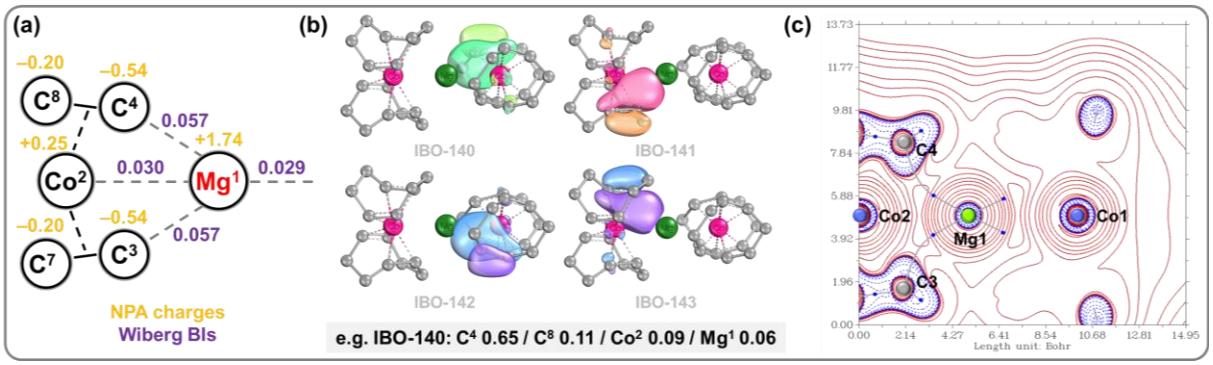

Figure 4-4: (a) NBO analysis including NPA charges and Wiberg BIs of 1; (b) Selected IBOs of 1. The interaction type and percentage of the electron density on C, Co and Mg are given exemplarily for IBO-140; (c) Plot of the Laplacian of the electron density on the C–Co–Mg plane of 1 fully displaying two of the four bond critical points between C_{π} and Mg (blue dots: bond critical points; grey lines: bond paths).

To assess the influence of the Mg^{2+} cation, we compared the properties of **1** with **J** in alkene hydrogenation reactions (see Figure 4-5).[1e] Various di-, tri- and tetra-substituted alkenes were hydrogenated quantitatively using **1** under mild H_2 pressure (1.5 mol%, 2-12 bar H_2, 30-60 °C). Catalyst **1** surpasses **J** in terms of yield and reaction rate for most of these substrates (see Figure S4-5, top and Table S1). The sterically most hindered substrate tetraphenylethylene was converted to the corresponding alkane with **1** in 88% yield, while a modest conversion of only 8% was achieved with **J**. This shows that the β-diketiminate motif is not an essential counterion component for the effective hydrogenation of alkenes. To gain initial information on the topicity of the catalyst, we conducted NMR spectroscopic reaction monitoring and mercury poisoning.[10] The hydrogenation of α-methylstyrene was not inhibited by the addition of Hg, while varying product formation was recorded for 1,1,2-triphenylethylene (52-89% yield), and significant inhibition was found for 1,1,2,2-triphenylethylene (35 vs. 88% yield; see Table 4-2).

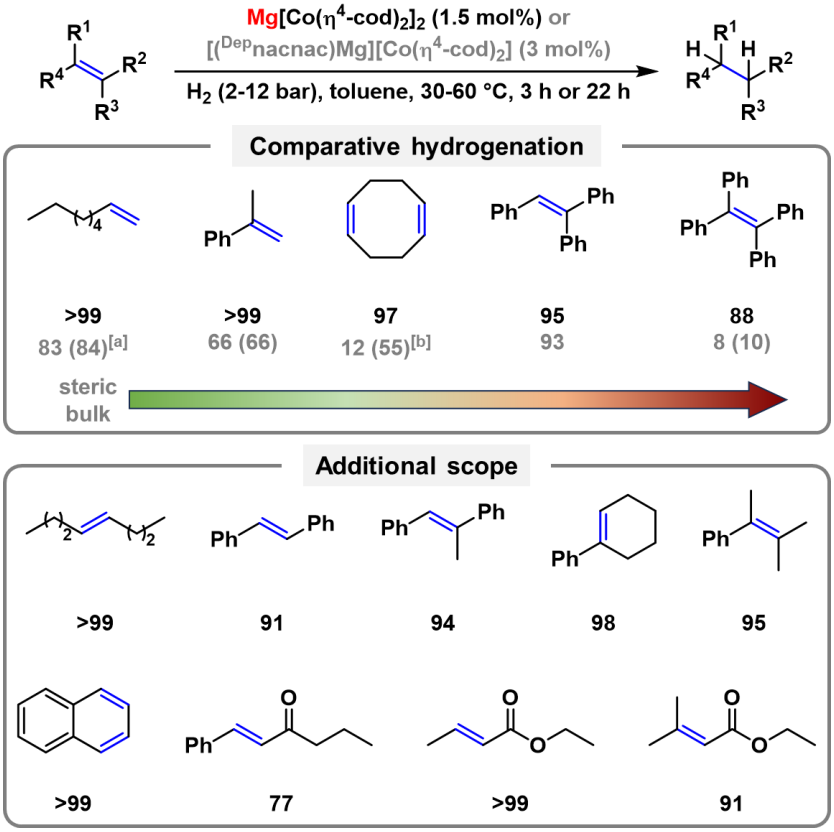

Figure 4-5: Hydrogenation of alkenes using $Mg[Co(\eta^4\text{-cod})_2]_2$ (1) and $[(^{Dep}nacnac)Mg][Co(\eta^4\text{-cod})_2]$ (J). Standard conditions: 0.2 mmol substrate (0.4 mol/L in toluene). 2-12 bar H_2, 30-60 °C, 3 h or 22 h (see the SI for the individual reaction conditions). Yields and conversions were determined by quantitative GC-FID analysis vs. internal *n*-pentadecane. [a] Isomerization to internal double bonds. [b] Formation of cis-cyclooctene as the major product.

These data suggest a homotopic catalyst predominantly operates at mild temperature and H_2 pressure, while heterotopic catalyst species are likely to contribute at higher temperatures and pressure required for challenging substrates such as 1,1,2,2-triphenylethylene. The ^{1}H NMR spectroscopic monitoring of the hydrogenation of α-methylstyrene with **1** (2 mol%, 2 bar H_2, ambient temperature, see Figure S4-11) revealed the complete formation of cumene in <71 min (see Figure S4-11). Moderate line broadening may indicate the formation of a minor amount of cobalt particles (after H_2 addition). While previous monitoring studies with **J** and **E** indicated that the spectroscopic line broadening is accompanied by termination of the hydrogenation reaction,[1e] the hydrogenation reaction with **1** did not cease when spectral broadening appeared. Thus, we suggest that the formed particles are inactive in the hydrogenation and are present alongside a molecular species, which facilitates the hydrogenation.

4.4 Conclusion

The complex $Mg[Co(\eta^4\text{-cod})_2]_2$ (**1**) features an unsupported linear Co–Mg–Co unit and can be synthesized through a simple salt metathesis reaction. Single crystal X-ray diffraction, DOSY NMR spectroscopy, and quantum chemical studies indicate that complex **1** exists as an intact ion triple in the solid state, characterized by an ionic magnesium-cobalt interaction and weak dative bonds between the 1,5-cyclooctadiene ligands and Mg^{2+}. This molecular structure is preserved in toluene solution. Complex **1** effectively catalyzes the hydrogenation of sterically demanding alkenes, surpassing the performance of related alkali metal salts **C**-**E** and the magnesium β-diketiminate salt **J**. These findings highlight a significant counterion effect on catalytic activity that is intrinsic to the Mg^{2+} cation.

4.5 Supporting information

Only the relevant sections of the Supporting Information that pertain to this thesis are displayed.

DOSY NMR Analysis of $Mg[Co(\eta^4\text{-cod})_2]_2$ (1) and $[Li(thf)_{1.92}][Co(\eta^4\text{-cod})_2]$ (C)

General Information

Diffusion-ordered NMR spectroscopy (DOSY) experiments were conducted on a Bruker Avance III HD 600 MHz spectrometer, equipped with a TBI 5 mm $^1H/^{19}F$-BB probe. All measurements were performed at 298 K, with the temperature validated using internal NMR calibration standards from Bruker.

The DOSY measurements were performed with convection compensating double stimulated echo (DSTE) pulse sequence developed by Jerschow and Müller.[12] The diffusion time delay was set to 40 ms. Smoothed square (SMSQ10.100) gradient shapes and a linear gradient ramp (32 increments, 5% to 95% of the maximum gradient strength) were used.

The NMR data were processed, analyzed, and plotted using TopSpin 3.2 software. Data evaluation was carried out using a Python script developed by Christian Scholtes, in which the DOSY data were fitted to the Stejskal-Tanner equation.[13]

$$I = I_0 \cdot \exp\left[-\gamma^2 G^2 \delta^2 \left(\Delta - \frac{\delta}{3}\right) D\right]$$

where I is the signal with the gradient, I_0 is the signal intensity without diffusion weighting, γ is the gyromagnetic ratio, G is the strength of the gradient pulse, δ is the duration of the pulse, Δ is the time interval between the two pulses and D the diffusion coefficient.

The calculated diffusion coefficient for TMS (D_{ref}) was applied to the Stokes-Einstein equation[14]

$$D_i = \frac{k_B T}{F c \pi \eta r_H}$$

to obtain viscosity correction for each individual sample. Here, k_B is the Boltzmann constant, T the temperature, F is the shape factor (set to 1 for a spherical shape), η the viscosity of the

sample, r_H the hydrodynamic radius of the analytes, and c a correction factor which was determined by using a semi-empirical modification by Chen.[15]

$$c_{Chen} = \frac{6F}{1 + 0.695 \left(\frac{r_{solv}}{r_{ref}}\right)^{2.234}}$$

The hydrodynamic radii values for TMS (r_{ref} = 2.96 Å) and toluene (r_{solv} = 2.88 Å) were calculated using hard-sphere increments.[16]

By inserting the Chen correction factor to the Stokes-Einstein equation,

$$\eta\ [kg/ms] = \frac{k_B T\ (1 + 0.695 \left(\frac{r_{solv}}{r_{ref}}\right)^{2.234})}{6\pi D_{ref}\ r_{ref}}$$

the correction factor for the viscosity of each respective sample (η) is determined. Finally, by incorporating all correction equations, the hydrodynamic radii can be iteratively calculated by

$$D = \frac{kT\ (1 + 0.695 \left(\frac{r_{solv}}{r_H}\right)^{2.234})}{6\pi\eta r_H}$$

Using the hydrodynamic radii, the respective Volumes (V_H) were calculated with the assumption of a spherical shape.

Sample Preparation

A 10 mM solution of either Mg[Co(η^4-cod)$_2$]$_2$ (**1**) or [Li(thf)$_{1.92}$][Co(η^4-cod)$_2$] (**C**) was prepared by dissolving the respective sample in toluene-d$_8$. The solution was then filtered from minor insolubles, and an aliquot (0.5 mL) was transferred into a J. Young NMR tube. Tetramethylsilane (TMS) was used as a reference and was added by withdrawing 500 µL from the headspace of a degassed TMS sample, just above the surface of the liquid and injected into the NMR tube, which was then sealed immediately afterwards.

Experimental Data for $Mg[Co(\eta^4\text{-cod})_2]_2$ (1)

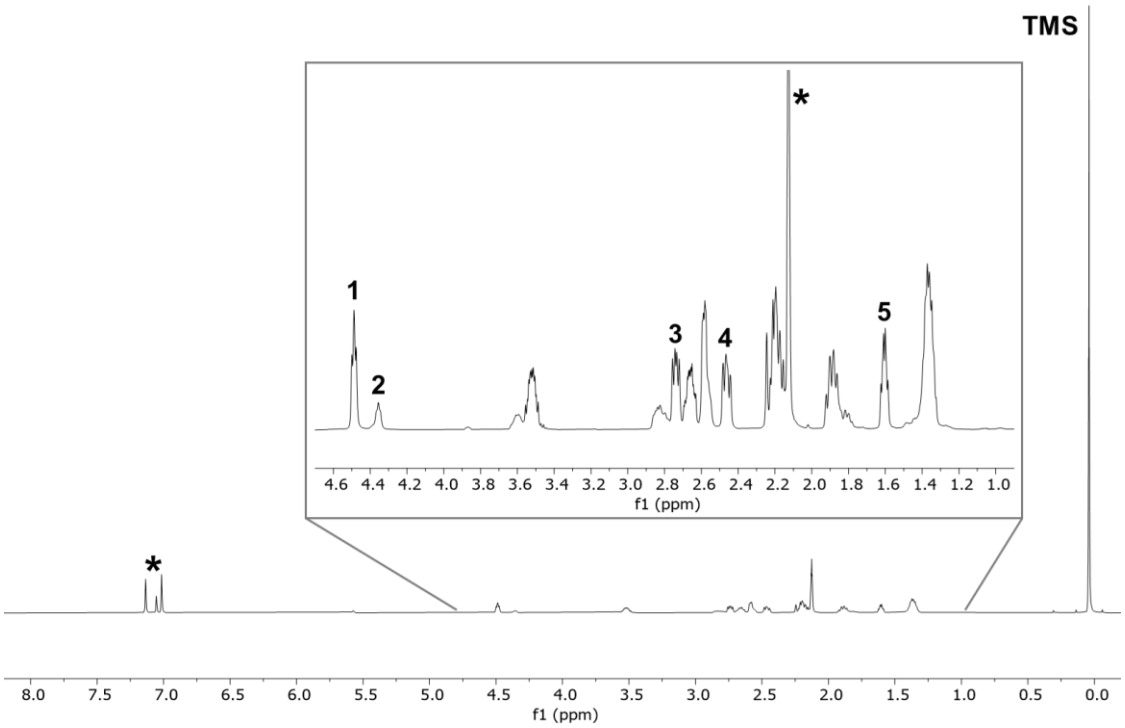

Figure S4-1: ^{1}H NMR spectrum of $Mg[Co(\eta^4\text{-cod})_2]_2$ (1) and TMS (600.13 MHz, 298 K, toluene-d_8), showing the signals 1-5 used for the DOSY analysis. *: toluene-d_8.

Table S4-3: Self-diffusion coefficients of signals 1-5 of $Mg[Co(\eta^4\text{-cod})_2]_2$ (1) in toluene-d_8. All signals correspond to the aliphatic and olefinic H atoms of the 1,5-cyclooctadiene ligand.

Signal	Chemical shift [ppm]	Diffusion coefficient D_i [$m^2 \cdot s^{-1}$]
I	TMS	2.48e-09 ± 1.14e-10
1	4.50-4.61	9.1464e-10 ± 1.54e-12
2	4.39-4.48	9.4051e-10 ± 4.26e-12
3	2.77-2.84	9.0042e-10 ± 1.32e-12
4	2.47-2.58	9.0448e-10 ± 1.98e-12
5	1.61-1.71	8.8644e-10 ± 1.96e-12
Mean diffusion coefficient *D* (**1**-**5**) [$m^2 \cdot s^{-1}$]		9.09e-10 ± 1.96e-12
Average radius r_H [Å]		5.646 ± 0.09643
Average volume V_H[a] [$Å^3$]		753.8 ± 38.63

[a] The average volume V_H was calculated assuming a spherical shape.

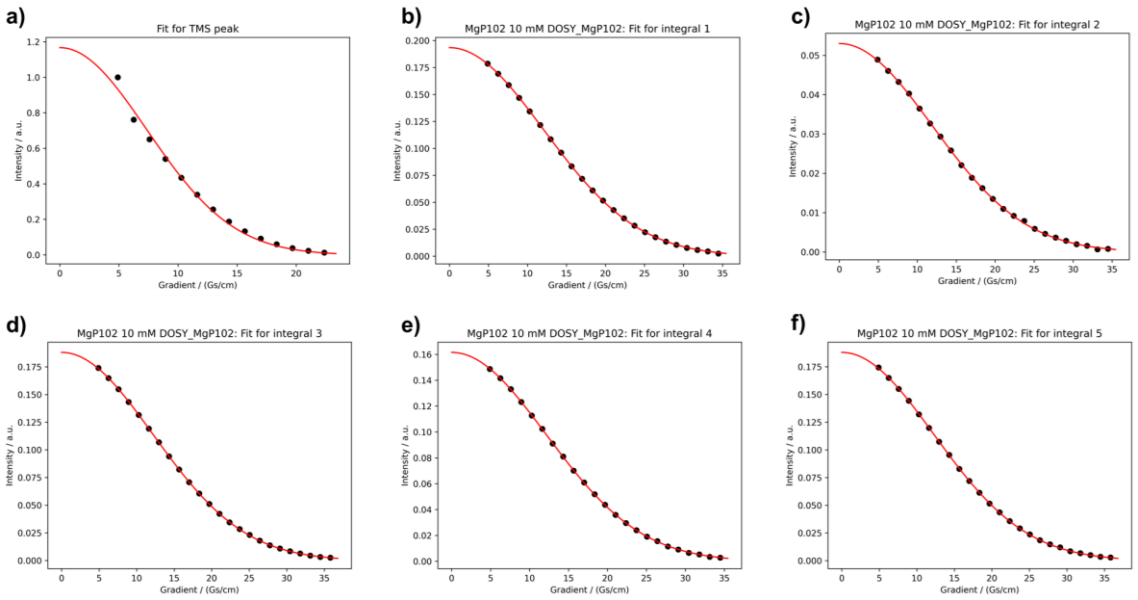

Figure S4-2: DOSY plots (signal intensity against gradient strength) of TMS and the signals 1-5 of $Mg[Co(\eta^4\text{-cod})_2]_2$ (1) in toluene-d_8.

Experimental Data for $[Li(thf)_{1.92}][Co(\eta^4\text{-cod})_2]$ (C)

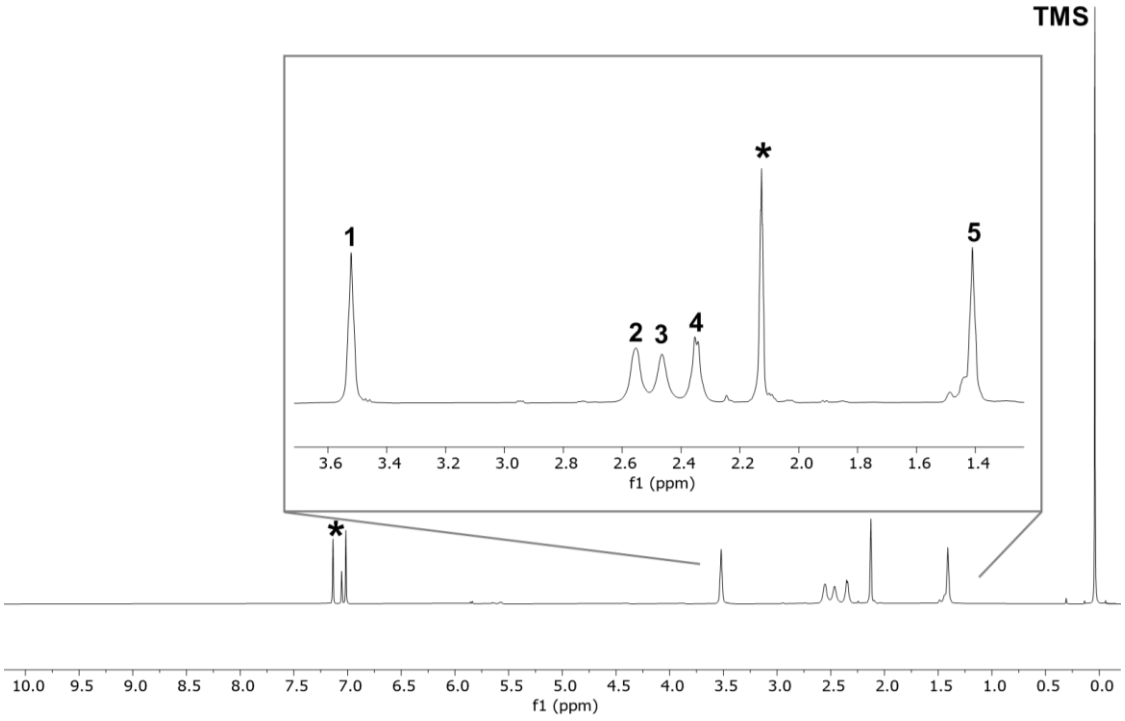

Figure S4-3: ^1H NMR spectrum of $[Li(thf)_{1.92}][Co(\eta^4\text{-cod})_2]$ (C) and TMS (600.13 MHz, 298 K, toluene-d_8), showing the signals 1-5 used for the DOSY analysis. *: Toluene-d_8.

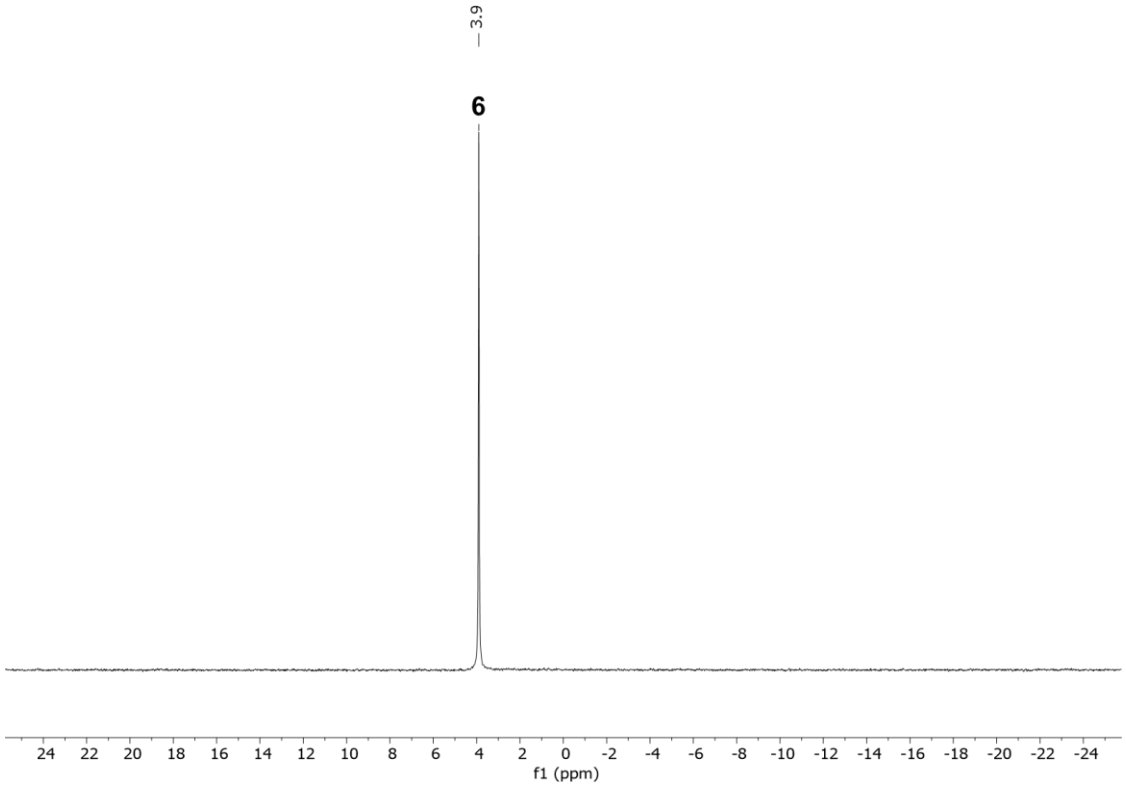

Figure S4-4: ^{7}Li NMR spectrum of $[Li(thf)_{1.92}][Co(\eta^4\text{-cod})_2]$ (C) and TMS (600.13 MHz, 298 K, toluene-d_8), showing the signal 6 used for the DOSY analysis.

Table S4-4: Self-diffusion coefficients of signals 1-6 of $[Li(thf)_{1.92}][Co(\eta^4\text{-cod})_2]$ (C) in toluene-d_8.

Signal	**Chemical shift [ppm]**	**Diffusion coefficient D_i [$m^2 \cdot s^{-1}$]**
	^{1}H NMR	
I	TMS	2.43e-09 ± 6.24e-11
1 (THF)	3.51-3.61	1.6395e-09 ± 2.42e-11
2 (1,5-cod)	2.57-2.67	1.0371e-09 ± 4.93e-12
3 (1,5-cod)	2.49-2.57	1.0026e-09 ± 3.94e-12
4 (1,5-cod)	2.35-2.47	1.014e-09 ± 5.08e-12
5 (THF)	1.41-1.48	1.6258e-09 ± 1.23e-11
	^{7}Li NMR	
6	3.90	9.92e-10 ± 9.19e-12
Mean diffusion coefficient *D* (**2**-**4**) [$m^2 \cdot s^{-1}$]		1.02e-09 ± 5.08e-12
Average radius r_H [Å]		5.132 ± 0.0656
Average volume V_H[a] [$Å^3$]		566.0 ± 21.71

Mean diffusion coefficient *D* (**1**&**5**) [$m^2 \cdot s^{-1}$]	1.63e-09 ± 1.23e-11
Average radius r_H [Å]	3.723 ± 0.01368
Average volume V_H[a] [$Å^3$]	216.2 ± 2.384
Mean diffusion coefficient *D* (**6**) [$m^2 \cdot s^{-1}$]	9.92e-10 ± 9.19e-12
Average radius r_H [Å]	4.746 ± 0.03109
Average volume V_H[a] [$Å^3$]	447.9 ± 8.802

[a] The average volume V_H was calculated assuming a spherical shape.

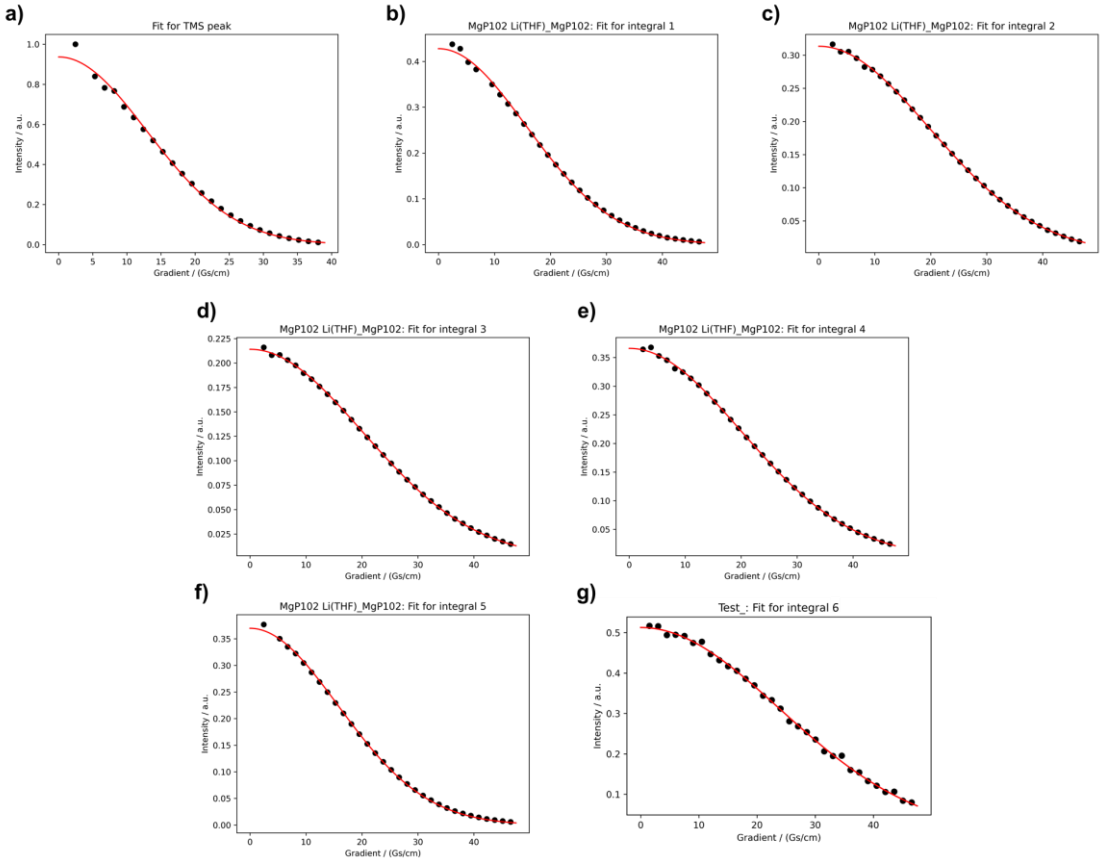

Figure S4-5: DOSY plots (signal intensity against gradient strength) of TMS and the signals 1-6 of $[Li(thf)_{1.92}][Co(\eta^4\text{-cod})_2]$ (C) in toluene-d_8.

Discussion

The DOSY NMR analysis of $Mg[Co(\eta^4\text{-cod})_2]_2$ (**1**) gives similar diffusion coefficients for all five cod ligand signals in the ^{1}H NMR spectrum, which results in a mean diffusion coefficient D = 9.09e-10 ± 1.96e-12 m^2 s^{-1} and a respective hydrodynamic volume V_H = 753.8 ± 38.63 Å^3 for the molecular entity (see Figure S4-1 and Table S4-3). The trinuclear complex **1** was then referenced to the mononuclear lithium cobaltate, $[Li(thf)_{1.92}][Co(\eta^4\text{-cod})_2]$ (**C**), which is the only toluene-soluble alkali metal cobaltate of the series. The diffusion coefficients for the cod ligand signals in the ^{1}H NMR spectrum are matching and give a mean diffusion coefficient D = 1.02 10e-09 ± 5.08e-12 m^2 s^{-1} and a respective hydrodynamic volume V_H = 566.0 ± 21.71 Å^3 for the molecular entity (see Figure S4-3 and Table S4-4). In agreement with this, the diffusion coefficient for the Li$^+$ cation in the ^{7}Li NMR spectrum was calculated at D = 9.92e-10 ± 9.19e-12 m^2 s^{-1}, resulting in a hydrodynamic volume V_H = 447.9 ± 8.802 Å^3 for the molecular unit (Figure S4-4 and Table S4-4). Interestingly, the THF ligands coordinated to the Li$^+$ cation of **C** exhibit a higher (mean) diffusion coefficient (D = 1.63e-09 ± 1.23e-11 m^2 s^{-1}) compared to that of the cod ligands (D = 1.02e-09 ± 5.08e-12 m^2 s^{-1}), which indicates that they are separate entities in solution. This suggests that a $Li[Co(\eta^4\text{-cod})_2]$ unit with close contact between the Li$^+$ cation and the $[Co(\eta^4\text{-cod})_2]^-$ anion is present in solution, which is solvated by THF molecules coordinating in an interchangeable mode (see [2] for a comparison of ion pair **C** in the solid state). The hydrodynamic volume V_H of **1** (753.8 ± 38.63 Å^3) is found to be approximately 33% and 68% larger, respectively, than the hydrodynamic volume V_H of **C** (^{1}H: 566.0 ± 21.71 Å^3 and ^{7}Li: 447.9 ± 8.802 Å^3, respectively; considered unit: $Li[Co(\eta^4\text{-cod})_2]$), indicating that **1** is present as a contact ion pair in solution.

4.6 References

[1] a) K. Jonas, R. Mynott, C. Krüger, J. C. Sekutowski, Y.-H. Tsay, *Angew. Chem.* **1976**, *88*, 808; b) K. Jonas (Studiengesellschaft Kohle mbH), US4169845 A, **1977**; c) D. Habermann, Organocobaltverbindungen aus (η-Cyclopentadienyl)cobalt-Komplexen durch reduktive C_5H_5-Ablösung, Doctoral Dissertation, Ruhr-Universität Bochum, **1980**; d) W. W. Brennessel, V. G. Young, Jr., J. E. Ellis, *Angew. Chem. Int. Ed.* **2002**, *41*, 1211; e) M. Gawron, F. Gilch, D. Schmidhuber, J. A. Kelly, T. M. Horsley Downie, A. Jacobi Von Wangelin, J. Rehbein and R. Wolf, *Angew. Chem. Int. Ed.* **2024**, *63*, e202315381.

[2] a) R. Wolf, A. W. Ehlers, J. C. Slootweg, M. Lutz, D. Gudat, M. Hunger, A. L. Spek, K. Lammertsma, *Angew. Chem. Int. Ed.* **2008**, *47*, 4584; b) C. G. P. Ziegler, F. Hennersdorf, J. J. Weigand, R. Wolf, *Z. Anorg. Allg. Chem.* **2020**, *646*, 552; c) G. Hierlmeier, P. Coburger, D. J. Scott, T. M. Maier, S. Pelties, R. Wolf, D. M. Pividori, K. Meyer, N. P. van Leest, B. de Bruin, *Chem. Eur. J.* **2021**, *27*, 14936; d) J. A. Kelly, J. Gramüller, R. M. Gschwind and R. Wolf, *Dalton Trans.* **2021**, *50*, 13985.

[3] a) D. Gartner, A. Welther, B. R. Rad, R. Wolf, A. Jacobi von Wangelin, *Angew. Chem. Int. Ed.* **2014**, *53*, 3722; b) P. Büschelberger, D. Gärtner, E. Reyes-Rodriguez, F. Kreyenschmidt, K. Koszinowski, A. Jacobi von Wangelin and R. Wolf, *Chem. Eur. J.* **2017**, *23*, 3139.

[4] B. N. Baumann, H. Lange, F. Seeberger, P. Büschelberger, R. Wolf, M. Hapke, *Mol. Catal.* **2023**, *550*, 113482.

[5] W. W. Brennessel, J. E. Ellis, *Inorg. Chem.* **2012**, *51*, 9076.

[6] a) S. Pelties, T. Maier, D. Herrmann, B. de Bruin, C. Rebreyend, S. Gärtner, I. G. Shenderovich, R. Wolf, *Chem. Eur. J.* **2017**, *23*, 6094; b) T. M. Maier, S. Sandl, I. G. Shenderovich, A. Jacobi von Wangelin, J. J. Weigand, R. Wolf, *Chem. Eur. J.* **2019**, *25*, 238; S. Sandl, T. M. Maier, N. P. van Leest, S. Kröncke, U. Chakraborty, S. Demeshko, K. Koszinowski, B. de Bruin, F. Meyer, M. Bodensteiner, C. Herrmann, R. Wolf, A. Jacobi von Wangelin, *ACS Catal.* **2019**, *9*, 7596; c) C. M. Hoidn, T. M. Maier, K. Trabitsch, J. J. Weigand, R. Wolf, *Angew. Chem. Int. Ed*. **2019**, *58*, 18931; d) S. Hauer, T. M. Horsley Downie, G. Balázs, K. Schwedtmann, J. J. Weigand, R. Wolf, *Angew. Chem. Int. Ed*. **2024**, *63*, e202317170.

[7] a) K. Jonas, G. Koepe and C. Krüger, *Angew. Chem. Int. Ed.* **1986**, *25*, 923; b) M. P. Blake, N. Kaltsoyannis and P. Mountford, *J. Am. Chem. Soc.* **2015**, *137*, 12352; c) R. Green, A. C. Walker, M. P. Blake and P. Mountford, *Polyhedron* **2016**, *116*, 64.

[8] a) G. M. Sheldrick, R. N. F. Simpson, *Chem. Commun. (London)* **1967**, 1015a; b) G. M. Sheldrick, R. N. F. Simpson, *J. Chem. Soc. (A)* **1968**, 1005.

[9] To the best of our knowledge, the only structurally related complex is $Zn[Co(\eta^4\text{-btd})_2]_2$ (btd = 1,3-butadiene), which was already reported in 1980 (ref. [1c]) but only subjected to a small reactivity study with nucleophiles. The solid state structure of $Zn[Co(\eta^4\text{-btd})_2]_2$ is shown in

section 1.4.10 (Figure S4-18), as it was not characterized by SC-XRD analysis in the original report.

[10] a) J. A. Widegren, R. G. Finke, *J. Mol. Catal. A* **2003**, *198*, 317; b) C. A. Jaska, I. Manners, *J. Am. Chem. Soc.* **2004**, *126*, 9776; c) R. H. Crabtree, *Chem. Rev.* **2012**, *112*, 1536; d) D. Gartner, S. Sandl, A. Jacobi von Wangelin, *Catal. Sci. Technol.* **2020**, *10*, 3502.

[11] Syringe filter ROTILABO® Mini-Tip (PTFE), pore size 0.2 µm, 15 mm diameter; available under: https://www.carlroth.com/de/de/spritzenvorsatzfilter/spritzenfilter-rotilabo-mini-tip-polytetrafluorethylen-%28ptfe%29/p/pp45.1, **2025**.

[12] a) A. Jerschow, N. Müller, *J. Magn. Reason., Ser. A* **1996**, *123*, 222; b) A. Jerschow, N. Müller, *J. Magn. Reson.* **1997**, *125*, 372.

[13] E. O. Stejskal, J. E. Tanner, *J. Chem. Phys.* **1965**, *42*, 288.

[14] A. Macchioni, G. Ciancaleoni, C. Zuccaccia, D. Zuccaccia, *Chem. Soc. Rev.* **2008**, *37*, 479.

[15] H. C. Chen, S. H. Chen, *J. Phys. Chem.* **1984**, *88*, 5118.

[16] a) D. Ben-Amotz, K. G. Willis, *J. Phys. Chem.* **1993**, *97*, 7736; b) D. Zuccaccia, A. Macchioni, *Organometallics* **2005**, *24*, 3476.

[17] NORELL® Valved NMR tubes are available under: https://secure.nmrtubes.com/nmr-epr-tubes/valved-for-intermediate-pressure, **2025**.

[18] a) Sheldrick, G. M. SADABS, Bruker AXS, Madison, USA **2007**; b) CrysAlisPro, Scale3 Abspack, Rigaku Oxford Diffraction, **2019**.

[19] R. C. Clark, J. S. Reid, *Acta Crystallogr. A* **1995**, *51*, 887.

[20] G. M. Sheldrick, *Acta Crystallogr. C* **2015**, *71*, 3.

[21] O. V. Dolomanov, L. J. Bourhis, R. J. Gildea, J. A. K. Howard, H. Puschmann, *J. Appl. Crystallogr.* **2009**, *42*, 339.

[22] G. M. Sheldrick, *Acta Crystallogr. A* **2008**, *64*, 112.

[23] a) Neese, F., The ORCA program system. *WIREs Comput. Mol. Sci.* **2012**, 2: 73, https://doi.org/10.1002/wcms.81; b) Neese, F. Software update: The ORCA program system—Version 5.0. WIREs *Comput. Mol. Sci.* **2022**; 12:e1606. https://doi.org/10.1002/wcms.1606.

[24] S. Grimme, A. Hansen, S. Ehlert, J.-M. Mewes, *J. Chem. Phys.* **2021**, *154*, 064103.

[25] a) J.-D. Chai and M. Head-Gordon, *J. Chem. Phys.* 2008, **128**, 084106; b) J.-D. Chai, M. Head-Gordon, *Phys. Chem. Chem. Phys.* **2008**, *10*, 6615; c) A. Schäfer, H. Horn, R. Ahlrichs, *J. Chem. Phys.* **1992**, *97*, 2571; d) A. Schäfer, C. Huber, R. Ahlrichs, *J. Chem. Phys.* **1994**, *100*, 5829; e) F. Weigend, R. Ahlrichs, *Phys. Chem. Chem. Phys.* **2005**, *7*, 3297; f) F. Weigend, *Phys. Chem. Chem. Phys.* **2006**, *8*, 1057; g) A. Hellweg, D. Rappoport, *Phys. Chem. Chem. Phys.* **2015**, *17*, 1010.

[26] NBO 7.0. E. D. Glendening, J. K. Badenhoop, A. E. Reed, J. E. Carpenter, J. A. Bohmann, C. M. Morales, P. Karafiloglou, C. R. Landis, and F. Weinhold, Theoretical Chemistry Institute, University of Wisconsin, Madison, WI (**2018**).

[27] a) G. Knizia, *J. Chem. Theory Comput.* **2013**, *9*, 4834; b) G. Knizia, J. E. M. N. Klein, *Angew. Chem. Int. Ed.* **2015**, *54*, 5518.

[28] a) E. R. Johnson, S. Keinan, P. Mori-Sánchez, J. Contreras-García, A. J. Cohen, W. Yang, *J. Am. Chem. Soc.* **2010**, *132*, 6498; b) J. Contreras-García, E. R. Johnson, S. Keinan, R. Chaudret, J.-P. Piquemal, D. N. Beratan, W. Yang, *J. Chem. Theory Comput.* **2011**, *7*, 625; c) R. A. Boto, F. Peccati, R. Laplaza, C. Quan, A. Carbone, J.-P. Piquemal, Y. Maday, J. Contreras-Garcia, *J. Chem. Theory Comput.* **2020**, *16*, 4150.

[29] T. Lu, F. Chen, *J. Comput. Chem.* **2011**, *33*, 580.

[30] W. Humphrey, A. Dalke, K. Schulten, *J. Mol. Graph.* **1996**, *14*, 33.

[31] a) F. London, *J. Phys. Radium* **1937**, *8*, 397; b) R. McWeeny, *Phys. Rev.* **1962**, *126*, 1028; c) R. Ditchfield, *Molec. Phys.* **1974**, *27*, 789; d) K. Wolinski, J. F. Hinton, P. Pulay, *J. Am. Chem. Soc.* **1990**, *112*, 8251; e) J. R. Cheeseman, G. W. Trucks, T. A. Keith, M. J. Frisch, *J. Chem. Phys.* **1996**, *104*, 5497; f) G. L. Stoychev, A. A. Auer, R. Izsák, F. Neese*, J. Chem. Theory Comput.* **2018**, 14, 619.

[32] A. V. Marenich, C. J. Cramer, D. G. Truhlar, *J. Phys. Chem. B* **2009**, *113*, 6378.

[33] a) J. Tao, J. P. Perdew, V. N. Staroverov, G. E. Scuseria, *Phys. Rev. Lett.* **2003**, *91*, 146401; b) V. N. Staroverov, G. E. Scuseria, J. Tao, J. P. Perdew, *J. Chem. Phys.* **2003**, *119*, 12129; c) V. N. Staroverov, G. E. Scuseria, J. Tao, J. P. Perdew, *J. Chem. Phys.* **2004**, *121*, 11507.

[34] a) J. P. Perdew, K. Burke, M. Ernzerhof, *Phys. Rev. Lett.* **1996**, *77*, 3865; b) J. P. Perdew, K. Burke, M. Ernzerhof, *Phys. Rev. Lett.* **1997**, *78*, 1396; c) C. Adamo, V. Barone, *J. Chem. Phys.* **1999**, *110*, 6158.

[35] F. Jensen, *J. Chem. Theory Comput.* **2014**, *11*, 132.

[36] B. Silvi, R.J. Gillespie, C. Gatti, “Electron Density Analysis” in In *Comprehensive Inorganic Chemistry II*, Elsevier, **2013**, pp. 187–226.

[37] P. Macchi, D. M. Proserpio, A. Sironi, *J. Am. Chem. Soc.* **1998**, *120*, 13429.

[38] R. Gericke, M. A. Bennett, S. H. Privér and S. K. Bhargava, *Inorg. Chem.* **2023**, *62*, 8846.

5 Conclusion

Over the past decades, the pivotal role of ion-pair interactions in catalysis has become increasingly evident, profoundly influencing both metal-catalyzed and organocatalytic transformations. These interactions stabilize reactive intermediates, modulate reaction kinetics, and enhance selectivity by fine-tuning the electronic and steric environment within catalytic cycles. As a result, researchers have recognized the necessity of in-depth investigations to unravel the precise functions of ion pairs in catalytic processes. A comprehensive understanding of how charged catalytic species interact with their counterions has led to the development of more efficient and selective catalytic systems. This growing awareness has driven extensive studies on solvent effects, ion-pair dynamics, and their broader implications for catalyst design, ultimately expanding the fundamental knowledge of ion-pairing interactions across diverse chemical transformations.

This study provides valuable insights into the catalytic behavior of both magnesium cobaltate salts and selenium-based organocatalysts, emphasizing the decisive role of ion-pairing interactions in their respective reaction mechanisms. The selenium-based organocatalyst was specifically examined with regard to its reactivity, selectivity, and the influence of ion pairs within the catalytic cycle. Although organocatalysis works metal-free, there is a significant impact of ion-pairing interactions on reaction dynamics. However, detailed investigations have revealed that these interactions between the catalyst and counterions play a crucial role in activation and selectivity, particularly by stabilizing reactive intermediates. This finding underscores the broader significance of ion-pairing effects, extending beyond traditional metal complexes to encompass non-metal-based catalytic systems.

Chapter one provides a comprehensive review on the key advancements in the development of highly acidic organocatalysts and their application for synthesis. While significant progress has been made in this field, many catalysts either disrupt the inherent C_2-symmetry of the BINOL backbone or introduce multiple acceptor sites. This not only complicates substrate binding but also increases the probability of multiple transition states, ultimately affecting reaction efficiency and selectivity.

This challenge is directly addressed in chapter two, where a novel chiral organocatalyst, DSA, is introduced. This catalyst retains the beneficial properties of chiral phosphoric acids while significantly improving applicability to more inert substrates, such as non-activated *N*-phenyl-aldimines and silyl enol ethers. The catalyst's high reactivity was successfully demonstrated in a Mukaiyama-Mannich reaction, showcasing its ability to activate challenging substrates. Additionally, the increased Lewis basicity of the P=Se moiety enhances substrate binding, potentially accelerating reaction rates. As a result, this study presents the development of a highly reactive catalyst that overcomes key limitations of chiral phosphoric acids.

Chapter three further advances this research by significantly improving the synthesis of DSA catalysts, allowing for the efficient incorporation of 3,3'-substituents. These modifications facilitate stereoselective transformations, as demonstrated in an Asymmetric Counteranion-Directed Catalysis (ACDC) reaction. The role of the presence of potassium ions within the reaction mixture on the selectivity of DSA-catalysis was thoroughly investigated, particularly in the context of salt metathesis. Additionally, structural insights were gained through the characterization of a dimeric crystal structure of a potassium-DSA salt catalyst. This finding provides a foundation for future NMR studies on aggregation in solution, paving the way for further optimization. In summary, these developments grant access to a highly reactive and selective catalyst system for applications in asymmetric ion-pair catalysis.

Chapter four shifts focus to the catalytic properties of a trinuclear magnesium cobaltate salt featuring a linear Co–Mg–Co arrangement, which has proven to be an effective system for alkene hydrogenation. Diffusion-Ordered Spectroscopy (DOSY) measurements revealed that this complex predominantly exists as a contact ion pair, ensuring close proximity between the cobaltate anion and the magnesium counterion. This ionic environment plays a crucial role in modulating the reactivity and stability of the active species, thereby influencing catalytic performance. Notably, magnesium counterions were found to outperform alkali metal counterions in fine-tuning catalytic activity, underscoring the potential of magnesium cobaltates as promising contact ion pair catalysts for selective hydrogenation reactions.

Overall, this work underscores the pivotal role of ion-pairing interactions in catalysis - an often overlooked yet fundamentally crucial factor in both metal-catalyzed and organocatalyzed transformations. This has been demonstrated through the effective synthesis of a novel chiral DSA organocatalyst, its application in asymmetric ion-pair catalysis, and detailed structural

investigations on both this DSA organocatalyst and a magnesium cobaltate metal catalyst. Gaining deeper insight into these interactions not only enhances our fundamental understanding but also unlocks new strategies for catalyst design, driving the precise optimization of efficiency, selectivity, and stability.

6 Curriculum Vitae

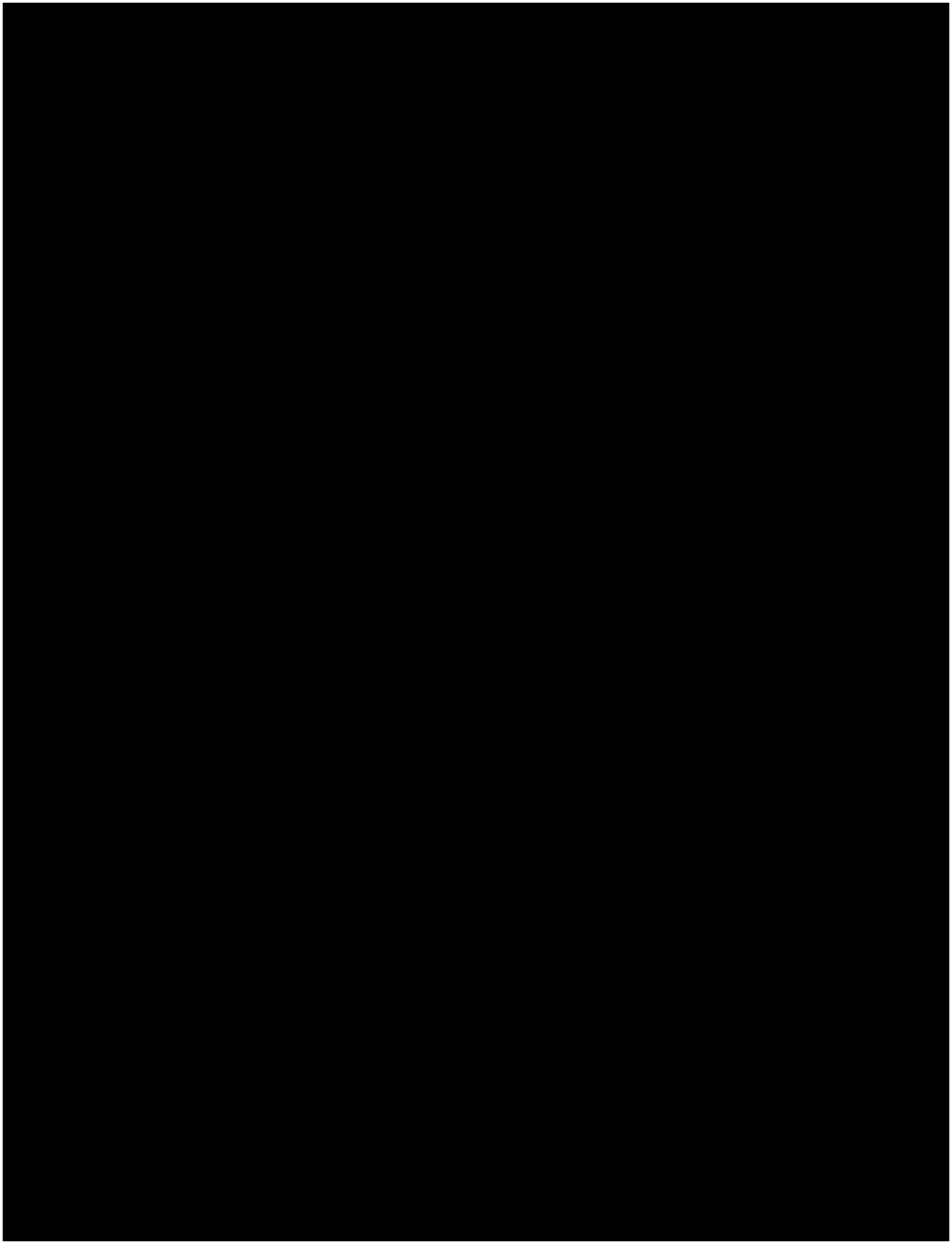

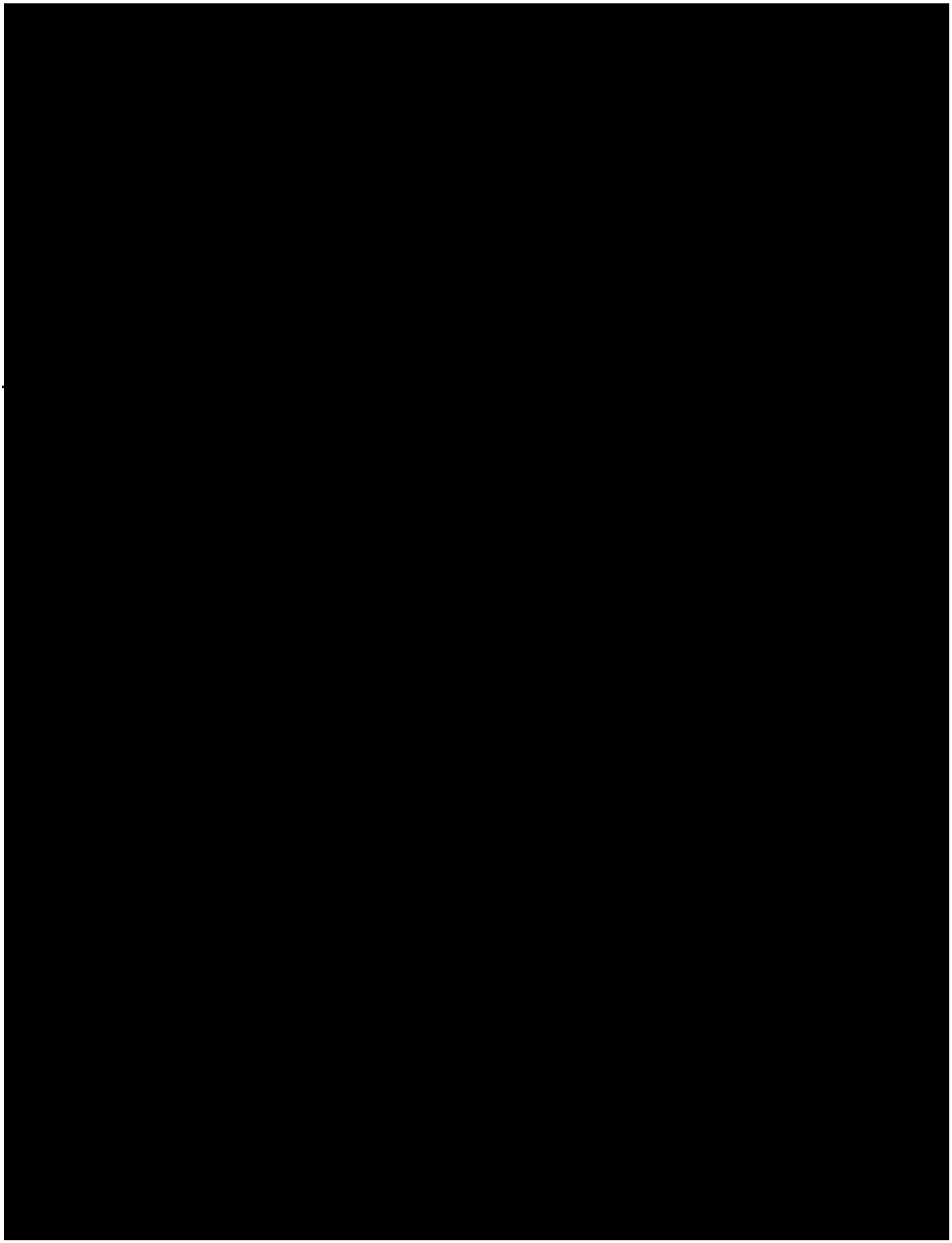

7 Danksagung

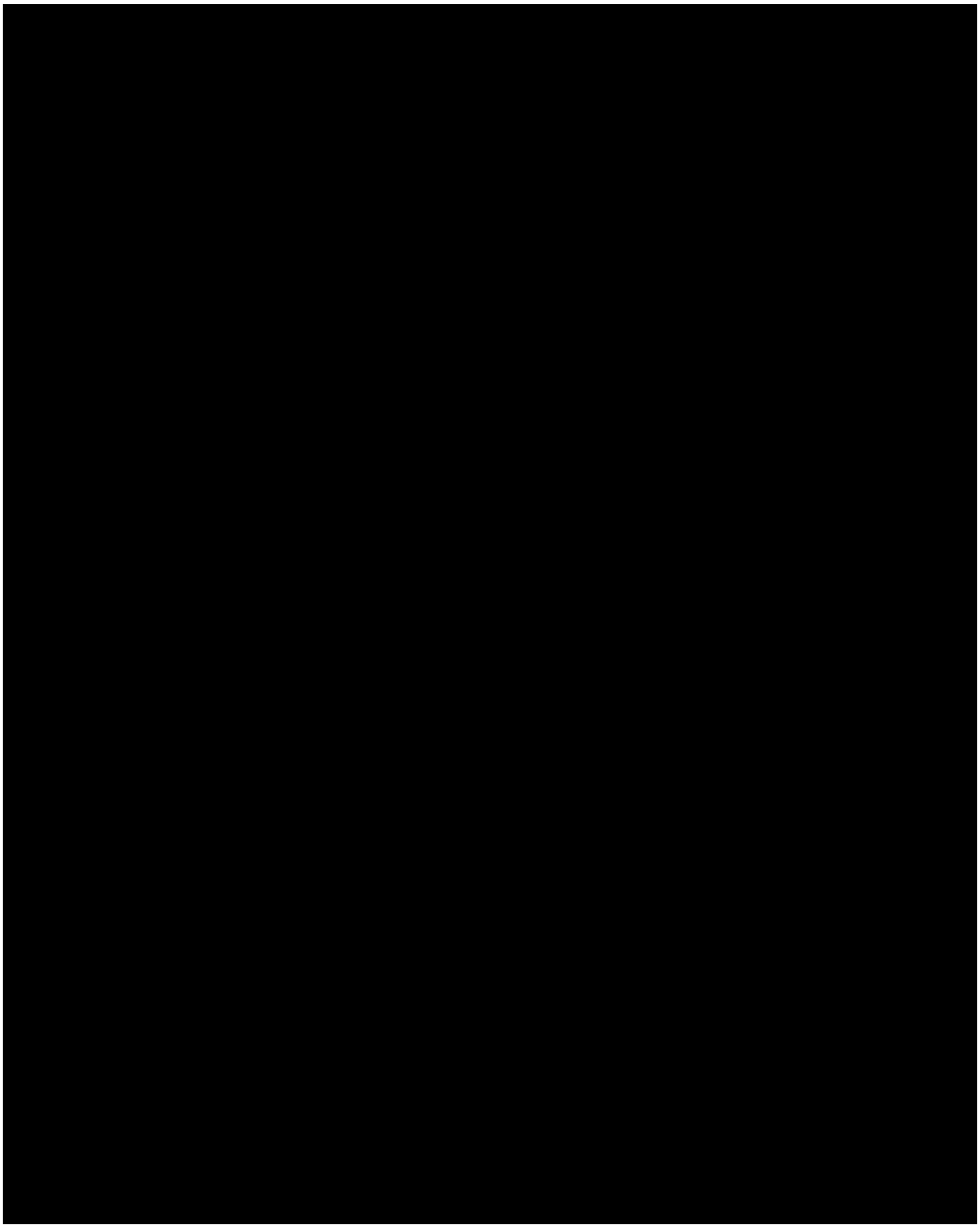

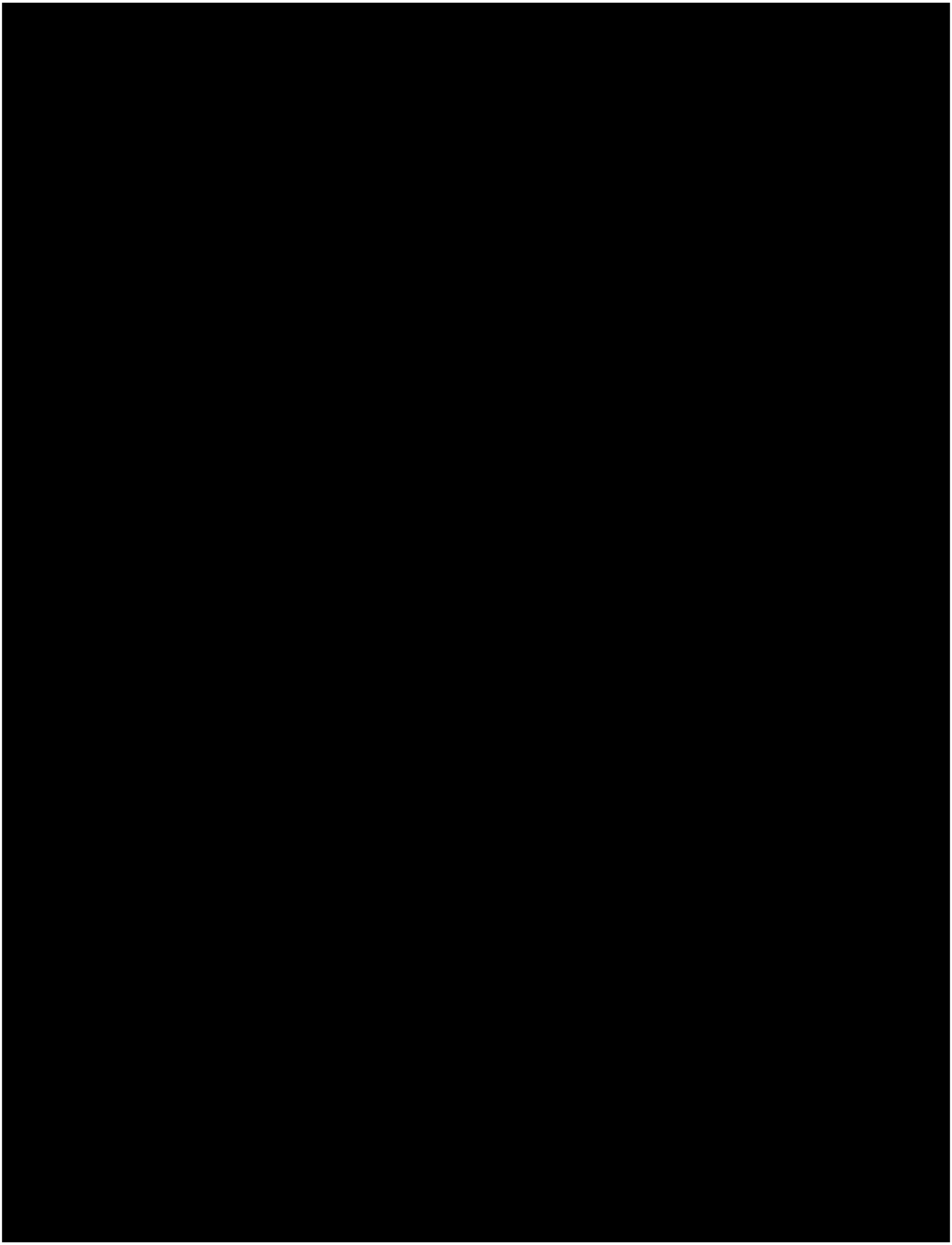

8 Eidesstattliche Versicherung

(1) Ich erkläre hiermit an Eides statt, dass ich die vorliegende Arbeit ohne unzulässige Hilfe Dritter und ohne Benutzung anderer als der angegebenen Hilfsmittel angefertigt habe; die aus anderen Quellen direkt oder indirekt übernommenen Daten und Konzepte sind unter Angabe des Literaturzitats gekennzeichnet.

(2) Bei der Auswahl und Auswertung folgenden Materials haben mir die zu Beginn des jeweiligen Kapitels aufgeführten Personen in der jeweils beschriebenen Weise unentgeltlich geholfen.

(3) Weitere Personen waren an der inhaltlich-materiellen Herstellung der vorliegenden Arbeit nicht beteiligt. Insbesondere habe ich hierfür nicht die entgeltliche Hilfe eines Promotionsberaters oder anderer Personen in Anspruch genommen. Niemand hat von mir weder unmittelbar noch mittelbar geldwerte Leistungen für Arbeiten erhalten, die im Zusammenhang mit dem Inhalt der vorgelegten Dissertation stehen.

(4) Die Arbeit wurde bisher weder im In- noch im Ausland in gleicher oder ähnlicher Form einer anderen Prüfungsbehörde vorgelegt.

Regensburg, den 07.02.2025 _____

Johannes Eder